EXPLORATION OF A TEMPLATE-DIRECTED APPROACH FOR THE SYNTHESIS OF SILVER NANOPARTICLES

By

HEBA ABBAS KASHMERY

A thesis submitted to the Department of Pure and Applied Chemistry, University of Strathclyde, in part fulfilment of the requirements for the degree of Doctor of Philosophy

September 2015

This thesis is the result of the author's original research. It has been composed by the author and has not been previously submitted for examination which has led to the award of a degree.

The copyright of this thesis belongs to the author under the terms of the United Kingdom Copyright Acts as qualified by University of Strathclyde Regulation 3.50. Due acknowledgement must always be made of the use of any material contained in, or derived from, this thesis.

Signed: Heba

Date: 04/09/2015

DEDICATION

I dedicate this thesis to:

My sweet Parents, Abbas & Buthaynah, whose love, prayers and efforts support me to achieve our dream to get such success. I am proud for your greatest care especially during my study abroad.

My grandmother, Amnah, who means to me a beautiful example of patience.

My sisters especially Alaa who shared my life abroad. Thank you for your cooperation to finish this work. I hope you graduate soon.

The memory of my inspiring person, Dr. Suzan Batterjee, who passed away while I was abroad. I hope I have fulfilled my promise to succeed this academic goal. Sadly, she will not see me graduate.

ACKNOWLEDGEMENTS

I thank ALLAH (SWT) for giving me the ability to achieve this level of work. I would like to express my appreciation to all those who gave me the opportunity to complete this thesis. First of all, I am grateful to King Abdul Aziz University in Jeddah for providing me with a generous scholarship and the opportunity to study abroad to undertake my PhD degree in the United Kingdom.

I would like to expend special thanks to the University of Strathclyde for the chance to complete my PhD studies. I am deeply indebted to my supervisor Dr. Glenn Burley who encouraged me to go forward with my thesis and I would like to express my gratitude to him for his stimulating support, continuous suggestions and advice. I also would like to thank my second supervisor, Dr John Reglinski for his generous feedback during my research. I am grateful for the collaboration with Dr. Alasdair W. Clark for his help with SEM and TEM imaging at the James Watt Nanofabrication Centre at the University of Glasgow. Thanks to Dr David G. Thompson at the Centre for Molecular Nanometrology at Strathclyde for SERS. I want to thank Dr Ruggero Dondi for the calculation of binding constants, Dr Mick Lee and Dr Andrew J. Fallows at the University of Leicester for their kind assistance in HRMS. I also want to thank all members of Burley group for generous support throughout the four years of my PhD.

Most especially, I would like to thank my parents for their prayers and for giving me the strength to pursue my studies. I also would like to thank my sisters, Hanady, Hala and Alaa who provided me with the moral support during a pleasant PhD journey.

I, of course, cannot forget my nephews (Moayad, Mohammed and Zeyad) and nieces (Reema and Rama) who make me happy every day. Finally, I offer my kind regards to all of my friends especially Thikryat, Saja and Taghreed for sharing advice during our PhD years.

ABSTRACT

The aim of this thesis is to develop a facile one-pot synthesis of silver nanoparticles (AgNPs) using Tollens' reagent as a silver source. The project focuses on the preparation of a series of sugar triazole ligands to template the formation of monodisperse AgNPs in a size- and shape-controlled manner.

Chapter 1 introduces the optical properties of metal nanoparticles and the common methods for the preparation of AgNPs, highlighting the limitations of typical methods and the motivations of this research. Chapter 2 describes the influence of the structural parameters of these sugar triazole ligands (i.e., sugar units, triazole and aromatic core) on the size, shape, stability and dispersity of AgNPs. The work highlights how the Ag(I) binding affinity of these ligands is a key parameter to tune the size and shape of the resultant AgNPs formed. Weaker Ag(I) binding ligands with a phloroglucinol core form monodisperse angular AgNPs over a range of sizes (12 ± 1 nm - 33 ± 7 nm), whereas resorcinol core triazole ligands exhibiting a higher Ag(I) binding affinity produce monodisperse spherical AgNPs of a single size (8 ± 5 nm). Chapter 3 describes the synthesis of AgNPs using sugar triazole ligands and Tollens' reagent using silver trifluoroacetate to investigate the counter-ion effect of silver salts on the size and the morphology of formed AgNPs. This salt produces AgNPs with similar shapes and sizes compared to that formed using silver nitrate. Chapter 4 describes the synthesis of PEG-functionalised sugar triazoles bearing PEG groups to investigate their effects on the formation of AgNPs. This work identifies the southernmost triazole as a modular site to tune the size and shape of AgNPs. Installation of PEG chains into the southernmost triazole ring shows a significant reduction in the Ag(I) binding affinity and produces monodisperse angular AgNPs

with diameters ranging from 15 ± 4 nm to 38 ± 7 nm. The surface enhanced Raman scattering properties of formed AgNPs are also discussed. Chapter 5 describes the synthesis of sugar-modified peptides to template the synthesis of AgNPs using Tollens' reagent. Increasing the sugar units using octamer peptide produces angular and smaller AgNPs (10 ± 2 - 23 ± 2) compared to that formed using pentamir peptide (16 ± 2 - 32 ± 4).

In conclusion, this thesis reports a novel template-directed triazole ligand strategy for the one-step synthesis of AgNPs in a size- and shape-controlled fashion. The mild synthetic methodology outlined in this thesis opens up new opportunities for the development of optical biosensing and imaging applications.

PUBLICATION

"Defining the Structural Parameters of Triazole Ligands in the Templated Synthesis of Silver Nanoparticles" **Kashmery, H. A**.; Clark, A. W.; Dondi, R.; Fallows, A. J.; Cullis, P. M.; Burley, G. A., *European Journal of Inorganic Chemistry* **2014,** *2014* (28), 4886-4895.

"SERS Enhancement of Silver Nanoparticles Prepared by a Template-Directed Triazole Ligand Strategy" **Kashmery, H. A**.; Thompson, D. G.; Dondi, R.; Mabbott, S.; Graham, D.; Clark, A. W. and Burley, G. A., *Chemical Communications* **2015,** (51), 13028-13031.

CONFERENCE PRESENTATIONS

"How can we make biocompatible silver nanoparticles with high size and shape control?" **Kashmery, H. A**.; Dondi, R.; Burley, G. A., University Research Day, University of Strathclyde, 2012 (Poster presentation).

"How can we make biocompatible silver nanoparticles with high size and shape control?" **Kashmery, H. A**.; Dondi, R.; Burley, G. A., 6th Saudi Scientific International Conference, London, UK, 2012 (Poster presentation).

"How can we make biocompatible silver nanoparticles with high size and shape control?" **Kashmery, H. A**.; Dondi, R.; Burley, G. A., 41st Scottish Regional Meeting of the RSC Organic Division, The University of St Andrews, 2012 (Poster presentation).

“Defining the Structural Parameters of Triazole Ligands in the Templated Synthesis of Silver Nanoparticles” **Kashmery, H. A**.; Clark, A. W.; Dondi, R.; Fallows, A. J.; Cullis, P. M.; Burley, G. A., 7th Saudi Scientific International Conference, Edinburgh, UK, 2014 (Oral presentation).

ABBREVIATIONS

µCP	Microcontact printing
µL	Microlitre
µM	Micromolar
AgNPs	Silver nanoparticles
AgNP@(**29**)	Silver nanoparticles prepared with compound (**29**)
AuNP	Gold nanoparticle
SCN	thiocyanate
BARAC	Biarylazacyclooctynone
BCN	Bicyclononyne
Bn	Benzyl
Boc	*tert*-butoxycarbonyl
Cbz	Carboxybenzyl
cm	Centimetre
Cq	Quaternary carbon
CuAAC	Copper(I)-catalysed alkyne-azide cycloaddition
ISE	Ion selective electrode
DBCO	Dibenzocyclooctyne
DCU	N,N'-dicyclohexylurea
DCC	N,N'-dicyclohexylcarbodiimide
DCM	Dichloromethane
DEG	Diethylene glycol
DIBAC	Aza-dibenzocyclooctyne

DIBO	Dibenzocyclooctynol
DIEA	Diisopropylethylamine
DIFO	Difluorinated cyclooctyne
DMAP	4-Dimethylaminopyridine
DIMAC	Di-methoxy-aza-cyclooctyne
DMF	Dimethylformamide
DMSO	Dimethyl sulfoxide
DNA	Deoxyribonucleic acid
dsDNA	Double-stranded DNA
EBL	Electron beam lithography
ε	Extinction coefficient
EDC	1-Ethyl-3-(3-dimethylaminopropyl)carbodiimide
EG	Ethylene glycol
EI	Electron impact
equiv.	Equivalents
ESI-MS	Electrospray Ionisation Mass Spectrometry
Fmoc	9-Fluorenylmethoxycarbonyl
FT-IR (ATR)	Fourier Transform Infrared Spectrometer (Attenuated Total Reflectance)
GC-MS	Gas Chromatography-Mass Spectrometry
GNP-Ag-Ab	Gold nanoparticle-antigen-antibody
GTP	Guanosine triphosphate
HBTU	O-(benzotriazole-1-yl)-1,1,3,3-tetramethyluronium hexafluorophosphate

HMBC	Heteronuclear Multiple-Bond Correlation
HOAt	1-Hydroxy-7-azabenzotriazole
HRMS	High-Resolution Mass Spectrometry
HSQC	Heteronuclear Single Quantum Coherence
Im	Imidazole
I-SPAAC	Interfacial strain-promoted alkyne azide cycloaddition
LRMS	Low Resolution Mass Spectrometry
LSPs	Localised surface plasmons
mg	Milligram
MGITC	Malachite green isothiocyanate
MGO	Malachite green oxalate
MHz	Megahertz
mL	Millilitre
mM	Millimolar
Mp	Melting point
NHS	N-hydroxysuccinimide
nm	Nanometre
nM	Nanomolar
NMR	Nuclear Magnetic Resonance
NOESY	Nuclear Overhauser Effect Spectroscopy
NPs	Nanoparticles
OCT	Octyne
ODN	Oligodeoxyribonucleotide
OTf^-	Trifluoromethanesulfonate

PCR	Polymerase chain reaction
PEG	Polyethylene glycol
PF_6^-	Hexafluorophosphate
Pfp-TFA	Pentafluorophenyl trifluoroacetate
PMMA	Poly methyl methacrylate
PSPs	Propagating surface plasmons
PVP	Poly(vinyl pyrrolidinone)
Py	Pyrrole
QD	Quantum dot
R6G	Rhodamine 6G
RNA	Ribonucleic acid
ROESY	Rotating-Frame Overhauser Effect Spectroscopy
ROS	Reactive oxygen species
RP-HPLC	Reverse-Phase High Performance Liquid Chromatography
RT	Room temperature
SEM	Scanning Electron Microscopy
SERS	Surface Enhanced Raman Scattering
ssDNA	Single-stranded DNA
SPAAC	Strain-promoted alkyne azide cycloaddition
SPPS	Solid phase peptide synthesis
SPR	Surface plasmon resonance
Sulfo-NHS	N-hydroxysulfosuccinimide

Sulfo-SMCC	Sulfosuccinimidyl-4-[N-maleimidomethyl]cyclohexane-1-carboxylate
TBTA	Tris-(benzyltriazolylmethyl)amine
TEM	Transmission Electron Microscopy
TES	Triethylsilane
TFA	Trifluoroacetic acid
THF	Tetrahydrofuran
Tm	Melting temperature
TOF	Time of flight
TP	Thiophenol
tpa	Tripyridylamine
TPW	TFA:phenol:water
UV-vis	Ultraviolet-visible

TABLE OF CONTENTS

LIST OF TABLES

LIST OF FIGURES

LIST OF SCHEMES

CHAPTER 1: INTRODUCTION

1.1 What is nanoscience and nanotechnology?

Nanoscience intends to exploit physical phenomena only available at scales 1 to 100 nanometres. The field of nanotechnology is defined as the way in which nanomaterials can be designed, characterised and controlled to provide several important uses.[1] For example, the small size and large surface-to-volume ratio of metal nanoparticles make them highly sensitive and selective nanoprobes to detect and image biomolecules including proteins, DNA and tumour cells.[2-4] Figure 1-1 shows general examples of functionalised gold nanoparticles and their biomedical applications.

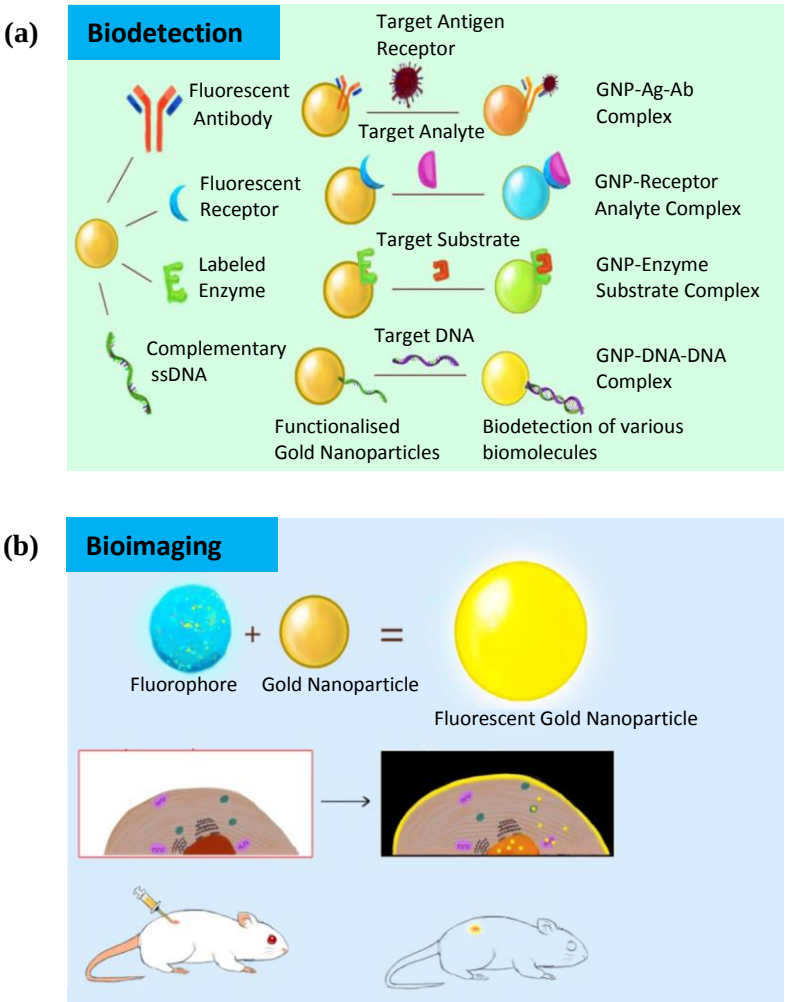

Figure 1-1: *Examples of functionalised gold nanoparticles for* ***(a)*** *biodetection and* ***(b)*** *bioimaging applications. Figure adapted with permission from Reference 3.*

A good illustration of advance in nanotechnology is the use of DNA to create nanoscale self-assembled structures programmed by the Watson-Crick base pairing of DNA (see Section 1.3.3).[5-8] The sequence selectivity imparted by Watson-Crick enables the formation of discrete 2D and 3D nanostructures in a highly programmable fashion.[9-15] These artificial structures can template other species such as proteins and metal nanoparticles (Figure 1-2).[16-18]

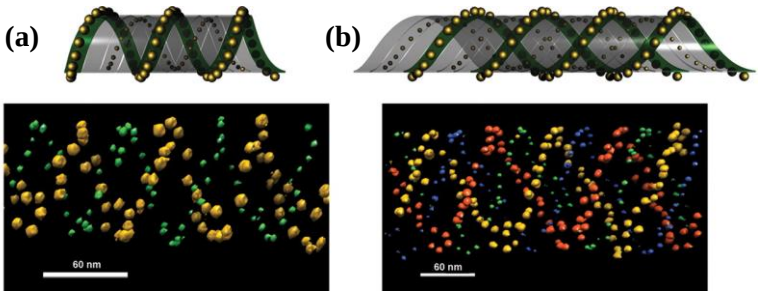

Figure 1-2: *Schematic representation of DNA self-assembly for the formation of 3D structures of gold nanoparticle tubes.* ***(a)*** *Single-spiral tubes and* ***(b)*** *double-spiral tubes formed with 5 and 10 nm AuNPs. Figure reproduced with permission from Reference 18. Copyright (2009) American Association for the Advancement of Science.*

1.2 Optical properties of metal nanoparticles

Metal nanoparticles (NPs) are of great interest due to their unique physical and chemical properties that are different from bulk materials.[19] For example, silver and gold NPs can strongly absorb and scatter light at specific wavelengths known as the surface plasmon resonance (SPR). This absorption occurs as a result of the movement of the electrons when a beam of light is incident on the surface molecules.[20] In contrast to bulk materials, the electronic motion in metal NPs is confined within a small length scale, which results in enhanced and tunable optical properties. This means that an increase in the particle size results in a shifting of the absorbance to a longer wavelength as seen in Figure 1-3.[21]

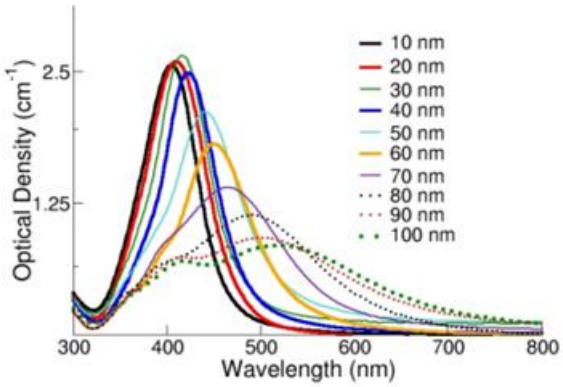

Figure 1-3: *Extinction (scattering + absorption) spectra of silver nanoparticles with diameters ranging from 10-100 nm at mass concentrations of 0.02 mg/mL. Figure reproduced with permission from Reference 21.*

The SPR characteristics of Ag and AuNPs occur by the interaction of light in two different modes and are contingent on the size of nanoparticles.[22-24] The first type is localised surface plasmons (LSPs) which are supported by spherical nanostructures.[25] The free electrons on the metal surfaces can oscillate when excited by incident light which has a wavelength longer than the NPs. In contrast, if the NPs have one-dimensional structures larger than the wavelength of the light, the free electrons will be excited and propagated along the metal surfaces to generate propagating surface plasmons (PSPs).[26] Figure 1-4 illustrates these two types of surface plasmons in silver nanoparticles.

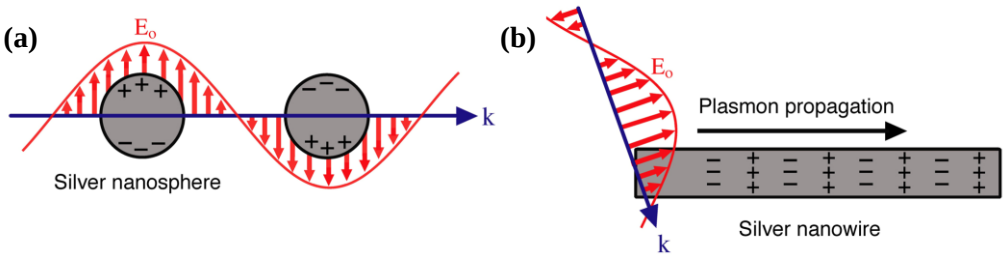

Figure 1-4: *Schematic illustration of the two types of plasmonic nanostructures.* ***(a)*** *Localised surface plasmons.* ***(b)*** *Propagating surface plasmon. (E_o) is the electric field of the incident light and (K) is a wave vector. Figure reproduced with permission from Reference 24. Copyright (2011) American Chemical Society.*

The optical properties of metal NPs are influenced not only by their size but also by their shape.[27-30] Figure 1-5 shows a variety of silver nanostructures with their absorption peaks.

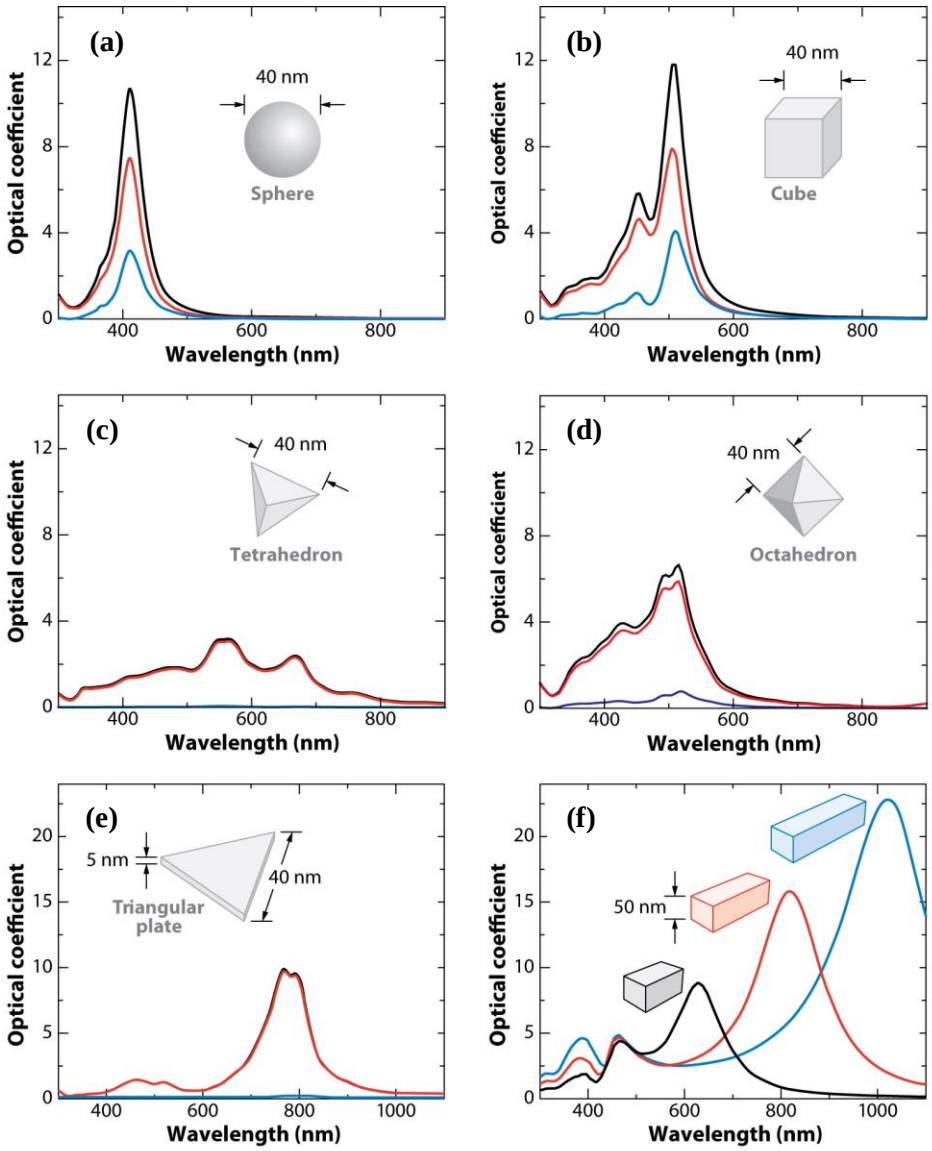

Figure 1-5: *Extinction (black), absorption (red), and scattering (blue) spectra calculated for Ag nanoparticles of different shapes:* ***(a)*** *a sphere displaying a single dipole resonance peak and* ***(b)*** *a cube;* ***(c)*** *a tetrahedron;* ***(d)*** *an octahedron and* ***(e)*** *a triangular plate.* ***(f)*** *Extinction spectra of rectangular bars with aspect ratios of 2 (black), 3 (red), and 4 (blue). Figure reproduced from Reference 30. Copyright (2009) Annual Reviews.*

1.3 Synthesis of metal nanoparticles

The development of rapid and ecofriendly processes for the synthesis of metal NPs is of great importance in the field of nanotechnology due to their optical properties. By virtue of their strong surface plasmon resonance that can extend throughout the visible and near infra-red regions, AgNPs are superior plasmonic candidates compared to other noble metal NPs such as gold and copper.[31,32] The spectroscopic and physical properties of AgNPs can vary significantly by the preparative methods used for their synthesis as a consequence of their optical properties being strongly affected by their size and the shape.[33] Conventionally, there are two fundamental routes for the preparation of AgNPs. The first is a physical based method such as photo- and electron beam-reductions.[34,35] The second approach is wet chemical based methods that depend on the chemical reduction of silver salt solutions using reducing agents.[36-38]

1.3.1 Preparation of AgNPs or nanostructures using physical methods

Lithographic fabrication such as electron beam lithography (EBL) is a common example of a physical method which uses an electron beam to produce metal nanoparticles on a substrate according to a determined pattern (Figure 1-6).[24,39] The substrate is covered with a polymer resist such as poly methyl methacrylate (PMMA), which is broken down after exposure to an electron beam. After removing the exposed regions of the resist with solvents, silver can be deposited by physical vapour deposition and the remaining resist is lifted off resulting in an array of silver nanostructures based on the desired pattern with a resolution of 20 nm.[40] The significant feature of EBL is the ability to produce nanostructures in different shapes.

However, a major limitation of this approach comes from the cost because it uses expensive instruments and consumes a significant amount of energy.[24]

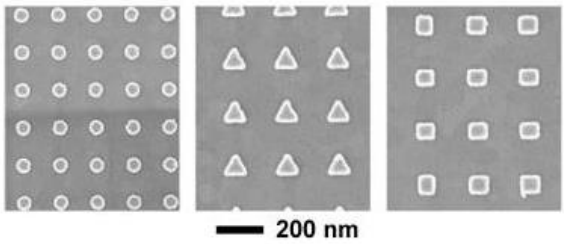

Figure 1-6: *General patterns used in electron beam lithography. Figure reproduced with permission from Reference 24. Copyright (2011) American Chemical Society.*

1.3.2 Preparation of AgNPs using wet methods

The most common method for the synthesis of AgNPs using wet chemistry methods is the reduction of silver salts (e.g., $AgNO_3$) using sodium borohydride or sodium citrate.[41] The formation of AgNPs starts with the reduction step of Ag(I) using, for example, $NaBH_4$ to form small clusters of Ag^0 atoms (nucleation). These small clusters can grow to form larger particles around 2-3 nm in diameter, stabilised by the borohydride species. Then, the stability of AgNPs decreases due to the hydrolysis of borohydride anions resulting in further growth of AgNPs with radius around 5-8 nm. Stabilising agents such as poly(vinyl pyrrolidinone) (PVP) can be added in order to stabilise the formed AgNPs. These compounds do not influence the growth mechanism of silver nanoparticles, but modify the growth rate of AgNPs and provide a greater electrostatic repulsion between the particles (Figure 1-7).[42] Although $NaBH_4$ reduction of Ag(I) is rapid, larger AgNPs are difficult to form using strong reducing agents due to a fast nucleation leading to the formation of small particles.[38] For this purpose, additional reducing agents such as ascorbate need to be added to produce small AgNPs that act as nuclei to grow larger particles.[43]

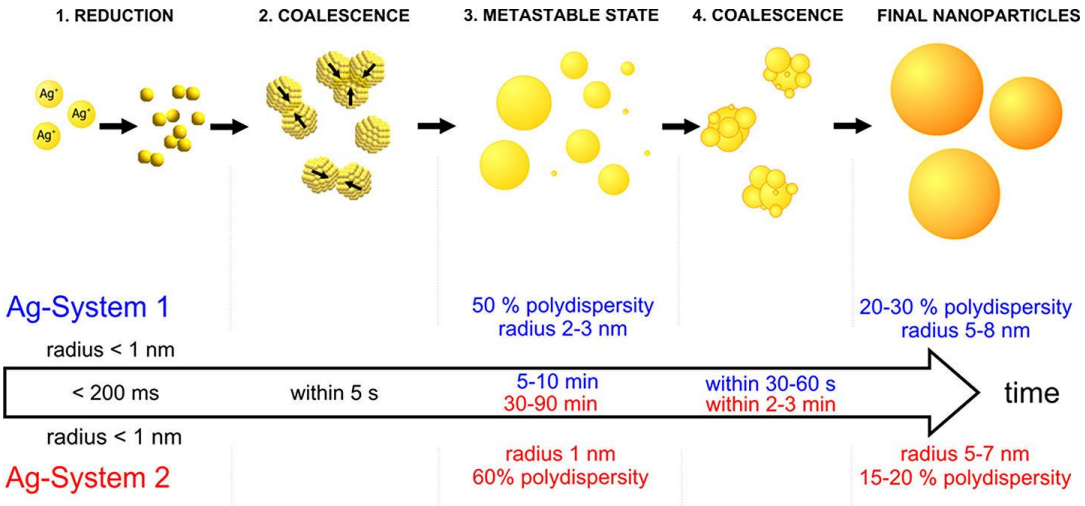

Figure 1-7: *Schematic illustration of the four-step growth mechanism deduced for AgNPs. System 1 is without a stabilising agent and System 2 is with stabilising agent. Figure reproduced with permission from Reference 42. Copyright (2012) American Chemical Society.*

In contrast, weaker reducing agents such as sodium citrate can produce larger nanoparticles with the size ranging from 20 to 600 nm.[24,44] A typical citrate reduction method involves the addition of sodium citrate to silver salts (e.g., $AgNO_3$) at temperature around 100°C.[45] One advantage of this method is the ability of citrate ions to act both as a reducing and a capping agent.[37] In the initial reduction step, citrate ions can interact strongly with the formed silver seeds forming the [Ag_2^+-citrate] complex that undergoes a slower growth resulting in the formation of larger stabilised Ag clusters (Figure 1-8).[45]

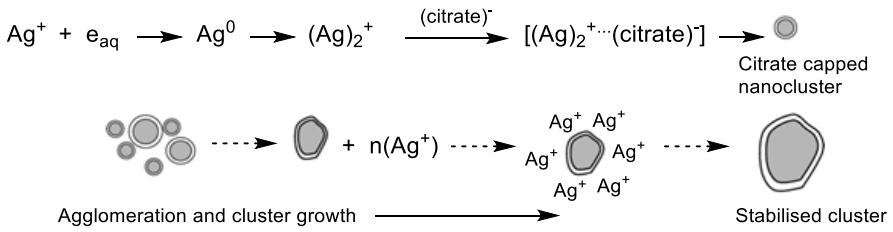

Figure 1-8: *Schematic illustration of the growth steps in the formation of AgNPs using citrate reduction method. Figure adapted with permission from Reference 45. Copyright (2004) American Chemical Society.*

A major limitation of these methods comes from the difficulty in controlling their size and shape, resulting in batch to batch variations.[24] For example, citrate reduction produces polydispersed AgNPs of various shapes such as plates and polyhedrons with a wide range of sizes (20-600 nm) in one reaction. Based on the citrate approach, a number of studies have been reported to control the shape of AgNPs. For example, Murphy *et al.*, developed a synthetic method to prepare silver nanowires using citrate reductant in the presence of NaOH.[46] The concentration of NaOH was the key parameter in this synthesis. The addition of small amounts of NaOH resulted in an increase in the pH from 5.5 to 6.5, which resulted in a decrease in the interaction of citrate to Ag seeds allowing the growth of Ag clusters into nanowire shapes. However, larger amounts of NaOH produced polydispersed AgNPs of irregular shapes.

The Yang group investigated a new method for the synthesis of AgNPs and illustrated the influence of tuning the pH of the solution from 5.7 to 11.1 on their morphology.[47] AgNPs formed at low pH exhibited triangular or polygonal shapes and proceeded with a slower nucleation and growth rate than those formed at high pH. Increasing the pH to 11.1 promoted the rate of Ag(I) reduction and produced polydispersed spherical and rod-like AgNPs.

1.3.2.1 Polyol process for the synthesis of AgNPs

Another common method for the preparation of AgNPs is the polyol process, which uses the polyol reagents such as ethylene glycol (**1**) both as a solvent and a reducing agent.[48,49] The key component for the reduction is the formation of glycolaldehyde (**2**) by heating ethylene glycol (**1**) in the presence of a silver salt such as $AgNO_3$ (Equation 1 and Equation 2).[50]

$$\underset{(\mathbf{1})}{2HOCH_2CH_2OH} + O_2 \longrightarrow \underset{(\mathbf{2})}{2HOCH_2CHO} + 2H_2O \qquad \text{Equation (1)}$$

$$2Ag^+ + (\mathbf{2}) \longrightarrow HCOOCH + 2Ag + 2H^+ \qquad \text{Equation (2)}$$

Polyol synthesis can form different structures of AgNPs ranging from cubes[51,52] and pentagonal wires[53] to right bipyramids[54] (Figure 1-9). The development of this approach provided a better understanding of the nucleation and growth mechanisms. The first process involves the reduction step to form a small cluster of fluctuating structure. Secondly, as the silver clusters grow, they become larger to form seeds which are usually produced in one of the common structures, multiply twinned, singly twinned or single crystalline that grow into different structures. Twinned particles are defined as a collection of symmetric single crystal subunits that share their boundary in a symmetrical manner.[48,49]

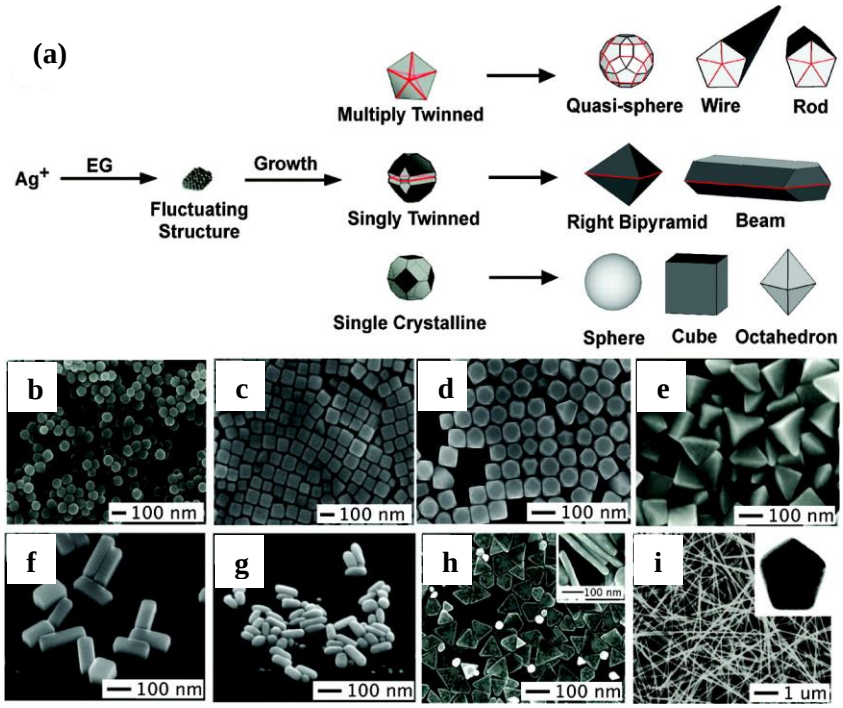

Figure 1-9: *Polyol method for synthesising Ag nanostructures.* ***(a)*** *Schematic illustration of the nucleation and growth mechanism for the formation of different structures:* ***(b)*** *spheres;* ***(c)*** *cubes;* ***(d)*** *truncated cubes;* ***(e)*** *right bipyramids;* ***(f)*** *bars;* ***(g)*** *spheroids;* ***(h)*** *triangular plates and* ***(i)*** *wires. Figure adapted with permission from Reference 24. Copyright (2011) American Chemical Society.*

The main advantage of the polyol synthesis over other wet chemical methods is the ability to control the formation of crystal seeds and to direct the growth of AgNPs to produce a specific shape by a process called oxidative etching.[55] This means that certain seeds can be removed during the growth phase of AgNPs by introducing trace ions such as chlorides in the presence of O_2. Chloride anions are strong ligands for etching and are able to dissolve singly and multiply twinned seeds to form cube structures.[51] Conversely, right bipyramids can be produced by weaker etchant ions such as bromides.[54] Finally, the addition of relatively high concentration of Fe(II) or Fe(III) ions (2.2 μM) decreases the oxidative etchant level leading to the formation of wire structures.[56] Decreasing the concentration of iron species (< 0.44 μM) produces nanocubes.

Other variations of the polyol method have been developed to control the Ag(I) reduction rate. For example, introducing sulfide ions into the synthesis can accelerate the formation of Ag nanocubes.[52] Other structures such as Ag nanoplates can be formed by the addition of polyacrylamide instead of PVP.[57] Polyacrylamide can coordinate to Ag ions through its amino group, slowing the reduction rate during the synthesis, and allowing the formation of thin nanoplate structures. Although a variety of methods exists for the preparation of AgNPs, very few of these can control both the size and shape of AgNPs under mild reductive conditions and at room temperature.[58,59] Table 1-1 summarises the key aspects of traditional methods for the preparation of AgNPs.

Table 1-1: *Summary of the preparative methods used to form AgNPs.*

Preparative Method	Advantages	Limitations
Lithographic methods.[24, 39, 40]	Formation of high monodisperse particles.	Need expensive instruments and produce low fluorescence particles, which limit their uses in biosensing.
Sodium borohydride reduction.[38]	Highly reactive reagent.	Difficult to form large nanoparticles.
Citrate reduction.[24, 37, 44]	Quick and easy method. Citrate ions can be used as both a reducing and a capping agent.	Difficult to form small nanoparticles. Produces polydisperse nanoparticles with a variety of shapes such as plates and polyhedrons in different sizes (20 - 600 nm) in one reaction.
Polyol Process.[24, 48, 49]	High degree of shape-controlled synthesis.	Require high temperature.

1.3.2.2 Preparation of silver nanoparticles using Tollens' reagent

Tollens' reaction has become a common method for silver deposition on a substrate such as glass since the invention of silver mirror in 1835.[60] Since its original development, this reaction has been under-utilised in the literature to prepare AgNPs.[59,61-67] One of the main advantages of this method is that the synthesis of

AgNPs proceeds at room temperature in the presence of aldehyde groups (**3**) as the corresponding reducing agent using Tollens' reagent $[Ag(NH_3)_2]OH$ (**4**, Equation 3).

$$\underset{(\mathbf{3})}{RCHO} + \underset{(\mathbf{4})}{2[Ag(NH_3)_2]OH} \longrightarrow RCOOH + 2Ag + 4NH_3 + H_2O \qquad \text{Equation (3)}$$

The open chain form of sugars such as glucose is a cheap and readily accessible aldehyde source. The open chain form of glucose exists in equilibrium with its cyclic hemiacetal, which is formed when the hydroxyl group of C_5, chiral centre, attacks the anomeric carbon atom (C_1) (Figure 1-10).[68] The importance of sugars in the formation of AgNPs refers to the presence of the aldehyde functional groups in the open chain form to reduce silver ions using Tollens' reagent.

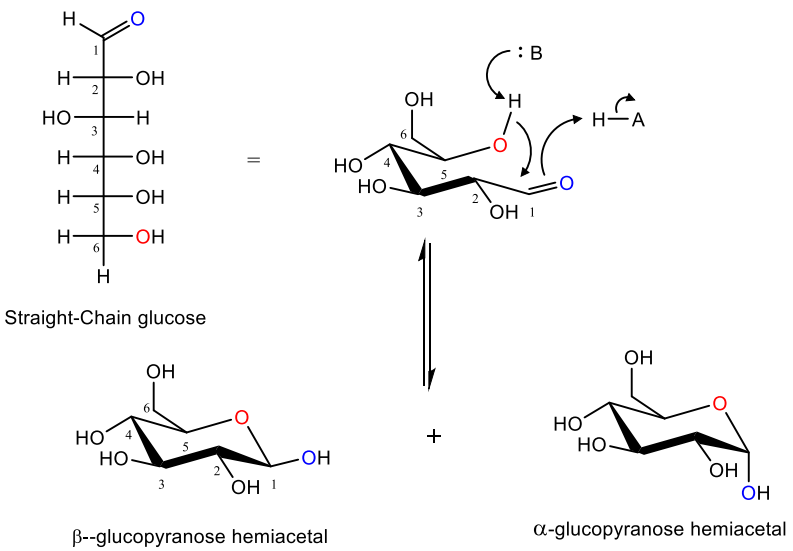

Figure 1-10: *Structures of open chain form and cyclic hemiacetal forms of glucose.*

According to Equation (3), AgNPs are formed by the chemical reduction of silver ion existing as $[Ag(NH_3)_2]^+$ cation. This complex is the main component of Tollens' reagent formed by the addition of ammonia to silver nitrate solution using sodium hydroxide. The synthesis of AgNPs proceeds under basic conditions [i.e., pH > 10].[69] Decreasing the pH value to 6 leads to aggregation of AgNPs.[62] In this method, both

the complex cation agents and the sugar reductants have a significant influence on the size of AgNPs formed. Kvitek *et al*. showed that a decrease in the concentration of ammonia from 0.2 to 0.005 M with pH 12.5 resulted in the formation of AgNPs from 380 to 45 nm.[66] Stronger reducing agents such as glucose produced smaller nanoparticles ~ 60 nm in diameter. The authors also proposed a correlation between the molecular structure of the reducing sugars used in Tollens'-mediated formation of AgNPs. Disaccharides (e.g., maltose), for example, produced smaller AgNPs around 45 nm with a narrower size distribution relative to monosaccharides (e.g., glucose). The justification given by the authors for this observation was that disaccharides had an increased number of reducing equivalents relative to monosaccharides.[66] Table 1-2 illustrates the differences in redox potential of common examples of saccharides.

Table 1-2: *Reduction potential of mono- and di-saccharides. The values are recorded at 98 °C using 1M of reducing agent and 2M NaOH.*[70]

Reducing Agent	**Redox Potential (-mV)**
D-arabinose	575
D(+)-galactose	569
α-D-glucose	552
β-D-lactose	549
D(-)fructose	521
D-maltose	451

1.3.3 DNA as a template to synthesise nanoparticles

The extraordinary features of DNA, especially the arrangement of its sequences in a well organised structure, render its potential as an excellent material in nanotechnology.[15-17, 71] The crucial consideration in this field is to study the capacity

of DNA to self-assemble in defined arrays and template other materials such as proteins and metal nanoparticles, rather than its ability to be hereditary material.

DNA is a double-helical structure; it consists of two anti-parallel long polymers of nucleotides that are formed by a phosphodiester linkage (Figure 1-11). Each nucleotide consists of a deoxyribose sugar, phosphate, and one of four nucleobases, which are adenine, guanine, cytosine and thymine.[72]

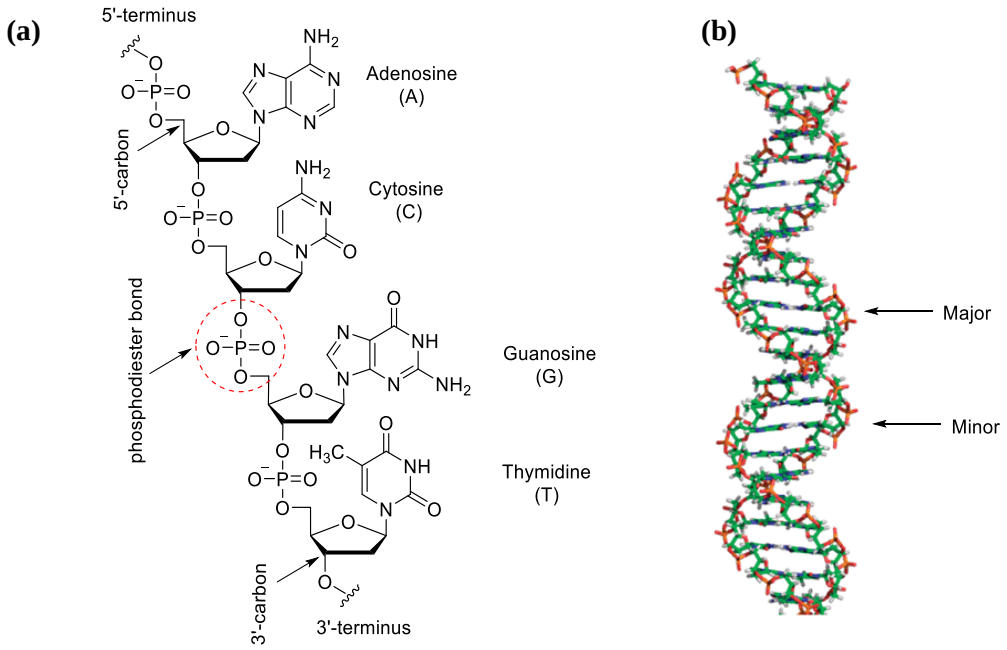

Figure 1-11: *Structures of DNA.* ***(a)*** *Chain of four nucleotides with the sequence 5′-ACGT-3′.* ***(b)*** *Right-handed B-DNA structure. Figure adapted from Reference 71 with permission from the Royal Society of Chemistry.*

The stability of the double helical structure of DNA is based on a natural intermolecular self-assembly of base pairing where each nucleobase on one strand interacts with a specific one on the other strand through hydrogen bonds.[68] This concept is called complementary Watson and Crick base pairing (Figure 1-12).

DNA is an excellent architecture for nano-assembly for the following reasons: (i) DNA can be manipulated by using commercial enzymes which are able to

perform several functions on DNA sequences such as amplification, ligation and cleavage at definite sites;[71] (ii) one can control its length by means of automated preparative methods such as solid phase synthesis and the polymerase chain reaction (PCR)[73] and (iii) the formation of the double helix is reversible, which provides thermodynamic control of the formation of higher order structures.[68]

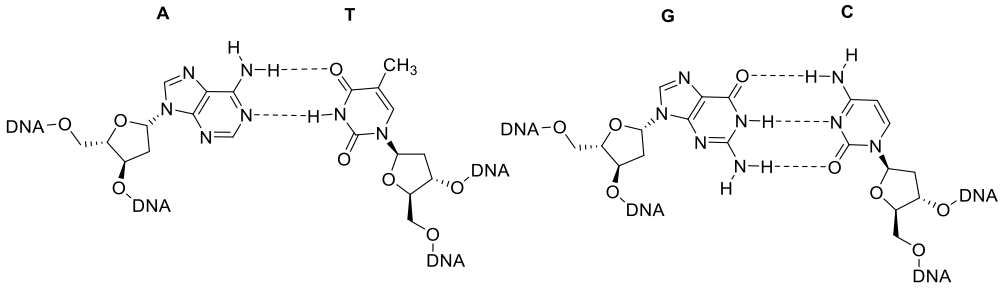

Figure 1-12*: Watson-Crick base pairs that are present in B-DNA.*

Considerable progress has been made in DNA research since the discovery of the Watson-Crick model. The formation of complex motifs is a natural consequence of the principle of complementary base pairing. According to Seeman (1982),[5] DNA molecules have the ability to form two dimensional (2D) structures. This case shows the importance of the naturally-occurring Holliday junction which describes the way in which four single stranded DNA (ssDNA) can be linked to form stable structures. Figure 1-13 elucidates the building block of 2D arrays, which are called "tiles", with the concept of cohesive ends. This means that the end of each tile can anneal to a complementary tile.

Since the development of DNA nanotechnology by Seeman, the programmable self-assembly features of DNA have been exploited to template the preparation of metal NPs.[16,17] Yan *et al.* reported an example of AuNPs arrays assembled on 2D DNA nanogrids.[74] The lattice was designed by the self-assembly of two DNA tiles (Figure

1-14a), resulted in the formation of a periodic square structure functionalised with a short single stranded DNA (A_{15}) (Figure 1-14b). Such structure provided selective hybridisation sites to organise AuNPs functionalised with T_{15} strands (Figure 1-14c).

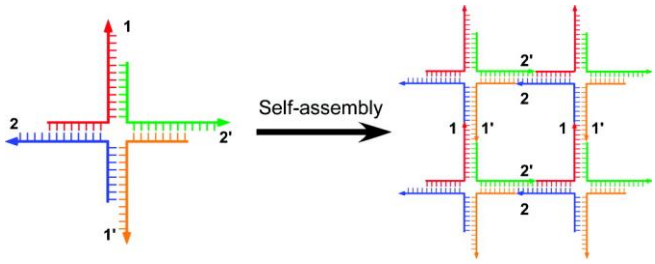

Figure 1-13: *Principle of DNA self-assembly, as proposed by N. Seeman. (1 is complementary to 1′ and 2 complementary to 2′). Figure adapted with permission from Reference 15. Copyright (2009) American Chemical Society.*

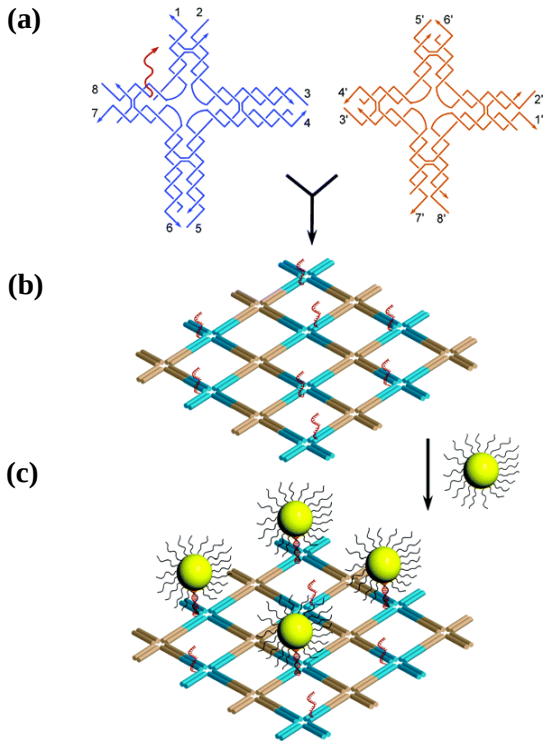

Figure 1-14: *Schematic representation of 2D square array of AuNP templated by DNA.* ***(a)*** *Two DNA tiles building block of 2D DNA nanogrids. The numbers indicate the complementary sticky ends. The red strand on tile A is the A_{15} sequence.* ***(b)*** *The 2D DNA nanogrids functionalised with the single strand A_{15}.* ***(c)*** *Assembly of 5-nm Au NPs on the DNA grids. The zigzag black lines surrounding the Au NPs represent the T_{15} strands. Figure reproduced with permission from Reference 74. Copyright (2006) American Chemical Society.*

DNA has the ability to control the formation of metal nanoparticles by a process called biomineralisation.[75] One of the key contributing factors for the use of DNA as a template for NP synthesis is the arrangement of the phosphate and amino groups that can interact with metals or metal ions in different ways to control nucleation, growth and passivation steps of NP synthesis (Figure 1-15).[75,76] These binding modes are attributed to the electrostatic attraction between the positive charge of metal cations and the electron-rich charge of the phosphate, carbonyl and amine groups on the DNA backbone. Another alternative type relies on the coordination interaction between the nucleobases or the phosphate oxygen and the transition metal cations. Table 1-3 illustrates these effective sites with different cations.

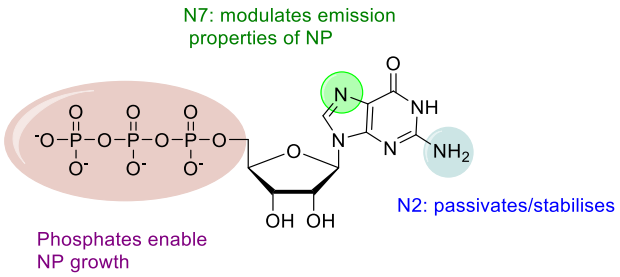

Figure 1-15: *Proposed roles of phosphate and base functionalities present on guanosine triphosphate (GTP) in nanoparticle nucleation, growth, termination, stabilisation and passivation. Figure adapted with permission from Reference 76. Copyright (2006) American Chemical Society.*

Table 1-3: *The most common binding sites of nucleic acids for representative examples of mono- and divalent metal ions. The ions are listed in increasing order of binding strength or in increasing order of affinity for the base. Table adapted by permission from Macmillan Publisher Ltd: Nature Nanotechnology from Reference 75. Copyright (2008).*

Binding Site	**Metal Ion**
Phosphate	Li^{+}, Na^{+}, K^{+}, Rb^{+}, Cs^{+}, Mg^{2+}, Ca^{2+}, Sr^{2+}, Ba^{2+}, trivalent lanthanides
Phosphate and base	Co^{2+}, Ni^{2+}, Fe^{2+}, Mn^{2+}, Zn^{2+}, Cd^{2+}, Pb^{2+}, Cu^{2+}
Base	Ag^{+}, Hg^{2+}, Pt^{2+}

In terms of the mechanism of NP formation, the growth of NPs such as AgNPs can occur in several steps (Figure 1-16).[75,76] The first process involves binding DNA ligands with metal cations to form a nanoparticle precursor. This initiation step is important to provide the required microenvironment for synthesis. Secondly, the small clusters formed from the previous stage are surrounded with a negative charged layer called capping molecules and start growth for forming larger clusters. This aggregation is usually balanced by a barrier that is produced by the capping of nucleic acids. After the barrier has reached an appropriate size, NPs are prevented from continuing to grow. Therefore, the major role of this step is to determine the termination point of the aggregation. A passivation step improves the physical and chemical properties of nanoparticle molecules by forming a protective layer of nucleic acid molecules on the surface of NPs. The final step is solubilisation to confirm the dispersion of nanoparticles in aqueous solution.

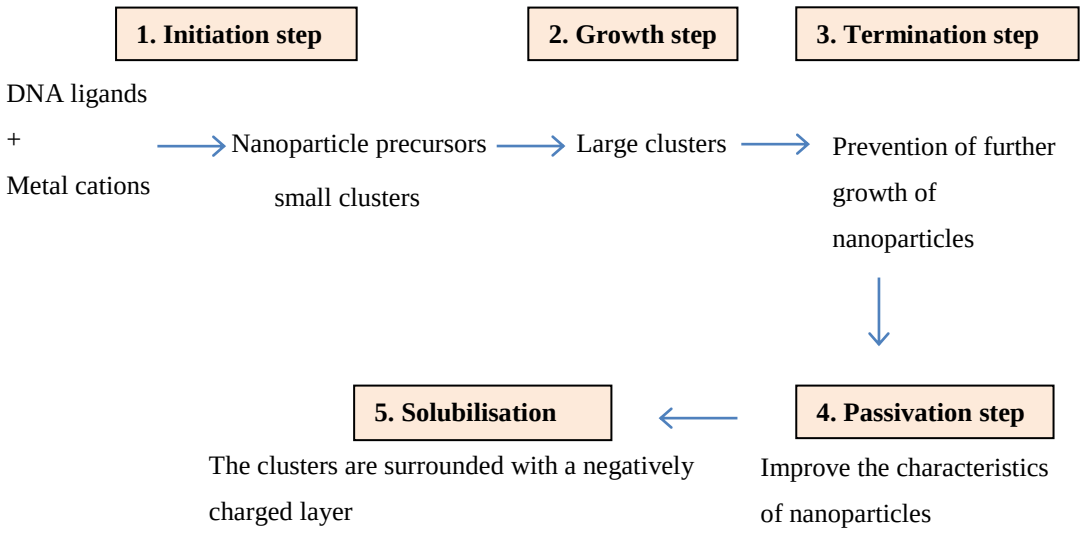

Figure 1-16: *Overview of the key steps in the formation of NP template by DNA.*

Developments to template the formation of metallic nanowires have focused on pre-complexation of metal cations, followed by chemical reduction using, for example, $NaBH_4$.[17] In 1998, Braun *et al.* conducted the first metallisation experiment to construct silver nanowires on DNA template.[77] Following this synthesis, efforts successfully generated several metal nanoparticles including, Pt,[78] Pd,[79] and Cu.[80] As an example, Richter *et al.*[79] applied these general procedures to accomplish the deposition of Pd metal along the DNA strand by $Pd(CH_3COO)_2$ to bind to duplex DNA followed by subsequent reduction with with dimethylaminoborane, lactic acid and sodium citrate. A further suggestion to develop this experiment was proposed by using other metal sources such as K_2PdCl_4 and K_2PtCl_4 instead of palladium acetate (Figure 1-17).[81]

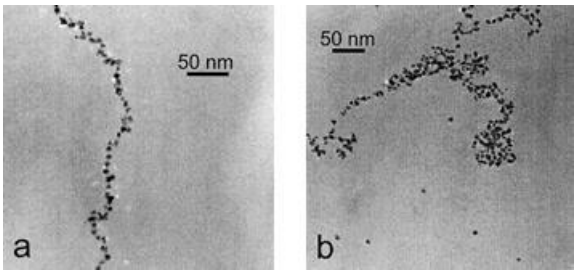

Figure 1-17: *TEM micrographs of chains of* ***(a)*** *Pt and* ***(b)*** *Pd clusters grown on λ-DNA. Figure reproduced with permission from Reference 81. Copyright (2004) American Chemical Society.*

1.3.3.1 Directed DNA metallisation via Click Chemistry

All the studies above depend on electrostatic and coordinative binding sites (Section 1.3.3) followed by a chemical reduction step. Although these procedures can produce molecular wires, they have some distinct disadvantages. A major limitation is that continuous metallisation lacks the selectivity required to direct the formation of metal nanoparticles to a precise location along the DNA strands.[82,83] Modifying DNA

allows one to incorporate functional groups at specific sites along DNA strands which can be post-synthetically functionalised.[84] A good illustration of these reactions is the application of "click chemistry" to address functional groups to specific sites along a DNA strand. These modifications can then direct the formation of metal nanostructures at defined sites. The incorporation of alkyne modifications into DNA either by chemical or enzymatic synthesis defines these sites. Click chemistry converts these alkynes into sugar triazoles which comprise a reducible aldehyde moiety in the open-chain form (Figure 1-18).[82] One advantage of this approach is the click chemistry reaction produces triazole products in high yield (Figure 1-19).[85,86]

Another example of the developments of a click reaction was reported by Carell's group to increase the alkyne density along a DNA strand (Figure 1-20a).[84] In this study, an alkyne-modified ODN series (Table 1-4) was prepared by way of solid phase synthesis. By comparing the results of click reactions using three different azides (**7**, **12-13**, Figure 1-20b), a flexible series (ODN-5 – ODN-8) produced higher yields of the triazole products than a rigid series (ODN-1 – ODN-4). For example, the reaction of azide (**7**) with ODNs containing (**10**) produced incomplete conversion to click products. In contrast, full conversion was achieved by using the flexible alkyne ODNs. This study also supported the view that it is possible to use this method to prepare long modified DNA strands (ODN-9 and ODN-10) by a PCR reaction without causing cleavage of the DNA strand.

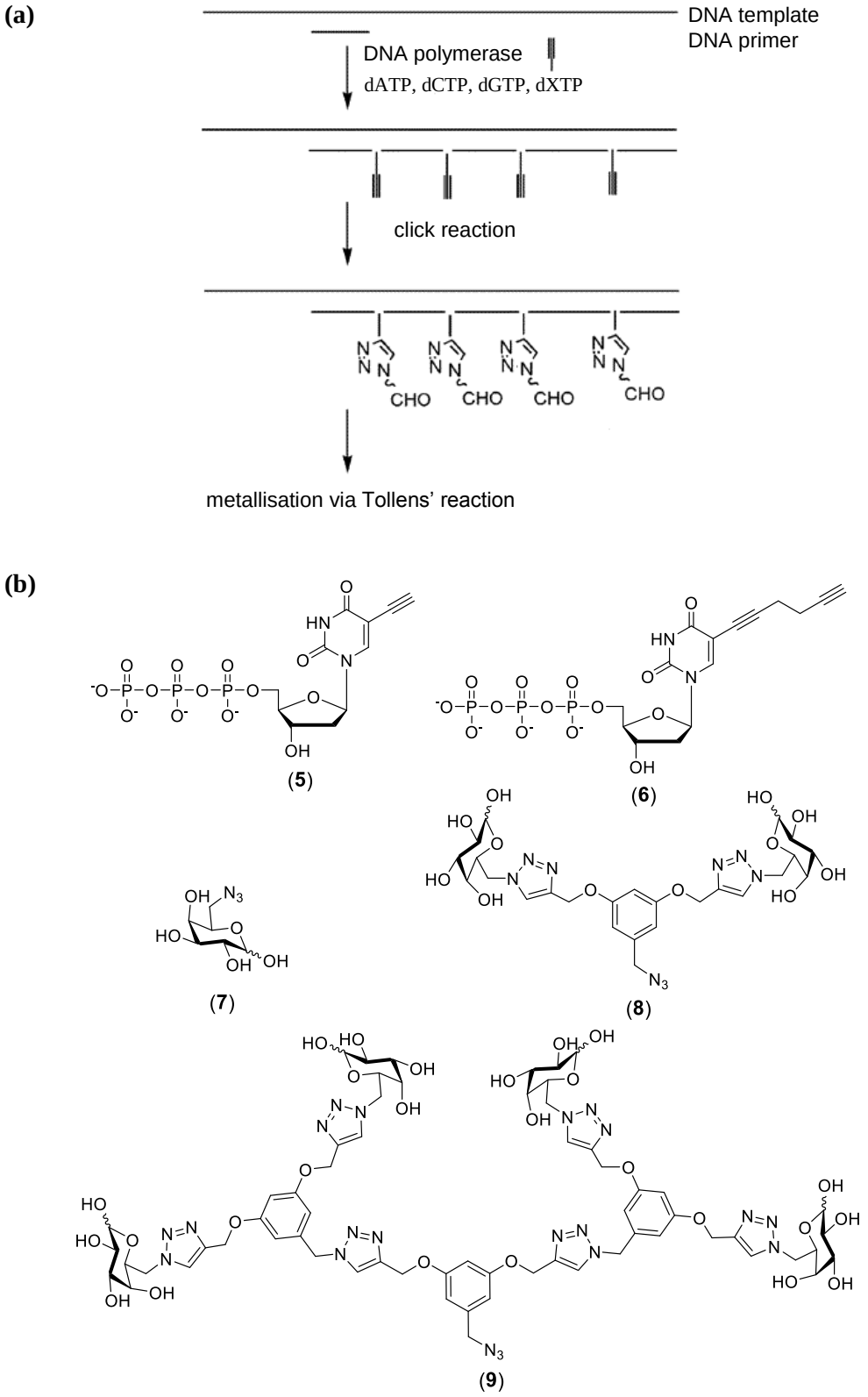

Figure 1-18: (a) *Schematic depiction of the selective metallisation process.* ***(b)*** *Structures of alkyne and azide molecules used for this study. Figure adapted with permission from Reference 82. Copyright (2006) American Chemical Society.*

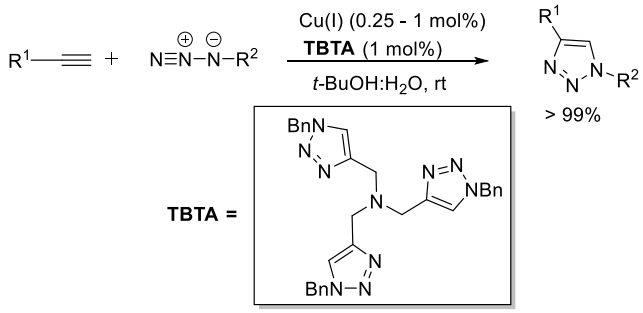

Figure 1-19: *Click Chemistry to synthesise 1,2,3-triazoles in the presence of TBTA.*

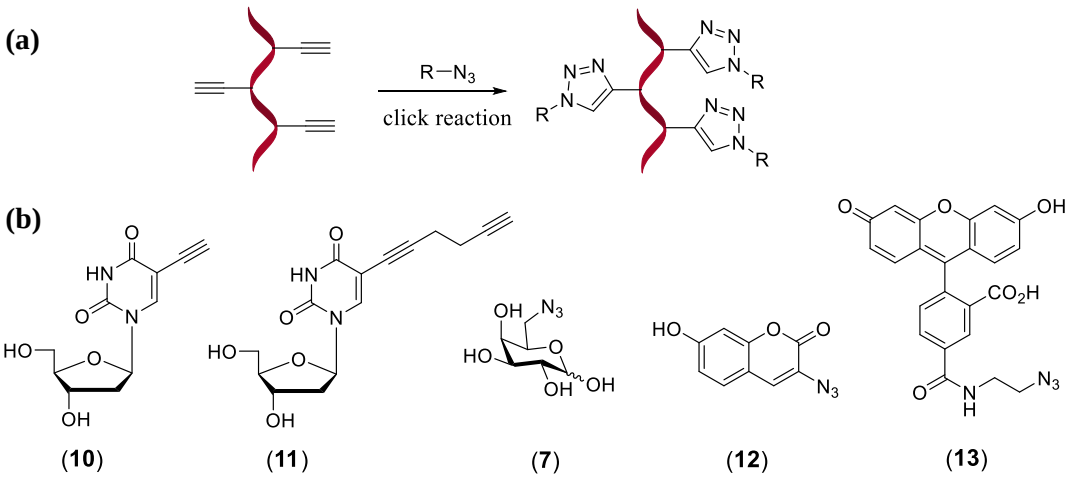

Figure 1-20: ***(a)*** *General scheme for the post-synthetic modification of DNA using a click reaction.* ***(b)*** *Structures of alkyne and azide molecules.*

Table 1-4: *Oligodeoxyribonucleotide (ODN) series comprising (**10**) or (**11**). Table adapted with permission from Reference 84. Copyright (2006) American Chemical Society.*

	X= (10)
ODN-1	5'- GCG CTG TXC ATT CGC G
ODN-2	5'- GCG CTG XXC ATT CGC G
ODN-3	5'- GCG CXG TXC AXT CGC G
ODN-4	5'- GCG CXX XXX XGT CGC G
	Y= (11)
ODN-5	5'- GCG CTG TYC ATT CGC G
ODN-6	5'- GCG CTG YYC ATT CGC G
ODN-7	5'- GCG CYG TYC AYT CGC G
ODN-8	5'- GCG CYY YYY YGT CGC G
ODN-9	5'-TTA ATT GAA TTC GAT TYG GGC CGG AYT TGT TTC
ODN-10	5'-GCA GGC YTCA YGC CAG AAT TAC CAG AAG

Simon and co-workers used a click reaction to form bimetallic nanowires along sugar-modified DNA duplex (**17**, Figure 1-21). Clicking DNA was employed by sugar azide (**7**) and alkyne-modified DNA strands (**14**).[83] Compared with their previous study, this research revealed the ability to use modified cytosine triphosphates as a source of alkyne groups instead of modified uridine triphosphates. In terms of metallisation, after the sliver had been deposited by Tollens' reagent, an enhancement gold solution was used.

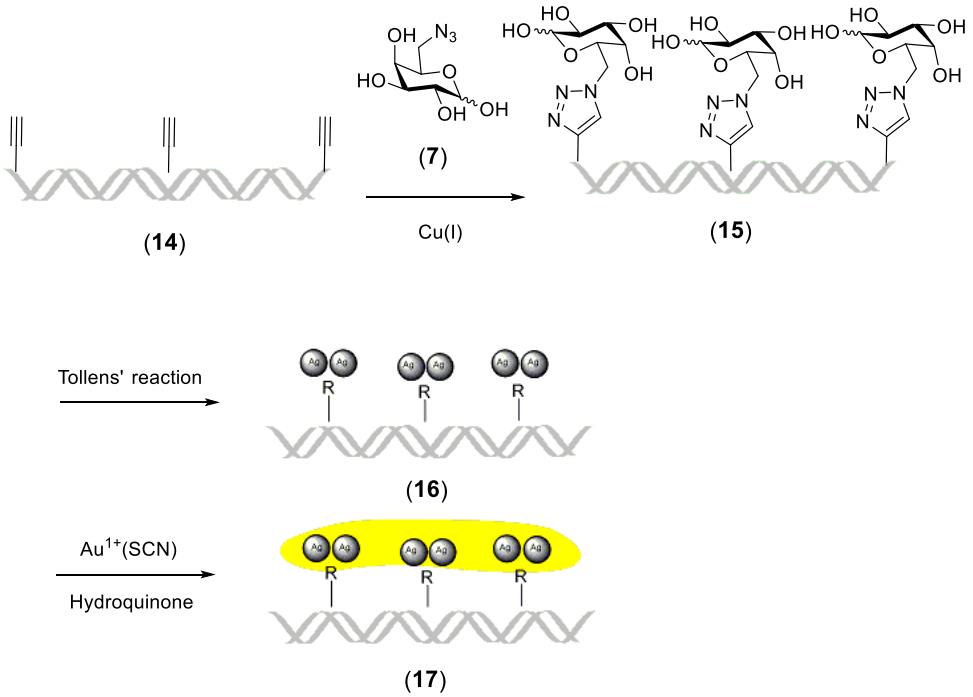

Figure 1-21: *General scheme for the metallisation procedure. Figure adapted with permission from Reference 83. Copyright (2007) John Wiley and Sons.*

1.3.4 Templated synthesis of silver nanoparticles using sugar triazoles

Despite the variety of methods that exist for the preparation of AgNPs using Tollens' reagent, an in-depth understanding of the mechanistic factors that control AgNP formation using Tollens' reagent is lacking. In order to address this shortfall, Burley *et al.* have recently developed a new templated reductive strategy using novel

triazole ligands to direct the synthesis of size- and shape-selected AgNPs using Tollens' reagent.[87] The underlying motivation for exploring this original design was based on a previous observation (Section 1.3.3.1) that ligand (**18**) was used to form Ag-nanostructures when covalently attached to DNA duplexes and exposed to Tollens' reagent.[82] This study reported the utility of the Ag(I)-binding ligand (**18**, Figure 1-22) to form monodisperse and stable suspensions of AgNPs with a diameter of 8 ± 5 nm. A central resorcinol scaffold in (**18**) was used to tether two galactose sugar units via a triazole linkage using click reaction.[88] A third triazole with different regiochemistry to the two resorcinol triazoles was installed in the southern part of (**18**) to complete a three-triazole ligand structure.

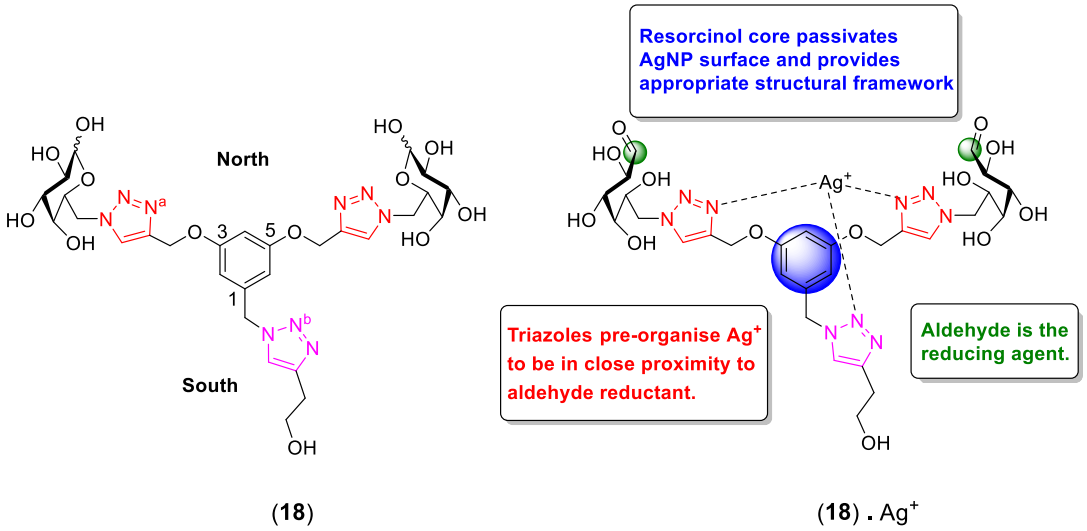

Figure 1-22: *Proposed binding model of the templated synthesis of AgNPs using ligand (**18**). Figure adapted with permission from Reference 87. Copyright (2012) John Wiley and Sons.*

The mechanistic rationale for the formation of monodispersed AgNP@(**18**) involved initial co-ordination of Ag(I) to the 3-position (N^a) of both the resorcinol triazole nitrogens (red in Figure 1-22) and the 2-position (N^b) of the southern-most triazole nitrogen (pink in Figure 1-22). Burley *et al.* surmised that the chelating effect of (**18**)

positioned Ag(I) atoms in close proximity to the aldehyde groups of the galactose sugars.[87] Once in position, these sugars facilitated the reduction of Ag(I) to putatively form nanoclusters of Ag nuclei[89] that can then form size-selected AgNPs by an exponential growth phase followed by termination and ligand capping.[67, 90]

Burley *et al.* studied the influence of increasing the number of reducing sugars on the size of produced nanoparticles.[87] In contrast to Kvitek *et al.* (Section 1.3.2.2), where an increase in the number of reducing equivalents of disaccharides produced smaller particles,[66] Burley *et al.* showed that increasing the number of sugar equivalents [i.e., (**19**)] did not result in the formation of smaller AgNPs.[87] However, this larger ligand can enhance the stability of AgNP in aqueous solutions containing high salt of NaCl up to 2.8 M.[87]

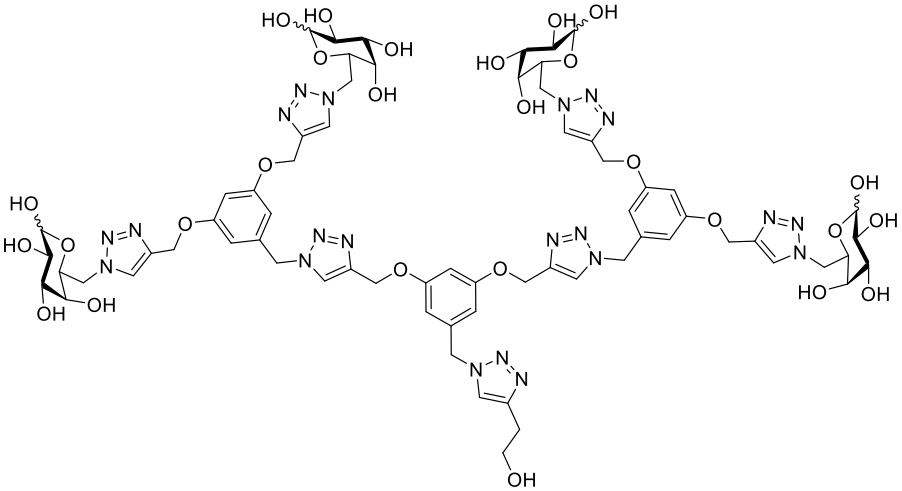

(**19**)

Figure 1-23: *Structure of sugar triazole ligand (**19**).*

1.4 Challenges in development of metal nanoparticles and their diagnostic applications

In contrast to a majority of micro- and macroparticles, metal NPs such as gold and silver have become key components of recent diagnostic and biophotonic devices due to their unique properties (see Section 1-2).[2-4] In 1996, Mirkin and co-workers introduced the concept of metal nanoparticle-based DNA detection and illustrated how the optical properties of these nanoparticles can be exploited for the detection of DNA.[91] In this work, two solutions of AuNPs functionalised with non complementary thiol-modified DNA that can bind to the complementary target DNA. (**20**, Figure 1-24). This hybridisation results in a red shift of surface plasmon absorption of AuNPs and consequently aggragation.[92]

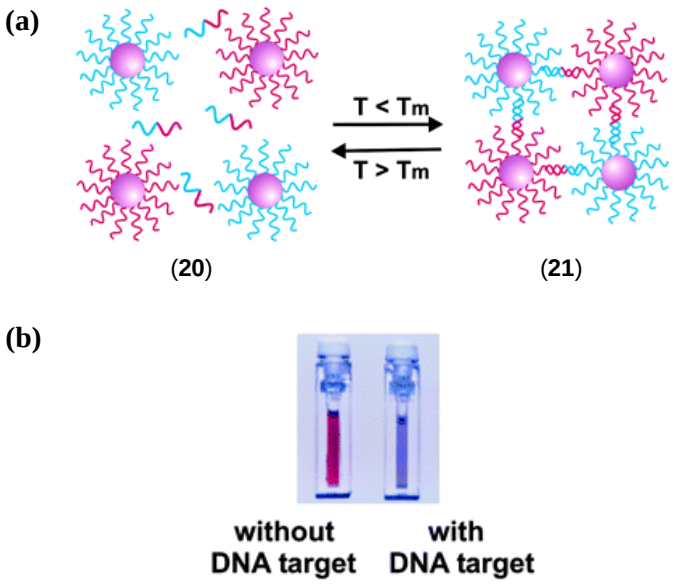

Figure 1-24: *Colorimetric detection of DNA based on the optical properties of gold nanoparticles.* ***(a)*** *Aggregation of oligonucleotide-functionalised gold nanoparticles in the presence of complementary target DNA. Tm is the melting temperature of DNA.* ***(b)*** *Changing the solution colour from red to blue due to aggregation. Figure reproduced with permission from Reference 2. Copyright (2005) American Chemical Society.*

Since this invention, the development of new highly sensitive methods to detect biological molecules has rapidly expanded, producing simple and quick effective nanoprobes for diagnostics of various diseases.[93] For example, modern and highly advanced spectroscopic techniques based upon surface enhanced Raman scattering (SERS) provide a huge enhancement of the Raman signal, by a factor of 10^{14}–10^{15} when molecules adsorb onto the surface of nanoparticles.[94,95] This enables the detection of DNA analytes at a much smaller concentration than is possible with Raman spectroscopy. The increase in Raman scattering by molecules adsorbed onto plasmonic nanoparticle surfaces is due to an enhancement in the electric field caused by a plasmon excitation through the laser incident light onto metal nanoparticle surfaces.[96,97] This novel tool offers a unique vibration spectrum of molecules as a fingerprint.[98] SERS has useful advantages because it can be used not only to detect the molecules, but also to identify their structures. Figure 1-25 illustrates the SERS effect to increase the intensity of the Raman bands of an adenine molecule using silver nanoparticles.[99]

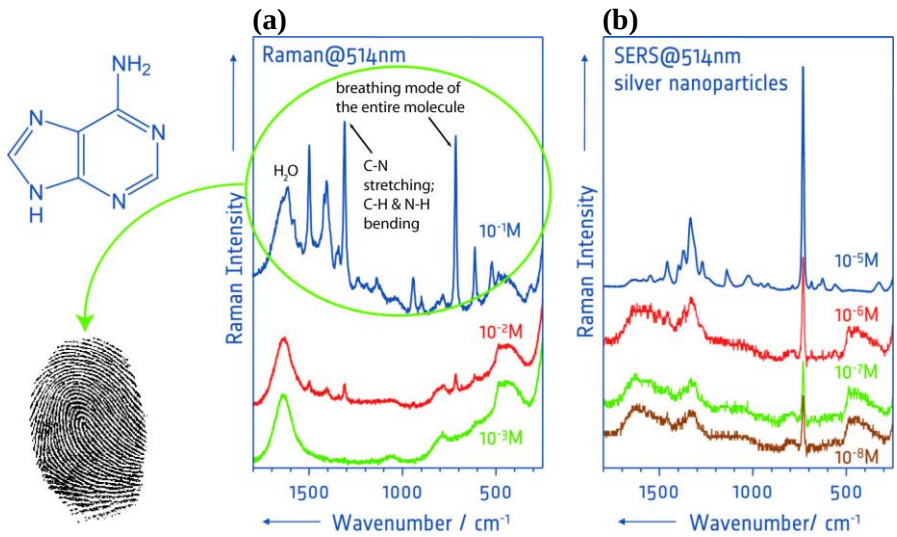

Figure 1-25: (a) *Raman spectroscopic investigation of adenine at high concentration.* ***(b)*** *SERS effect to enhance Raman bands and improve the detection limit using silver nanoparticles. Figure reproduced with permission from Reference 99.*

Mirkin and colleagues demonstrated an example of SERS nanoprobes to detect DNA and RNA based on scanometric detection methods.[98] This tool has three crucial components: (i) a DNA capture strand immobilised on a glass surface; (ii) DNA-modified gold nanoparticles and (iii) a single stranded DNA target (Figure 1-26a). In the presence of the target, the DNA capture strand binds to the complementary sequences of the target. Hybridisation of the DNA attached to the nanoparticles with the overhanging sequences of the target, generates grey visible spots after the addition of silver enhancement solution. This solution is to induce silver deposition on the surface of gold particles and can be used to amplify gold-labelled samples for the detection of DNA and RNA biomolecules. The vital feature of this class of nanoprobes is the potential for multiplexed DNA detection by using different Raman active dyes as a tag to label the sequences of DNA-modified nanoparticles (Figure 1-26b-c). Using this method, silver deposition can enhance the Raman signals of these dyes which provide the ability to identify DNA sequences based on fingerprint Raman spectroscopy.

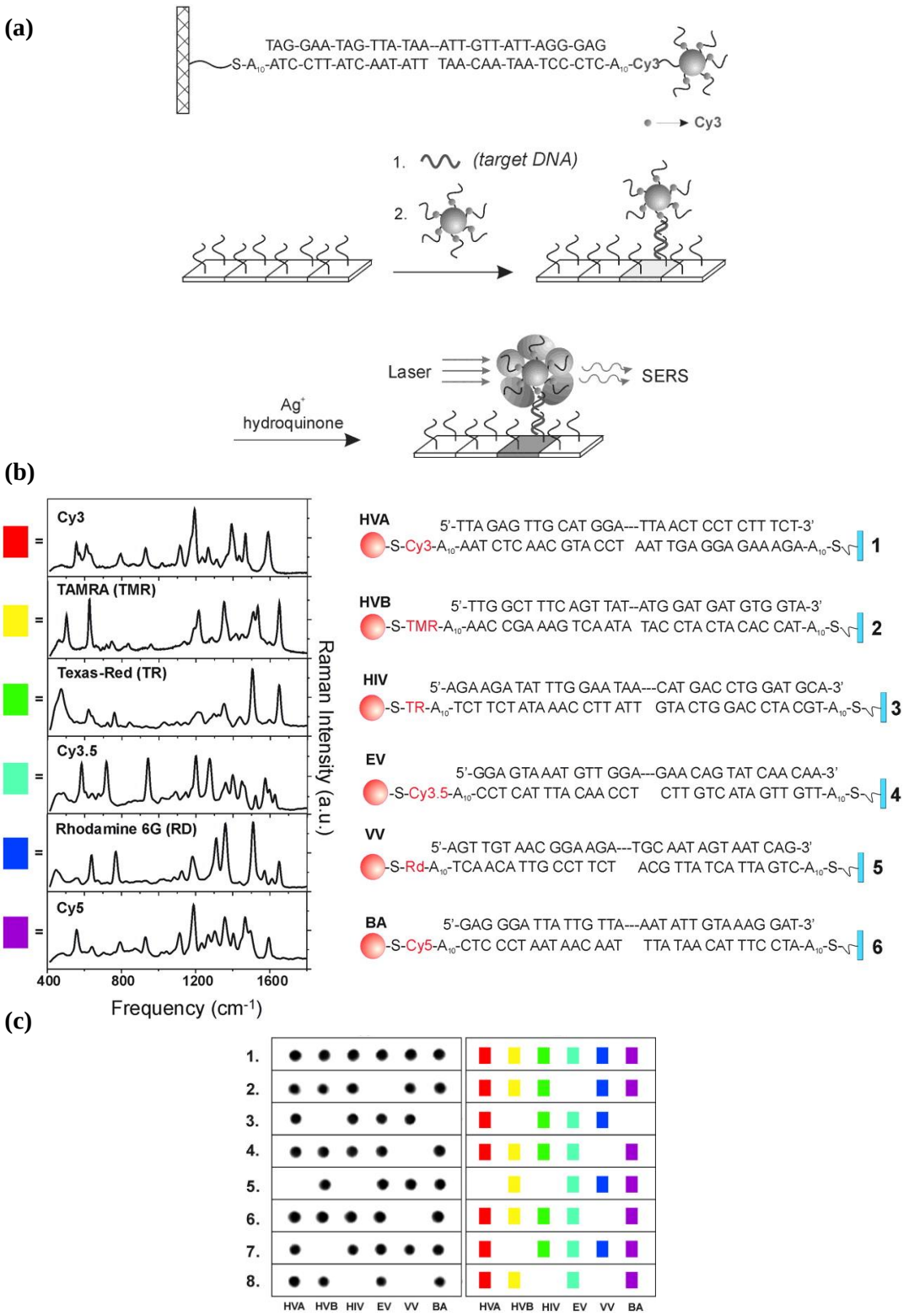

Figure 1-26: (a) *Scheme of the DNA and RNA detection by using SERS.* ***(b)*** *Raman spectra of six different dye-label nanoparticle probes for multiplexed DNA detection.* ***(c)*** *Images of Ag-enhanced microarrays with corresponding Raman spectra. The coloured boxes correlate with the colour coded Raman spectra. Figure reproduced with permission from Reference 98. Copyright (2002) American Association for the Advancement of Science.*

1.4.1 Importance of size- and shape-controlled methods of nanoparticle synthesis for biodiagnostic applications

One of the major challenges to develop the application of metal NPs is to tune the size and shape of these NPs for specific application requirements. For example, Graham's group studied the effect of tuning the size of AgNPs on SERS enhancement by preparing different sizes of spherical and monodispersed AgNPs.[100] They proved that the increase in the particle sizes results in an increase in the enhancement of Raman signals using three different analytes, namely thiophenol (TP), malachite green oxalate (MGO) and rhodamine 6G (R6G). Another example of the size tunability and application potentials of NPs in biosensing is the study of size-dependent antibacterial activity of AgNPs. It has been shown that smaller NPs with the diameter of 5 nm are more efficient against different types of bacteria including aerobic and anaerobic bacteria, such as *Escherichia coli* (*E. coli*)[44] and *Streptococcus mutans* (*S. mutans*).[101] Song's group investigated the way in which the shape of silver nanoparticles can promote their properties as antibacterial agents.[102] In this study, truncated triangular silver nanoplates have the greatest activity to inhibit the growth of *E. coli* compared to spherical and rod nanoparticles.

Besides the size and shape of nanoparticles, the stability of these particles in high salt concentrations is a key property for biosensing applications. This is particularly important because salts are highly important for DNA modifications and hybridisation process while nanoparticles can aggregate in the presence of high concentration of salts.

1.5 Hypothesis

Previous work on the metallisation using sugar-modified DNA suggests that sugar triazoles can template the formation of Ag nanowires (Figure 1-27a).[83] Based on this method, sugar triazole ligands such as (**18**, Figure 1-27b) provide highly controlled size AgNPs with spherical shape as reported by Burley *et al.*[87] The working hypothesis of this work will be that size, shape and properties of AgNPs can be tuned according to the structure of triazole ligands such as (**22-26**, Figure 1-27c).

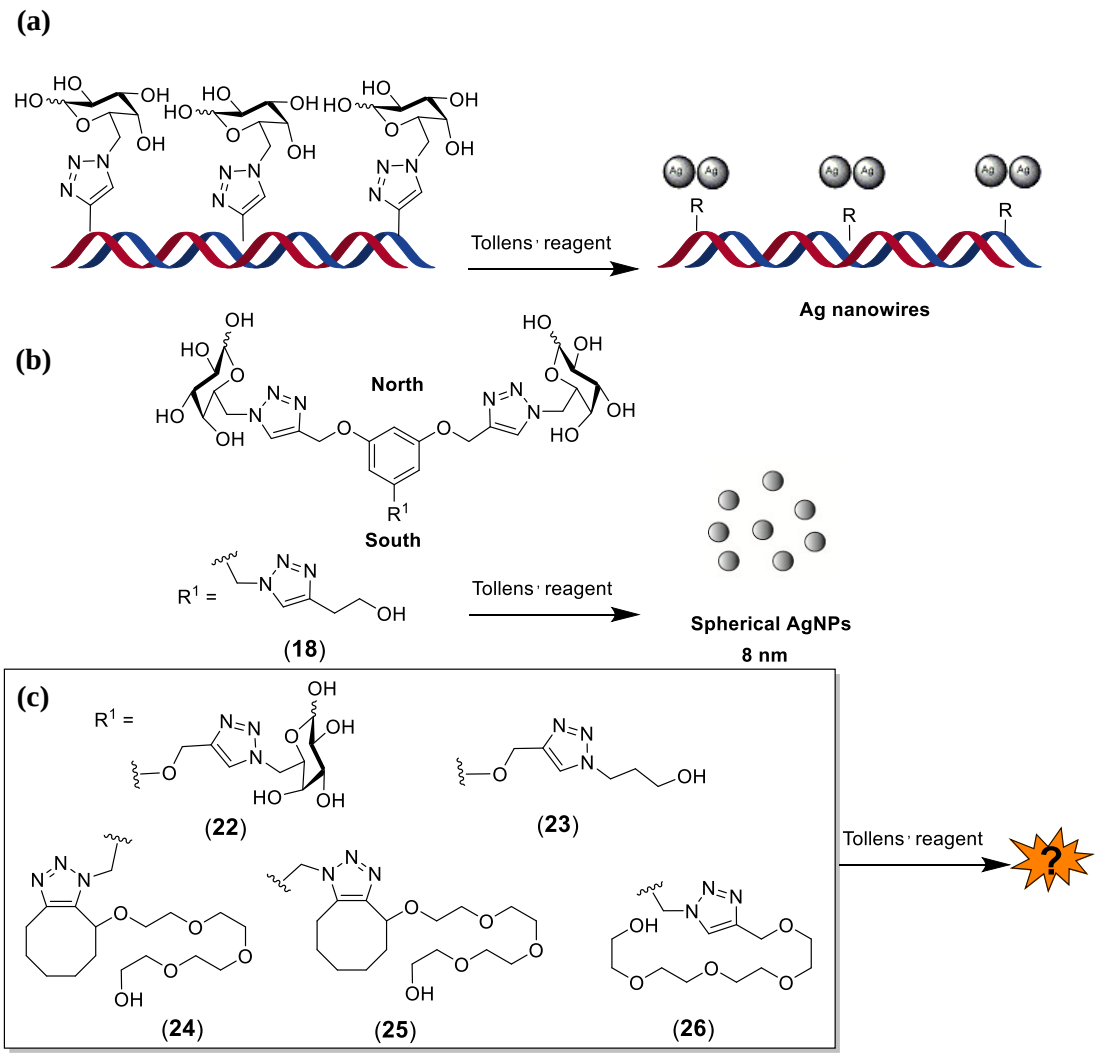

Figure 1-27: *Templated synthesis of AgNPs using sugar triazole ligands and Tollens' reagent.* ***(a)*** *Ag nanowires formed on sugar-modified DNA.* ***(b)*** *Spherical AgNPs using ligand (**18**).* ***(c)*** *Structures of sugar triazole ligands (**22-26**) prepared in this study.*

1.6 Aims

The aim of this thesis is to develop a facile one-pot synthesis of AgNPs based on a template-directed approach using sugar triazole ligands and Tollens' reagent. A series of sugar triazole ligands (e.g., **22-26**, Figure 1-27c) were prepared to investigate the influence of their structural parameters on the formation of AgNPs.

This thesis focuses on four major aims:

1) Determination of the role of the aromatic core of sugar triazole ligand (**18**, Figure 1-27b) in the formation of AgNPs.
2) Exploration of the role of the counter-ion of silver salts on the size and the morphology of AgNPs formed using sugar triazole ligands (**18**, Figure 1-27b) and (**22-23**, Figure 1-27c).
3) Synthesis of PEG-functionalised sugar triazoles (**24-26**, Figure 1-27c) and investigation of the effects of changing the southern part of the ligand structure on AgNP formation.
4) Exploration of a template-directed synthesis approach for the synthesis of AgNPs using sugar-modified peptides (**27-28**, Figure 1-28).

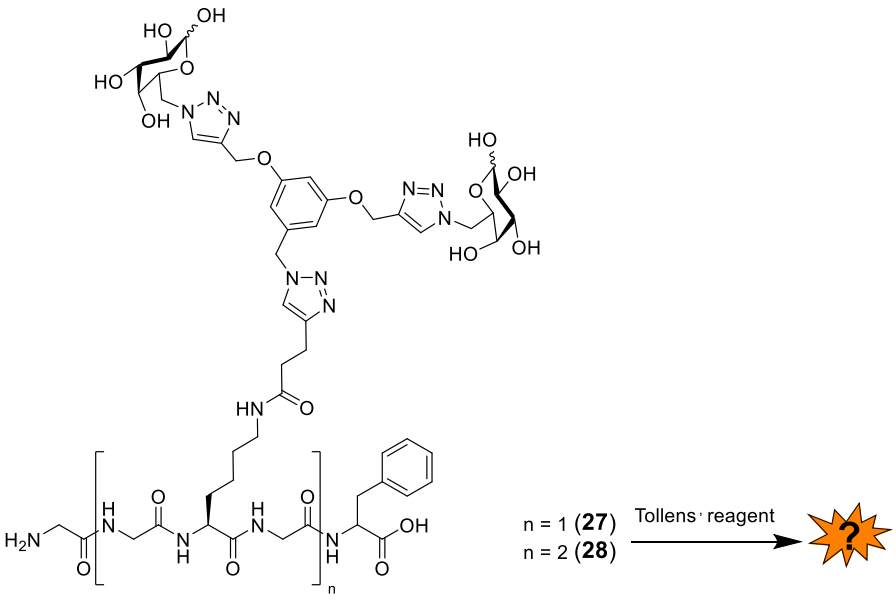

Figure 1-28: *Structures of sugar-functionalised peptides (**27-28**).*

CHAPTER 2: DEVELOPMENT OF TEMPLATE-BASED METHODS FOR THE SIZE- AND SHAPE-CONTROLLED SYNTHESIS OF SILVER NANOPARTICLES

2.1 Introduction

In chapter one (Section 1.3), a variety of methods for the preparation of AgNPs were presented. Among these methods, the formation of AgNPs using Tollens' reagent $[Ag(NH_3)_2]OH$ in the presence of aldehyde is one such method that can be utilised under mild reductive conditions and at room temperatures (Section 1.3.2.2). Based on the work of Burley *et al.*, a new template-directed approach for the synthesis of AgNPs using sugar triazole ligands and Tollens' reagent has been reported (Section 1.3.4). This method has some advantages over current approaches. For example, the polyol synthesis method requires high temperatures to oxidise an alcohol to an aldehyde. A current disadvantage of Tollens'-mediated synthesis of AgNPs using ligand (**18**) is the long preparative routes needed to access (**18,** Scheme 2-1a).

2.2 Aims of the study

The aims of this chapter are:

1) To develop an efficient preparative route for the generation of sugar triazole ligands to direct the synthesis of AgNPs using Tollens' reagent.

2) To investigate how each of the constituent structural elements of these ligands [i.e., sugar unit, triazole and aromatic core] influences the size, morphology, stability and dispersity of AgNPs.

3) To establish how the Ag(I)-binding affinity of these triazole ligands influences the size and shape of the resultant AgNPs formed.

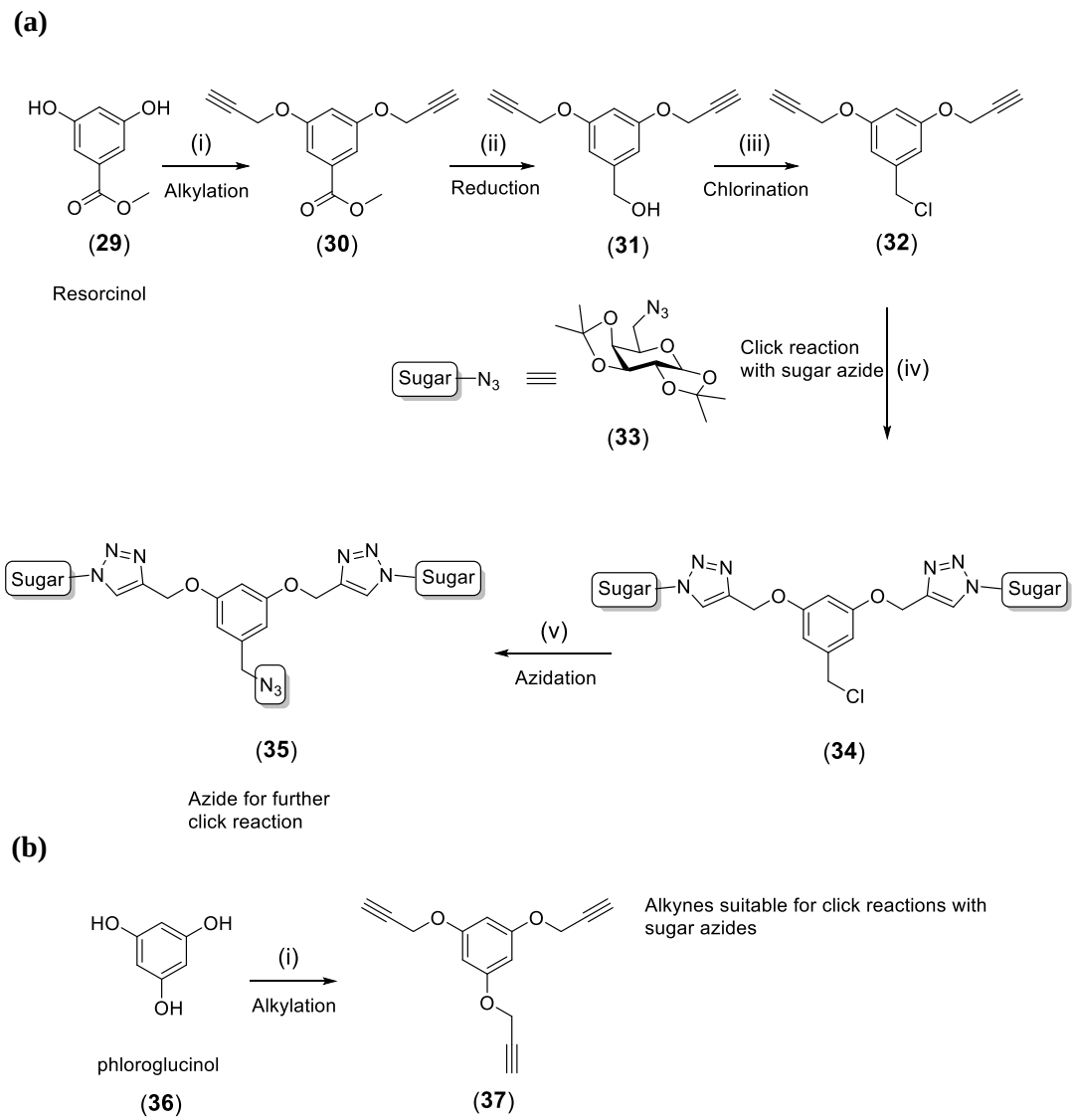

Scheme 2-1: (a) *Synthetic route for the preparation of sugar triazole ligand with resorcinol core.*[82,88] ***(b)*** *Proposed synthetic route for the preparation of sugar triazole ligand with phloroglucinol core.*

2.3 Results and Discussion

2.3.1 Design of sugar triazole ligands

In order to study the structural parameters of triazole ligands in the templated synthesis of AgNPs, new ligand scaffolds were prepared in which the resorcinol core

as present in (**18,** Figure 1-27) was replaced with phloroglucinol (**22, 23** and **39,** Figure 2-1).

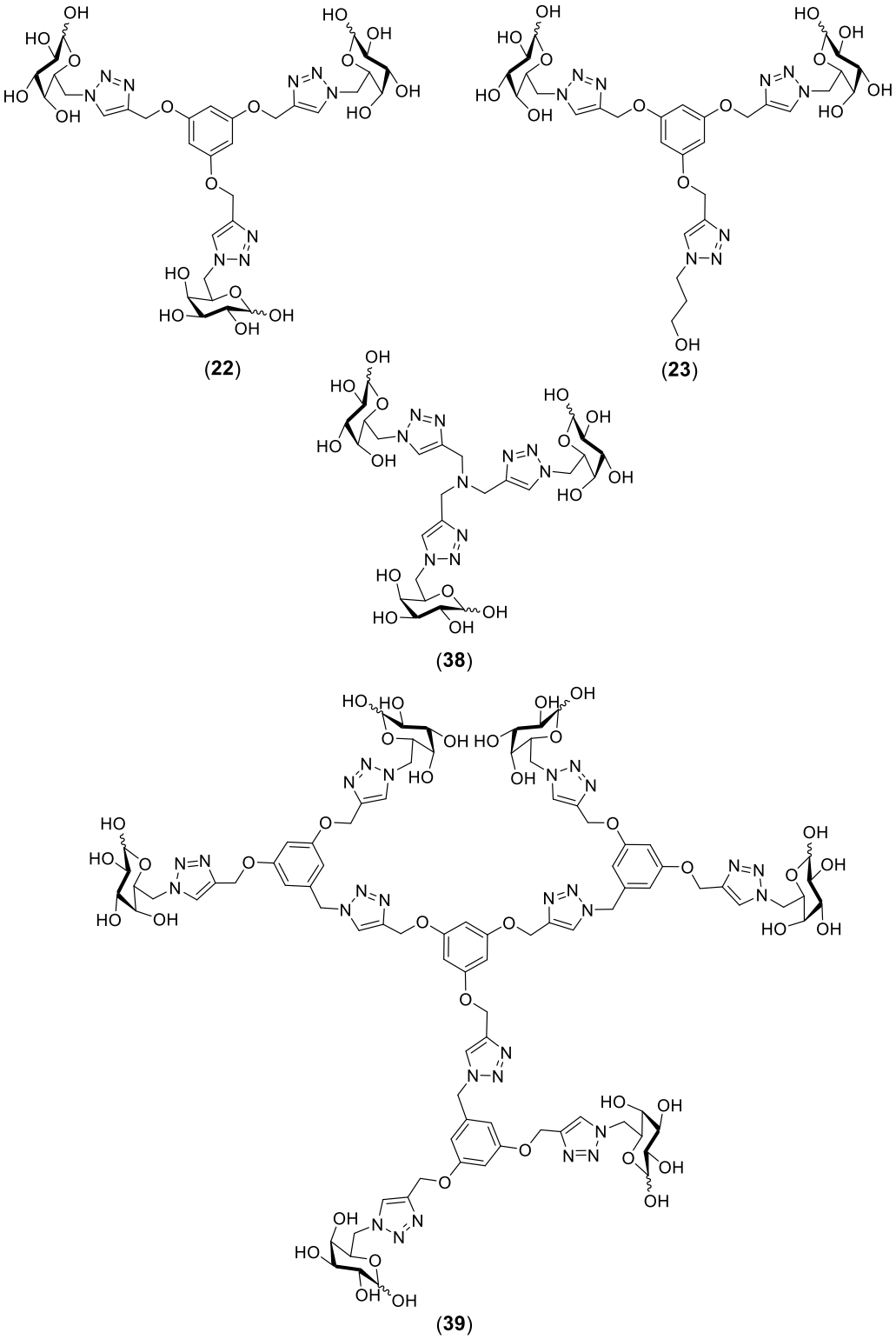

Figure 2-1: *Structures of sugar triazoles (**22-23, 38-39**) prepared in this study.*

Changing the core structure subtly alters the triazole regiochemistry and inter-triazole distance in the southern part of the ligand (Figure 2-2). The effect of this change on AgNP formation was studied using a three-sugar triazole (**22**) and two-sugar triazole (**23**) ligand system. The role of the central aromatic ring was probed by the replacement of the resorcinol core with a central nitrogen atom (**38**). To further explore how sugar density plays a role in the size and shape of AgNPs, the hybrid ligand (**39**) was synthesised.

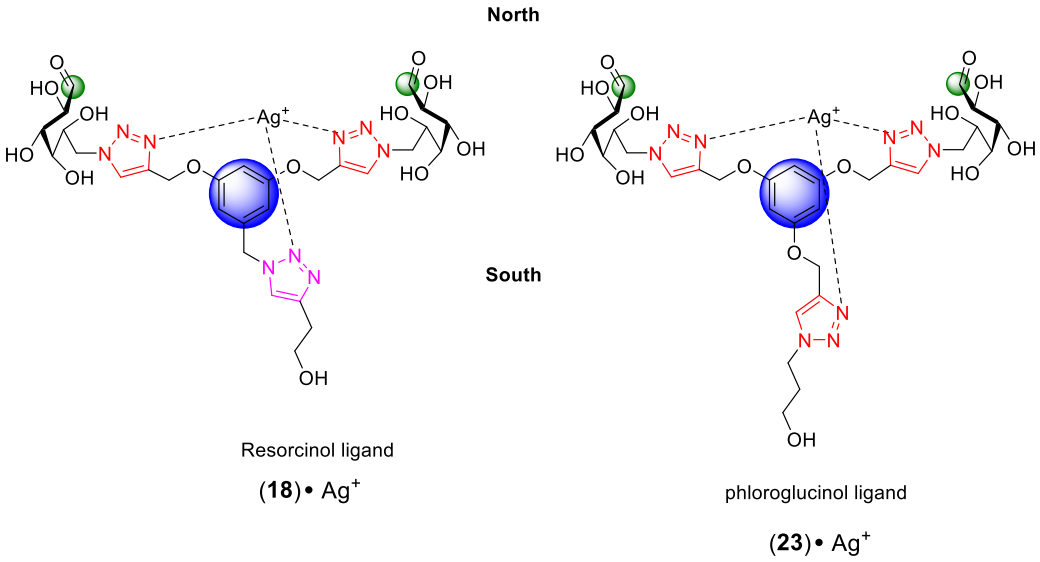

Figure 2-2: *Comparison between a putative binding model of the templated synthesis of AgNPs using resorcinol and phloroglucinol ligands.*

The sugar triazole ligands in this study were prepared by copper-catalysed Huisgen cycloaddition between azides and terminal alkynes. Scheme 2-2 shows the synthetic route used to prepare the alkynylated scaffold for the synthesis of sugar triazole ligands (**22**), (**23**) and (**39**). This facile one-pot procedure involved the reaction of phloroglucinol (**36**) with propargyl bromide to afford (**37**) as a cream-coloured powder in 50% yield after purification by column chromatography and recrystallisation.[103]

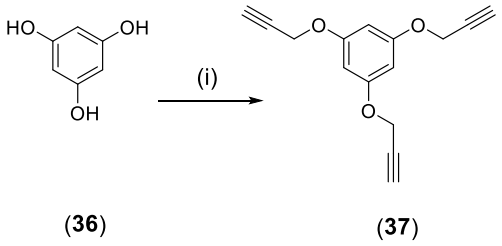

Scheme 2-2: *Reagents and conditions: (i) propargyl bromide (4.5 equiv.), K_2CO_3 (4.1 equiv.), DMF, RT, 4d, 50%.*

The central phloroglucinol core was chosen as the scaffold for connecting two or three galactose units via triazole rings. This new system allows for the investigation of the effect of the southernmost sugar units on the formation of AgNPs.

2.3.1.1 Synthesis of sugar azides

Azide (**33**) was prepared in two steps according to a literature procedure (Scheme 2-3).[104] The first step was the conversation of alcohol in isopropylidene-protected galactose (**40**) into the corresponding mesylate (**41**) using mesityl chloride. Mesylate (**41**) was then reacted with sodium azide to afford galactose (**33**) as a clear oil in 97% after purification by column chromatography.

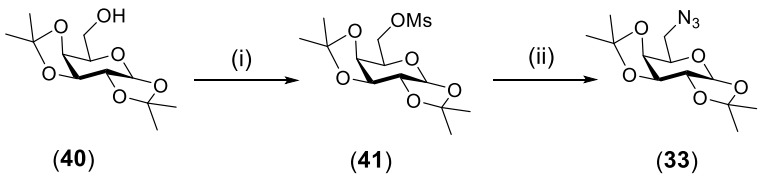

Scheme 2-3: *Reagents and conditions: (i) CH_3SO_2Cl (4.0 equiv.), DIEA (4.0 equiv.), dry THF, 0°C to RT, 24h, 96%; (ii) NaN_3 (10 equiv.), DMF, Δ, 120°C, 24h, 97%.*

2.3.1.2 Synthesis of sugar triazole (22)

Sugar triazole (**22**) was prepared in two steps as shown in Scheme 2-4. The first step was the click reaction between (**37**) and four equivalents of galactose azide (**33**)

using copper sulfate in the presence of sodium ascorbate afforded (**42**) as a white solid in 67% yield after purification by column chromatography. Subsequently, acid deprotection of the isopropylidene groups of (**42**) afforded (**22**) as a white powder in 60% yield after purification by RP-HPLC.

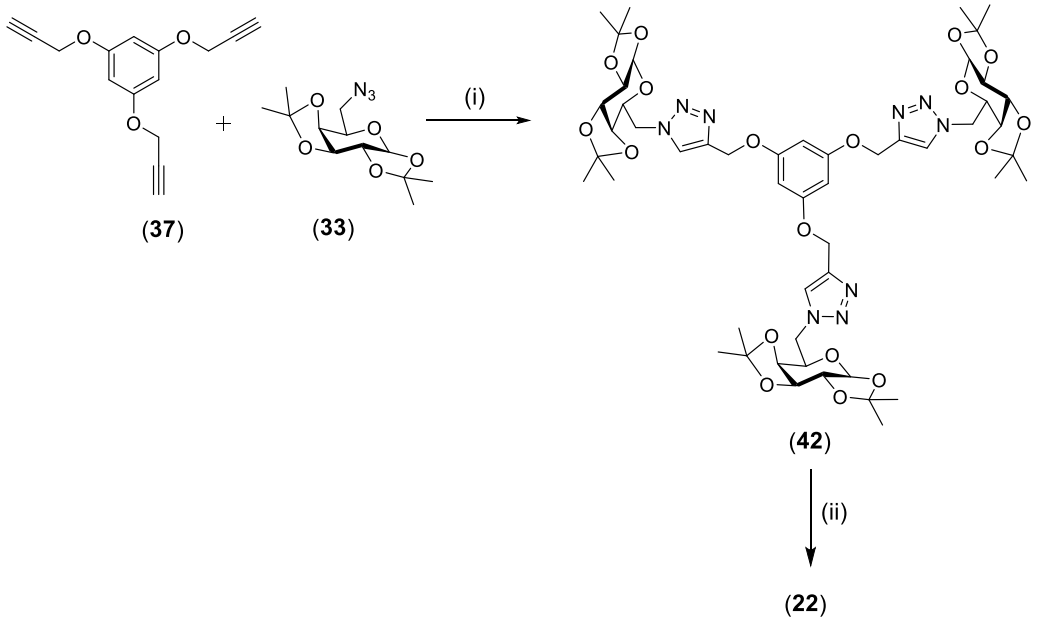

Scheme 2-4: *Reagents and conditions: (i) Compound (**33**) (4.0 equiv.), $CuSO_4$ (0.08 M, 0.3 equiv.), sodium ascorbate (2.0 equiv.), THF:H_2O (3:1), RT, 67%; (ii) TFA:H_2O (1:1), Δ, 70°C, 3h, 60%.*

2.3.1.3 Synthesis of sugar triazole ligand (23)

A click reaction between (**37**) and (**33**) using copper sulfate in the presence of sodium ascorbate afforded a mixture of mono-, bi- and tri-click products (Scheme 2-5). Purification by column chromatography afforded the bi- click product (**44**) as a pale yellow solid in 24% yield. Mass spectroscopy provided evidence for the formation of (**44**) and gave *m/z* 811 corresponding to $[M+H]^+$ (Appendix B10). Then, 3-iodo-1-propanol (**45**) was heated to reflux in the presence of sodium azide for 24 hours to afford the azide (**46**) in 99% yield. Compound (**46**) was used for a further

click reaction with (**44**) and afforded (**47**) followed by acid deprotection of the isopropylidenes and purification by RP-HPLC to yield (**23**).

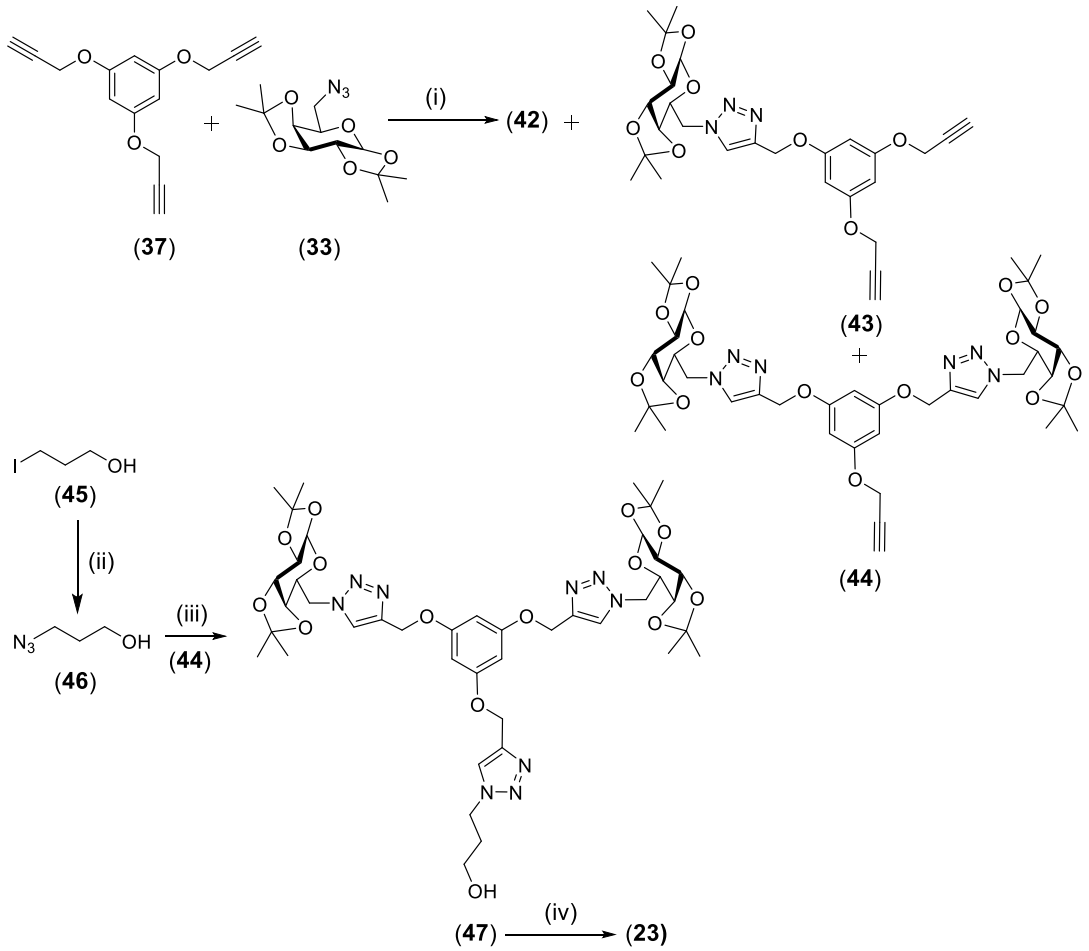

Scheme 2-5: *Reagents and conditions: (i) Compound (**33**) (2.0 equiv.), $CuSO_4$ (0.22 M, 0.35 equiv.), sodium ascorbate (2.0 equiv.), THF:H_2O (3:1), RT, 24% (**44**); (ii) NaN_3 (10 equiv.), H_2O, Δ, 90°C, 24h, 99%; (iii) (**46**) (5.0 equiv.), $CuSO_4$ (0.8 M, 1.2 equiv.), sodium ascorbate (2.0 equiv.), THF:H_2O (3:1), RT; (iv) TFA:H_2O (1:1), Δ, 70°C, 3h, 70% over 2 steps.*

2.3.1.4 Synthesis of sugar triazole (38)

The synthesis of sugar triazole (**38**) commenced with a three-fold click reaction between commercially available tripropargylamine (**48**) and galactose azide (**33**) to afford (**49**) as a white solid in 36% after purification by column chromatography

(Scheme 2-6).[86] Compound (**49**) was then treated with TFA:H_2O and purified by RP-HPLC to afford deprotected sugar triazole (**38**) as a white powder in 60% yield.

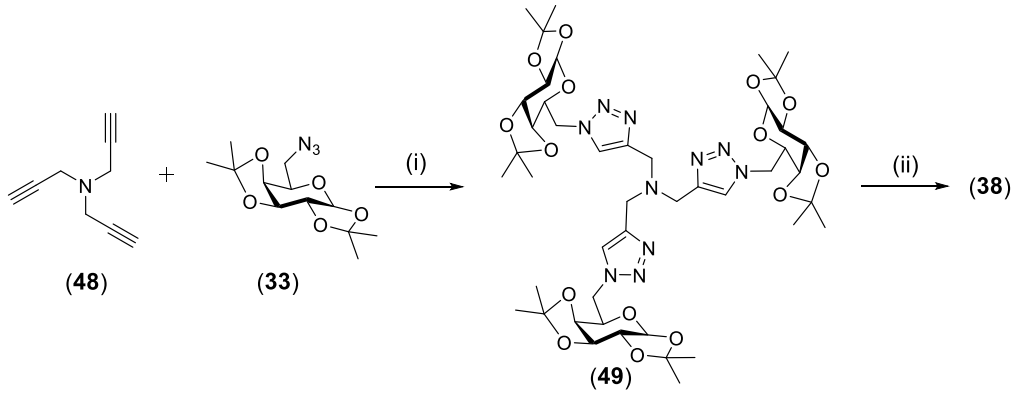

Scheme 2-6: *Reagents and conditions: (i) Compound (**33**) (4.5 equiv.), 2.6-lutidine (1.0 equiv.), $[Cu(CH_3CN)_4]PF_6$ (0.01 equiv.), CH_3CN, 0°C to RT, 24h, 36%; (ii) TFA:H_2O (1:1), Δ, 70°C, 3h, 60%.*

2.3.1.5 Synthesis of sugar triazole (39)

Compound (**39**) was prepared in several steps. The first step was to prepare compound (**35**) in which galactose units (**33**) were linked to a central resorcinol core via triazole rings (Scheme 2-7).[88,82] The synthesis commenced with alkylation of methyl-3,5-dihydroxybenzoate (**29**) with propargyl bromide to afford (**30**) as a pale yellow crystalline solid in 80% yield. Reduction of (**30**) by lithium aluminium hydride afforded (**31**), which was then reacted with thionyl chloride in the presence of pyridine for 24 hours at room temperature to yield the corresponding benzyl chloride (**32**). After purification by column chromatography, a two-fold click reaction with (**32**) was carried out with 2.4 equivalents of galactose azide (**33**) under standard copper-catalysed Huisgen cycloaddition conditions to afford (**34**). Compound (**34**) was purified by column chromatography and reacted with NaN_3 to yield the corresponding azide (**35**) as a white solid in 60% yield. The next step involved a three-fold click reaction using alkyne (**37**) and 3.3 equivalents of (**35**) in

the presence of copper(I) to yield (**50**) as a white solid in 41% yield after column chromatography. Finally, acid deprotection of the isopropylidene groups of (**50**) and purification by RP-HPLC afforded (**39**) as a white powder in 47% yield.

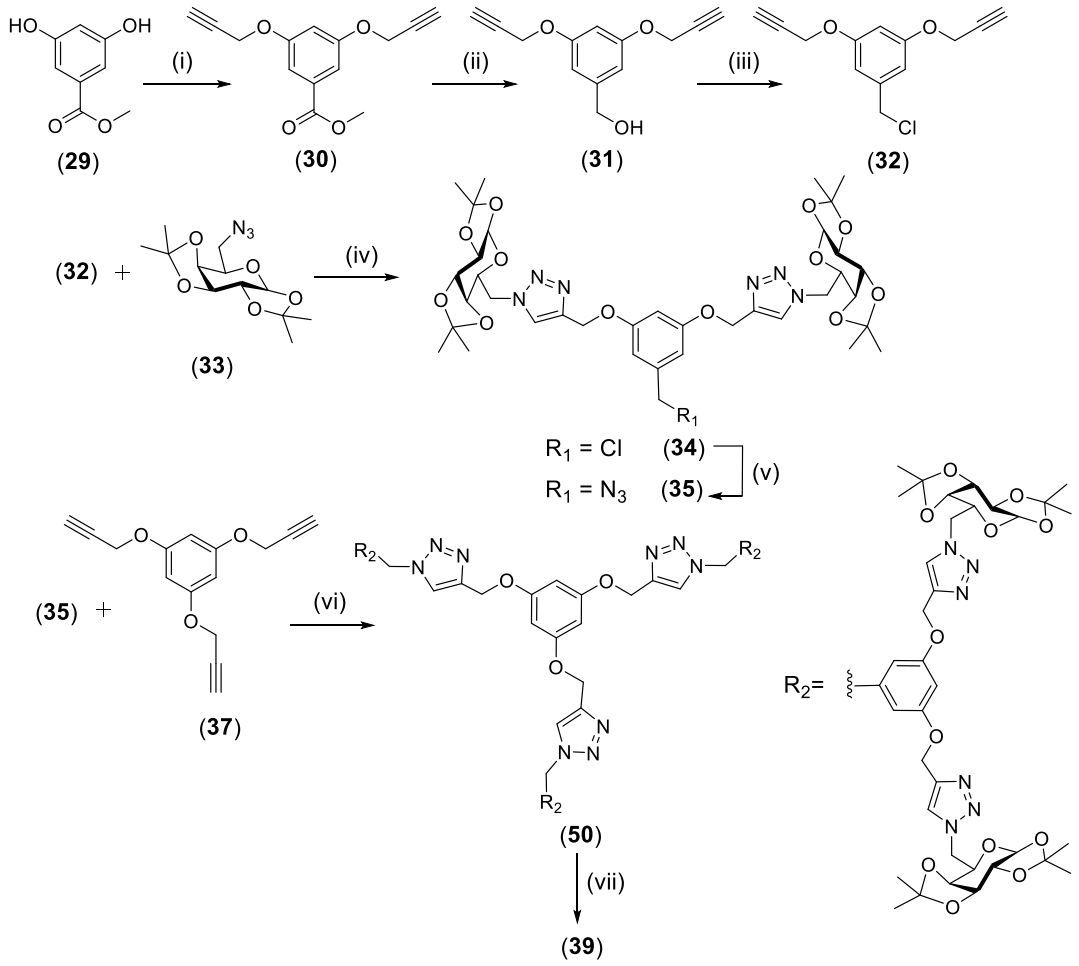

Scheme 2-7: *Reagents and conditions: (i) propargyl bromide (2.2 equiv.), K_2CO_3 (3.0 equiv.), 18-crown-6 (0.007 equiv.), acetone, Δ, 70°C, 24 h, 80%; (ii) $LiAlH_4$ (10 equiv.), dry THF, 0°C, 1h, 80%; (iii) $SOCl_2$ (3.0 equiv.), dry DCM, pyridine (2.0 equiv.), 0°C to RT, 48h, 35%; (iv) Compound (**33**) (2.4 equiv.), $CuSO_4$ (0.08 M, 0.32 equiv.), sodium ascorbate (2.0 equiv.), THF:H_2O (3:1), RT, 24h, 91%; (v) NaN_3 (10 equiv.), acetone:H_2O (4:1), Δ, 90°C, 24h, 60%; (vi) (**35**) (3.3 equiv.), $CuSO_4$ (0.08 M, 1.47 equiv.), sodium ascorbate (2.0 equiv.), THF:H_2O (3:1), RT, 24h, 41%; (vii) TFA:H_2O (1:1), Δ, 70°C, 24h, 47%.*

2.3.2 Synthesis of silver nanoparticles using sugar triazole ligands

AgNPs were prepared in a single step at room temperature based on previous work reported by Burley *et al.*[87] The synthesis of AgNPs was conducted by screening the

concentration of the triazole sugars and Tollens' reagent to determine the optimal conditions for the preparation of AgNPs. This method allowed an understanding of the factors that can control the synthesis and tune the properties of AgNPs. The formation of AgNPs was confirmed by UV-vis spectroscopy which exhibited a diagnostic SPR peak at 420 nm.

2.3.2.1 Silver nanoparticles derived from sugar triazole (22)

A AgNP array using compound (**22**) was constructed over concentration ranges of 1 µM - 25 mM [(**22**)] and 10 µM - 50 mM [Tollens'] (Table 2-1).

Table 2-1: *AgNP@(**22**) screening array prepared using sugar triazole (**22**) and Tollens' reagent. White boxes represent no AgNP formation, yellow boxes represent AgNP formation and grey boxes represent the formation of silver mirrors.*

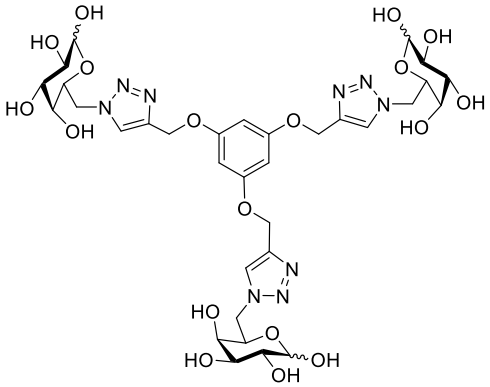

[(22)]

[Tollens']

	25 mM	10 mM	1 mM	100 µM	10 µM	1 µM
10 µM	#1	#2	#3	#4	#5	#6
100 µM	#7	#8	#9	#10	#11	#12
1 mM	#13	#14	#15 21 ± 3 nm	#16	#17	#18
10 mM	#19 17 ± 3 nm	#20	#21	#22	#23	#24
20 mM	#25	#26	#27	#28	#29	#30
50 mM	#31 18 ± 5 nm	#32	#33	#34	#35	#36

The reaction screen of [(**22**)] and [Tollens'] produced AgNP@(**22**) in three regions (yellow boxes in Table 2-1): (i) a region of low concentration of Tollens' [i.e., 1mM]; (ii) a region of intermediate concentration of Tollens' [10 mM] and lastly

(iii) a high concentration region of Tollens' [20 mM - 50 mM]. The dependence on concentration of both ligand and Tollens' was similar to AgNP@(**18**) prepared by Burley *et al.*[87] Silver aggregates were also observed in some reaction vessels (grey boxes, Table 2-1). UV-vis spectra of AgNP@(**22**) formed in these three exemplar regions all exhibited a diagnostic surface plasmon resonance peak ~ 420 nm (Figure 2-3).

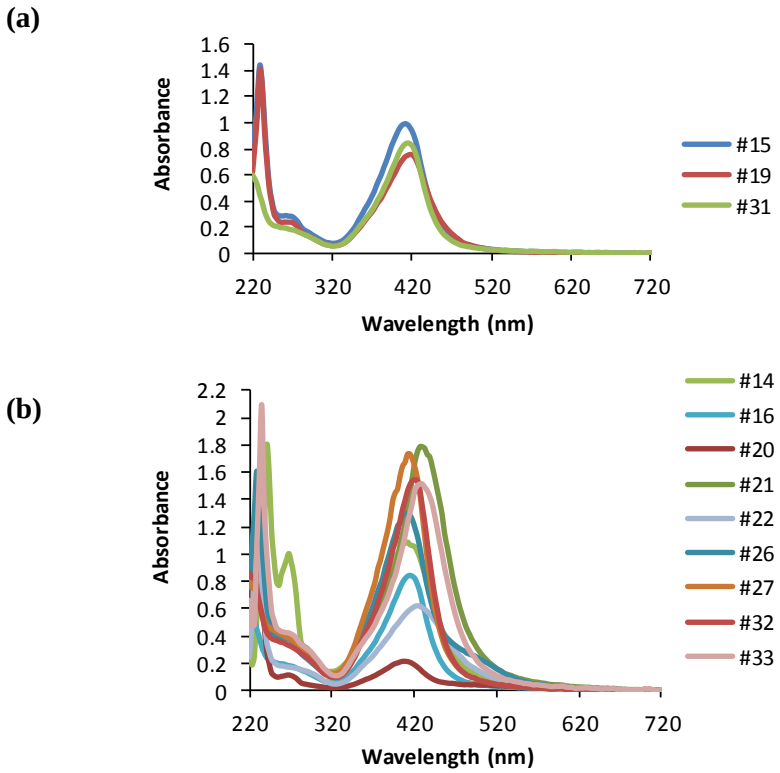

Figure 2-3: *UV-vis spectra of reactions which formed AgNP@(**22**) as observed by a SPR peak at 420 nm.* ***(a)*** *#15, 19 and 31;* ***(b)*** *#14, 16, 20-22, 26-27 and 32-33. Samples #19-20, 21, 26 were diluted 1:10, #27 was diluted 1:20, #32 was diluted 1:50 and #31 was diluted 1:70 prior to each measurement.*

TEM analysis revealed AgNP@(**22**) formed angular AgNPs of similar diameter (Figure 2-4). For example, #15 (lower concentration of Tollens') and #31 (high concentration of Tollens') afforded angular AgNP@(**22**) with diameters of 21 ± 3 nm and 18 ± 5 nm respectively. AgNP@(**22**) formed using an intermediate concentration

of Tollens' [i.e., #19], produced AgNPs [Ø = 17 ± 3 nm]. In contrast, Burley *et al*. reported that ligand (**18**) produced spherical AgNPs [Ø = 8 ± 5 nm].[87]

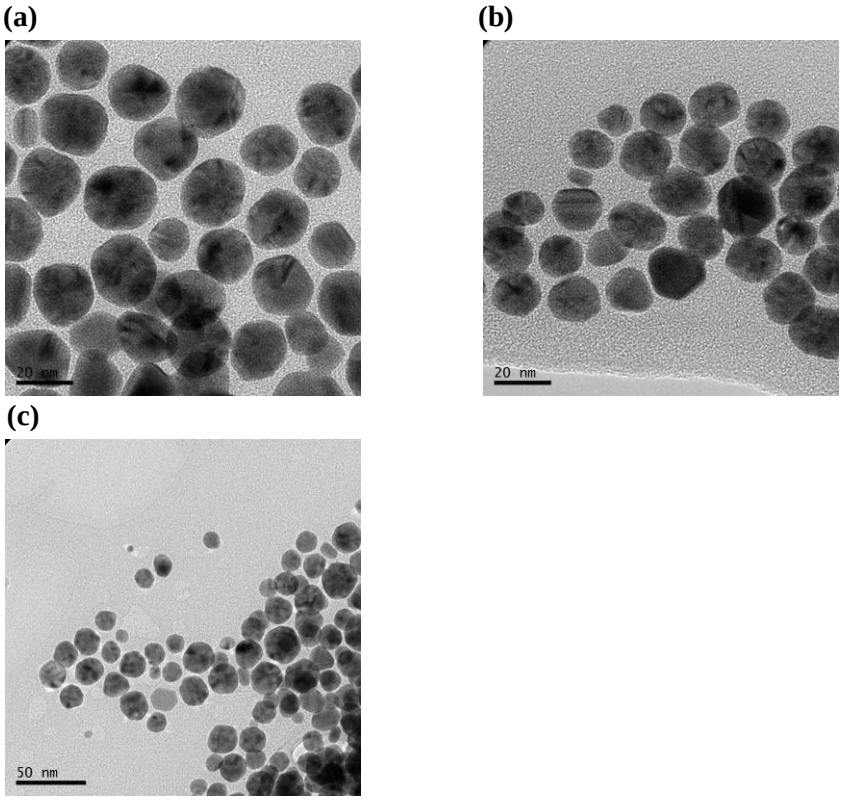

Figure 2-4: *TEM images of AgNP@(**22**) prepared using reaction conditions in Table 2-1.* ***(a)*** *#15, Ø = 21 ± 3 nm;* ***(b)*** *#19, Ø = 17 ± 3 nm;* ***(c)*** *#31, Ø = 18 ± 5 nm.*

These results suggested that ligand (**22**) templated the formation of AgNPs much larger in diameter and of different shape to AgNP@(**18**).

2.3.2.2 Silver nanoparticles derived from sugar triazole (23)

The formation of AgNP@(**23**) was screened as a function of [(**23**)] and [Tollens'] with a similar concentration range used to prepare AgNP@(**22**) (Table 2-2).

Table 2-2: *AgNP@(**23**) screening array prepared using sugar triazole (**23**) and Tollens' reagent. White boxes represent no AgNP formation and yellow boxes represent AgNP formation.*

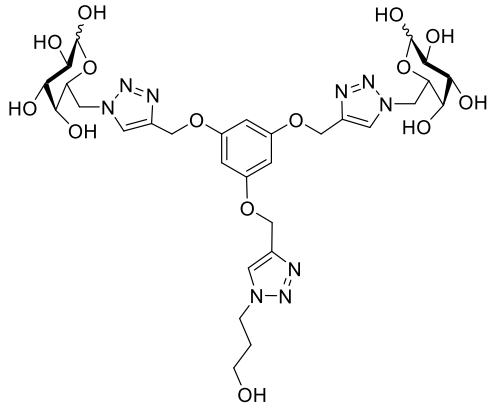

[(23)]

[Tollens']

	25 mM	10 mM	1 mM	100 µM	10 µM	1 µM
10 µM	#1	#2	#3	#4	#5	#6
100 µM	#7	#8	#9	#10	#11	#12
1 mM	#13	#14	#15	#16	#17	#18
10 mM	#19 33 ± 7 nm	#20	#21	#22	#23	#24
20 mM	#25	#26	#27 14 ± 3 nm	#28	#29	#30
50 mM	#31 12 ± 3 nm	#32	#33	#34	#35	#36

The size distribution of the array using (**23**) [i.e., AgNP@(**23**)] was slightly different from AgNP@(**22**). AgNP@(**23**) were formed over concentration ranges of 1 mM - 25 mM [(**23**)] and 10 mM - 50 mM [Tollens']. One obvious difference was that no silver mirrors or formation of Ag aggregates were observed using (**23**). This suggested that the third galactose sugar present in (**22**) is not playing an influential role in AgNP formation. Another aspect is that the addition of low concentration of Tollens' at 1mM to ligand (**23**) did not form silver nanoparticles. The formation of AgNP@(**23**) was more dependent on the reaction conditions than AgNP@(**22**). All samples which formed silver nanoparticles displayed a characteristic SPR peak ~ 420 nm (Figure 2-5).

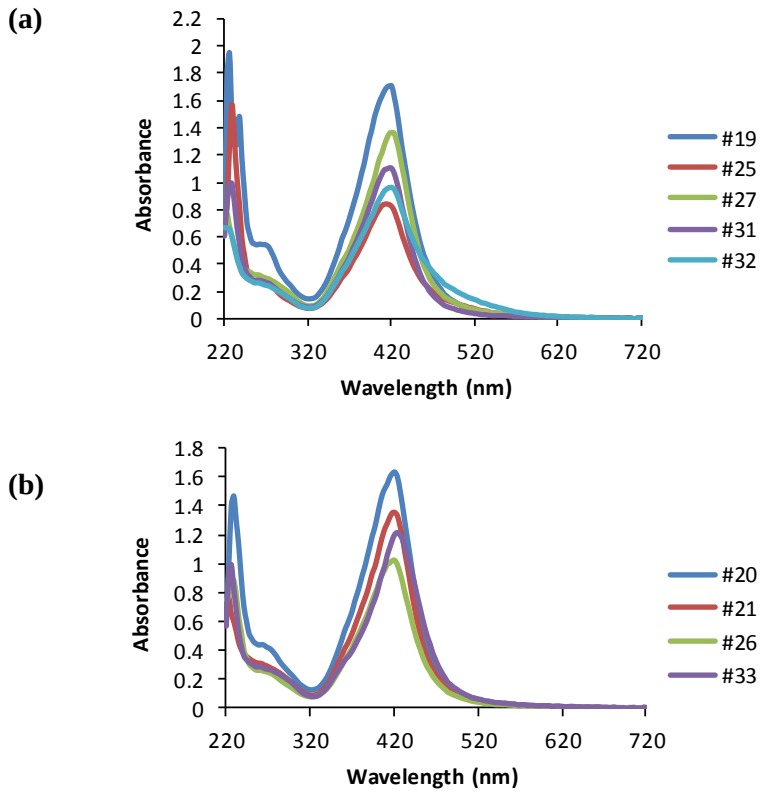

Figure 2-5: *UV-vis spectra of reactions which formed AgNP@(**23**) as observed by a SPR at 420 nm.* ***(a)*** *#19, 25, 27 and 31-32;* ***(b)*** *#20-21, 26 and 33. Samples #19-21, 27 and 33 were diluted 1:10, #25-26 were diluted 1:20 and #31-32 were diluted 1:50 prior to each measurement.*

TEM analysis of several examples in this series produced angular AgNP@(**23**) of tunable sizes that ranged from 12 ± 3 nm in diameter when a higher concentration of Tollens' was used (#31, Figure 2-6c) through to 33 ± 7 nm when an intermediate concentration of Tollens' was used (#19, Figure 2-6a).

The key conclusion from this series was the formation of different sizes of AgNP@(**23**) was tunable.

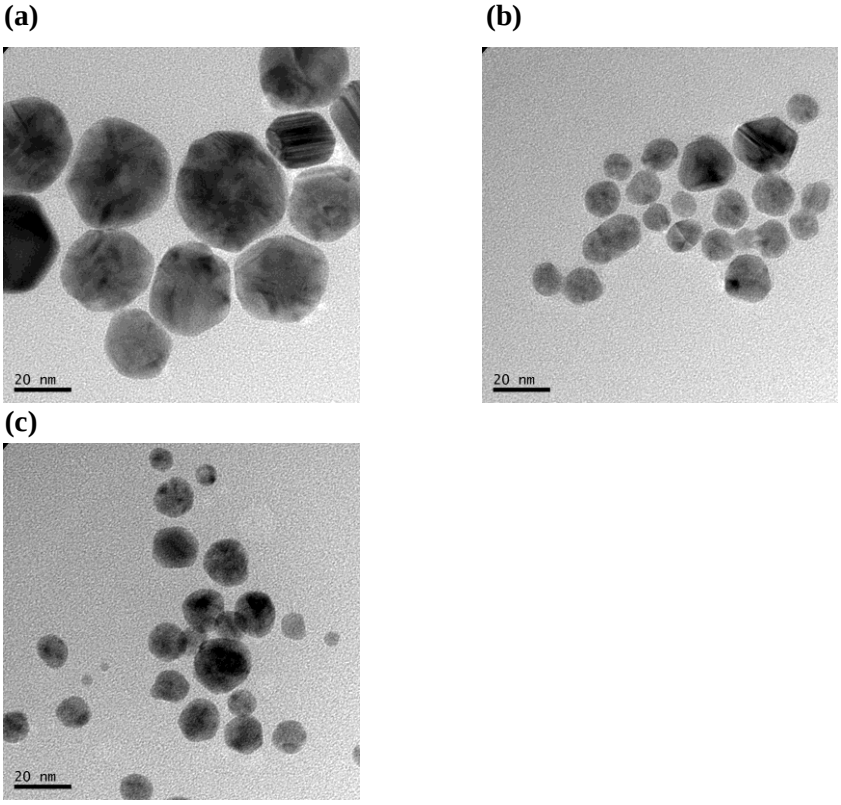

Figure 2-6: *TEM images of AgNP@(**23**) prepared using reaction conditions in Table 2-2.* ***(a)*** *#19, Ø = 33 ± 7 nm;* ***(b)*** *#27, Ø = 14 ± 3 nm;* ***(c)*** *#31, Ø = 12 ± 3 nm.*

2.3.2.3 Silver nanoparticles derived from sugar triazole (38)

Table 2-3 represents the AgNP@(**38**) array prepared over a concentration range of 1 µM - 25 mM [(**31**)] and 10 µM - 50 mM [Tollens']. In contrast to AgNP@(**22**) and AgNP@(**23**), a narrow reaction window was observed for the formation of poor quality and polydisperse AgNPs using ligand (**38**) [i.e., AgNP@(**38**)]. Yellow samples with comparatively weak SPR (maximum absorption at 0.1, Figure 2-7) were formed at [Tollens'] 100µM - 1mM and 1µM - 1 mM [(**38**)] with silver mirrors and aggregates predominating outside the optimal conditions (Table 2-3, grey boxes).

Table 2-3: *AgNP@(**38**) screening array prepared using sugar triazole (**38**) and Tollens' reagent. White boxes represent no AgNP formation, yellow boxes represent AgNP formation and grey boxes represent the formation of silver mirrors.*

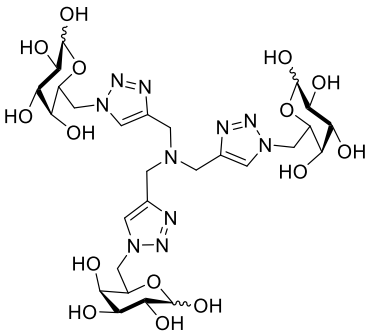

[(38)]

[Tollens']

	25 mM	10 mM	1 mM	100 µM	10 µM	1 µM
10 µM	#1	#2	#3	#4	#5	#6
100 µM	#7	#8	#9	#10	#11	#12
1 mM	#13	#14	#15	#16	#17	#18
10 mM	#19	#20	#21	#22	#23	#24
20 mM	#25	#26	#27	#28	#29	#30
50 mM	#31	#32	#33	#34	#35	#36

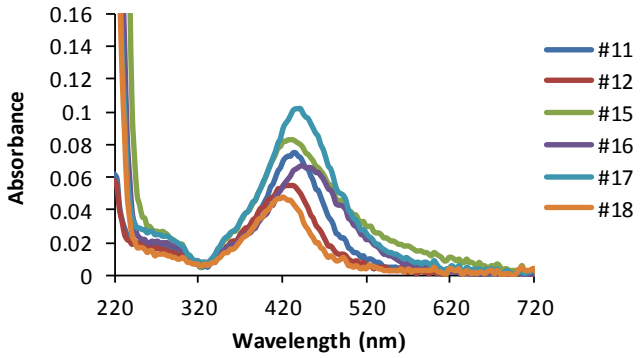

Figure 2-7: *UV-vis spectra of reactions #11-12 and 15-18, which formed AgNP@(**38**) with poor quality as observed by a weak SPR at 420 nm.*

The poor dispersity and size control of AgNP@(**38**) was confirmed by SEM analysis (Figure 2-8).

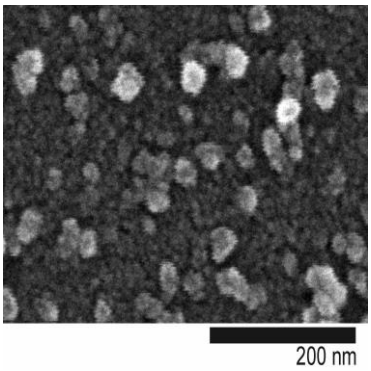

Figure 2-8: *SEM image of AgNP@(**38**) prepared using reaction conditions of #33 in Table 2-3.*

2.3.2.4 Silver nanoparticles derived from sugar triazole (39)

A AgNP array using compound (**39**) was constructed over concentration ranges of 1 µM - 5 mM [(**39**)] and 10 µM - 50 mM [Tollens'] (Table 2-4). The concentration of (**39**) in this array was lower than that used for the preparation of previous arrays due to its high molecular weight and lower solubility in water.

The particle distribution on the array of AgNP@(**39**) showed that ligand (**39**) facilitated the formation of AgNP@(**39**) over much wider concentration ranges of ligand and Tollens' compared to ligands (**22**) and (**23**). This observation revealed that AgNP@(**39**) displayed a significantly weaker dependence on the reaction conditions. All samples which formed silver nanoparticles showed surface plasmon resonance peak ~ 420 nm (Figure 2-9). TEM analysis of several examples in this series produced angular AgNP@(**39**) with similar diameters ranging from 12 ± 1 nm (#22, Figure 2-10a) to 15 ± 2 nm (#24, Figure 2-10b).

Table 2-4: *AgNP@(**39**) screening array prepared using sugar triazole (**39**) and Tollens' reagent. White boxes represent no AgNP formation and yellow boxes represent AgNP formation.*

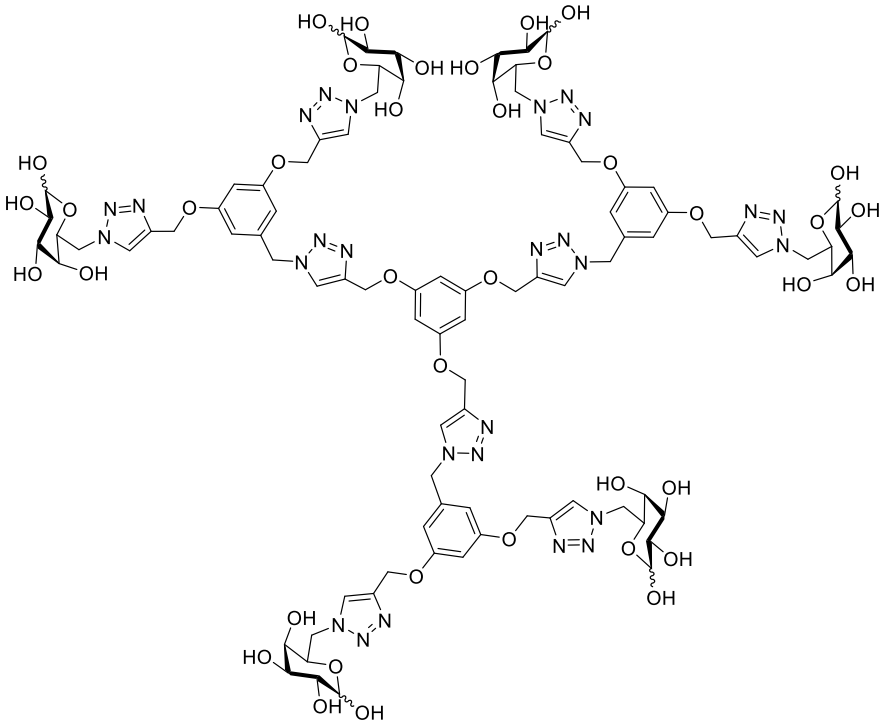

[(39)]

[Tollens']

	5 mM	1 mM	100 µM	10 µM	1 µM
10 µM	#1	#2	#3	#4	#5
100 µM	#6	#7	#8	#9	#10
1 mM	#11	#12	#13	#14	#15
10 mM	#16	#17	#18	#19	#20
20 mM	#21	#22 12 ± 1 nm	#23	#24 15 ± 2 nm	#25
50 mM	#26 13 ± 2 nm	#27	#28	#29	#30

The key conclusion arising from this study was the size tunability observed in the formation of AgNP@(**23**) was significantly reduced when (**39**) was used as a ligand to form AgNP@(**39**). The lack of the tunability was previously observed by Burley *et al*. using large ligand such as (**19**) (Section 1.3.4) which produced 10 ± 2 nm AgNP@(**19**) over a similarly wide concentration range of [(**19**)] and [Tollens'].[87]

This result suggested that triazole ligands using the resorcinol core [i.e., (**39**)] tended to override the influence of the central phloroglucinol core.

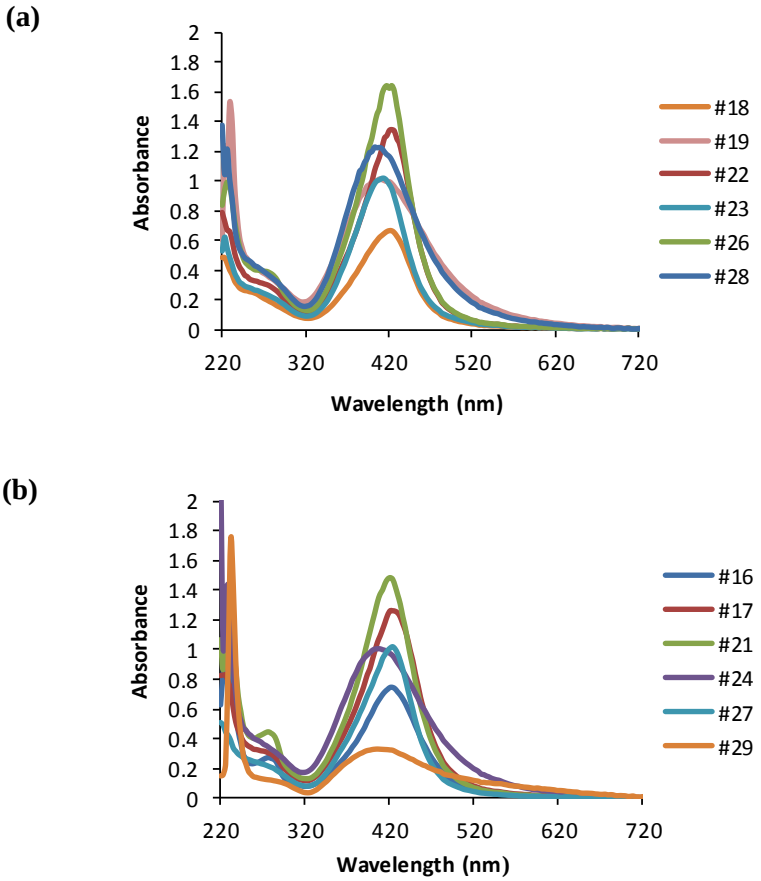

Figure 2-9: *UV-vis spectra of reactions which formed AgNP@(**39**) as observed by a SPR at 420 nm.* ***(a)*** *#18-19, 22-23, 26 and 28;* ***(b)*** *#16-17, 21, 24, 27 and 29. Samples #17-18, 23 and 28 were diluted 1:10, #16 and 21-22 were diluted 1:20 and #27 was diluted 1:50 prior to each measurement.*

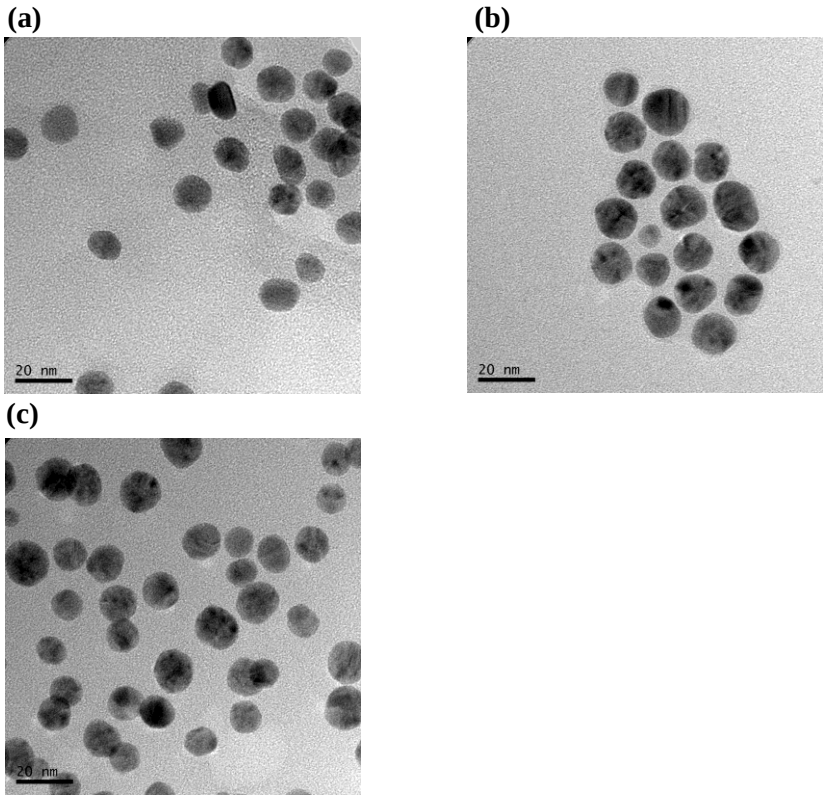

Figure 2-10: *TEM images of AgNP@(**39**) prepared using reaction conditions in Table 2-4.* ***(a)*** *#22, Ø = 12 ± 1 nm;* ***(b)*** *#24, Ø = 15 ± 2 nm;* ***(c)*** *#26, Ø = 13 ± 2 nm.*

2.3.3 Stability of AgNPs in high salt buffers

The preparation of AgNPs that can resist aggregation in the presence of high salts is a key property for the potential utility of these NPs in biological applications. This is an important feature because salts are common reagents for the functionalisation of biomolecules such as DNA. The stability of AgNP@(**22**) and AgNP@(**39**) to increasing concentrations of an aqueous solution of NaCl was tested after 24 hours at room temperature. AgNP@(**22**) remained dispersed in aqueous solutions up to 0.3 M NaCl (Figure 2-11a), whereas AgNP@(**39**) remained dispersed in higher concentration up to 4.5 M (Figure 2-11b). This result supported the study by Burley *et al.* that reported that AgNPs prepared using (**19**) were stable up to 2.8 M, while AgNPs prepared using (**18**) aggregated at 30 mM.[87]

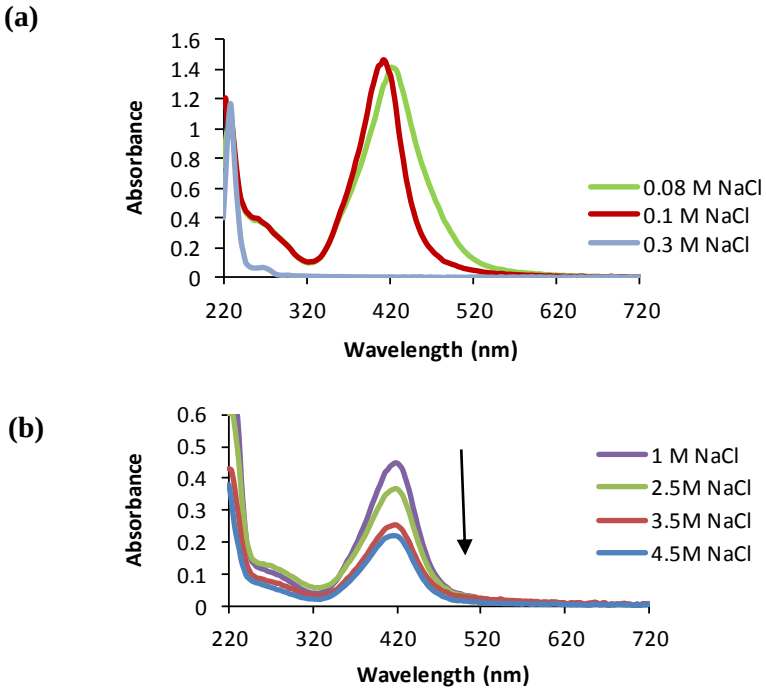

Figure 2-11: *Stability of* ***(a)*** *AgNP@(**22**) and* ***(b)*** *AgNP@(**39**) to increasing concentrations of an aqueous solution of NaCl. Aggregation was observed by a loss of the SPR peak at ~ 420 nm.*

2.3.4 Summary of AgNPs synthesis and properties

AgNPs were prepared in a one-pot method using Tollens' reagent and sugar triazole ligands (**22**), (**23**) and (**39**). Using these ligands, these results highlighted the utility of the phloroglucinol core to form of angular shapes of AgNPs, larger in size to that of spherical AgNPs reported previously using a resorcinol core triazole ligand (**18**).[87] Triazole ligand (**23**) facilitated the formation of monodisperse AgNPs where the size was controlled according to the reaction conditions. Increasing the size of the ligand such as (**39**) reduced size tunability but enhanced the colloidal stability of the resulting particles. Taken collectively, these results suggest that merely increasing the number of reducing equivalents [i.e., number of galactose units] in the system

does not necessarily equate to the formation of monodispersed AgNPs with smaller diameters. Table 2-5 summarises the results of AgNPs formed in this study.

Table 2-5: *Summary of AgNPs formed using ligands (**22**, **23** and **39**).*

Ligand	Tollens' : Ligand	AgNP size (nm)
(**22**)	1 mM : 1 mM (1:1)	21 ± 3
	10 mM : 25 mM (2:5)	17 ± 3
	50 mM : 25 mM (2:1)	18 ± 5
(**23**)	10 mM : 25 mM (2:1)	33 ± 7
	20 mM : 1 mM (20:1)	14 ± 3
	50 mM : 25 mM (2:1)	12 ± 3
(**39**)	20 mM : 1 mM (20:1)	12 ± 1
	20 mM : 10 µM (2000:1)	15 ± 2
	50 mM : 5 µM (10:1)	13 ± 2

The availability of methods to vary the size and shape of AgNPs produced using these new ligands (**22**, **23** and **39**) led to the hypothesis that the nature of the central aromatic core could be influential on the formation of AgNPs. To detect this effect, kinetic experiments and NMR spectroscopic methods were conducted to understand how these ligands bind to Ag(I) and whether the binding affinity of Ag(I) for these ligands can influence the size and shape of formed AgNPs. Mass spectrometric analysis was also used to further explore the chelating properties of these ligands to the silver ions.

2.3.5 The kinetics of AgNP formation

The kinetics of AgNP formation was explored using ligands (**22**), (**23**) and (**39**) by monitoring the onset of the SPR peak at 400 nm using 100 µM [(ligand)] and 10

mM [Tollens']. The onset of formation of AgNP@(**22**) was observed at ~ 180 s with an end-point at ~ 420 s (Figure 2-12). A similar rate of onset of formation of AgNP@(**23**) was also observed but with a slower end-point (570 s). This infers that the southernmost galactose in (**22**) increases the rate of AgNP formation. However, at certain [(**22**)] and [Tollens'], the southernmost galactose sugar destabilises the growth of AgNP formation and can result in Ag mirrors under certain conditions as seen previously in the formation of AgNP@(**22**) (Section 2.3.2.1). The most significant difference in the kinetics of AgNP formation was observed for AgNP@(**39**). A slower rate of onset (~ 192 s) and a significantly slower end-point (~ 1200 s) were observed for the formation of AgNP@(**39**). In contrast to the previous study, an increase in the number of sugars using (**19**) resulted in a virtually identical kinetic profile to the two-sugar ligand system **(18)** [the rate of onset ~ 120 s and end- point ~ 588 s].[87] This could be a contributing factor to the slightly larger observed size of AgNP@(**39**) compared to AgNP@(**19**).

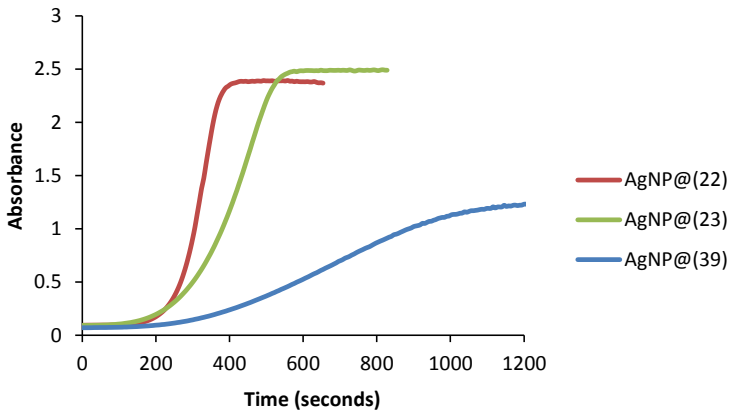

Figure 2-12: *Kinetics of formation of AgNP using (**22**, red), (**23**, green) and (**39**, blue) as monitored by the formation of the SPR peak at 400 nm.*

2.3.6 NMR spectroscopic experiments

The chemistry of triazoles has been a great interest due to their ability to act as N-donor ligands to coordinate with metals such as Ag(I).[105-107] The chelating properties of these type of ligands allow prediction of the mechanism of AgNP formation using sugar triazole ligands in the presences of Ag(I) as reported by Burley *et al.*[87] In this study, ^{1}H NMR titrations were used to evaluate the complexation behaviour of Ag(I) to the triazole groups by studying the changes in chemical shift of ^{1}H NMR signals with increasing concentration of $AgNO_3$. Triazole protons (H^c/H^d) and aromatic protons (H^e) were used as diagnostic markers of Ag(I) coordination (Figure 2-13).

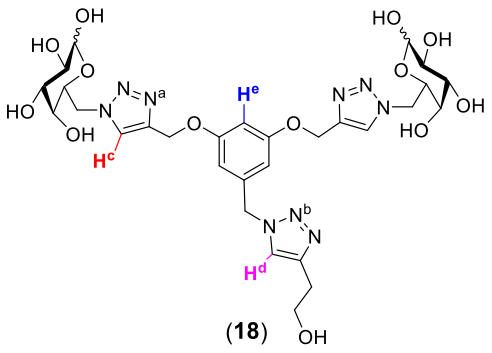

Figure 2-13: *Triazole protons (H^c/H^d) and aromatic proton (H^e) used as diagnostic markers in ^{1}H-NMR titration study.*

A ^{1}H NMR titration study using (**18**) revealed a significant downfield shift (0.2 ppm) for both H^c and H^d upon the addition of one equivalent of Ag(I). This downfield shift of H^d reached a maximum at a Ag(I):(**18**) ratio of 1:1, whereas the downfield shift of H^c reached maximum at a 2:1 Ag(I):(**18**) ratio. This suggested that in the presence of one equivalent of Ag(I), all three triazole units were participating in the coordination of a single Ag(I) cation. In contrast, an upfield shift of the aromatic H^e in (**18**) was observed upon the addition of one equivalent of Ag(I) followed by a gradual return to its original position after the addition of six equivalents of Ag(I).[87]

A ^{1}H NMR titration study using ligands (**22**) and (**23**) in the presence of up to six equivalents of $AgNO_3$ was conducted in order to gain further insight into the Ag(I) binding characteristics. Triazole protons (H^f) and aromatic protons (H^g) of (**22**) were used as diagnostic markers of Ag(I) coordination (Figure 2-14). Titration of up to one equivalent of Ag(I) resulted in a significantly smaller downfield shift (0.04 ppm) of H^f compared to that observed for H^c/H^d in (**18**). A further marked divergence in Ag(I)-chelating behaviour between (**18**) and (**22**) was the observation of a further 0.08 ppm downfield shift of H^f in (**22**) upon the addition of six equivalents of Ag(I). The behaviour of aromatic H^g in (**22**) was also divergent from H^e in (**18**). A 0.16 ppm upfield shift of the aromatic H^g was observed upon the addition of up to three equivalents of Ag(I). Surprisingly, the chemical shift of this proton did not change as H^g after addition of a further three equivalents of Ag(I).

A ^{1}H NMR titration was then conducted using ligand (**23**). A similar Ag(I)-chelating behaviour to (**22**) was observed using triazole (H^h/H^j) and aromatic protons (H^i) of (**23**) as diagnostic markers of Ag(I) coordination (Figure 2-15). Titration of up to one equivalent of Ag(I) resulted a downfield shift (0.04 ppm) of (H^h/H^j), similar to that observed for H^f in (**22**). A further 0.1 ppm downfield shift was observed up to the addition of six equivalents Ag(I). A 0.18 ppm upfield shift of the aromatic H^i was observed upon the addition of up to three equivalents of Ag(I), again consistent with that observed for H^g in (**22**).

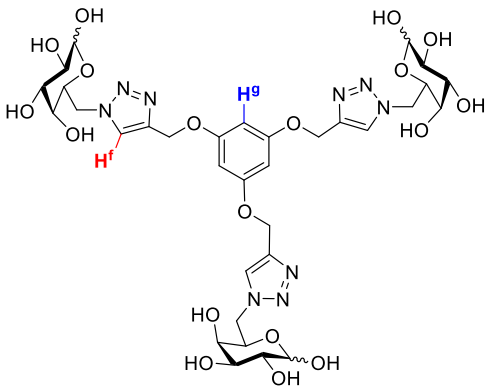

(**22**)

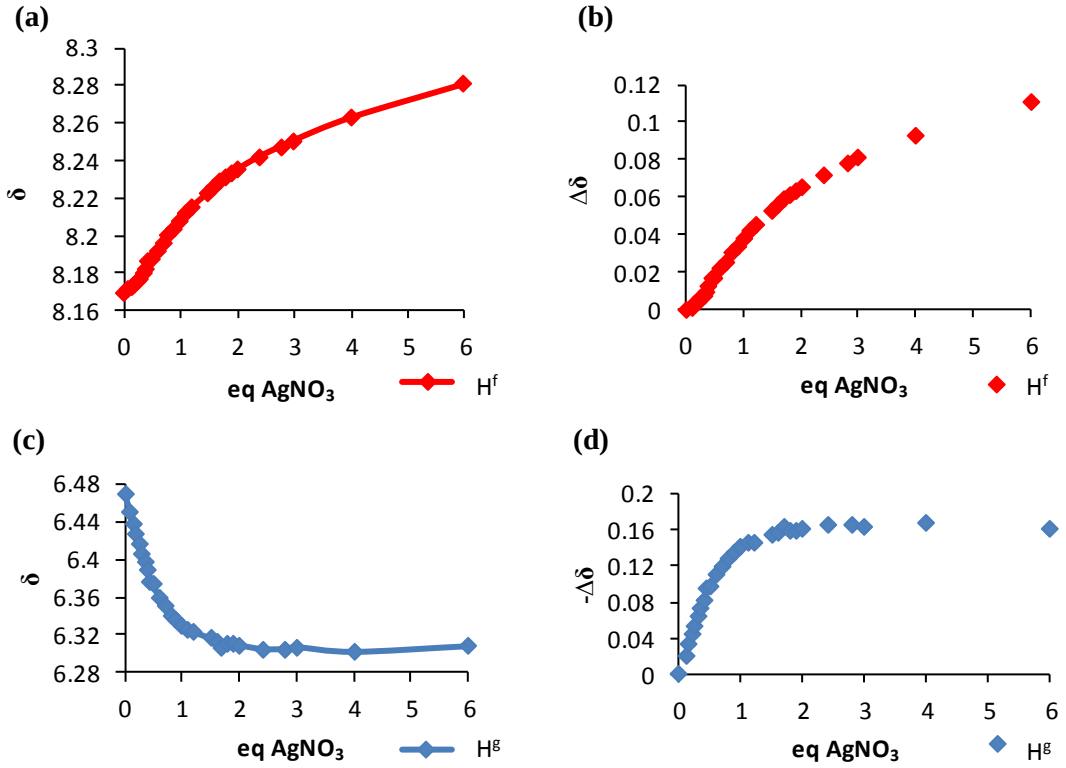

Figure 2-14: *Plots of the ^{1}H-NMR titration of sugar triazole ligand (**22**) with an increasing amount of $AgNO_3$ in D_2O.* ***(a** and **c)** Plots of the ^{1}H-NMR titration of H^f and H^g with $AgNO_3$.* ***(b** and **d)** Change in chemical shift of H^f and H^g as a function of $AgNO_3$.*

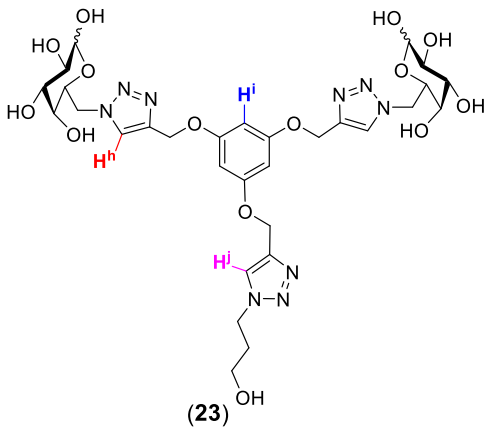

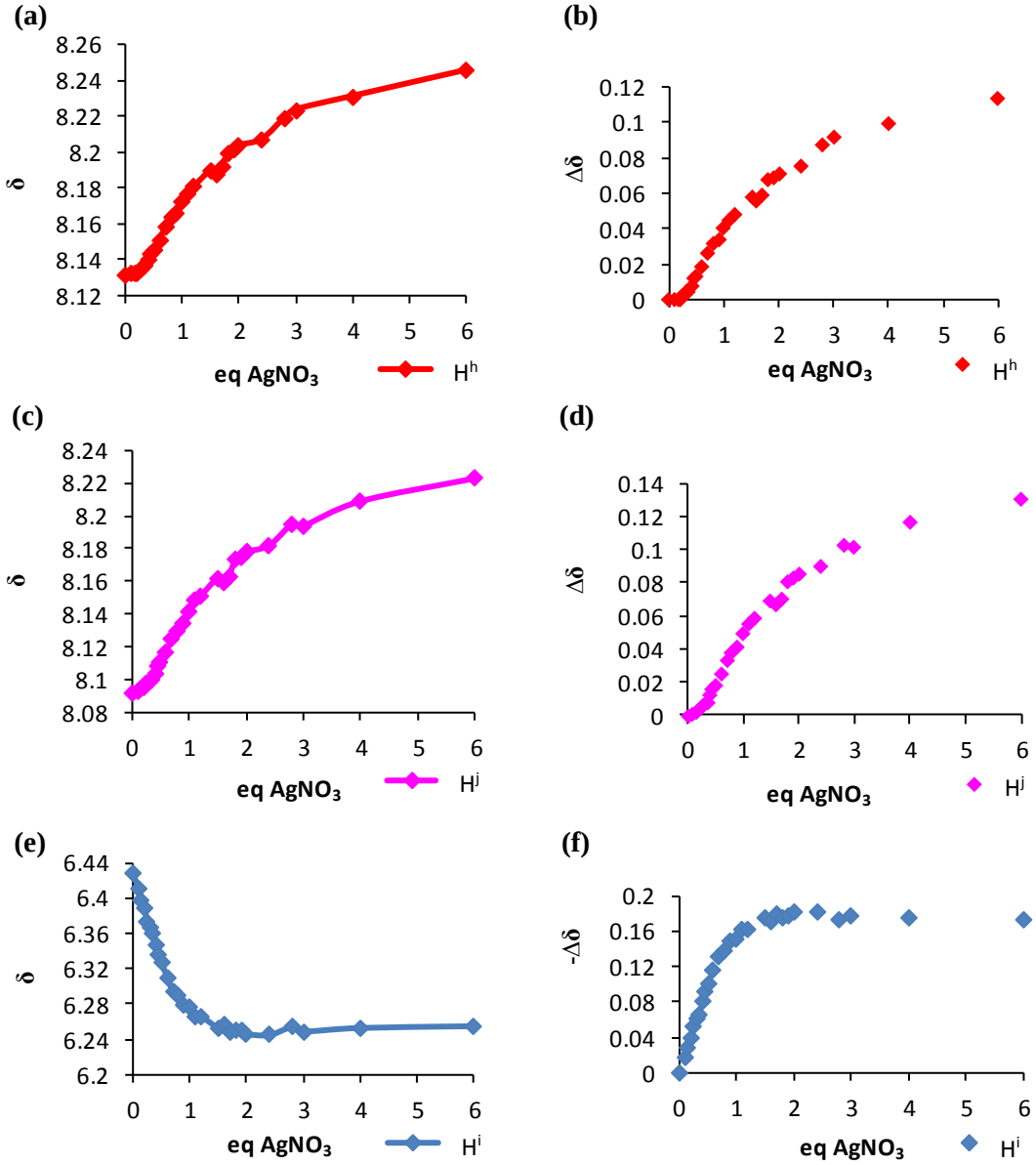

Figure 2-15: *Plots of the ^{1}H-NMR titration of sugar triazole ligand (**23**) with an increasing amount of $AgNO_3$ in D_2O.* ***(a, c** and **e)*** *Plots of the ^{1}H-NMR titration of H^h, H^j and H^i with $AgNO_3$.* ***(b, d** and **f)*** *Change in chemical shift of of H^h, H^j and H^i as a function of $AgNO_3$.*

Taken collectively, the small downfield shift of triazole protons in ligands (**22**) and (**23**) compared with (**18**) suggested that the Ag(I)-binding affinity of these ligands was weaker and markedly different to (**18**). To test this hypothesis, the binding affinity of Ag(I) for ligands (**22**) and (**23**) was calculated in collaboration with Ruggero Dondi using non-linear least squares fitting computer models (Table 2-6).[108,109] The acquired ^{1}H NMR data of the triazole sugar ligands and the concentration of the Ag(I) was used to calculate the Ag(I) binding constants using WinEQNMR2 software.

Table 2-6: *Ag(I) binding constant of (**22-23**) calculated by non-linear curve fitting of ^{1}H NMR chemical shift data of the triazole protons using the software program WinEQNMR2.*[108]

Compound	**K** (M^{-1})	**Log K**
(**22**)	533 ± 22	2.727 ± 0.018
(**23**)	743 ± 69	2.871 ± 0.040

A significant observation of Ag(I) binding affinity of these ligands compared with previous study is that K values of (**22**) and (**23**) were much smaller than (**18**) with K ~ 72 393 ± 38011 M^{-1}.[87,109] Ligand (**18**) has a Ag(I) binding affinity 136 times higher than ligand (**22**) and 97 times higher than ligand (**23**) (Table 2-6).

All of these observations combined with kinetic results suggested the effect of Ag(I) binding affinity of triazole sugar ligands plays an influential role on the formation of AgNPs. As a consequence of the significantly higher Ag(I)-binding affinity, the rate of nucleation of (**18**) (120 s) is faster than in (**22**) (180 s). While this increase in binding affinity in (**18**) increases the rate of Ag nucleation, the rate of growth of these nuclei into AgNP@(**18**) slows down compared to AgNP@(**22**) as reflected by the longer end-point of (**18**) (588 s) relative to (**22**) (420 s). In the case of

AgNP@(**18**), we assume that the increase in Ag(I)-binding affinity would produce a larger population of Ag nuclei in complex with (**18**) compared to (**22**) in the initial nucleation stages, however once these nuclei are formed, the rate of growth of these nuclei into AgNPs slows down. The slower rate of growth of AgNP@(**18**) was similar to AgNP@(**23**) as reflected by end-point (570 s) while ligand (**23**) exhibited smaller binding affinity. At present, it is not clear if this slower growth rate is directly related to the binding affinity of Ag clusters to these ligands, and this aspect will be a subject of further investigation.

In conclusion, subtle changes in the ligand cores significantly alter the overall Ag(I) binding behaviour. The binding properties of these ligands have been well studied in literature, however, to the best of our knowledge, there have been no reports highlighting the role of Ag(I) binding affinity to tune the size and shape of the resultant AgNPs formed. This study showed that weaker Ag(I) binding ligands using phloroglucinol core triazole ligands (**22**) and (**23**) can be used to form monodisperse angular AgNPs over wider a range of sizes (12 ± 3 nm - 33 ± 7 nm), whereas resorcinol core triazole ligand (**18**) exhibiting a high Ag(I) binding affinity produce monodisperse spherical AgNPs of a single size (8 ± 5 nm).

2.3.7 Probing AgNP formation using non-sugar triazole

In order to compare the differences in Ag(I) binding of the two core scaffolds in more detail, (**51**) and (**52**) were prepared in which galactose sugars in (**23**) and (**18**) were replaced with aliphatic alcohol chains (Figure 2-16). The synthesis of these ligands allowed the investigation of how the Ag(I)-binding affinity is influenced by the galactose sugar units. In particular, if these ligands show a significant difference

in binding constants, it can be said that the sugar units did not affect the binding behaviour of sugar triazole ligands during the early stages of the synthesis of AgNPs.

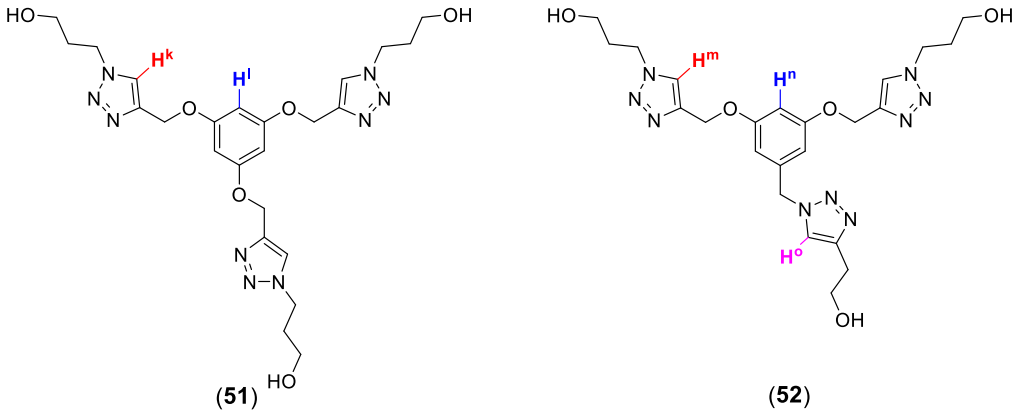

Figure 2-16: *Structures of triazole control molecules (**51**) and (**52**). Red and pink colours represent triazole protons and blue colour represents aromatic protons used as diagnostic markers in ^{1}H-NMR titration study.*

2.3.7.1 Synthesis of triazole ligand (51)

Compound (**51**) was prepared by a one-pot two-step azidation and copper-catalysed Huisgen [3+2] cycloaddition using 3-iodo-1-propanol to prepare azide *in situ* (Scheme 2-8).[110] This reaction was conducted using thermal heating (reflux) instead of microwave irradiation as per the original report. The crude mixture was diluted with H_2O followed by washing with DCM. Unfortunately after work up, the desired compound dissolved in both the organic and the aqueous layers. Therefore, it was difficult to purify the desired compound and alternative procedure was sought.

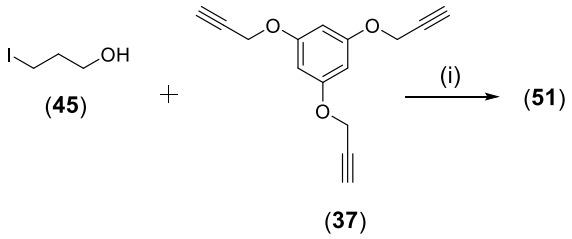

Scheme 2-8: *Reagents and conditions: (i) Compound (**45**) (3.2 equiv.), NaN_3 (3.2 equiv.), Cu(0) (0.8 equiv.), $CuSO_4$ (1M), t-BuOH:H_2O (1:1), Δ, 135°C, 24h.*

An alternative approach was used to prepare (**51**) in three steps under standard azide-alkyne Huisgen cycloaddition conditions (Scheme 2-9). The first step was the reaction of azido propanol (**46**) with acetic anhydride and triethylamine to afford azido-propyl acetate (**53**) in 78% as a yellow oil. A click reaction between (**53**) and (**37**) afforded (**54**) as a yellow solid after purification by column chromatography. Then, base-mediated acetyl deprotection and purification by RP-HPLC afforded the trihydroxylated ligand (**51**) in 50% yield.

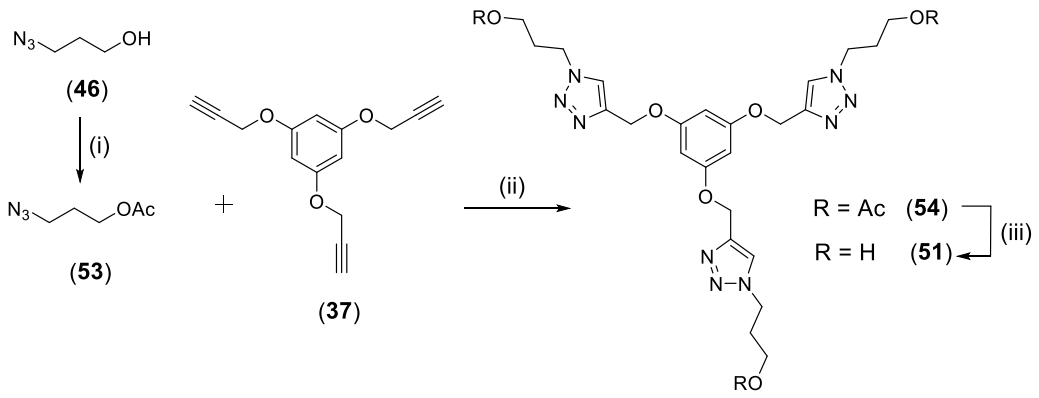

Scheme 2-9: *Reagents and conditions: (i) Acetic anhydride (5.0 equiv.), Et_3N (5.0 equiv.), DCM, RT, 24h, 78%; (ii) Compound (**53**) (11.2 equiv.), $CuSO_4$ (0.14 M, 0.72 equiv.), sodium ascorbate (4.4 equiv.), THF:H_2O (3:1), RT, 24h; (iii) ammonia in methanol (2 M), Δ, 40°C, 24h, 50% over 2 steps.*

2.3.7.2 Synthesis of triazole ligand (52)

Ligand (**52**) was prepared by triazole formation between (**32**) and three equivalents of (**53**) in the presence of copper(I) to yield (**55**). Chloride displacement of (**55**) using NaN_3 yielded azide (**56**). Deprotection of the acetyl groups of (**56**) with ammonia produced the dihydroxylated compound (**57**). The installation of the southernmost triazole group was achieved by a click reaction between (**57**) and 3-butyn-1-ol (**58**) using an immobilised copper(I) species PS-NHC-Cu(I) (**59**) in 31% yield (Scheme 2-10). The copper catalyst was prepared in three steps according to a known

procedure using Merrifield resin (**60**) instead of activated SiO_2-Cl (Scheme 2-11).[111]

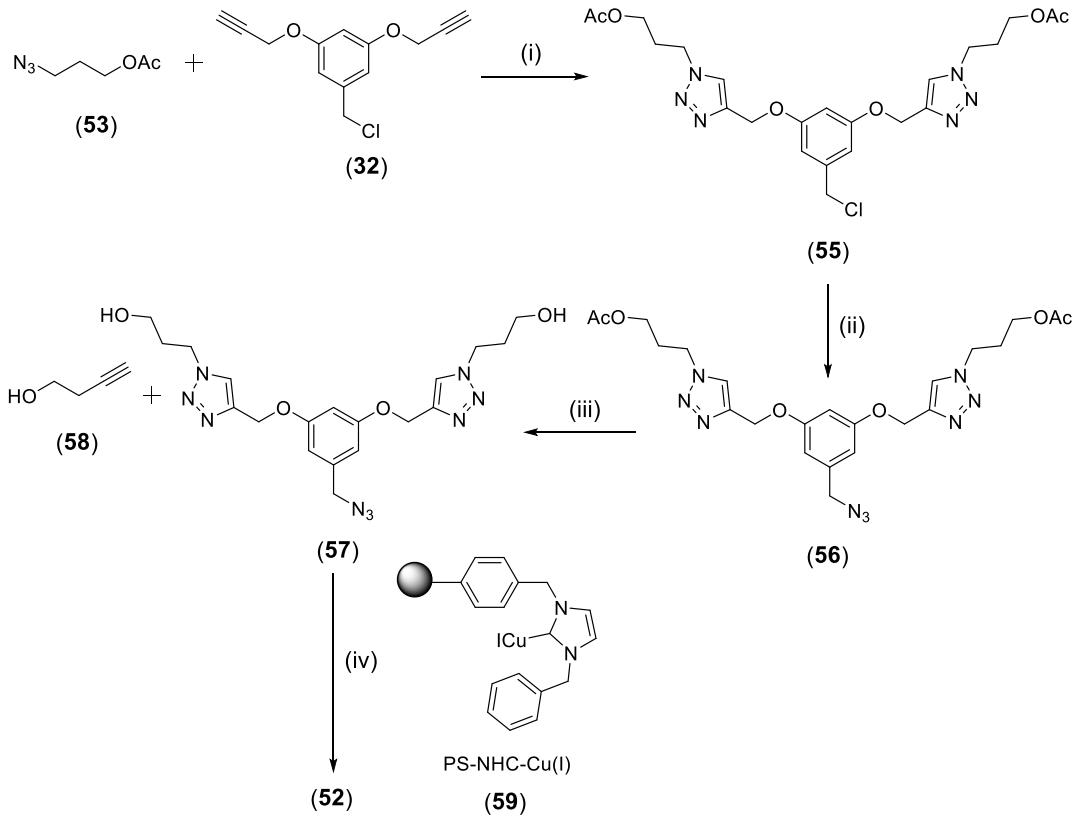

Scheme 2-10: *Reagents and conditions: (i) Compound (**53**) (3.0 equiv.), $CuSO_4$ (0.08 M, 0.3 equiv.), sodium ascorbate (2.0 equiv.), THF:H_2O (3:1), RT, 24h, 76%; (ii) NaN_3 (10 equiv.), acetone:H_2O (4:1), Δ, 3h, 87%; (iii) ammonia in methanol (2 M), Δ, 40°C, 24h, 99%; (iv) (**58**) (3.0 equiv.), (**59**) (1.1 equiv.), DMSO, RT, 24h, 31%.*

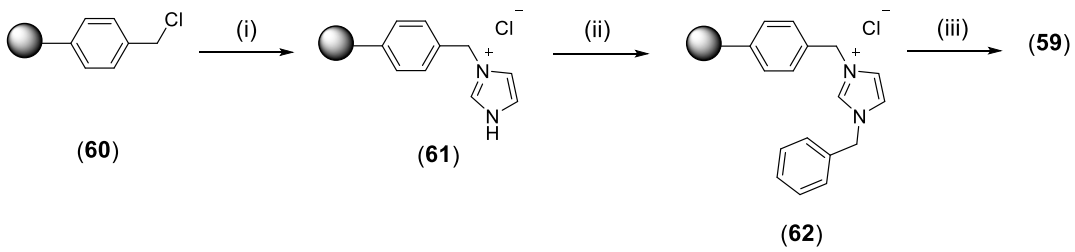

Scheme 2-11: *Reagents and conditions: (i) imidazole (4.3 equiv.), toluene, Δ, 80°C, 24h; (ii) benzyl bromide (4.3 equiv.), toluene, Δ, 110°C, 24h; (iii) CuI (1.07 equiv.), t-BuOK (1.07 equiv.), THF, RT, 24h.*

2.3.7.3 ^{1}H NMR titration experiments using triazole ligand controls

A comparative analysis of the Ag(I)-binding characteristics of ligands (**51**) and (**52**) by ^{1}H NMR titration with $AgNO_3$ was conducted using the method as described previously in sugar ligands (Section 2.3.6). Titration of up to one equivalent of Ag(I) resulted in a 0.04 ppm downfield shift of the traizole proton H^k in (**51**) (Figure 2-17b). A further 0.1 ppm downfield shift was observed upon the addition of a further three equivalents of Ag(I). For ligand (**52**), titration of up to one equivalent of Ag(I), a 0.06 ppm downfield shift of H^m and a 0.02 ppm downfield shift of H^o was observed (Figure 2-18b, d). A further downfield shift of 0.1 ppm in H^m and 0.07 ppm in H^o occurred upon the addition of a further three equivalents of Ag(I). For the aromatic protons, a 0.2 ppm upfield shift of H^l in (**51**) and H^n in (**52**) was observed upon the addition of up to three equivalents of Ag(I) (Figure 2-17d and Figure 2-18f).

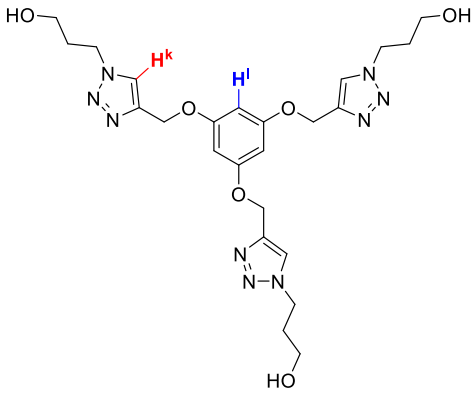

(**51**)

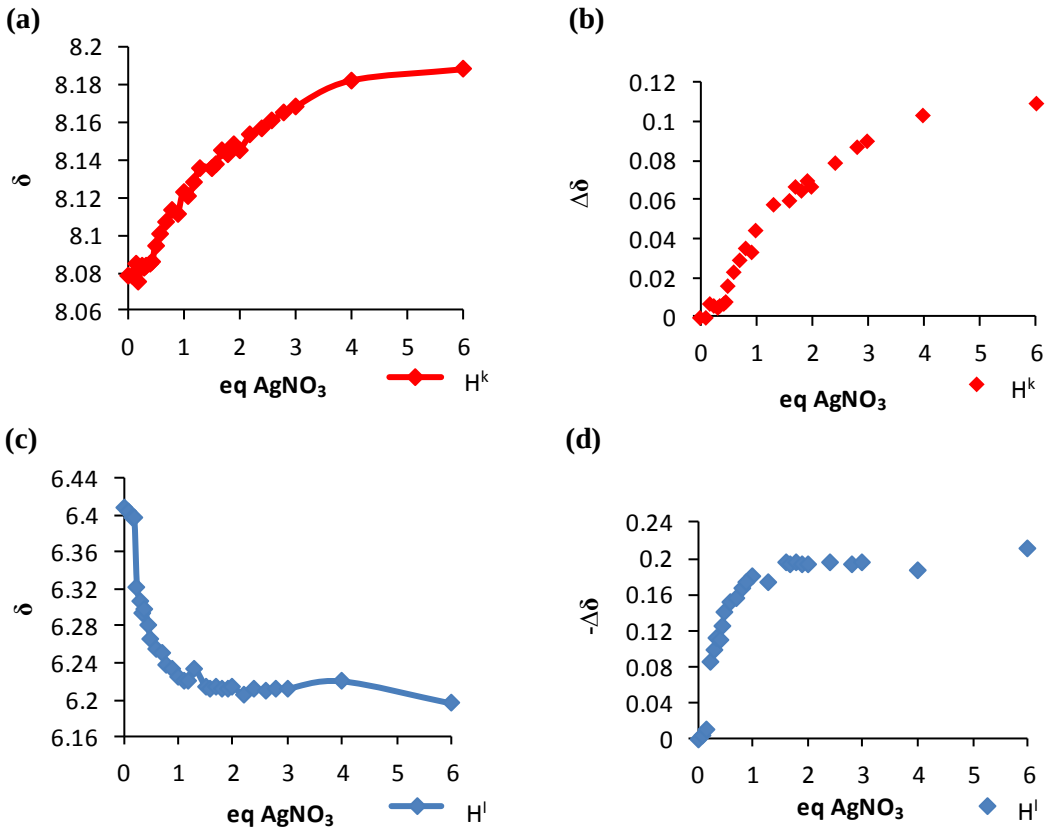

Figure 2-17: *Plots of the ^{1}H-NMR titration of sugar triazole ligand (**51**) with an increasing amount of $AgNO_3$ in D_2O.* ***(a** and **c)** Plots of the ^{1}H-NMR titration of H^k and H^l with $AgNO_3$.* ***(b** and **d)** Change in chemical shift of H^k and H^l as a function of $AgNO_3$.*

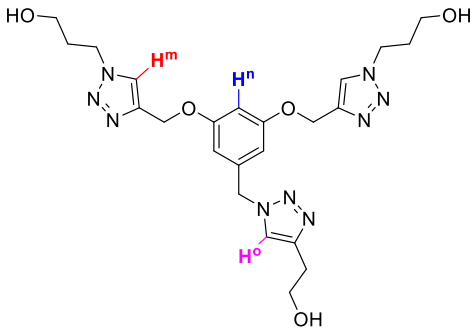

(**52**)

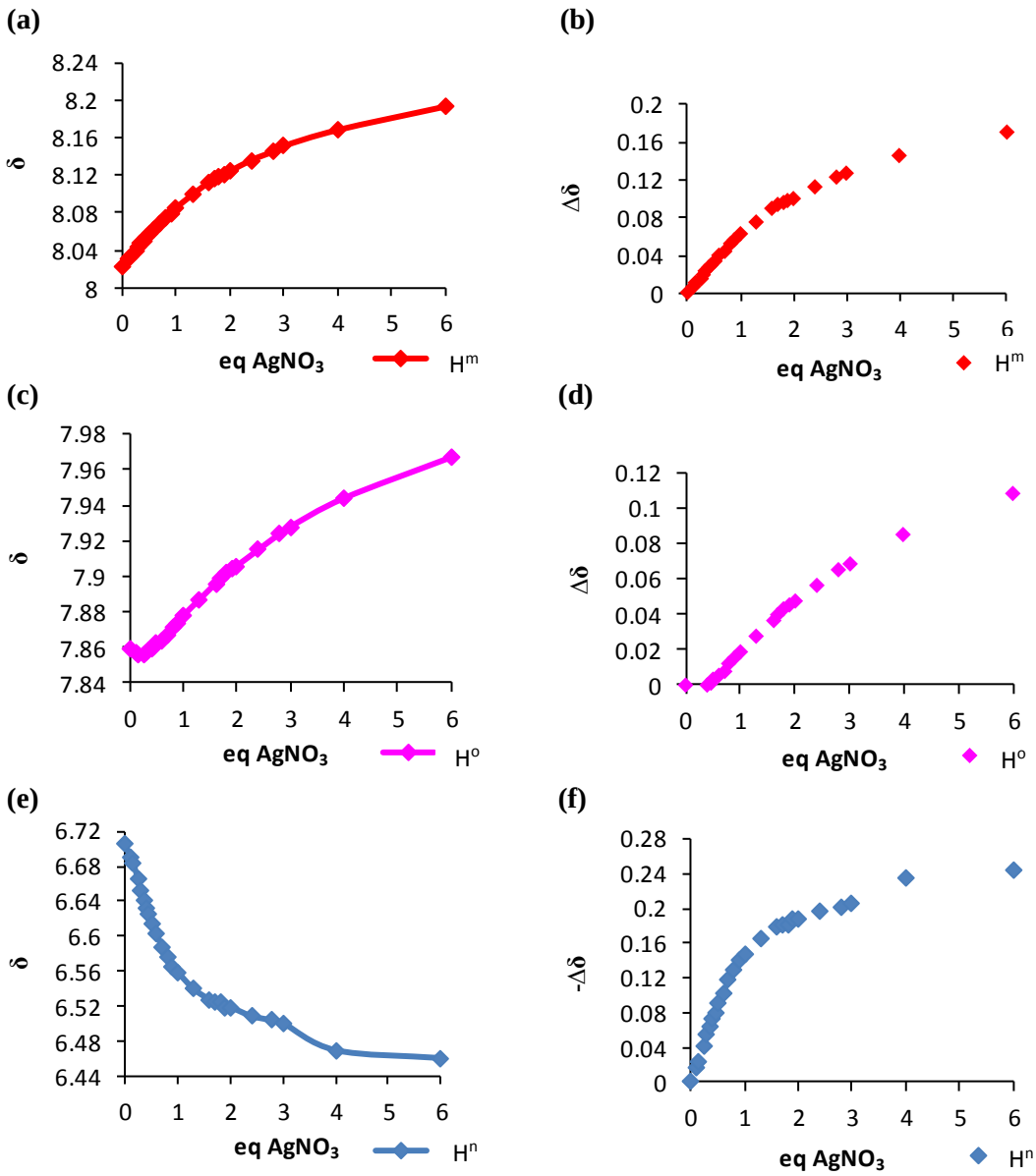

Figure 2-18: *Plots of the ^{1}H-NMR titration of sugar triazole ligand (**52**) with an increasing amount of $AgNO_3$ in D_2O.* ***(a, c** and **e)*** *Plots of the ^{1}H-NMR titration of H^m, H^o and H^n with $AgNO_3$.* ***(b, d** and **f)*** *Change in chemical shift of of H^m, H^o and H^n as a function of $AgNO_3$.*

The binding affinity of Ag(I) for ligands (**51**) and (**52**) was then calculated by WinEQNMR2 software (Table 2-7).[108]

Table 2-7: *Ag(I) binding constant of (**51-52**) calculated by non-linear curve fitting of ^{1}H NMR chemical shift data of the triazole protons using the software program WinEQNMR2.*[108]

Compound	**K** (M^{-1})	**Log K**
(**51**)	794 ± 105	2.900 ± 0.057
(**52**)	489 ± 14	2.689 ± 0.012

An unexpected result was the higher binding constant of (**51**) (794 ± 105 M^{-1}) compared to (**52**) (489 ± 14 M^{-1}). This result was inconsistent with sugar triazole ligands because it shows that the phloroglucinol core structure has a higher affinity of Ag(I) compared to the resorcinol core. Crucially, when the galactose sugars replaced aliphatic alcohol chains [i.e., (**52**) → (**18**)], the binding affinity increased markedly, whereas a similar binding affinity was observed when the structure was changed from (**51**) → (**23**). The significant reduction in Ag(I) binding affinity of (**52**) compared to ligand (**18**), suggests that the two northernmost galactose sugars in (**18**) collectively enhance Ag(I) binding. However, Burley *et al.* reported that the southern triazole is essential for AgNP formation.[87] In this study, a AgNPs array using ligand (**63**) (Figure 2-19) and Tollens' reagent was prepared which produced Ag aggregates instead of stable colloidal particles. Therefore, all of these results conclude that the three triazoles and the sugars work in concert to bind Ag(I).

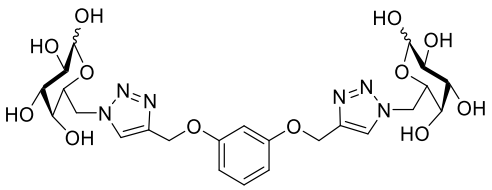

(**63**)

Figure 2-19: *Structure of sugar triazole ligand (**63**) used to study the effect of the absence of the third triazole on the formation of AgNPs.*

2.3.7.4 Preparation of AgNP with triazole ligand control

In order to investigate the importance of linked reducing sugar species in the formation of AgNPs, a new array was conducted using ligand (**51**) and Tollens' reagent in the presence of three equivalents of galactose (Table 2-8). A ratio of galactose:(**51**) (3:1) was chosen as this correlated to the same stoichiometry of reducing sugars in (**22**). Surprisingly, no AgNPs were formed over all concentrations of (**51**) and Tollens' surveyed. Figure 2-20b indicates the absence of the formation of AgNPs. Therefore, the covalent attachment of galactose sugars to the triazole scaffold is essential for these ligands to facilitate AgNP formation.

Table 2-8: *AgNP screening array prepared using (**51**+galactose) and Tollens' reagent. Grey boxes represent the formation of silver mirrors.*

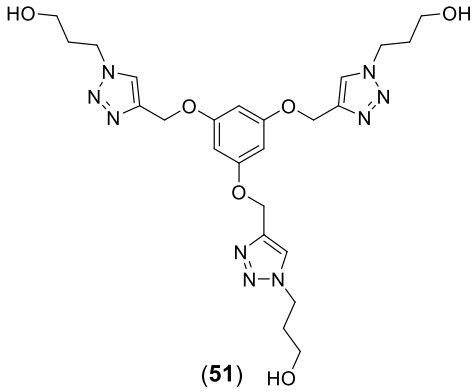

(**51**)

[(51)+Galactose]

[Tollens']

	25 mM of (**51**) + 75 mM of galactose	10 mM of (**51**) + 30 mM of galactose	1 mM of (**51**) + 3 mM of galactose	100 µM of (**51**) + 300 µM of galactose	10 µM of (**51**) + 30 µM of galactose
1mM	#1	#2	#3	#4	#5
10mM	#6	#7	#8	#9	#10
20mM	#11	#12	#13	#14	#15
50mM	#16	#17	#18	#19	#20

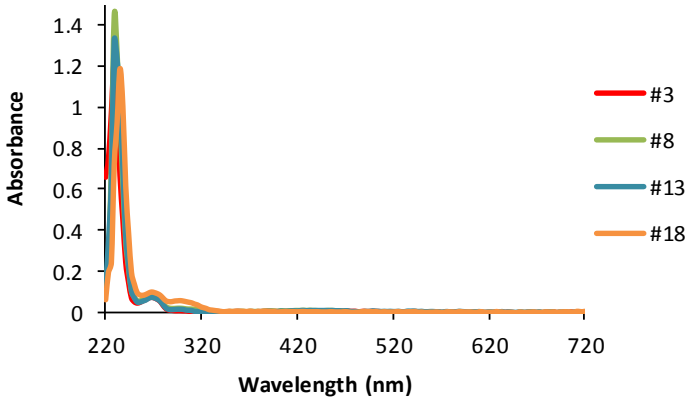

Figure 2-20: *UV-vis spectra of reactions #3, 8, 13 and 18 using reaction conditions in Table 2-8.*

2.3.8 Mass spectrometric analysis

The final analysis presented in this chapter is ESI-MS analysis of the Ag(I)-binding using sugar triazole ligands (**22**), (**23**) and (**39**). In this technique, a mixture of ligand and $AgNO_3$ solutions in water:MeOH (9:1) were injected into an ESI-MS spectrometer to detect the ions of silver complexes. ESI-MS analysis of (**22**) in complex with one equivalent of Ag(I) resulted in the predominant formation of the $[M+Ag]^+$ ion (*m/z* 962) (Appendix A1a). A minor amount of the 2:1 (**22**)•Ag(I) complex $[2M+Ag]^+$ at *m/z* 1819 was observed, indicative of the formation of a metallocyclic species as reported previously by Crowley *et al.* using other Ag(I)-chelating triazole ligands.[105-107] The $[M+Ag]^+$ ion still predominated in the presence of two equivalents of Ag(I); however the formation of a small amount of $[M+2Ag-H]^+$ at *m/z* 1070 was also observed (Appendix A1b). Increasing the number of equivalents of Ag(I) up to four afforded a range ions corresponding to $[M+Ag]^+$, $[M+2Ag-H]^+$ and $[M+3Ag-2H]^+$, but with the 1:1 complex still predominating (Appendix A1d). Thus in the presence of one equivalent of Ag(I), ligand (**22**) predominantly formed (**22**)•Ag(I) complex with a 1:1 stoichiometry. Increasing the number of equivalents of Ag(I) resulted in the formation of a range of other minor Ag(I)-chelating species.

ESI-MS analysis of the Ag(I)-chelating properties was then investigated using ligand (**23**). A molecular ion $[M+Na]^+$ with *m/z* 774 was the predominant species when one equivalent of Ag(I) was added to (**23**). A minor amount of $[M+Ag]^+$ at *m/z* 860 was also observed (Appendix A2a). The $[M+Ag]^+$ peak was the predominant species in the presence of two equivalents of Ag(I) (Appendix A2b). As the number of equivalents of Ag(I) was increased up to four, the $[M+Ag]^+$ ion still predominated

with the formation of a small amount of $[M+2Ag-H]^+$ at *m/z* 966 and a complete loss of $[M+Na]^+$ at *m/z* 774 (Appendix A2d).

ESI-MS analysis of the Ag(I)-chelating properties was then investigated using ligand (**39**). The major molecular ion was *m/z* 1205 corresponding to $[M+2Ag]^{2+}$ when one equivalent of Ag(I) was added to (**39**). A series of other minor adducts were also observed in the mixture, such as *m/z* 2303 $[M+Ag]^+$ and 839 $[M+3Ag]^{3+}$ (Appendix A3a). The wide range of molecular ions observed in this ligand complex was in stark contrast to the predominant $[M+Ag]^+$ observed in the 1:1 (**22**)•Ag(I) complex. As the number of equivalents of Ag(I) was increased from one up to six, the $[M+3Ag]^{3+}$ peak became more pronounced (Appendix A3d). At 7.5 equivalents of Ag(I), $[M+3Ag]^{3+}$ was the dominant peak in the spectrum with a complete loss of $[M+Ag]^+$ at *m/z* 2303 (Appendix A3e). The Ag(I)-binding behaviour of ligand (**39**) therefore diverges quite markedly from (**22**) and (**23**) by its ability to chelate a much wider dynamic range of Ag(I) ions. This Ag(I) binding behaviour also varies according to the stoichiometric ratio of ligand (**39**).

2.4 Conclusion

Using copper-catalysed click chemistry, sugar triazole ligands (**18-19**) were prepared by Burley *et al.* as a template for the synthesis of size- and shape-controlled AgNPs using Tollens' reagent. This chapter reported the synthesis of sugar triazole ligands (**22-23** and **38-39**) for the study of the structural parameters of these ligands in the templated synthesis of AgNPs. The structure of the central core was critical to control the size and shape of formed AgNPs. Phloroglucinol ligands (**22**) and (**23**) that display weaker Ag(I) binding affinity produced angular AgNPs that were larger in diameter than spherical AgNPs prepared by using resorcinol ligand (**18**) with high

Ag(I) binding affinity. The sizes of the AgNPs formed using (**23**) were inherently tunable and dependent on the reaction conditions. The use of tertiary amine ligand (**38**) resulted in no formation of AgNPs, showing that the aromatic core is important in this synthesis. Ligand (**39**) was a highly versatile ligand that can be used to form stable suspensions of AgNPs in high salt buffers.

2.5 Experimental

Silver nitrate (99.9999% and NH_4OH (28%) were purchased from Sigma Aldrich. UV-Vis measurements were acquired in ultrapure H_2O using a Thermo-Scientific Nanodrop 1000. Time-course kinetics experiments were acquired using a Varian CaryWin 300Bio UV-Visible spectrometer. Electron microscopy images were taken using an FEI Tecnai T20 TEM and a Hitachi S4700 SEM. High resolution mass spectrometry was performed on a Water Acquity XEVO QToF machine. Elemental analysis was performed on PerkinElmer 2400 Series 2. Nuclear magnetic resonance (NMR) (^{1}H and ^{13}C) spectra were recorded using a Bruker 400 and 500 MHz spectrometer. Analytical and semi-preparative RP-HPLC were performed at room temperature on an ULTIMAT 3000 Instrument (DIONEX). UV absorbance was measured using a photodiode array detector at 210 and 260 nm. An ACE C18 column (4.6 × 250 mm, 5 μm, 300 Å) was used for analytical RP-HPLC. A solvent gradient of increasing amount of MeCN was used for HPLC of compounds (**22-23, 38-39** and **51-52**). A typical gradient started with 90% H_2O (solvent A) and 10% MeCN (solvent B). This was held at 2 min, then increased to 90% solvent B over 20 min. For semi-preparative HPLC, an ACE C18 column (21.2 × 250 mm, 5 μm, 300 Å) was used.

2.5.1 Synthesis of sugar triazole (22)

Synthesis of 1,3,5-tris(prop-2-yn-1-yloxy)benzene (37)[103]

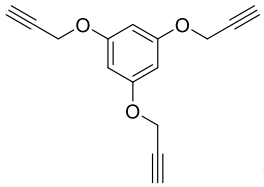

To a stirred solution of propargyl bromide (80% in toluene, 42.45 g, 357 mmol) and anhydrous potassium carbonate (44.39 g, 321 mmol) in DMF (100 mL) was added a solution of phloroglucinol (**36**) (10.00 g, 79 mmol) in DMF (60 mL) dropwise in 30 min. The reaction mixture was stirred for 4 days at room temperature. The mixture was filtered and the filtrate concentrated *in vacuo* to a small volume. The crude residue was diluted with DCM (400 mL) and the organic layer washed with H_2O (3 × 100 mL), followed by brine (3 × 100 mL). The organic layer was then dried over Na_2SO_4, filtered and concentrated *in vacuo.* Purification by column chromatography (SiO_2) eluting with 1:3 Et_2O:hexane followed by recrystallisation from Et_2O:petroleum ether afforded 1,3,5-tris(prop-2-yn-1-yloxy)benzene (**37**) (9.50 g, 50%) as a cream coloured powder.

GC-MS (EI) *m/z*: $[M + H]^+$ 241.

MP. 80-81°C.

^{1}H NMR ($CDCl_3$, 500 MHz): δ 2.54 (t, 3H, *J* = 2.4 Hz, C≡CH), 4.66 (d, 6H, *J* = 2.4 Hz, CH_2), 6.28 (s, 3H, Ar).

^{13}C NMR ($CDCl_3$, 100 MHz): δ 56.2 (CH_2, 3C), 75.9 (C≡**C**H, 3C), 78.5 (**C**≡CH, 3C), 95.7 (Ar-CH, 3C), 159.6 (Ar-C, 3C).

Synthesis of 1,2,3,4-di-O-isopropylidene-6-mesyloxy-6-deoxy-α-D galactopyranose (41)[104]

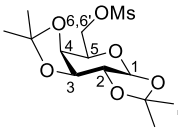

To a stirred solution of 1,2-3,4-diacetonide-6-hydroxy-galactopyranose (**40**) (25.00 g, 96 mmol) in anhydrous THF (300 mL) at 0°C was added mesityl chloride (44.06 g, 385 mmol, 29.89 mL) followed by DIEA (49.62 g, 385 mmol, 66.87 mL) dropwise. The reaction mixture was stirred overnight at room temperature. The mixture was then quenched by addition of cold water (150 mL), concentrated *in vacuo* to a small volume and extracted with EtOAc (500 mL). The organic phase was washed with HCl 0.1 M (2 × 100 mL), followed by $NaCO_3$ sat. (2 × 100 mL) and brine (2 × 100 mL). The organic layer was then dried over Na_2SO_4, filtered and concentrated *in vacuo*. The product was then suspended in hexane (50 mL), sonicated for 20 min and dried under vacuum overnight to afford 1,2-3,4-diacetonide-6-mesyloxy-galactopyranose (**41**) (31.20 g, 96%) as a yellow powder. LRMS (ESI) *m/z*: $[M + Na]^+$ 361.

MP. 135-136°C.

^{1}H NMR (DMSO-d_6, 400 MHz): δ 1.29 (s, 6H, CH_3), 1.36 (s, 3H, CH_3), 1.45 (s, 3H, CH_3), 3.20 (s, 3H, CH_3S), 3.97-3.40 (m, 1H/H_5), 4.15 (dd, 1H, J = 8.1, 11.0 Hz, H_6'), 4.29 (dd, 1H, J = 1.9, 7.9 Hz, H_4), 4.35-4.40 (m, 2H, H_2/H_6), 4.64 (dd, 1H, J = 2.5, 7.9 Hz, H_3), 5.50 (d, 1H, J = 5.0 Hz, H_1).

^{13}C NMR (DMSO-d_6, 100 MHz): δ 24.2 (CH_3), 24.8 (CH_3), 25.7 (CH_3), 25.8 (CH_3), 36.9 (CH_3S), 66.0 (C_6), 69.2 (C_5), 69.5 (C_2), 70.0 ($C_{4,3}$), 95.5 (C_1), 108.1 (Cq), 108.7 (Cq).

Synthesis of 1,2,3,4-di-O-isopropylidene-6-azido-6-deoxy-α-D-galactopyranose (33)[104]

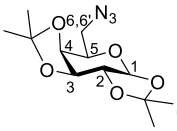

To a solution of 1,2,3,4-di-O-isopropylidene-6-mesyloxy-6-deoxy-α-D-galactopyranose (**41**) (31.00 g, 92 mmol) in DMF (280 mL) was added NaN_3 (59.56 g, 916 mmol) followed by H_2O (15 mL). The reaction mixture was heated to 120°C overnight. The mixture was then cooled to room temperature, concentrated *in vacuo* to a small volume and extracted with EtOAc (600 mL). The organic layer was washed with brine (3 × 200 mL), followed by H_2O (2 × 30 mL), dried over Na_2SO_4, filtered and concentrated *in vacuo* to orange oil. Purification by column chromatography (SiO_2) eluting with 10% EtOAc in hexane afforded 1,2-3,4-diacetonide-6-azido-galactopyranose (**33**) (25.36 g, 97%) as a clear oil.

LRMS (ESI) *m/z*: $[M + Na]^+$ 308.

FT-IR (ATR): ν_{max} (cm^{-1}): 2104 (N_3).

^1H NMR ($CDCl_3$, 400 MHz): δ 1.34 (s, 3H, CH_3), 1.35 (s, 3H, CH_3), 1.46 (s, 3H, CH_3), 1.55 (s, 3H, CH_3), 3.37 (dd, 1H, *J* = 5.4, 12.7 Hz, $H_{6'}$), 3.52 (dd, 1H, *J* = 7.9, 12.7 Hz, H_6), 3.90-3.94 (m, 1H, *J* = 1.9, 7.9 Hz, H_5), 4.20 (dd, 1H, *J* = 2.0, 7.9 Hz, H_4), 4.34 (dd, 1H, *J* = 2.5, 5.0 Hz, H_2), 4.64 (dd, 1H, *J* = 2.5, 7.9 Hz, H_3). 5.55 (d, 1H, *J* = 5.0 Hz, H_1).

^{13}C NMR ($CDCl_3$, 100 MHz): δ 24.6 (CH_3), 25.1 (CH_3), 26.2 (CH_3), 26.24 (CH_3), 50.9 (C_6), 67.2 (C_5), 70.6 (C_2), 71.0 (C_3), 71.4 (C_4), 96.6 (C_1), 109.0 (Cq), 109.8 (Cq).

Synthesis of compound (42)

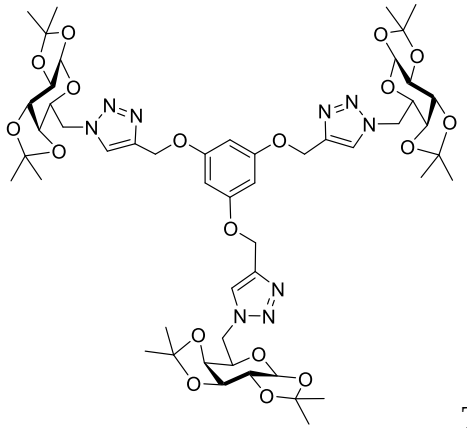

To a solution of (**37**) (1.87 g, 8 mmol) and (**33**) (8.87 g, 31 mmol) in THF:H_2O (3:1, 25 mL) was added an aqueous solution of $CuSO_4$ (0.5 M, 5 mL) followed by solid sodium ascorbate (3.08 g, 16 mmol). The reaction mixture was stirred overnight at room temperature. The suspension was diluted with H_2O (32 mL), cooled to 0°C and treated with conc. NH_4OH (3.12 mL) for 10 min. The reaction mixture was diluted with DCM (300 mL) and the organic layer washed with brine (2 × 30 mL), followed by H_2O (2 × 30 mL), 0.1 M HCl (1×30 mL), brine (2 × 30 mL) and finally H_2O (2 × 30 mL). The organic layer was then dried over Na_2SO_4, filtered and concentrated *in vacuo*. Purification by column chromatography (SiO_2) eluting with 60:35:5 EtOAc:hexane:MeOH afforded **(42)** (5.70 g, 67%) as white crystals.

HRMS (ESI-TOF) *m/z*: $[M + H]^+$ Calcd for $C_{51}H_{70}N_9O_{18}$ 1096.4839; Found 1096.4884.

Anal. Calcd for $C_{51}H_{69}N_9O_{18}$: C, 55.83; H, 6.29; N, 11.49. Found: C, 54.95; H, 6.27; N, 11.23.

MP. 146-148°C.

^{1}H NMR ($CDCl_3$, 500 MHz): δ 1.29 (s, 9H, CH_3), 1.36 (s, 9H, CH_3), 1.39 (s, 9H, CH_3), 1.50 (s, 9H, CH_3), 4.19-4.22 (m, 6H), 4.33-4.34 (m, 3H), 4.45-4.50 (m, 3H),

4.62-4.65 (m, 6H), 5.15 (s, 6H, CH_2O), 5.52 (d, 3H, J = 5.0 Hz), 6.28 (s, 3H, Ar), 7.80 (s, 3H, NCH=C).

^{13}C NMR ($CDCl_3$, 125 MHz): δ 24.6 (CH_3, 3C), 25.1 (CH_3, 3C), 26.1 (CH_3, 3C), 26.2 (CH_3, 3C), 50.8 (NCH_2, 3C), 62.3 (OCH_2, 3C), 67.4 (CH, 3C), 70.5 (CH, 3C), 71.0 (CH, 3C), 71.4 (CH, 3C), 95.2 (Ar-CH, 3C), 96.4 (CH, 3C), 109.3 (Cq, 3C), 110.1 (Cq, 3C), 124.3 (N**C**H=C, 3C), 143.8 (NCH=**C**, 3C), 160.4 (Ar-C, 3C).

Synthesis of compound (22)

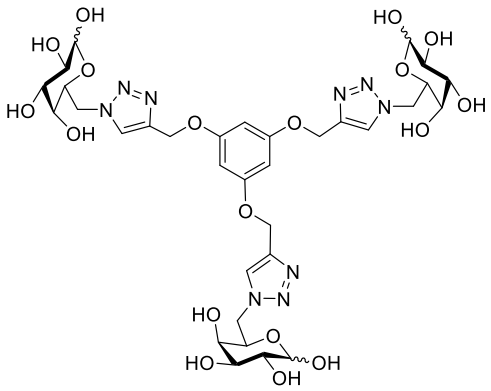

To a mixture of TFA:H_2O (1:1, 30 mL) was added (**42**) (1.50 g, 1 mmol) under a nitrogen atmosphere. The reaction mixture was heated to 70°C for 3 h. The mixture was then cooled to room temperature followed by concentration *in vacuo*. The crude residue was diluted with H_2O (30 mL) and concentrated *in vacuo* again to remove excess TFA. The product was diluted with MeOH and precipitated using Et_2O. The crude residue was diluted in 5% MeCN in H_2O and purified by semi-preparative HPLC using H_2O and MeCN. The gradient was started at 5% MeCN (solvent B), held at 5 min, then increased to 90% solvent B over 20 min. The product was freeze-dried to afford **(22)** (0.70 g, 60%) as a white powder. This compound was isolated as a mixture of diastereomers (see Appendix B7).

HRMS (ESI-TOF) *m/z*: $[M + H]^+$ Calcd for $C_{33}H_{46}N_9O_{18}$ 856.2961; Found 856.2958.

MP. 154-156°C.

^{1}H NMR (DMSO-d_6, 500 MHz): δ 3.25-3.33 (m), 3.54-3.63 (m), 3.70 (d, J = 1.9 Hz), 3.90-3.92 (m), 4.19-4.29 (m), 4.48-4.53 (m), 4.76 (bs), 4.90 (s), 5.09 (d , J = 5.1 Hz), 6.23 (bs), 6.36 (s), 6.62 (bs), 8.20 (s).

^{13}C NMR (DMSO-d_6, 125 MHz): δ 51.0, 61.2, 68.3, 68.9, 69.5, 71.6, 72.8, 72.9, 92.7, 94.5, 97.3, 125.3, 142.1, 142.2, 159.9.

2.5.2 Synthesis of sugar triazole (23)

Synthesis of compound (44)

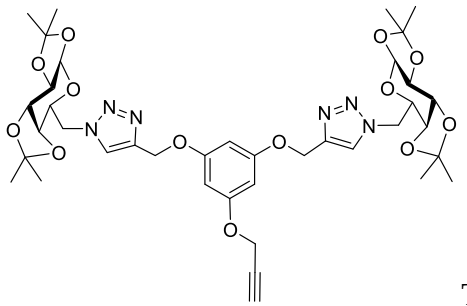

To a solution of (**37**) (0.50 g, 2 mmol) and (**33**) (1.19 g, 4 mmol) in THF:H_2O (5.25:1.75 mL) was added an aqueous solution of $CuSO_4$ (0.5 M, 1.40 mL) followed by solid sodium ascorbate (0.41 g, 4 mmol). The reaction mixture was stirred overnight at room temperature. The suspension was diluted with H_2O (9 mL), cooled to 0°C and treated with conc. NH_4OH (0.83 mL) for 10 min. The reaction mixture was diluted with DCM (100 mL) and the organic layer washed with brine (2 × 20 mL), followed by H_2O (2 × 20 mL). The organic layer was then dried over Na_2SO_4, filtered and concentrated *in vacuo*. Purification by column chromatography (SiO_2) eluting with 20% EtOAc in hexane afforded (**44**) as a yellow solid. (0.40 g, 24%).

HRMS (ESI-TOF) *m/z*: $[M + H]^+$ Calcd for $C_{39}H_{51}N_6O_{13}$ 811.3514; Found 811.3538. MP. 128-130°C.

^{1}H NMR ($CDCl_3$, 500 MHz): δ 1.29 (s, 6H, CH_3), 1.36 (s, 6H CH_3), 1.39 (s, 6H CH_3), 1.50 (s, 6H CH_3), 2.53 (t, 1H, *J* = 2.4 Hz, C≡CH), 4.18-4.22 (m, 4H), 4.33-4.34 (m, 2H), 4.44-4.49 (m, 2H), 4.61-4.65 (m, 6H), 5.16 (s, 4H, CH_2O), 5.52 (d, 2H, *J* = 4.9 Hz), 6.26 (d, 2H, *J* = 2.1 Hz, *o*-Ar), 6.30 (t, 1H, *J* = 2.1 Hz, *p*-Ar), 7.80 (s, 2H, NCH=C).

^{13}C NMR ($CDCl_3$, 125 MHz): δ 24.6 (CH_3, 2C), 25.0 (CH_3, 2C), 26.1 (CH_3, 2C), 26.2 (CH_3, 2C), 50.7 (NCH_2, 2C), 56.1 (**C**H_2C≡C, 1C), 62.3 (OCH_2, 2C), 67.3 (CH, 2C), 70.5 (CH, 2C), 70.9 (CH, 2C), 71.3 (CH, 2C), 75.8 (C≡**C**H, 1C), 78.6 (**C**≡CH, 1C), 95.3 (*o*-Ar-CH, 2C), 95.6 (*p*-Ar-CH, 1C), 96.4 (CH, 2C), 109.3 (Cq, 2C), 110.1 (Cq, 2C), 124.3 (N**C**H=C, 2C),143.7 (NCH=**C**, 2C), 159.6 (*p*-Ar-C, 1C), 160.3 (*o*-Ar-C, 2C).

Synthesis of 3-azidopropan-1-ol (46)[112]

To a solution of 3-iodopropanol (**45**) (6.67 g, 36 mmol) in H_2O (200 mL) was added NaN_3 (23.31 g, 359 mmol). The reaction mixture was stirred and heated to reflux overnight. The mixture was extracted with DCM (3 × 100 mL) and the organic layer dried over Na_2SO_4, filtered and concentrated *in vacuo* afforded 3-azidopropan-1-ol (**46**) (3.59 g, 99%) as a pale yellow oil.

Caution! This compound was not completely dry and safety consideration should be taken to avoid explosion risks associated with isolation of low molecular weight organic azides.

^{1}H NMR ($CDCl_3$, 400 MHz): δ 1.80-1.86 (m, 2H, CH_2**CH_2**CH_2), 2.01 (bs, 1H, OH), 3.44 (t, 2H, *J* = 6.6 Hz, CH_2N), 3.74 (t, 2H, *J* = 6.0 Hz, CH_2OH).

^{13}C NMR ($CDCl_3$, 100MHz): δ 31.6 (CH_2**C**H_2CH_2, 1C), 48.6 (CH_2N, 1C), 60.0 (CH_2OH, 1C).

Synthesis of compound (47)

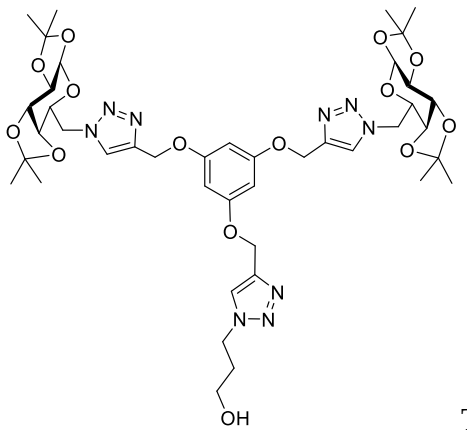

To a solution of (**44**) (0.27 g, 0.33 mmol) and (**46**) (0.17 g, 1.66 mmol) in THF:H_2O (3:1, 4 mL) was added an aqueous solution of $CuSO_4$ (0.5 M, 0.8 mL) followed by solid sodium ascorbate (0.13 g, 0.67 mmol). The reaction mixture was stirred overnight at room temperature. The suspension was diluted with H_2O (5 mL), cooled to 0°C and treated with conc. NH_4OH (0.45 mL) for 10 min. The reaction mixture was diluted with DCM (100 mL) and the organic layer washed with brine (2 × 20 mL), followed by H_2O (2 × 20 mL). The organic layer was then dried over Na_2SO_4, filtered and concentrated *in vacuo* afforded (**47**). The crude product was used directly for the next step.

Synthesis of compound (23)

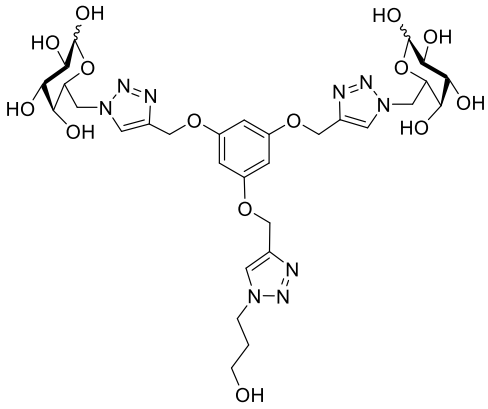

To a mixture of TFA:H_2O (1:1, 10 mL) was added (**47**) under a nitrogen atmosphere. The reaction mixture was heated to 70°C for 3 h. The mixture was then cooled to room temperature followed by concentration *in vacuo*. The residue was diluted with H_2O (30 mL) and concentrated *in vacuo* again to remove excess TFA. The product was precipitated with MeOH. The crude residue was diluted in H_2O and purified by semi-preparative HPLC using H_2O and MeCN. The gradient was started at 5% MeCN (solvent B), held at 5 min, then increased to 90% solvent B over 20 min. The product was freeze-dried to afford (**23**) (0.175 g, 70%) as a white powder. This compound was isolated as a mixture of diastereomers (see Appendix B17).

HRMS (ESI-TOF) *m/z*: $[M + H]^+$ Calcd for $C_{30}H_{42}N_9O_{14}$ 752.2851; Found 752.2871.

MP. 120-122°C.

^{1}H NMR (D_2O, 400 MHz): δ 2.03-2.10 (m), 3.51-3.58 (m), 3.63-3.66 (m), 3.76 (bs), 3.86-3.88 (m), 3.92-3.96 (m), 4.00-4.05 (m), 4.26-4.30 (m), 4.40-4.46 (m), 4.48-4.51 (m), 4.57-4.64 (m), 5.01-5.05 (m), 5.12 (bs), 5.23 (d, J = 3.1 Hz), 6.21 (s), 7.97 (s), 8.05 (s).

^{13}C NMR (D_2O, 100 MHz): δ 31.8, 47.2, 50.8, 51.0, 58.0, 61.1, 68.2, 68.7, 68.9, 69.0, 69.4, 71.6, 72.6, 73.1, 92.3, 95.6, 96.5, 125.0, 125.6, 125.7, 142.9, 159.4.

2.5.3 Synthesis of sugar triazole (38)

Synthesis of compound (49)

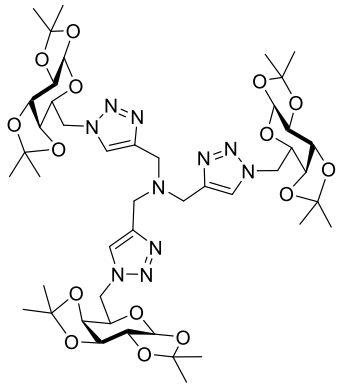

To a solution of tripropargylamine (**48**) (1.00 g, 7.62 mmol) in MeCN (12 mL) was added in succession (**33**) (9.78 g, 34.31 mmol), 2,6-lutidine (0.82 g, 7.62 mmol) and $[Cu(CH_3CN)_4]PF_6$ (0. 28 g, 0.76 mmol) at 0°C. After 1 h, the reaction mixture was allowed to warm to room temperature and stirred overnight. The solvent was then evaporated *in vacuo*. The resulting residue was diluted with H_2O (20 mL), cooled to 0°C and treated with conc. NH_4OH (2 mL) for 10 min. The reaction mixture was diluted with DCM (170 mL) and the organic layer washed with brine (2 × 50 mL), followed by H_2O (2 × 50 mL), 0.1 M HCl (1×50 mL), brine (2 × 50 mL) and finally H_2O (2 × 50 mL). The organic layer was then dried over Na_2SO_4, filtered and concentrated *in vacuo* followed by purification by column chromatography (SiO_2) eluting with 20% hexane in Et_2O afforded (**49**) (2.7 g, 36%) as white crystals.

HRMS (ESI-TOF) *m/z*: $[M + H]^+$ Calcd for $C_{45}H_{67}N_{19}O_{15}$ 987.4787; Found 987.4778.

MP. 218-220°C.

^{1}H NMR ($CDCl_3$, 500 MHz): δ 1.26 (s, 9H, CH_3), 1.36 (s, 9H, CH_3), 1.37 (s, 9H, CH_3), 1.50 (s, 9H, CH_3), 3.75-3.83 (m, 6H), 4.17-4.22 (m, 6H), 4.30-4.32 (m, 3H),

4.45 (dd, 3H, *J* = 8.5, 14.2 Hz), 4.61-4.65 (m, 6H), 5.52 (d, 3H, *J* = 4.9 Hz), 7.85 (s, 3H).

^{13}C NMR ($CDCl_3$, 125 MHz): δ 24.6 (CH_3, 3C), 25.1 (CH_3, 3C), 26.17 (CH_3, 3C), 26.2 (CH_3, 3C), 47.6 (CH_2, 3C), 50.6 (CH_2, 3C), 67.6 (CH, 3C), 70.6 (CH, 3C), 71.0 (CH, 3C), 71.4 (CH, 3C), 96.4 (CH, 3C), 109.2 (Cq, 3C), 110.1 (Cq, 3C), 125.2 (N**C**H=C, 3C), 144.3 (NCH=**C**, 3C).

Synthesis of compound (38)

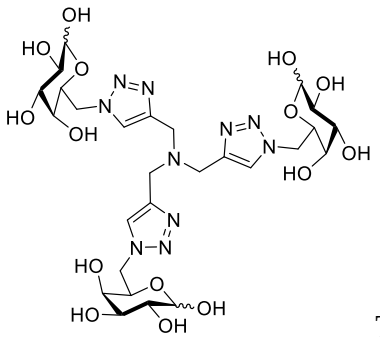

To a mixture of TFA:H_2O (1:1, 30ml) was added (**49**) (1.5 g, 2 mmol). The reaction mixture was heated to 70°C for 3 h. The mixture was then cooled to room temperature followed by concentration *in vacuo*. The crude residue was diluted with H_2O (30 mL) and concentrated *in vacuo* again to remove excess TFA. The product was precipitated with MeOH. The crude residue was diluted in 5% MeCN in H_2O and purified by semi-preparative HPLC using water and MeCN. The gradient was started at 1% MeCN (solvent B), held at 5 min, then increased to 90% solvent B over 13 min. The product was freeze-dried to afford (**38**) (1.20 g, 60%) as a white powder. This compound was isolated as a mixture of diastereomers (see Appendix B26).

HRMS (ESI-TOF) m/z: $[M + H]^+$ Calcd for $C_{27}H_{43}N_{10}O_{15}$ 747.2909; Found 747.2911.

MP. 162-164°C.

^{1}H NMR (D_2O, 500 MHz): δ 3.56 (dd, *J* = 7.9, 9.9 Hz), 3.70 (dd, *J* = 3.5, 10 Hz), 3.87-3.92 (m), 3.97 (d, *J* = 3.5 Hz), 4.04 (d, *J* = 3.0 Hz), 4.11-4.14 (m), 4.48-4.50 (m), 4.56 (d, *J* = 7.9 Hz), 4.63-4.76 (m), 4.84 (s), 5.26 (d, *J* = 3.7 Hz), 8.04 (s).

^{13}C NMR (D_2O, 100 MHz): δ 46.1, 50.5, 50.6, 67.5, 68.1, 68.3, 68.4, 68.8, 71.0, 72.0, 72.4, 91.8, 95.9, 127.9, 128.1, 135.45, 135.5.

2.5.4 Synthesis of sugar triazole (39)

Synthesis of methyl 3,5-bis(prop-2-yn-1-yloxy)benzoate (30)[88]

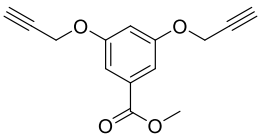

To a stirred solution of methyl 3,5-dihydroxybenzoate (**29**) (50.00 g, 297 mmol) in acetone (500 mL) was added propargyl bromide (80% in toluene, 77.82 g, 654 mmol), anhydrous and freshly ground potassium carbonate (123.29 g, 892 mmol) and 18-crown-6 (629.08, 2 mmol) under a nitrogen atmosphere. The reaction mixture was stirred and heated to reflux overnight. The solvent was then evaporated *in vacuo*. The resulting residue was diluted with DCM (500) and H_2O (300). The organic layer was washed with brine (3 × 250 mL), dried over $MgSO_4$, filtered and concentrated *in vacuo* afforded methyl 3,5-bis(prop-2-ynyloxy)benzoate (**30**) as yellow crystals (58.20 g, 80%) after recrystallisation from MeOH.

MP. 80-81°C.

^{1}H NMR ($CDCl_3$, 500 MHz): δ 2.55 (t, 2H, *J* = 2.4 Hz, C≡CH), 3.92 (s, 3H, CH_3), 4.72 (d, 4H, *J* = 2.4 Hz, CH_2), 6.82 (t, 1H, *J* = 2.4 Hz, *p*-Ar), 7.30 (d, 2H, *J* = 2.4 Hz, o-Ar).

^{13}C NMR ($CDCl_3$, 100 MHz): δ 52.5 (CH_3, 1C), 56.3 (CH_2, 2C), 76.2 (C≡**C**H, 2C),

78.2 (**C**≡CH, 2C), 107.8 (*p*-Ar-CH, 1C), 109.1 (*o*-Ar-CH, 2C), 132.4 (*p*-Ar-C, 1C), 158.7 (*m*-Ar-C, 2C), 166.7 (**C**OOCH$_3$, 1C).

Synthesis of (3,5-bis(prop-2-yn-1-yloxy)phenyl)methanol (31)[88]

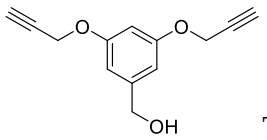

To a stirred anhydrous THF (70 mL) was added LiAlH$_4$ (10.00 g, 262 mmol) at 0°C slowly in small portions under a nitrogen atmosphere followed by a solution of methyl 3,5-bis(prop-2-ynyloxy)benzoate (**30**) (6.4 g, 26 mmol) in anhydrous THF (70 mL) dropwise and left stirring for 1 h. The reaction was quenched by addition of EtOAc (50 mL), followed by H$_2$O (50 mL). The mixture was then filtered and the solution concentrated *in vacuo* to a small volume. The residue was diluted with DCM (300 mL) and the organic layer washed with brine (150 mL), dried over MgSO$_4$, filtered and concentrated *in vacuo* afforded (3,5-bis(prop-2- ynyloxy)phenyl)methanol (**31**) (4.54 g, 80%) as an off-white solid.

MP. 93-94°C.

^{1}H NMR (CDCl$_3$, 400 MHz): δ 2.53 (t, 2H, *J* = 2.4 Hz, C≡CH), 4.65 (s, C**H$_2$**OH), 4.53 (d, 4H, *J* = 2.4 Hz, C**H$_2$**C≡CH), 6.55 (t, 1H, *J* = 2.3 Hz, *p*-Ar), 6.63 (d, 2H, *J* = 2.3 Hz, o-Ar).

^{13}C NMR (CDCl$_3$, 100 MHz): δ 56.1 (**C**H$_2$C≡CH, 2C), 65.3 (**C**H$_2$OH, 1C), 75.9 (C≡**C**H, 2C), 78.6 (**C**≡CH, 2C), 101.8 (*p*-Ar-CH, 1C), 106.5 (*o*-Ar-CH, 2C), 143.8 (*p*-Ar-C, 1C), 159.1 (*m*-Ar-C, 2C).

Synthesis of 1-(chloromethyl)-3,5-bis(prop-2-yn-1-yloxy)benzene (32)[88]

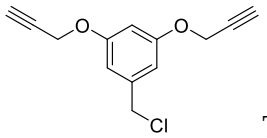

To a stirred solution of (3,5-bis(prop-2-ynyloxy)phenyl)methanol (**31**) (4.40 g, 20 mmol) in anhydrous DCM (80 mL) were added anhydrous pyridine (3.22 g, 41 mmol, 3.3 mL) and thionyl chloride (3.63 g, 31 mmol, 2.2 mL) dropwise at 0°C. The reaction mixture was stirred overnight at room temperature. Additional thionyl chloride (3.63 g, 31 mmol, 2.2 mL) was added to the mixture and stirred for a further 24 h. The reaction was then quenched with H_2O (100 mL). The mixture was diluted with DCM (100 mL) and the organic phase washed with H_2O (3 × 50 mL), $NaHCO_3$ sat. (1 × 50 mL) brine (3 × 50 mL), dried with $MgSO_4$ and concentrated *in vacuo.* Purification by column chromatography (SiO_2) eluting with 20% acetone in hexane afforded 1-(chloromethyl)-3,5- bis(prop-2-ynyloxy)benzene (**32**) (1.67 g, 35%) as a pale cream solid.

MP. 68-70°C.

^{1}H NMR ($CDCl_3$, 400 MHz): δ 2.55 (t, 2H, *J* = 2.4 Hz, C≡CH), 4.53 (s, **CH$_2$**Cl), 4.69 (d, 4H, *J* = 2.4 Hz, C**H$_2$**C≡CH), 6.59 (t, 1H, *J* = 2.3 Hz, *p*-Ar), 6.66 (d, 2H, *J* = 2.3 Hz, o-Ar).

^{13}C NMR ($CDCl_3$, 100 MHz): δ 46.3 (**C**H$_2$Cl, 1C), 56.2 (**C**H$_2$C≡CH, 2C), 76.0 (C≡**C**H, 2C), 78.4 (**C**≡CH, 2C), 102.5 (*p*-Ar-CH, 1C), 108.5 (*o*-Ar-CH, 2C), 139.9 (*p*-Ar-C, 1C), 159.0 (*m*-Ar-C, 2C).

Synthesis of compound (34)[82]

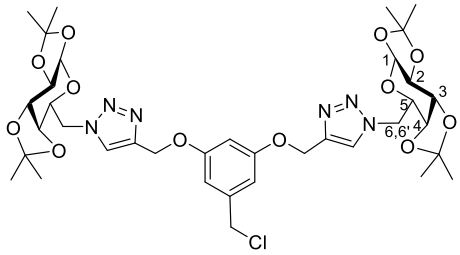

To a solution of 1-(chloromethyl)-3,5- bis(prop-2-ynyloxy)benzene (**32**) (1.3 g, 5.54 mmol) and 1,2-3,4-diacetonide-6-azido-galactopyranose (**33**) (3.79 g, 13.30 mmol) in THF:H_2O (3:1, 18 mL) was added an aqueous solution of $CuSO_4$ (0.5 M, 3.5 mL) followed by solid sodium ascorbate (2.20 g, 11.08 mmol). The reaction mixture was stirred overnight at room temperature. The suspension was diluted with H_2O (20 mL), cooled to 0°C and treated with conc. NH_4OH (2.2 mL) for 10 min. The reaction mixture was diluted with DCM (300 mL) and the organic layer washed with brine (2 × 50 mL), followed by H_2O (2 × 50 mL). The organic layer was then dried over $MgSO_4$, filtered and concentrated *in vacuo*. Purification by column chromatography (SiO_2) eluting with 1:1 EtOAc:petroleum ether afforded (**34**) (4.05 g, 91%) as white crystals.

LRMS (ESI) m/z: $[M + Na]^+$ 827.

MP. 184-185°C.

^{1}H NMR (CDCl3, 400 MHz): δ 1.29 (s, 6H, CH_3), 1.36 (s, 6H, CH_3), 1.38 (s, 6H, CH_3), 1.49 (s, 6H, CH_3), 4.18-4.21 (m, 4H, H_4/H_5), 4.33 (dd, 2H, *J* = 2.5, 4.9 Hz, H_2), 4.46 (dd, 3H, *J* = 8.4, 14.4 Hz, $H_{6'}$), 4.51 (s, 2H, CH_2Cl), 4.61-4.63 (m, 2H, H_3), 4.65-4.66 (m, 2H, H_6), 5.19 (s, 4H, CH_2O), 5.52 (d, 2H, *J* = 4.9 Hz, H_1), 6.59 (t, 1H, J = 2.2 Hz, *p*-Ar), 6.64 (d, 2H, J = 2.2 Hz, o-Ar), 8.00 (s, 2H, NCH=C).

^{13}C NMR ($CDCl_3$, 100 MHz): δ 24.6 (CH_3), 25.1 (CH_3), 26.1 (CH_3), 26.2 (CH_3), 46.4 (CH_2Cl), 50.8 ($C_{6,6'}$), 62.4 (OCH_2), 67.4 (C_4), 70.5 (C_2), 71.0 (C_3), 71.3 (C_5),

96.4 (C_1), 102.2 (*p*-Ar-CH), 108.1 (*o*-Ar-CH), 109.3 (Cq), 110.1 (Cq), 124.3 (N**C**H=C), 139.9 (*p*-Ar-C), 143.7 (NCH=**C**), 159.8 (*m*-Ar-C).

Synthesis of compound (35)[82]

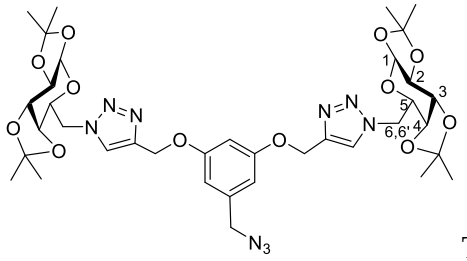

To a solution of (**34**) **(**4.00 g, 5 mmol) in acetone:H_2O (4:1, 100 mL) was added NaN_3 (3.23 g, 50 mmol) and heated to reflux under a nitrogen atmosphere overnight. The reaction mixture was diluted with EtOAc (500 mL) and the organic layer washed with brine (2 × 50 mL), followed by H_2O (2 × 50 mL). The organic layer was then dried over $MgSO_4$, filtered and concentrated *in vacuo* afforded (**35**) (2.40 g, 60%) as a white amorphous solid.

LRMS (ESI) m/z: $[M + Na]^+$ 834.

MP. 181-183°C.

^{1}H NMR (Acetone-d_6, 400 MHz): δ 1.28 (s, 6H, CH_3), 1.36 (s, 6H, CH_3), 1.37 (s, 6H, CH_3), 1.45 (s, 6H, CH_3), 4.30-4.33 (m, 2H, H_5), 4.36 (dd, 2H, *J* = 1.9, 7.8 Hz, H_4), 4.37 (s, 2H, CH_2N_3), 4.39 (dd, 2H, *J* = 2.5, 5.0 Hz, H_2), 4.50 (dd, 2H, *J* = 8.9, 14.2 Hz, $H_{6'}$), 4.63 (dd, 2H, *J* = 3.6, 14.2 Hz, H_6), 4.70 (dd, 2H, *J* = 2.5, 7.8 Hz, H_3), 5.21 (s, 4H, CH_2O), 5.47 (d, 2H, *J* = 5 Hz, H_1), 6.67 (d, 2H, *J* = 2.2, *o*-Ar), 6.76 (t, 1H, J = 2.2, *p*-Ar), 8.06 (s, 2H, NCH=C).

^{13}C NMR (Acetone-d_6, 100 MHz): δ 24.8 (CH_3), 25.2 (CH_3), 26.3 (CH_3), 26.5 (CH_3), 51.3 (CH_2N_3), 55.2 ($C_{6,6'}$), 62.7 (OCH_2), 68.1 (C_4), 71.4 (C_2), 71.8 (C_3), 72.2 (C_5), 97.3 (C_1), 102.2 (*p*-Ar-CH), 108.6 (*o*-Ar-CH), 109.5 (Cq), 110.3 (Cq), 125.3 (N**C**H=C), 139.1 (*p*-Ar-C), 143.9 (NCH=**C**), 161.7 (*m*-Ar-C).

Synthesis of compound (50)

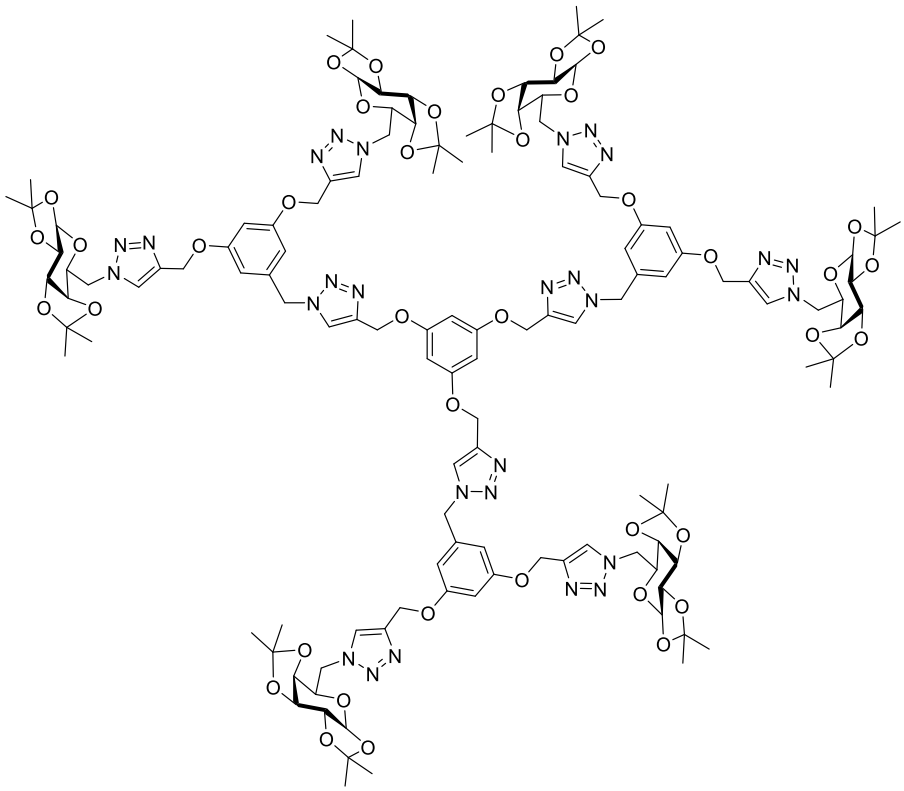

To a solution of (**37**) (0.40 g, 1.67 mmol) and (**35**) (4.46 g, 5.49 mmol) in THF:H_2O:DMSO (3:1: 0.5, 25 mL) was added an aqueous solution of $CuSO_4$ (0.5 M, 4.9 mL) followed by solid sodium ascorbate (0.6 g, 3.33 mmol). The reaction mixture was stirred overnight at room temperature. The suspension was diluted with H_2O (10 mL), cooled to 0°C and treated with conc. NH_4OH (0.70 mL) for 10 min. The reaction mixture was diluted with DCM (250 mL) and the organic layer washed with brine (2 × 50 mL), followed by H_2O (2 × 50 mL), 0.1 M HCl (1 × 50 mL), brine (2 × 50 mL) and concentrated *in vacuo*. Purification by column chromatography (SiO_2) eluting with 10% of MeOH in chloroform afforded (**50**) (1.83 g, 41%) as white crystals.

HRMS (ESI-TOF) m/z: $[M + H]^+$ Calcd for $C_{126}H_{160}N_{27}O_{39}$ 2675.1367; Found 2675.1375.

Anal. Calcd for $C_{126}H_{159}N_{27}O_{39}$: C, 56.50; H, 5.94; N, 14.12. Found: C, 55.76; H, 5.96; N, 13.50.

MP. 158-160°C.

^{1}H NMR ($CDCl_3$, 400 MHz): δ 1.28 (s, 18H, CH_3), 1.35 (s, 18H, CH_3), 1.36 (s, 18H, CH_3), 1.48 (s, 18H, CH_3), 4.18-4.20 (m, 12H, CH), 4.32 (dd, 6H *J* = 2.5, 4.9 Hz, CH), 4.46 (dd, 6H, *J* = 8.4, 14.3 Hz, CH), 4.60-4.65 (m, 12H, CH), 5.11 (s, 6H, CH_2), 5.13 (s, 12H, CH_2) , 5.44 (s, 6H, CH_2), 5.51 (d, 6H, *J* = 4.9 Hz, CH), 6.26 (s, 3H, Ar-CH), 6.51 (d, 6H, *J* = 2.1 Hz, Ar-CH), 6.62 (t, 3H, *J* = 2.1 Hz, Ar-CH), 7.62 (s, 3H, NCH=C), 7.79 (s, 6H, NCH=C).

^{13}C NMR ($CDCl_3$, 125 MHz): δ 24.6 (CH_3, 6C), 25.1 (CH_3, 6C), 26.1 (CH_3, 6C), 26.2 (CH_3, 6C), 50.8 (CH_2, 6C), 54.3 (CH_2, 3C), 62.2 (CH_2, 6C), 67.4 (CH, 6C), 70.5 (CH, 6C), 70.9 (CH, 6C), 71.3 (CH, 6C), 96.4 (CH, 6C), 102.1 (Ar-CH), 107.6 (Ar-CH), 109.3 (Cq, 6C), 110.1 (Cq, 6C), 123.2 (N**C**H=C, 3C), 124.4 (N**C**H=C, 6C), 137.0 (Ar-C, 3C), 143.4 (NCH=**C**, 6C), 144.4 (NCH=**C**, 3C), 160.1 (Ar-C, 6C), 160.3 (Ar-C, 3C).

Synthesis of compound (39)

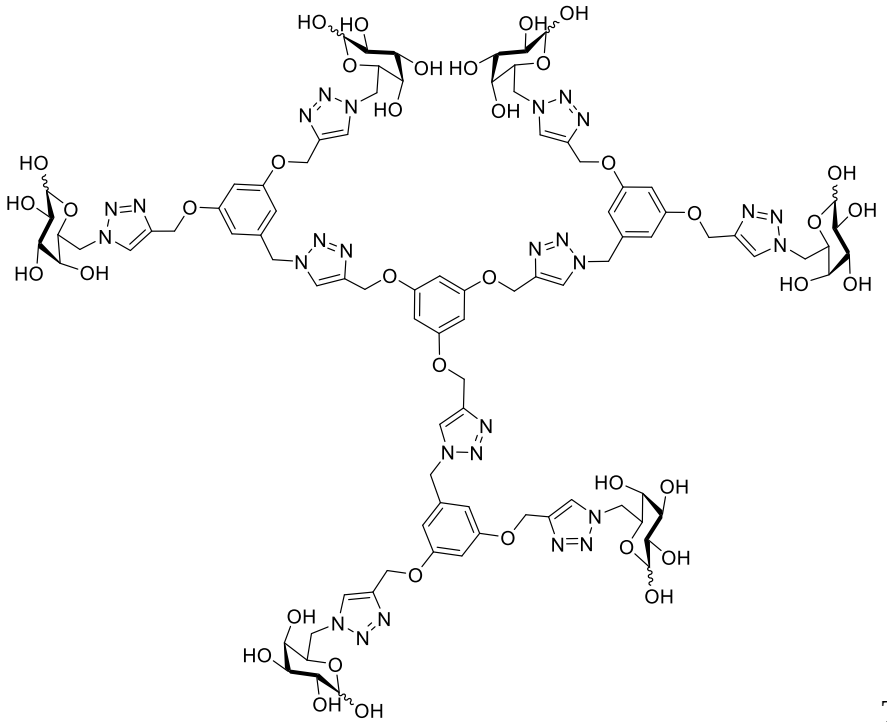

To a mixture of TFA:H_2O (1:1, 30 mL) was added (**50**) (1.50 g, 0.56 mmol) under a nitrogen atmosphere. The reaction mixture was heated to 70°C overnight. The mixture was then cooled to room temperature followed by concentration *in vacuo*. The crude residue was diluted with H_2O (30 mL) and concentrated *in vacuo* again to remove excess TFA. The product was diluted with MeOH and precipitated using Et_2O. The crude residue was diluted in 5% MeCN in H_2O and purified by semi-preparative HPLC using H_2O and MeCN. The gradient was started at 5% MeCN (solvent B), held at 5 min, then increased to 90% solvent B over 13 min. The product was freeze-dried to afford (**39**) (578 mg, 47%) as a white powder. This compound was isolated as a mixture of diastereomers (see Appendix B35).

HRMS (ESI-TOF) m/z: $[M + H]^+$ Calcd for $C_{90}H_{112}N_{27}O_{39}$ 2194.7611; Found 2194.7615.

MP. 164-166°C.

^{1}H NMR (DMSO-d_6, 500 MHz): δ 3.25-3.37 (m), 3.54-3.62 (m), 3.70-3.74 (m), 3.89-3.92 (m), 4.20 (t, J = 7.0 Hz), 4.26-4.28 (m), 4.36 (d, J = 6.7 Hz), 4.48-4.52 (m), 4.61 (d, J = 5.4 Hz), 4.74-4.79 (m), 4.90-4.91 (m), 5.08-5.11 (m), 5.53 (s), 6.23 (d, J = 4.8 Hz), 6.32 (s), 6.60-6.63 (m), 6.75 (s), 8.18 (s), 8.30 (s).

^{13}C NMR (DMSO-d_6, 100 MHz): δ 51.0, 52.8, 61.2, 61.23, 68.3, 68.8, 68.9, 69.5, 71.6, 72.8, 72.9, 76.0, 81.9, 82.6, 92.7, 94.5, 97.3, 100.9, 101.8, 107.2, 124.8, 125.3, 125.4, 138.2, 142.0, 142.1, 142.8, 159.4, 159.9.

2.5.5 Synthesis of triazole ligand controls (51-52)

Synthesis of 3-azidopropyl acetate (53)[112]

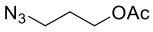

To a solution of 3-azidopropan-1-ol (**46**) (3.59 g, 36 mmol) in DCM (200 mL) was added in succession acetic anhydride (18.13 g, 178 mmol, 16.75 mL) and triethylamine (17.97 g, 178 mmol, 24.76 mL). The reaction mixture was stirred overnight at room temperature. The reaction mixture was washed with a 0.1 M NaOH (2 × 50), followed by 0.1 M HCl (2 × 50 mL) and finally with brine (1 × 50 mL). The organic layer was then dried over Na_2SO_4, filtered and concentrated *in vacuo* afforded 3-azidopropyl acetate (**53**) as a yellow oil (3.96 g, 78%).

Caution! This compound was not completely dry and safety consideration should be taken to avoid explosion risks associated with isolation of low molecular weight organic azides.

^{1}H NMR ($CDCl_3$, 400 MHz): δ 1.89-1.95 (m, 2H, CH_2**CH_2**CH_2), 2.07 (s, CH_3), 3.40 (t, 2H, J = 6.7 Hz, CH_2N), 4.16 (t, 2H, J = 6.2 Hz, CH_2O).

^{13}C NMR ($CDCl_3$, 100MHz): δ 21.1 (CH_3, 1C), 28.4 (CH_2**C**H_2CH_2, 1C), 48.4 (CH_2N, 1C), 61.6 (CH_2O, 1C), 171.2 (CO, 1C).

Synthesis of compound (54)

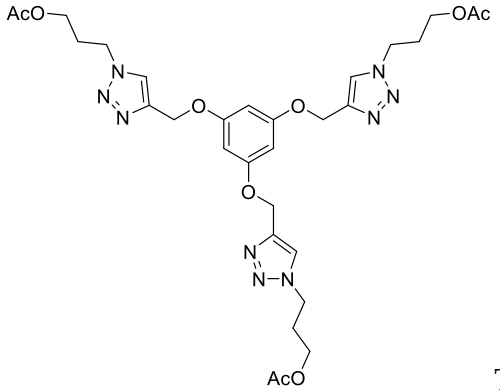

To a solution of (**37**) (1.31 g, 5 mmol) and (**53**) (4.00 g, 28 mmol) in THF:H_2O (3:1, 18 mL) was added an aqueous solution of $CuSO_4$ (0.5 M, 3.60 mL) followed by solid sodium ascorbate (2.15 g, 11 mmol). The reaction mixture was stirred overnight at room temperature. Additional sodium ascorbate (2.15 g, 11 mmol), $CuSO_4$ in H_2O (3.60 mL) and (**53**) (4.00 g, 28 mmol) were added to the mixture and stirred for a further 24 h. The suspension was diluted with H_2O (22 mL), cooled to 0°C and treated with conc. NH_4OH (2.20 mL) for 10 min. The reaction mixture was diluted with DCM (220 mL) and the organic layer washed with brine (2 × 50 mL), followed by H_2O (2 × 50 mL). The organic layer was then dried over Na_2SO_4, filtered and concentrated *in vacuo* afforded (**54**) as a yellow solid. The crude product was used directly for the next step.

Synthesis of compound (51)

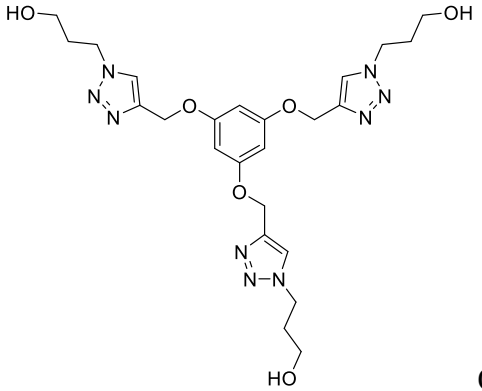

Compound (**54**) was treated with ammonia in MeOH (2 M, 100 ml) and stirred overnight at 40°C. The solution was concentrated *in vacuo* and then dissolved in H_2O (40 mL). The copper ions were removed by passing the solution through a DOWEX 50-X8 ion exchange column. The eluted fractions were concentrated *in vacuo* and the residue was dissolved in H_2O and freeze-dried. The crude residue was diluted in H_2O and purified by semi-preparative HPLC using H_2O and MeCN. The gradient was started at 5% MeCN (solvent B), held at 5 min, then increased to 90% solvent B over 20 min. The product was freeze-dried to afford (**51**) (1.48 g, 50%) as orange oil.

HRMS (ESI-TOF) *m/z*: $[M + H]^+$ Calcd for $C_{24}H_{34}N_9O_6$ 544.2632; Found 544.2634. Anal. Calcd for $C_{24}H_{33}N_9O_6$: C, 52.98; H, 56.07; N, 23.18 Found: C, 50.91; H, 6.18; N, 22.05.

^{1}H NMR (DMSO-d_6, 500 MHz): δ 1.94-1.99 (m, 6H, $CH_2C\mathbf{H_2}CH_2$), 3.41 (t, 6H J = 6.1 Hz, $C\mathbf{H_2}N$), 4.43 (t, 6H, J = 7.1 Hz, $C\mathbf{H_2}OH$), 5.09 (s, 6H, CH_2O), 6.34 (s, 3H, Ar-CH), 8.22 (s, 3H, NCH=C).

^{13}C NMR (DMSO-d_6, 125 MHz): δ 32.9 ($CH_2\mathbf{C}H_2CH_2$, 3C), 46.7 (CH_2N, 3C), 57.4 (CH_2OH, 3C), 61.2 (CH_2O, 3C), 94.6 (Ar-CH, 3C), 124.6 (N**C**H=C, 3C), 142.4 (NCH=**C**, 3C), 159.9 (Ar-C, 3C).

Synthesis of compound (55)

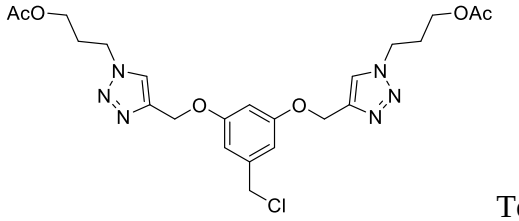

To a solution of (**32**) (0.86 g, 4 mmol) and (**53**) (1.57 g, 11 mmol) in THF:H_2O (3:1, 12 mL) was added an aqueous solution of $CuSO_4$ (0.5 M, 2.40 mL) followed by solid sodium ascorbate (1.45, 7 mmol). The reaction mixture was stirred overnight at room temperature. The suspension was diluted with H_2O (15 mL), cooled to 0°C and treated with conc. NH_4OH (1.43 mL) for 10 min. The reaction mixture was diluted with DCM (150 mL) and the organic layer washed with brine (2 × 30 mL), followed by H_2O (2 × 30 mL). The organic layer was then dried over Na_2SO_4, filtered and concentrated *in vacuo*. Purification by column chromatography (SiO_2) eluting with 10% MeOH in DCM afforded (**55**) (1.45 g, 76).

HRMS (ESI-TOF) *m/z*: $[M + H]^+$ Calcd for $C_{23}H_{30}N_6O_6Cl$ 521.1915; Found 521.1931.

Anal. Calcd for $C_{23}H_{29}N_6O_6Cl$: C, 52.97; H, 5.56; N, 16.12. Found: C, 53.18; H, 5.60; N, 15.77.

MP. 54-55°C.

^{1}H NMR ($CDCl_3$, 500 MHz): δ 2.06 (s, 6H, CH_3), 2.25-2.30 (m, 4H, $CH_2C\mathbf{H_2}CH_2$), 4.12 (t, 4H, *J* = 6.0 Hz, CH_2N), 4.47 (t, 4 H, *J* = 7.0 Hz, $C\mathbf{H_2}OAc$), 4.50 (s, 2H, CH_2Cl), 5.19 (s, 4H, CH_2O), 6.60 (t, 1H, *J* = 2.1 Hz, *p*-Ar), 6.64 (d, 2H, *J* = 2.1 Hz, *o*-Ar), 7.65 (s, 2H, NCH=C).

^{13}C NMR ($CDCl_3$, 125 MHz): δ 21.0 (CH_3, 2C), 29.6 ($CH_2\mathbf{C}H_2CH_2$, 2C), 46.3 (CH_2Cl, 1C), 47.5 (CH_2N, 2C), 61.1 (CH_2OAc, 2C), 62.3 (CH_2O, 2C), 102.2 (*p*-Ar-

CH, 1C), 108.2 (*o*-Ar-CH, 2C), 123.2 (N**C**H=C, 2C), 140.0 (*p*-Ar-C, 1C), 144.1 (NCH=**C**, 2C), 159.7 (*m*-Ar-C, 2C), 171.0 (CO, 2C).

Synthesis of compound (56)

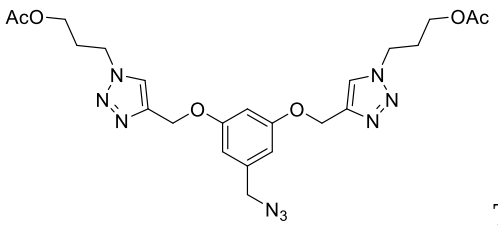

To a solution of (**55**) (0.80 g, 1.54 mmol) in acetone:H_2O (4:1, 18 mL) was added (1.00 g, 15.4 mmol) NaN_3 and heated to reflux under a nitrogen atmosphere for 3 h. The reaction mixture was diluted with EtOAc (100 mL) and the organic layer washed with brine (2 × 20 mL), followed by H_2O (2 × 20 mL). The organic layer was then dried over Na_2SO_4, filtered and concentrated *in vacuo* afforded (**56**) (0.71 g, 87%). The crude product was used directly for the next step.

Synthesis of compound (57)

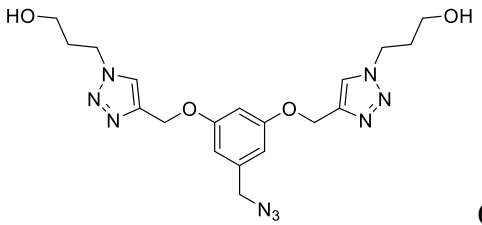

Compound (**56**) (0.71 g, 1 mmol) was treated with ammonia in MeOH (2 M, 100 ml) and stirred overnight at 40°C. The solution was concentrated *in vacuo* afforded (**57**) (0.59 g, 99%).

HRMS (ESI-TOF) *m/z*: $[M + H]^+$ Calcd for $C_{19}H_{26}N_9O_4$ 444.2108; Found 444.2116.

^{1}H NMR ($CDCl_3$, 500 MHz): δ 2.11-2.16 (m, 4H, $CH_2C\mathbf{H_2}CH_2$), 3.63 (t, 4H, *J* = 5.8 Hz, $C\mathbf{H_2}CH_2CH_2$), 4.25 (s, 2H, CH_2N_3), 4.53 (t, 4H, *J* = 6.7 Hz, $CH_2CH_2C\mathbf{H_2}OH$),

5.19 (s, 4H, CH_2O), 6.56 (d, 2H, J = 2.2 Hz, *o*-Ar), 6.62 (t, 1H, J = 2.2 Hz, *p*-Ar), 7.69 (s, 2H, NCH=C).

^{13}C NMR ($CDCl_3$, 100 MHz): δ 32.7 (CH_2**C**H_2CH_2, 2C), 47.2 (**C**$H_2CH_2CH_2OH$, 2C), 54.8 (CH_2N_3, 1C), 58.7 (CH_2OH, 2C), 62.2 (CH_2O, 2C), 102.0 (*p*-Ar-CH, 1C), 108.0 (*o*-Ar-CH, 2C), 123.7 (N**C**H=C, 2C), 138.0 (*p*-Ar-C, 1C), 143.8 (NCH=**C**, 2C), 159.8 (*m*-Ar-C, 2C).

2.5.6 Synthesis of PS-NHC-Cu(I) catalyst for click-chemistry (59)[111]

Synthesis of compound (61)

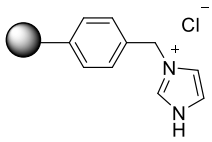

To a mixture of Merrifield resin (**60**) (1.46 mmol/g catalyst loading, 2.00 g, 3 mmol) in toluene (15 mL) was added imidazole (0.89 g, 13 mmol) under nitrogen atmosphere. The reaction mixture was stirred and refluxed at 80°C overnight. Then the solution was filtered and the solid washed with chloroform, MeOH and EtOAc, respectively, and dried under vacuum (**61**) as a pale yellow powder. The crude product was used directly for the next step.

Synthesis of compound (62)

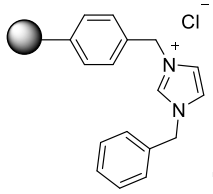

To a mixture of (**61**) in toluene (15 mL) was added benzyl bromide (2.24 g, 13 mmol, 1.55 mL) under nitrogen atmosphere. The reaction mixture was stirred and refluxed at 110°C overnight. Then the solution was filtered and the solid washed with chloroform, MeOH and EtOAc, respectively, and dried under vacuum

afforded (**62**) as a pale yellow powder. The crude product was used directly for the next step.

Synthesis of compound (59)

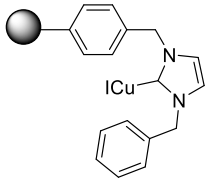

To a mixture (**62**) in THF (5 mL) were added CuI (0.61 g, 3.2 mmol) and *t*-BuOK (0.36 g, 3.2 mmol) under nitrogen atmosphere. The suspension was stirred overnight. Then the solution was filtered and the solid washed with H_2O, MeOH and acetone, respectively, and dried under vacuum afforder (**59**) (1.1 g) as a grey green powder.

Synthesis of compound (52)

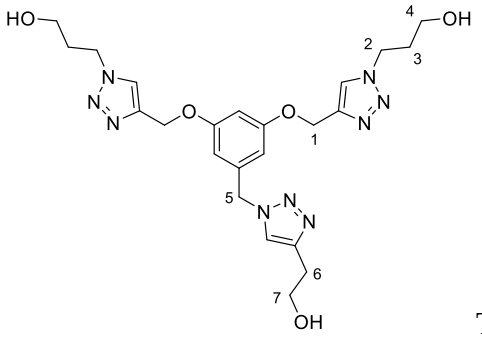

To a solution of **(57)** (0.59 g, 1.33 mmol) in DMSO (3 mL) was added 3-butyn-1-ol (**58**) (0.28 g, 3.99 mmol), and PS-NHC-Cu(I) (**59**) (1.46 mmol/g catalyst loading, 1 g, 1.46 mmol) and stirred overnight under a nitrogen atmosphere. The reaction mixture was then filtered and the solid catalyst washed with DMSO (1 mL). The combined filtrate was concentrated to a small volume, diluted with H_2O and purified by semi-preparative HPLC using H_2O and MeCN. The gradient was started at 5% MeCN (solvent B),

held at 5 min, then increased to 90% solvent B over 20 min. The product was freeze-dried to afford (**52**) (0.212 g, 31%) as a yellow amorphous solid.

HRMS (ESI-TOF) *m/z*: $[M + H]^+$ Calcd for $C_{23}H_{32}N_9O_5$ 514.2526; Found 514.2516.

Anal. Calcd for $C_{23}H_{31}N_9O_5$: C, 53.74; H, 6.03; N, 24.53. Found: C, 53.49; H, 6.04; N, 23.99.

MP. 100-101°C.

^{1}H NMR (Methanol-d_4,, 500 MHz): δ 2.07-2.12 (m, 4H, CH_2 ^{3}), 2.90 (t, 2H, *J* = 6.6 Hz, CH_2 ^{6}), 3.55 (t, 4H, *J* = 6.0 Hz, CH_2 ^{4}), 3.80 (t, 2H, *J* = 6.6 Hz, CH_2 ^{7}), 4.51 (t, 4H, *J* = 7.0 Hz, CH_2 ^{2}), 5.13 (s, 4H, CH_2 ^{1}), 5.48 (s, 2H, CH_2 ^{5}), 6.59 (d, 2H, *J* = 2.0 Hz, *o*-Ar), 6.65 (t, 1H, *J* = 2.0 Hz, *p*-Ar), 7.79 (s, 1H,), 8.03 (s, 2H).

^{13}C NMR (MeOD, 125 MHz): δ 30.1 (CH_2), 34.1 (CH_2) , 54.9 (CH_2), 59.4 (CH_2), 62.2 (CH_2), 62.7 (CH_2), 103.2 (*p*-Ar-CH, 1C), 108.7 (*o*-Ar-CH, 2C), 124.3 (N**C**H=C, 1C), 125.8 (N**C**H=C, 2C), 139.4 (*p*-Ar-C, 1C), 144.8 (NCH=**C**, 3C), 161.4 (*m*-Ar-C, 2C).

2.5.7 Silver nanoparticle (AgNP) formation

Preparation of sugar stock solutions: The corresponding sugar triazoles (**22-23** and **38-39**) were dissolved in ultrapure H_2O and diluted to a standard concentration of 50 mM. These stock solutions were then used to screen the optimal conditions for AgNP formation.

Preparation of Tollens' reagent stock solutions: Stock solutions of Tollens' reagent were prepared in three different concentrations (100, 20 and 3 mM) and diluted as required with ultrapure H_2O for the preparation of the nanoparticle arrays.

100 mM Tollens: To 1.8 mL H_2O was added $AgNO_3$ (0.5 M, 500 µL), followed by NaOH (3 M, 100 µL) and finally NH_4OH (28%, 110 µL).

20 mM Tollens: To 4.1 mL H_2O was added $AgNO_3$ (0.5 M, 279 µL), followed by NaOH (3 M, 56 µL) and finally NH_4OH (28%, 61 µL).

3 mM Tollens: To 9.9 mL H_2O was added $AgNO_3$ (0.5 M, 60 µL), followed by NaOH (3 M, 12 µL) and finally NH_4OH (28%, 13 µL).

AgNPs were formed by the addition of 300 µL of Tollens' reagent to 300 µL of a solution of an appropriate sugar ligand in a plastic eppendorf. The solution was vortexed and left in the dark overnight. The mixture was centrifuged for 30 seconds to afford a suspension of colloidal of AgNPs.

2.5.8 Reaction kinetics of AgNP formation

Time course: 200 µL of sugar solutions (**22**, **23** or **39**) at 200 µM and 200 µL of Tollens' solution (20 mM) were mixed in a low-volume quartz cuvette; UV-Vis measurements were taken at 400 nm every 5 seconds using a UV-Vis spectrophotometer.

2.5.9 General procedure for ^{1}H NMR titration studies

Stock solutions of triazole ligands (**22, 23, 51** or **52**) at 2 mM and $AgNO_3$ (12 mM) were prepared in D_2O. 300 µL of aliquots of the ligands were mixed with increasing amounts of $AgNO_3$ and diluted with D_2O up to 600 µL. The recorded spectra are shown in Appendix C1-C4 and ordered at different concentrations of $AgNO_3$ from 0 to 6 mM.

The acquired ^{1}H NMR data of the triazole sugar ligands and the concentration of the Ag(I) was used to calculate the Ag(I) binding constants using WinEQNMR2 software.[108] The data was fitted-permited according to the following equations:[113]

$$Ag + L \underset{}{\overset{K}{\rightleftharpoons}} AgL \qquad \text{Equation (4)}$$

$$K = \frac{[\mathrm{AgL}]}{[\mathrm{Ag}][\mathrm{L}]}$$ Equation (5)

$$[L]_0 = [L] + [AgL]$$ Equation (6)

$$[Ag]_0 = [Ag] + [AgL]$$ Equation (7)

$$[Ag] = \frac{1}{2}\left(Ag_0 - L_0 - \frac{1}{K}\right) - \sqrt{\left(Ag_0 + L_0 + \frac{1}{K}\right)^2 + 4\frac{Ag_0}{K}}$$ Equation (8)

$$[AgL] = \frac{1}{2}\left(Ag_0 + L_0 + \frac{1}{K}\right) - \sqrt{\left(Ag_0 + L_0 + \frac{1}{K}\right)^2 + 4[Ag]_0[L]_0}$$ Equation (9)

$$\Delta\delta = \delta_{\Delta AgL}\left(\frac{[AgL]}{[L]_0}\right)$$ Equation (10)

CHAPTER 3: EXPLORATION OF THE COUNTER-ION EFFECT OF SILVER SALTS ON THE FORMATION OF SILVER NANOPARTICLES

3.1 Introduction

Chapter two explored the structural parameters of triazole ligands in the templated synthesis of AgNPs using Tollens' reagent. In this study, silver nitrate was used as a silver source for the preparation of Tollens' reagent. This chapter focuses on the investigation of the effect of counter-ions on the templated synthesis of AgNPs by replacing silver nitrate with other silver salts.

It is well known in literature that ligands containing nitrogenous donor atoms coordinate to a silver ion in different modes that is dependent on the counter ion of silver salts.[114-116] For example, Wang *et al*. reported 1:1 Ag(I) complexes using the tripyridylamine (tpa) ligand.[115] This design formed three different complexes that were dependent on the type of silver salt used. For example, using silver trifluoroacetate, a dimer structure was formed through coordination of two silver ions with two pyridyl groups in each tpa ligand (Figure 3-1a). In this bonding mode, the trifluoroacetate counter ion chelated to the silver centre and linked the dimer units through Ag-O bonds. Changing the counter ion to nitrate (NO_3^-) resulted in the formation of a zigzag structure through Ag-N bonds (Figure 3-1b). Silver trifluoromethanesulfonate (OTf^-) formed a ribbonlike structure in which all three pyridyl groups of the tpa ligand coordinated to three silver ions (Figure 3-1c). Hexafluorophosphate (PF_6^-) and perchlorate (ClO_4^-) silver salts coordinated to the tpa in a similar manner to OTf^-.

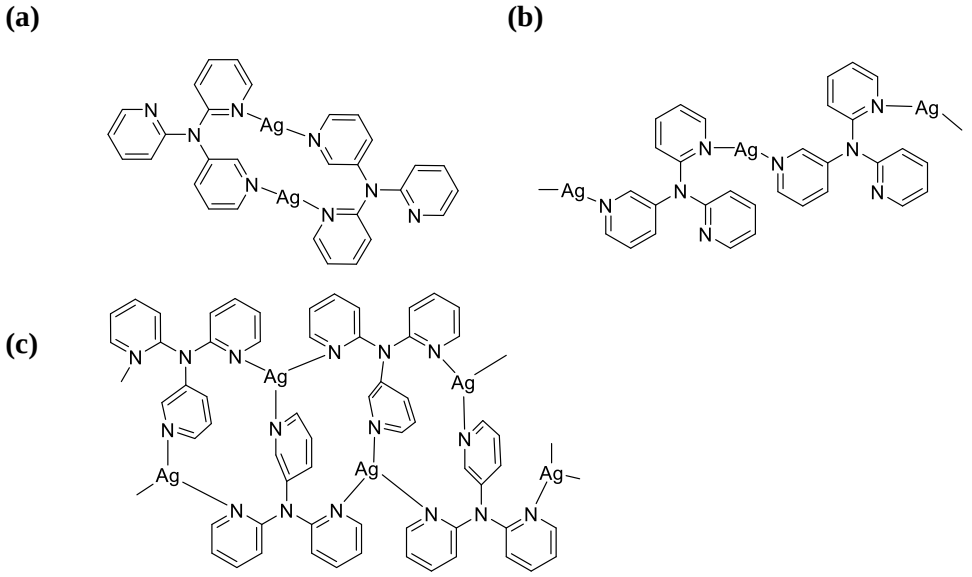

Figure 3-1: *Silver (I) complexation of tripyridylamine ligand:* ***(a)*** *dimer;* ***(b)*** *zigzag and* ***(c)*** *ribbonlike structures.*

Recent research has reported the effect of different counter ions of silver salts on the preparation of size- and shape-controlled AgNPs. In 2010, Xia *et al*. extended the polyol synthesis (Section 1.3.2.1) for the preparation of Ag nanocubes using ethylene glycol and CF_3COOAg in the presence of NaSH, HCl and PVP.[117] The authors suggested that CF_3COO^- is more stable than NO_3^- at high temperature (150°C) required in polyol synthesis. Another advantage of using CF_3COO^- is the slower growth rate of AgNPs (15-90 min) compared to typical method using NO_3^- (8-10 min). This feature enabled greater tunability of the size of AgNPs ranging from 30 to 42, 50 and 70 nm by monitoring the UV-vis spectra of AgNPs during the synthesis at different reaction time (15, 30, 60 and 90 min). A linear correlation was observed between the intensity of the SPR peak and the length of Ag nanocubes. In contrast, the size of AgNPs produced using NO_3^- increased from 25 to 45 nm in 2 min.[52]

Following this study, Xia *et al*. prepared Ag nanocubes with the length of 18-32 nm by switching the ethylene glycol (EG) to diethylene glycol (DEG).[118] The authors

attributed the smaller size of AgNPs to the higher viscosity of DEG resulted in the rapid formation of a large number of Ag nuclei.[119] The lower reducing power of DEG allowed these nuclei to grow at a slower rate (30-180 min).

Another example of the influence of the counter ions on the formation of AgNPs was reported by Lee and Oh using five different salts: $AgNO_3$, $AgClO_4$, AgF, $AgBF_4$ and $AgPF_6$.[120] The synthesis was accomplished in ethanol at 80°C in the presence of PVP afforded spherical AgNPs with the average size around 4-8 nm. This study showed the following aspects:

(i) AgNPs prepared using fluorinated salts (e.g., AgF, $AgBF_4$ and $AgPF_6$.) exhibited higher intensity of the UV absorbance. The maximum peak was observed using AgF at 400 nm with a shoulder peak at 500 nm related to aggregation due to the higher concentration of AgNPs.

(ii) ISE analysis showed that the yield of the reduction increased from 2% using $AgNO_3$ or $AgClO_4$ to 25%, 46% and 89% using $AgBF_4$, $AgPF_6$ and AgF respectively. This study showed how the fluoride ions influenced the formation of AgNPs. This effect was probed by the formation of AgNPs using $AgNO_3$ in the presence of NaF. The UV absorbance of these AgNPs was 13 times higher than those prepared without NaF salt. In this respect, the authors inferred that the highest silver nanoparticle formation corresponding to the higher pK_a of the conjugate acid of AgF [i.e., HF, with pK_a = 3.17] than the conjugate acids of $AgNO_3$ [pK_a = -1.37] and $AgClO_4$ [pK_a = -10].

3.2 Hypothesis

Based on literature precedent, the counter ions of silver salts have a significant effect on the formation of AgNPs. To the best of our knowledge, there have been no

reports highlighting the utility of silver salts beyond silver nitrate for the synthesis of AgNPs using Tollens' reagent. We therefore hypothesise that the nature of the counter ion of silver salts used to form Tollens' reagent will affect the size and shape of AgNPs.

3.3 Aims of the study

The aim of this chapter is to investigate the synthesis of AgNPs using ligands (**18**, **22** and **23**, Figure 3-2) and Tollens' reagent derived from CF_3COOAg. The underlying motivation for exploring this method was based on previous work by Xia *et al*. who reported that CF_3COOAg slowed the growth rate of AgNPs formation with a high degree of size- and shape-control compared to $AgNO_3$ (Section 3.1).[117] A possible reason for this effect is the weaker acidity of the conjugate acid of CF_3COOAg [pK_a = -0.3] than $AgNO_3$ [pK_a = -1.37].

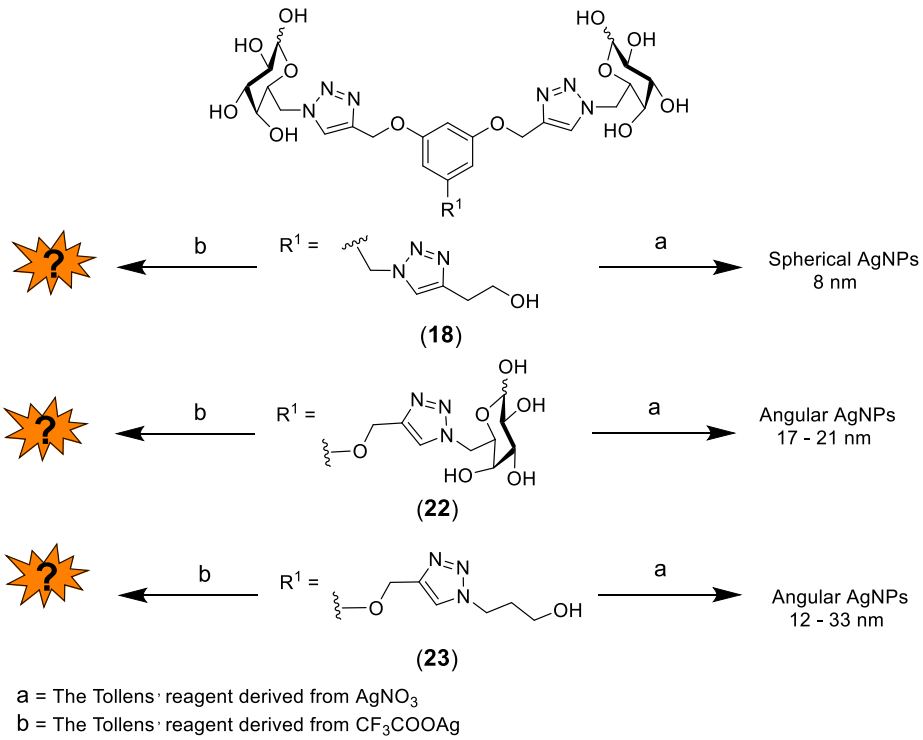

Figure 3-2: *Structures of sugar triazoles used for studying the effect of changing the silver salts on the preparation of AgNPs using Tollens' reagent.*

3.4 Results and Discussion

3.4.1 Synthesis of AgNPs using sugar triazole ligands and Tollens' reagent derived from CF_3COOAg

3.4.1.1 AgNPs derived from sugar triazole (18)

A silver nanoparticle array using compound (**18**) was constructed over concentration ranges of 1 µM - 25 mM [(**18**)] and 10 µM - 50 mM [Tollens'] derived from CF_3COOAg (Table 3-1).

Table 3-1: *AgNP@(**18**) screening array prepared using sugar triazole (**18**) and Tollens' reagent derived from CF_3COOAg. White boxes represent no AgNP formation, yellow boxes represent AgNP formation and grey boxes represent the formation of silver mirrors.*

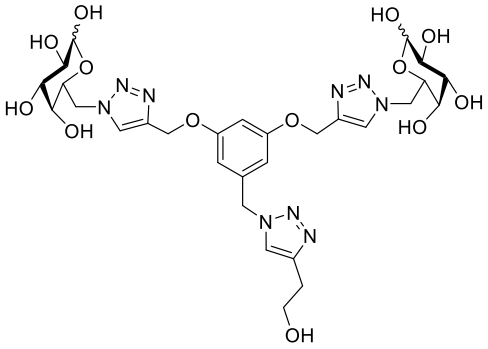

[(18)]

[Tollens']

	25 mM	10 mM	1 mM	100 µM	10 µM	1 µM
10 µM	#1	#2	#3	#4	#5	#6
100 µM	#7	#8	#9	#10	#11	#12
1 mM	#13	#14	#15	#16	#17	#18
10 mM	#19 12 ± 2 nm	#20	#21	#22	#23	#24
20 mM	#25	#26 12 ± 2 nm	#27	#28	#29	#30
50 mM	#31 12 ± 2 nm	#32	#33	#34	#35	#36

The reaction screen of [(**18**)] and [Tollens'] produced AgNP@(**18**) in three regions (yellow boxes in Table 3-1): (i) a region of low concentration of Tollens' [i.e., 1mM]; (ii) a region of intermediate concentration of Tollens' [10 mM] and lastly

(iii) a high concentration region of Tollens' [20 mM - 50 mM]. Figure 3-3 shows the UV-vis spectra of several examples of AgNP@(**18**) formed in these regions. Silver aggregates were also observed at 50 mM [Tollens'] and 100 µM - 10 mM [(**18**)] (grey boxes in Table 3-1). The particle distribution of this array was different from AgNP@(**18**) prepared by Burley *et al*. using Tollens' reagent derived from $AgNO_3$.[87] For example, no silver mirrors or aggregates were observed at 100 µM - 10 mM (**18**) and 50 mM [Tollens'] derived from $AgNO_3$. Instead, a yellow colloidal solution was formed at 10 mM [(**18**)] and no AgNPs were formed at 1 mM - 100 µM (**18**).

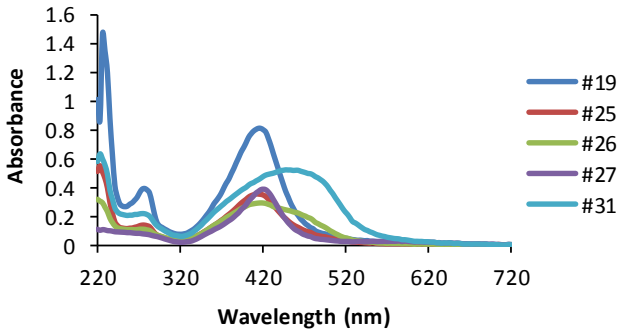

Figure 3-3: *UV-vis spectra of reactions #19, 25-27 and 31, which formed AgNP@(**18**) using Tollens' reagent derived from CF_3COOAg. Sample #19 was diluted 1:20 and #25-27, 31 were diluted 1:75 prior to each measurement.*

TEM analysis of several examples in this series produced spherical AgNPs of diameter [Ø = 12 ± 2 nm] (Figure 3-4). These results were similar to Burley's previous study (Section 1.3.4) that ligand (**18**) produced spherical AgNP [Ø = 8 ± 5 nm] using Tollens' reagent derived from $AgNO_3$.

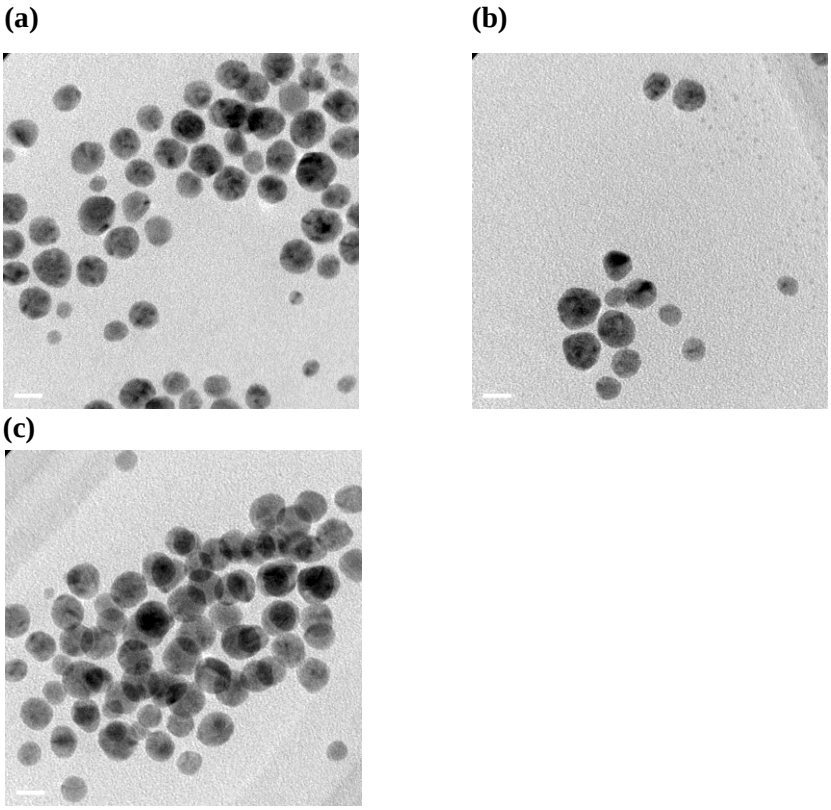

Figure 3-4: *TEM images of AgNP@(**18**) prepared using reaction conditions in Table 3-1.* ***(a)*** *#19, Ø = 12 ± 2 nm;* ***(b)*** *#26, Ø = 12 ± 2 nm;* ***(c)*** *#31, Ø = 12 ± 2 nm.*

3.4.1.2 AgNPs derived from sugar triazole (22)

The formation of AgNPs using compound (**22**) was screened as a function of [(**22**)] and [Tollens'] derived from CF_3COOAg (Table 3-2) with a similar concentration range used for the preparation of AgNPs array using compound (**18**). The particle distribution of this array was similar to AgNP@(**22**) prepared using Tollens' reagent derived from $AgNO_3$ (Table 2-1, Section 2.3.2.1). Figure 3-5 shows the UV-vis spectra of several examples of AgNP@(**22**) formed in this array.

Table 3-2: *AgNP@(**22**) screening array prepared using sugar triazole (**22**) and Tollens' reagent derived from CF_3COOAg. White boxes represent no AgNP formation, yellow boxes represent AgNP formation and grey boxes represent the formation of silver mirrors.*

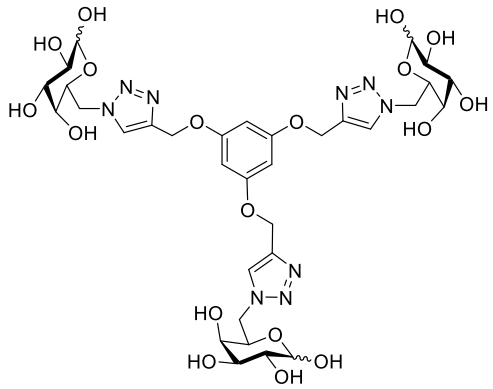

[(22)]

[Tollens']

	25 mM	10 mM	1 mM	100 µM	10 µM	1 µM
10 µM	#1	#2	#3	#4	#5	#6
100 µM	#7	#8	#9	#10	#11	#12
1 mM	#13	#14	#15	#16	#17	#18
10 mM	#19 14 ± 4 nm	#20	#21	#22	#23	#24
20 mM	#25	#26 12 ± 2 nm	#27	#28	#29	#30
50 mM	#31 17 ± 3 nm	#32	#33	#34	#35	#36

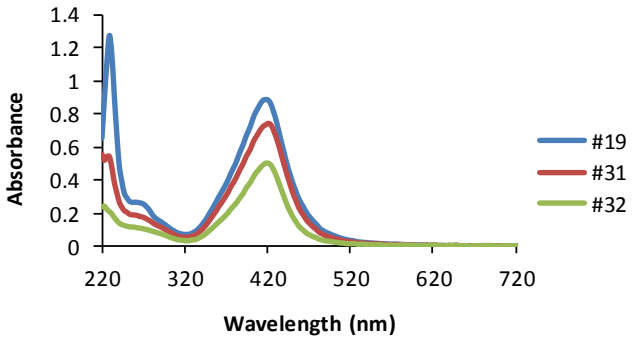

Figure 3-5: *UV-vis spectra of reactions #19 and 31-32, which formed AgNP@(**22**) using Tollens' reagent derived from CF_3COOAg. Sample #19 was diluted 1:20 and #31-32 were diluted 1:75 prior to each measurement.*

TEM analysis revealed AgNP@(**22**) using Tollens' reagent derived from CF_3COOAg formed angular AgNPs of similar diameter . For example, #19 and #31

afforded angular AgNP@(**22**) with diameters of 14 ± 4 nm and 17 ± 3 nm respectively. Similar results were observed using ligand (**22**) and Tollens' reagent derived from $AgNO_3$ that afforded angular AgNP@(**22**) with a diameter of 17 ± 3 nm and 18 ± 5 [i.e., #19 and #31 respectively] (Figure 2-4, Section 2.3.2.1).

(a) **(b)**

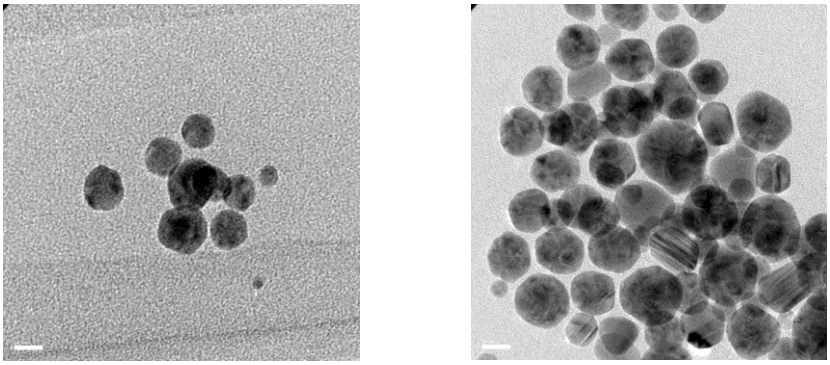

Figure 3-6: *TEM images of AgNP@(**22**) prepared using reaction conditions in Table 3.2.* ***(a)*** *#19, Ø = 14 ± 4 nm;* ***(b)*** *#31, Ø = 17 ± 3 nm.*

3.4.1.3 AgNPs derived from sugar triazole (23)

Table 3-3 represents the AgNPs array prepared over a concentration range of 1 µM - 25 mM [(**23**)] and 10 µM - 50 mM [Tollens'] derived from CF_3COOAg.

The particle distribution of this array was similar to AgNP@(**23**) prepared using Tollens' reagent derived from $AgNO_3$ (Table 2-2, Section 2.3.2.2). The only difference was the formation of Ag aggregates at 50 mM of Tollens' and 1mM (**23**). Figure 3-7 shows the UV-vis spectra of several examples of AgNP@(**23**) formed in this array.

***Table 3-3**: AgNP@(**23**) screening array prepared using sugar triazole (**23**) and Tollens' reagent derived from CF_3COOAg. White boxes represent no AgNP formation, yellow boxes represent AgNP formation and grey box represents the formation of silver mirrors.*

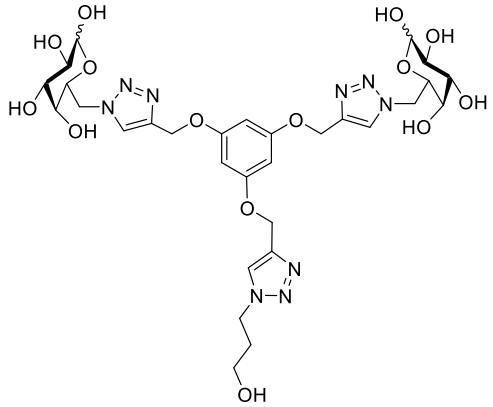

[(23)]

[Tollens']

	25 mM	10 mM	1 mM	100 µM	10 µM	1 µM
10 µM	#1	#2	#3	#4	#5	#6
100 µM	#7	#8	#9	#10	#11	#12
1 mM	#13	#14	#15	#16	#17	#18
10 mM	#19 10 ± 3 nm	#20 15 ± 4 nm	#21 29 ± 6 nm	#22	#23	#24
20 mM	#25	#26	#27 23 ± 5 nm	#28	#29	#30
50 mM	#31 17 ± 6 nm	#32 15 ± 6 nm	#33	#34	#35	#36

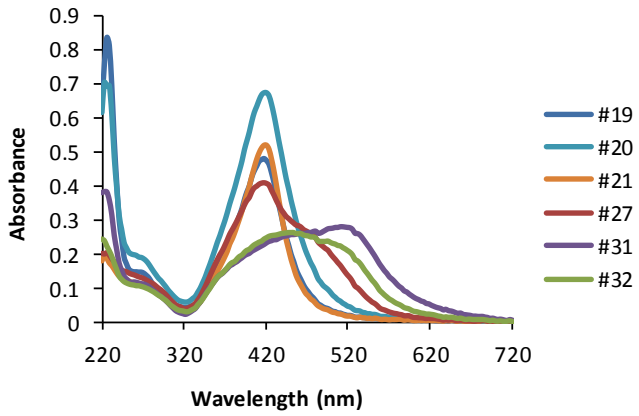

***Figure 3-7:** UV-vis spectra of reactions #19-21, 27 and 31-32, which formed AgNP@(**23**) using Tollens' reagent derived from CF_3COOAg. Sample #19-21 were diluted 1:40, #27, 32 were diluted 1:75 and #31 was diluted 1:90 prior to each measurement.*

An interesting observation was that the surface SPR peak of the samples were highly dependent on the reaction conditions used for the preparation of AgNP@(**23**) using Tollens' reagent derived from CF_3COOAg. For example, samples #19, #20 and #21 exhibited the most sharp and narrow peaks at 420 nm. Broader peaks at 475 nm were formed using #31 and #32. A shoulder peak at 520 nm was observed in #31. Such a red shift in the formation of the shoulder peak has been previously reported by El-Sayed and Misra that attributed to the high particle concentration or the smaller interparticle distance than particle dimensions.[121,122] Conversely, all samples of AgNP@(**23**) prepared using Tollens' reagent derived from $AgNO_3$ showed sharp and narrow peaks at 420 nm over a similarly wide concentration range of [(**23**)] and [Tollens'] (Figure 2-5, Section 2.3.2.2). The changes in UV-vis spectral properties of AgNP@(**23**) using Tollens' reagent derived from two different silver salts tend to override the influence of the counter ion on the formation of AgNP@(**23**).

TEM analysis of several examples in this series produced angular AgNP@(**23**) of tunable sizes that ranged from 10 ± 3 nm in diameter (#19, Figure 3-8a) through to 29 ± 6 nm (#21, Figure 3-8c). The inherent tunability of the size of AgNP@(**23**) was also observed using $AgNO_3$ (Figure 2-6, Section 2.3.2.2). However, the sizes of AgNP@(**23**) under certain conditions were different compared to these new results. For example, #19 using $AgNO_3$ produced angular AgNPs of much larger diameter [Ø = 33 ± 7 nm].

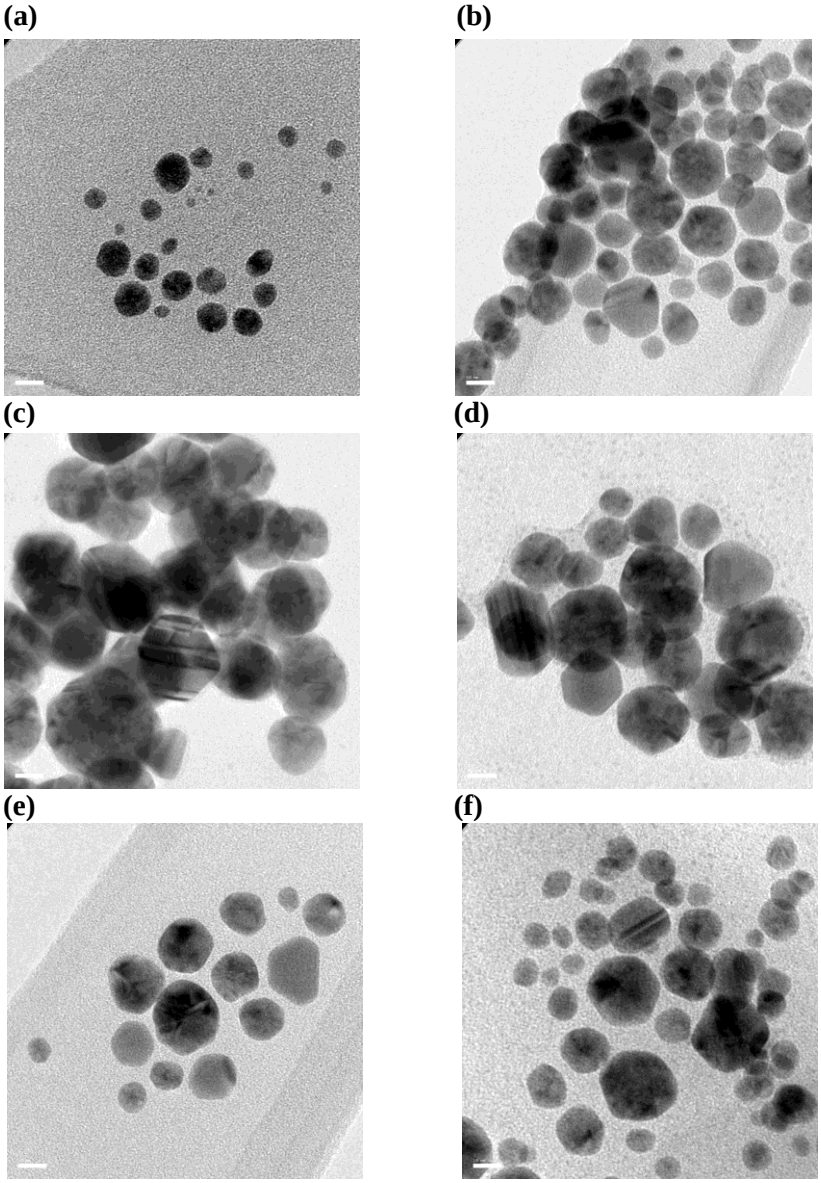

Figure 3-8: *TEM images of AgNP@(**23**) prepared using reaction conditions in Table 3-3.* ***(a)*** *#19, Ø = 10 ± 3 nm;* ***(b)*** *#20, Ø = 15 ± 4 nm;* ***(c)*** *#21, Ø = 29 ± 6 nm;* ***(d)*** *#27, Ø = 23 ± 5 nm;* ***(e)*** *#31, Ø = 17 ± 6 nm;* ***(f)*** *#32, Ø = 15 ± 6 nm.*

The key conclusion arising from this study was that changing the counter ion from NO_3^- to CF_3COO^- in Tollens' reagent using the same ligand (**18**), (**22**) or (**23**) produced similar shapes of AgNPs and influenced the size of AgNP@(**23**) more than AgNP@(**18**) and AgNP@(**22**). Table 3-4 summarises the results of AgNPs prepared using Tollens' reagent derived from two different salts, CF_3COOAg and $AgNO_3$.

Table 3-4: *Summary of AgNPs formed using ligands (**18**, **22** and **23**) and Tollens' reagent derived from two different salts, CF_3COOAg and $AgNO_3$.*

Ligand	Tollens' : Ligand	AgNP size (nm) using CF_3COOAg	AgNP size (nm) using $AgNO_3$
(**18**)	10 mM : 25 mM (2:5)	12 ± 2	8 ± 5
	20 mM :10 mM (2:1)	12 ± 2	8 ± 5
	50 mM : 25 mM (2:1)	12 ± 2	8 ± 5
(**22**)	10 mM : 25 mM (2:5)	14 ± 4	17 ± 3
	50 mM : 25 mM (2:1)	17 ± 3	18 ± 5
(**23**)	10 mM : 25 mM (2:1)	10 ± 3	33 ± 7
	20 mM : 1 mM (20:1)	23 ± 5	14 ± 3
	50 mM : 25 mM (2:1)	17 ± 6	12 ± 3

Taken collectively, the size of formed AgNP was depended on the counter ion and the nature of the sugar triazole ligands (**18**, **22,** and **23**). For example, ligands (**18**) and (**22**) produced similar sizes of AgNP@(**18**) and AgNP@(**22**) using $AgNO_3$ and CF_3COOAg. For ligand (**23**), at certain concentrations of Tollens' and (**23**), smaller AgNPs were formed using CF_3COOAg. This result was inconsistent with the Xia *et al*. study in polyol synthesis that reported the synthesis of larger Ag nanocubes ranging from 30 to 70 nm using CF_3COOAg compared to the size of 25 to 45 nm using $AgNO_3$ (Section 3-1).[117] In contrast to the greater control of AgNPs reported by Xia *et al.* using CF_3COO^-,[117] the size tunability observed in the formation of AgNP@(**23**) using NO_3^- reduced when CF_3COO^- was used.

All of these observations combined with UV-vis spectra results suggested that AgNP@(**23**) was affected by the counter ions of silver salts used in Tollens' reagent. Another interesting observation is that although ligands (**22**) and (**23**) have the same

core, ligand (**22**) produced similar sizes of AgNP@(**22**). Therefore, the increase in the number of reducing equivalents [i.e., galactose units] from two (**23**) to three (**22**) could be a possible reason for reducing the counter ion effects in the formation of AgNP@(**22**). To detect this effect, kinetic experiments and NMR spectroscopic studies were conducted to understand how counter ion of silver salts can influence the formation of AgNPs.

3.4.2 The kinetics of AgNP formation using sugar triazole ligands and Tollens' reagent derived from CF_3COOAg

The kinetics of AgNP formation was explored using ligands (**18**), (**22**) and (**23**) by monitoring the onset of the surface plasmon peak at 400 nm using 100 µM [(ligand)] and 10 mM [Tollens'] derived from CF_3COOAg. The onset of formation of AgNP@(**18**) was observed at ~ 48 s with an end-point at ~ 240 s (Figure 3-9). AgNP@(**22**) showed a significant slower rate of onset (~ 1600 s) with an end-point at (~ 2900 s). A similar slower rate of onset of formation of AgNP@(**23**) was also observed but with a faster end-point (2400 s). In contrast to the kinetics results in chapter two (Figure 2-12), the rate of the formation of AgNP@(**22**) and AgNP@(**23**) using CF_3COOAg was dramatically slower than those formed using $AgNO_3$ [the rate of onset ~ 180 s with an end-point ~ 420 s in AgNP@(**22**) and ~ 570 s in AgNP@(**23**)]. We suggested that this effect was attributed to the lower reduction potential of CF_3COOAg relative to $AgNO_3$. The slower growth rate of AgNPs using CF_3COOAg was consistent with Xia's *et al*. results (Section 3-1).[117] However, this behaviour was not observed in the formation of AgNP@(**18**) [the rate of onset ~ 120 s and end-point ~ 588 s] using $AgNO_3$]. Thus, by switching the counter ion

from NO_3^- to CF_3COO^-, the rate of AgNP@(**18**) formation was not affected compared to AgNP@(**22**) and AgNP@(**23**).

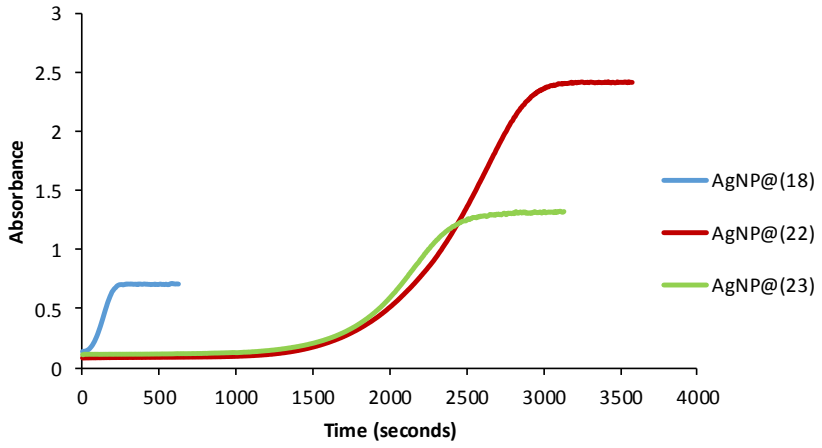

Figure 3-9: *Kinetics of formation of AgNP using (**18**, blue), (**22**, red) and (**23**, green) and Tollens' reagent derived from CF_3COOAg as monitored by the formation of the SPR peak at 400nm.*

3.4.3 NMR spectroscopic experiments

^{1}H NMR titration experiments were then conducted using ligands (**18**), (**22**) and (**23**) in the presence of CF_3COOAg to explore the binding characteristics of these ligands to the silver ions. Triazole protons and aromatic protons were used as diagnostic markers of Ag(I) coordination. A ^{1}H NMR titration study using ligands (**18**) revealed a downfield shift (0.05 ppm for H^c and 0.01 ppm for H^d) upon the addition of one equivalent of Ag(I) (Figure 3-10b, d). A further downfield shift [0.15 ppm for H^c and 0.09 for H^d] was observed up to the addition of six equivalents of Ag(I). In contrast, a 0.15 ppm upfield shift of the aromatic H^e was observed upon the addition of up to three equivalents of Ag(I) (Figure 3-10f). The chemical shift of this proton did not change after addition of a further three equivalents of Ag(I). An interesting observation was that the behaviour of both triazole and aromatic protons in this

experiment was different from that reported in Burley *et al.* work in the presence of $AgNO_3$ (Section 2.3.6).[87]

A ^{1}H NMR titration was then conducted using ligands (**22**) and (**23**). Titration of up to one equivalent of Ag(I) resulted a downfield shift (0.04 ppm) of the triazole protons [H^f in (**22**) and H^h/H^j in (**23**)], similar to that observed for H^c in (**18**) in the presence of CF_3COOAg (Figure 3-11b and Figure 3-12b, d). A 0.16 ppm upfield shift of the aromatic protons [H^g in (**22**) and H^i in (**23**)] was observed upon the addition of up to six equivalents of Ag(I), again consistent with that observed for H^e in (**18**) in the presence of CF_3COOAg (Figure 3-11d and Figure 3-12f). The behaviour of both triazole and aromatic protons in both ligands (**22**) and (**23**) was similar to that observed in the presence of $AgNO_3$ (Section 2.3.6).

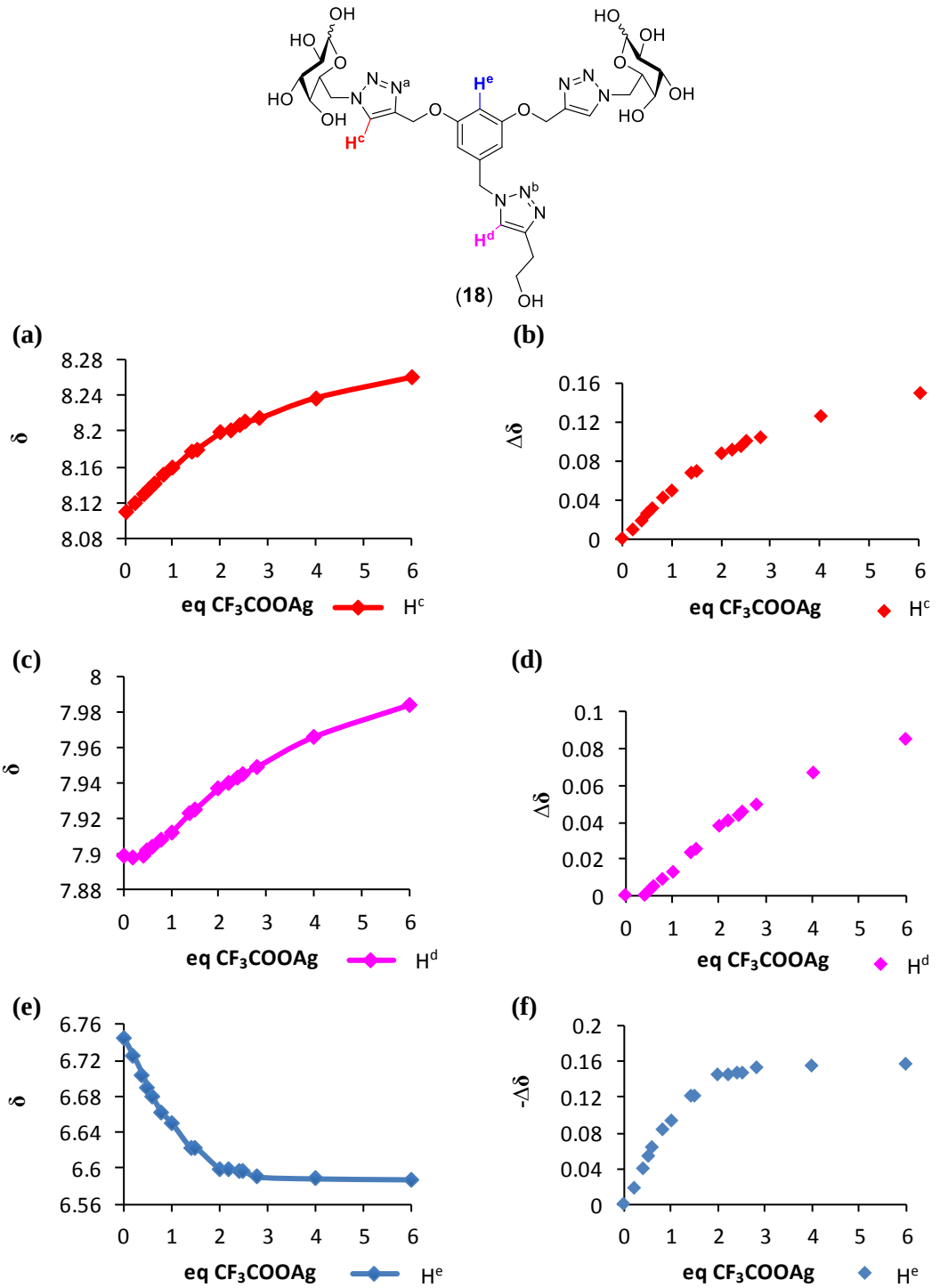

Figure 3-10: *Plots of the ^{1}H-NMR titration of sugar triazole ligand (**18**) with an increasing amount of CF_3COOAg in D_2O.* ***(a, c,*** *and* ***e)*** *Plots of the ^{1}H-NMR titration of H^c, H^d and H^e with CF_3COOAg.* ***(b, d,*** *and* ***f)*** *Change in chemical shift of H^c, H^d and H^e as a function of CF_3COOAg.*

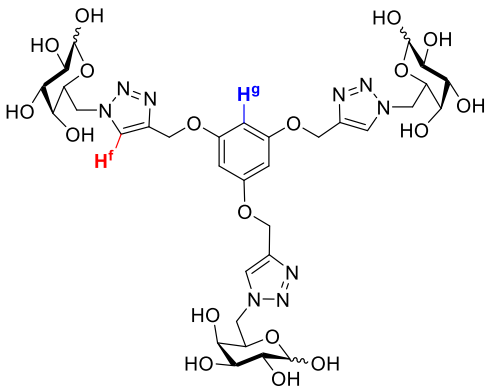

(**22**)

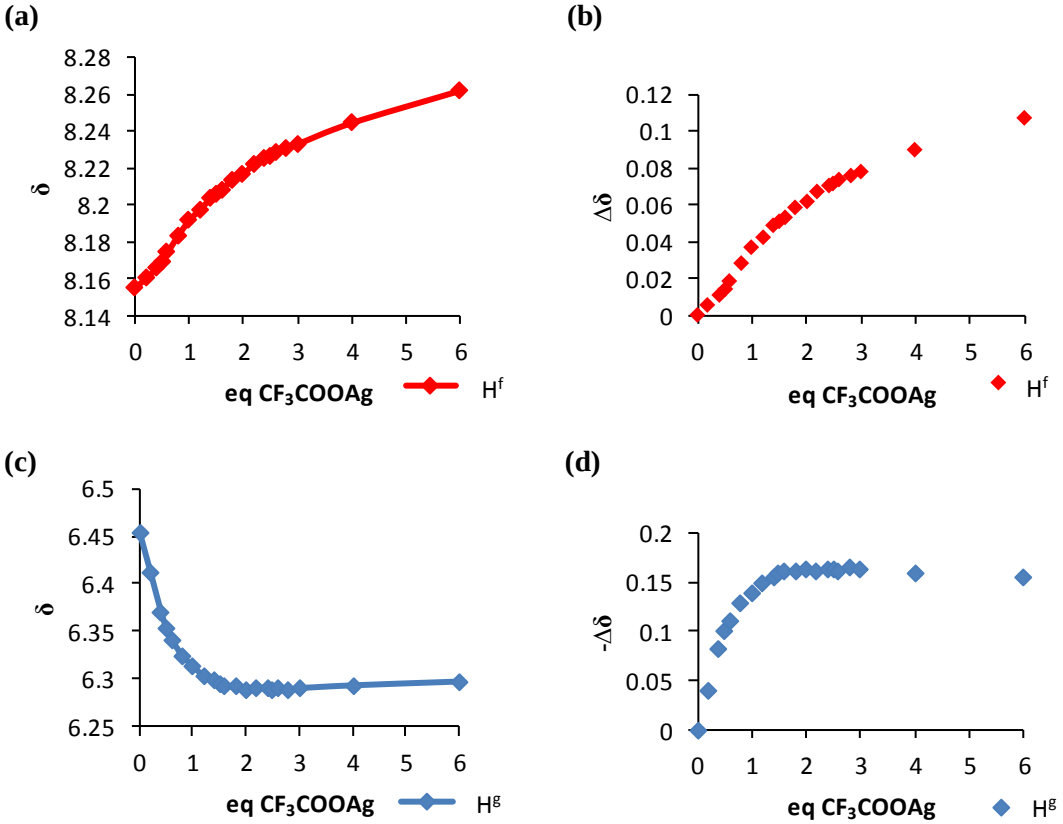

Figure 3-11: *Plots of the ^{1}H-NMR titration of sugar triazole ligand (**22**) with an increasing amount of CF_3COOAg in D_2O.* ***(a** and **c)** Plots of the ^{1}H-NMR titration of H^f and H^g with CF_3COOAg.* ***(b** and **d)** Change in chemical shift of H^f and H^g as a function of CF_3COOAg.*

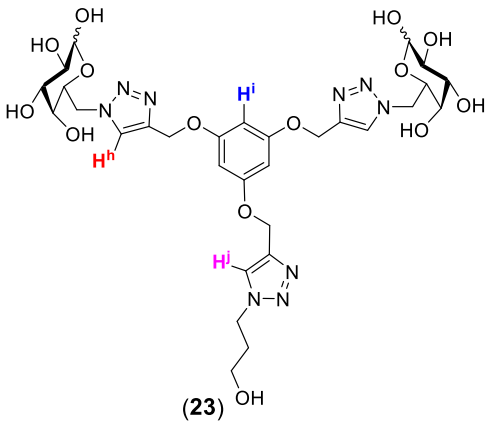

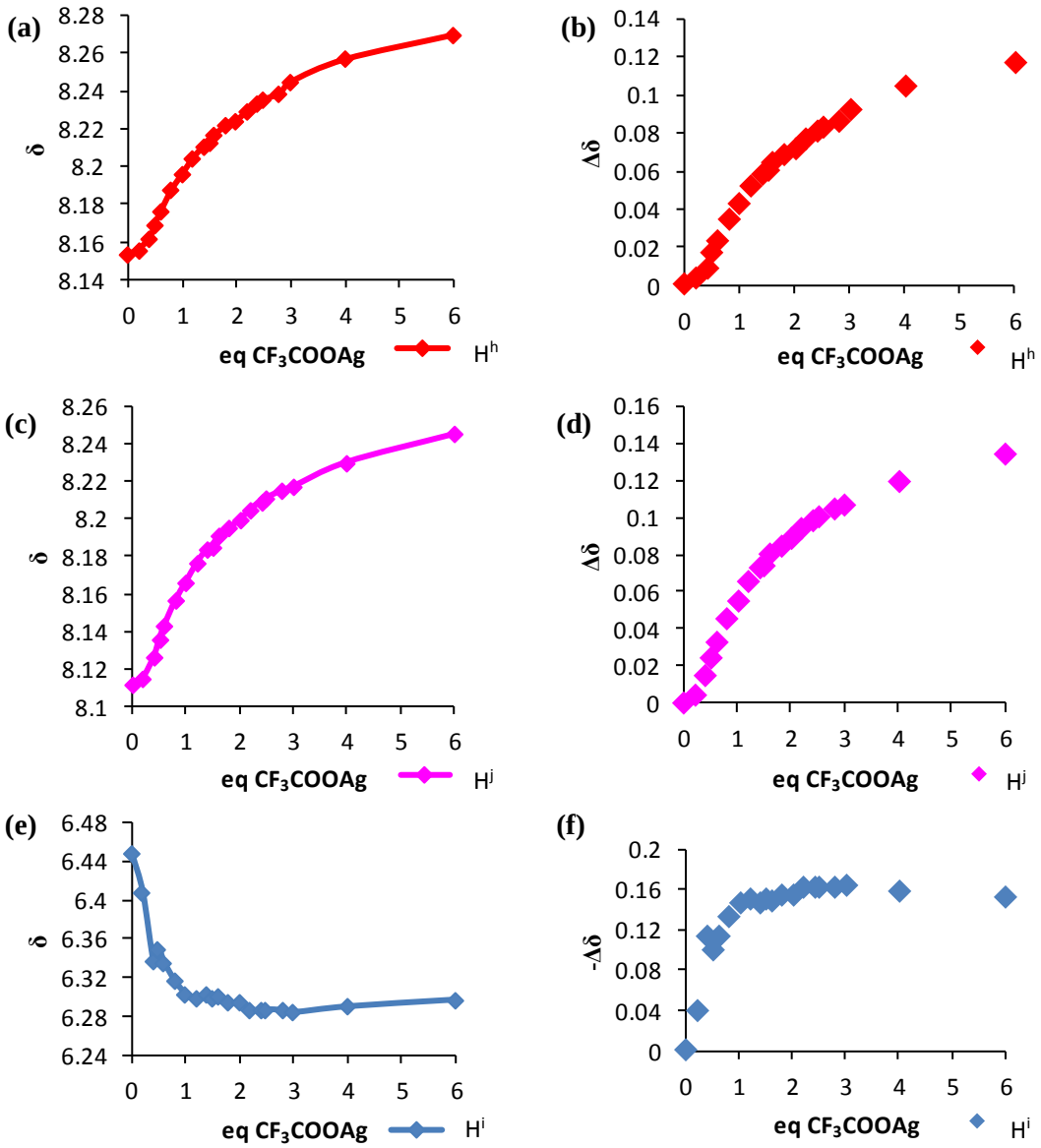

Figure 3-12: *Plots of the ^{1}H-NMR titration of sugar triazole ligand (**23**) with an increasing amount of CF_3COOAg in D_2O.* ***(a, c** and **e)** Plots of the ^{1}H-NMR titration of H^h, H^j and H^i with CF_3COOAg.* ***(b, d** and **f)** Change in chemical shift of of H^h, H^j and H^i as a function of CF_3COOAg.*

The binding affinity of Ag(I) for ligands (**18**), (**22**) and (**23**) was then calculated by WinEQNMR2 software.[108]

Table 3-5: *Comparison of Ag(I) binding constant of (**18, 22** and **23**) using two different silver salts calculated by non-linear curve fitting of ^{1}H NMR chemical shift data of the triazole protons using the software program WinEQNMR2.*[108]

	In the presence of CF_3COOAg		**In the presence of $AgNO_3$**	
Compound	**K** (M^{-1})	**Log K**	**K** (M^{-1})	**Log K**
(**18**)	425 ± 23	2.629 ± 0.023	72 393 ± 38011	4.859 ± 0.219
(**22**)	513 ± 31	2.710 ± 0.026	533 ±22	2.727 ± 0.018
(**23**)	745 ± 52	2.872 ± 0.030	743 ± 69	2.871 ± 0.040

An interesting observation of Ag(I) binding affinity of these ligands is that changing the counter ion from NO_3^- to CF_3COO^- resulted in a significant reduction in Ag(I) binding of (**18**). In contrast, ligands (**22**) and (**23**) binded to Ag(I) in a similar manner using $AgNO_3$ and CF_3COOAg.

In order to further explore the effect of CF_3COO^- counter ion on the binding characteristics of these ligands to the silver, ^{19}F NMR titration was conducted using ligand (**22**) as an example in the presence of CF_3COOAg. Titration of up to two equivalents of (**22**) resulted in a slight upfield shift (0.006 ppm) of fluorine chemical shift (Figure 3-13). A 0.009 ppm upfield shift was observed upon the addition of a further four equivalents of (**22**). This slight shift provides further justification of the weak Ag(I) binding affinity of ligand(**22**) using CF_3COOAg. Further ^{19}F NMR titration studies will be required in order to understand the role of CF_3COO^- in Ag(I) binding affinity of ligands (**18**) and (**23**).

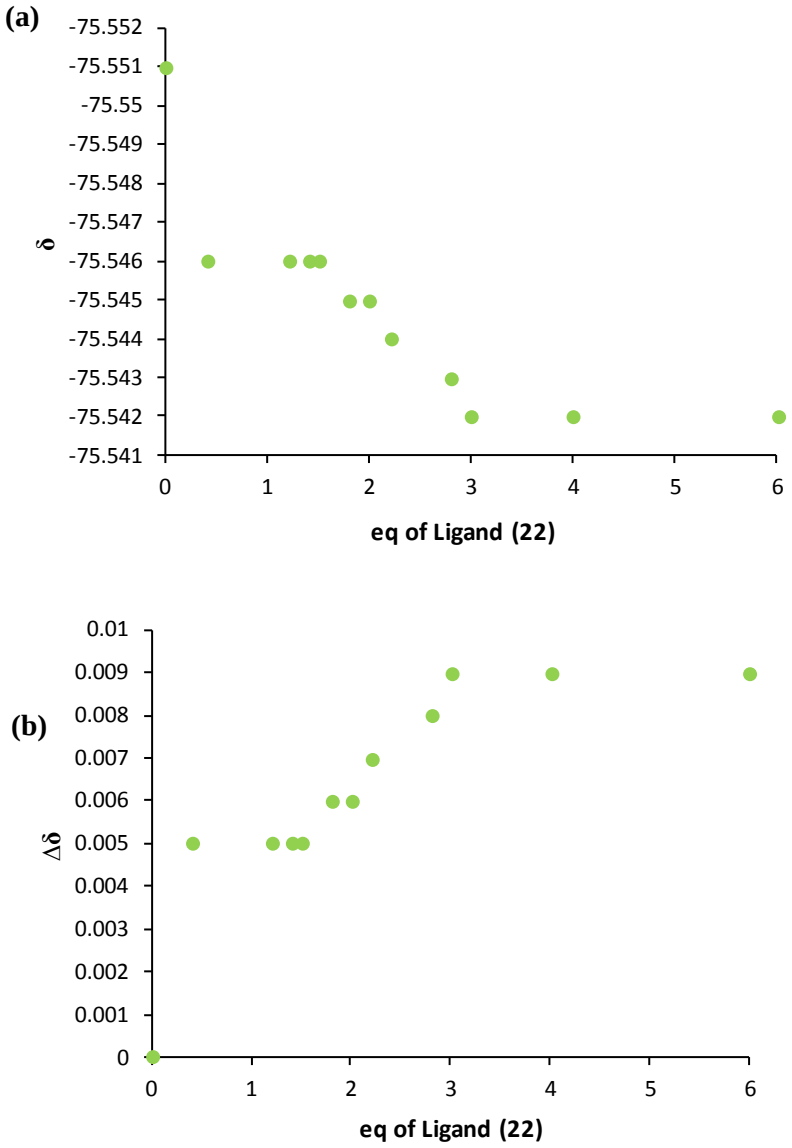

Figure 3-13: (a) *Plots of the ^{19}F-NMR titration of CF_3COOAg with an increasing amount of sugar triazole ligand (**22**) in D_2O.* ***(b)*** *Change in fluorine chemical shift as a function of ligand (**22**).*

3.5 Conclusion

This chapter reported the effect of using CF_3COOAg to form AgNPs in the presence of sugar triazole ligands (**18**), (**22**) and (**23**). The morphology of AgNPs was not affected by switching the counter ion from NO_3^- to CF_3COO^-. However, different sizes of AgNPs were produced depending on the nature ligand. Among these ligands,

(**23**) produced tunable sizes of AgNPs using $AgNO_3$ and CF_3COOAg. Reducing the acidity of the conjugate acid of silver salt by using CF_3COOAg resulted in the reduction of the size tunability of AgNP@(**23**) compared to that observed when $AgNO_3$ was used. Incorporation of a third sugar unit on the southern part of ligand (**22**) reduced the effect of the counter ions on the size of AgNP@(**22**). Ligand (**18**) produced similar sizes of AgNP@(**18**) using both salts while the CF_3COO^- counter ion significantly reduced the Ag(I) binding affinity of ligand (**18**) compared to $AgNO_3$. At present, the actuale role of CF_3COO^- in the formation of AgNPs is not clear, and this aspect will be a subject of further investigation.

3.6 Experimental

3.6.1 Synthesis of sugar triazole (18)

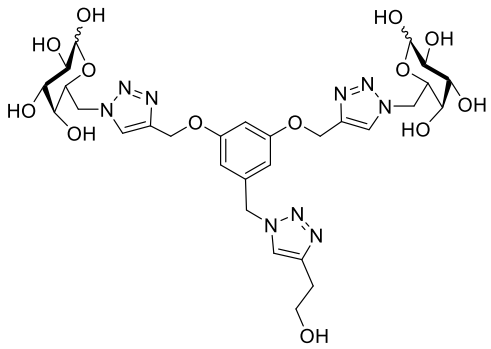

To a stirred solution of (**35**) (0.56 g, 0.7 mmol) in DMSO (5 mL) was added 3-butyn-1-ol (**58**) (0.48 g, 7 mmol) and Ps-NHC-Cu(I) (**59**) (1.46 mmol/g catalyst loading, 0.67 g, 0.98 mmol) under a nitrogen atmosphere and left stirring overnight at room temperature. The reaction mixture was quenched with brine (10 mL) and filtered to remove the catalyst. The solution was then extracted with EtOAc (3 × 20 mL) and the combined organic layers were washed with brine (5 × 50 mL), 1.3% NH_3 (2 × 50 mL) and finally brine (50 mL). The organic layer was then dried over $MgSO_4$, filtered and concentrated

in vacuo. The crude residue was added to a mixture of TFA:water (1:1, 8 mL) under a nitrogen atmosphere and heated to reflux for 3 h. The mixture was then cooled to room temperature followed by concentration *in vacuo*. The residue was diluted with H_2O (30 ml) and concentrated *in vacuo* again to remove excess TFA. The product was precipitated with Et_2O. The crude residue was diluted in H_2O and purified by semi-preparative HPLC using H_2O and MeCN. The product was freeze-dried to afford (**18**) (0.4 g, 79%) as a white powder. This compound was isolated as a mixture of diastereomers (see Appendix B60).

LRMS (ESI) m/z: $[M + Na]^+$ 744.

MP. 178-180°C.

^{1}H NMR (D_2O, 500 MHz): δ 2.88 (t, 6.3 Hz), 3.53-3.57 (m), 3.64-3.66 (m), 3.81 (t, 6.3 Hz), 3.87 (bs), 3.93 (bs), 4.00 (bs), 4.03-4.05 (m), 4.43-4.44 (m), 4.50 (d, 7.8 Hz), 4.56-4.69 (m), 5.09 (s), 5.23 (bs), 5.43 (s), 6.54 (s), 6.56 (s), 7.80 (s), 8.04 (s).

^{13}C NMR (D_2O, 125 MHz): δ 27.8, 50.8, 50.9, 53.4, 60.5, 61.2, 68.1, 68.7, 68.9, 69.0, 69.4, 71.6, 72.6, 73.1, 92.3, 96.5, 102.4, 107.9, 123.9, 125.7, 125.8, 137.8, 142.9, 145.4, 159.0.

3.6.2 Silver nanoparticle (AgNP) formation

Preparation of sugar stock solutions: The corresponding sugar triazoles (**18**, **22** and **23**) were dissolved in ultrapure H_2O and diluted to a standard concentration of 50 mM. These stock solutions were then used to screen the optimal conditions for AgNP formation.

Preparation of Tollens' reagent stock solutions: Stock solutions of Tollens' reagent were prepared in three different concentrations (100, 20 and 3 mM) and diluted as required with ultrapure H_2O for the preparation of the nanoparticle arrays.

100 mM Tollens: To 1.8 mL H_2O was added CF_3COOAg (0.5 M, 500 µL), followed by NaOH (3 M, 100 µL) and finally NH_4OH (28%, 110 µL).

20 mM Tollens: To 4.1 mL H_2O was added CF_3COOAg (0.5 M, 279 µL), followed by NaOH (3 M, 56 µL) and finally NH_4OH (28%, 61 µL).

3 mM Tollens: To 9.9 mL H_2O was added CF_3COOAg (0.5 M, 60 µL), followed by NaOH (3 M, 12 µL) and finally NH_4OH (28%, 13 µL).

AgNPs were formed by the addition of 300 µL of Tollens' reagent to 300 µL of a solution of an appropriate sugar ligand in a plastic eppendorf. The solution was vortexed and left in the dark overnight. The mixture was centrifuged for 30 seconds to afford a suspension of colloidal of AgNPs.

3.6.3 Reaction kinetics of AgNP formation

Time course: 200 µL of sugar solutions (**18**, **22** or **23**) at 200 µM and 200 µL of Tollens' solution (20 mM) were mixed in a low-volume quartz cuvette; UV-Vis measurements were taken at 400 nm every 5 seconds using a UV-Vis spectrophotometer.

3.6.4 General procedure for ^{1}H NMR titration studies

Stock solutions of triazole ligands (**18, 22** or **23**) at 2 mM and CF_3COOAg (12 mM) were prepared in D_2O. 300 µL of aliquots of the ligands were mixed with increasing amounts of CF_3COOAg and diluted with D_2O up to 600 µL. The recorded spectra are shown at different concentrations of CF_3COOAg from 0 to 6 mM. The acquired ^{1}H NMR data of the triazole sugar ligands and the concentration of the Ag(I) was used to calculate the Ag(I) binding constants using WinEQNMR2 software.[108]

3.6.5 General procedure for ^{19}F NMR titration studies

Stock solutions of CF_3COOAg at 2 mM and triazole ligands (**18, 22** or **23**) (12 mM) were prepared in D_2O. 300 µL of aliquots of CF_3COOAg were mixed with increasing amounts of the ligands and diluted with D_2O up to 600 µL. The recorded spectra are shown at different concentrations of the ligands from 0 to 6 mM.

CHAPTER 4: POLYETHYLENE GLYCOL-MEDIATED FORMATION OF SILVER NANOPARTICLES

4.1 Inroduction

The chemistry of polyethylene glycol (PEG) has received a great interest in biological research due to their hydrophilicity, biocompatibility and reduced immunogenicity.[123-127] PEG is a polymer of ethylene glycol with the general structure shown in Figure 4.1.

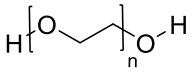

Figure 4-1: *General structure of a PEG polymer, n refers to the number of repeating ethylene oxide units.*

The high flexibility and non-toxicity of PEG molecules renders these polymers key building blocks for the conjugation to other molecules such as proteins, polypeptides[126] and nanoparticles[124]. This concept is known as "PEGylation". The ability of PEG to hydrogen-bond with water can mask proteins from the immune system and can therefore reduce immunogenicity.[128,129] Since the original development of PEGylation in 1977,[128,129] considerable progress has been made to graft PEG groups onto biomolecules and nanoparticles to improve efficient synthetic methods for this class of bioconjugation.[130-134]

Current challenges in this field focus on the development of environmentally friendly methods for the synthesis of hydrophilic and size-controlled functionalised polymeric metal NPs.[135-139] Beside these aspects, understanding the factor that can affect the stability of NPs to provide the required biocompatibility for sensing applications has been a great challenge.[140] Taking into consideration the unique advantages of PEGylated metal NPs, this chapter will focus on the investigation of sugar triazole

ligands bearing small PEG chains and how they influence the preparation of AgNPs using Tollens' reagent.

4.1.1 PEGylation of metal nanoparticles

PEG-functionalised metal NPs have emerged as a promising tool for diagnostics and therapeutics due to their following properties: (i) one of the crucial features of PEG molecules is increasing the solubility of NPs in water;[135] (ii) PEG hydrophilic molecules can reduce the interaction between nanoparticles and therefore protect them from aggregation due to the steric repulsion between the PEG chains;[140] (iii) PEG molecules reduce the surface charge of nanoparticles, thus reducing their immunogenicity[141] and (iv) one of the essential aspects of PEG molecules is the ability to modify the terminal hydroxyl groups with functional groups suitable for bioconjugation such as thiol,[142-146] aldehyde[147] and carboxylic acid.[145]

Generally, there are two fundamental methods for the modification of NPs with PEG polymers. The first approach is to attach PEG molecules directly to the surface of NPs by electrostatic interaction between the negatively polarized oxygen groups of PEG and the positively charged NP.[138] This method can be achieved by the preparation of NPs directly in PEG polymeric media as discussed in the polyol process for AgNPs synthesis using PEG as a reducing agent (Section 1.3.2.1) or in the presence of an appropriate reducing agent such as β-D-glucose (Scheme 4-1). The synthesis of AgNPs involves the addition of silver nitrate into an aqueous PEG solution to putatively form a $[Ag(PEG)]^+$ complex, which is then reduced by β-D-glucose to form PEG-capped AgNPs and gluconic acid (**57**) (Equation 11 and Equation 12).[138]

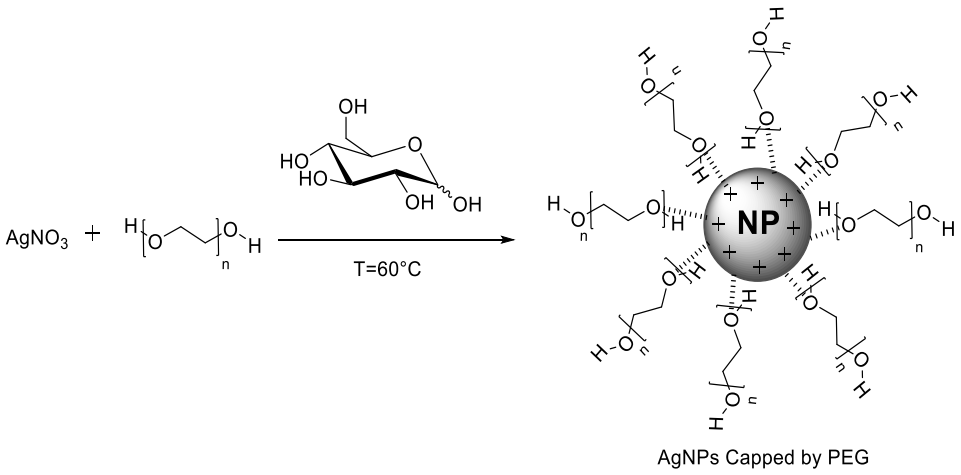

Scheme 4-1: *Synthesis of AgNPs capped by PEG using $AgNO_3$ and β-D-glucose. Scheme adapted with permission from Reference 138.*

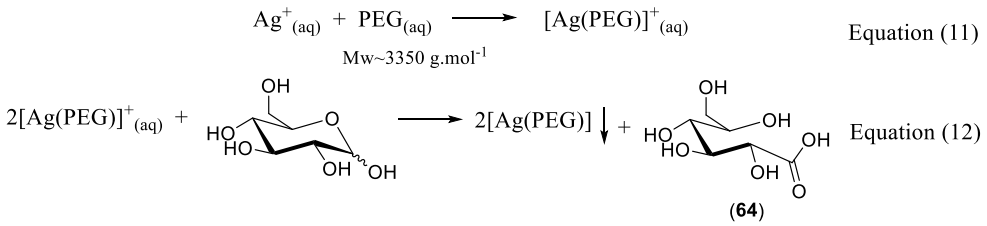

The second approach to PEGylated metal NP synthesis is to modify one of the terminal ends of PEG with functional groups such as thiol to passivate the surface of AuNP.[142,144] For example, Brust's group developed a synthetic route to prepare biocompatible AuNPs stabilised by thioalkylated PEG ligand (Figure 4-2).[144,145] An interesting feature of this ligand is that the hydrophopic alkane chain can enhance the interaction of the thiol group with the surface of gold NPs and increase their colloidal stability in "high salt" buffer solutions.[148] This polymer can provide the required biocompatibility for biological applications due to the facility to prepare other derivatives with carboxyl and amino groups that target biomolecules such as proteins and peptides using standard amine coupling methods (Scheme 4-2).[145] In these reactions, carboxyl group-modified NP (**65**) activates with EDC or sulfo-NHS to form the activated ester (**66**) that can react with an amino group of a protein to form a

stable amide bond (**67**). In the case of amino-modified NP, the sulfo-SMCC ester (**69**) is commonly used to cross-link amino- and thiol biomolecules to form (**71**).[125]

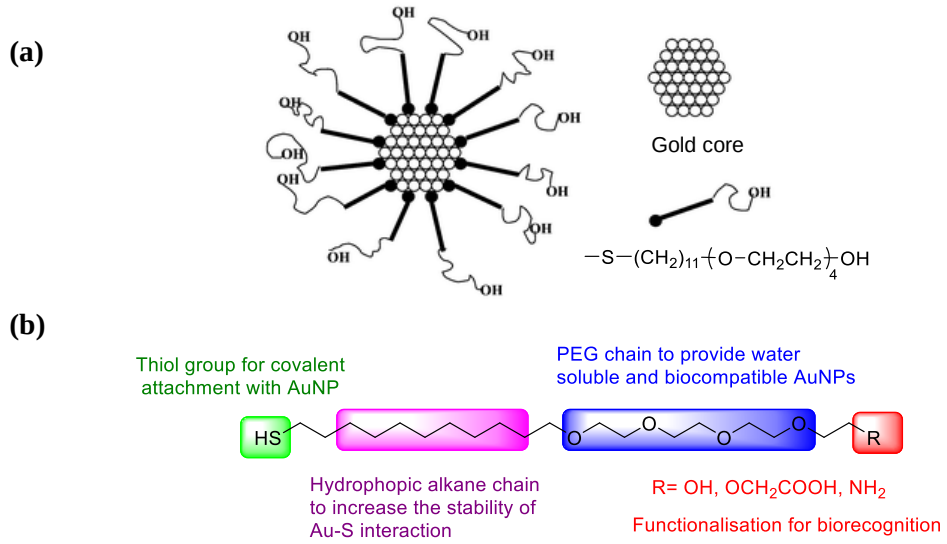

Figure 4-2: ***(a)*** *Schematic representation of AuNPs capped by thioalkylated PEG molecules.* ***(b)*** *Chemical structure of thioalkylated PEG molecule and its properties for biological applications.* ***(a)*** *Adapted from Reference 144 with permission of The Royal Society of Chemistry.*

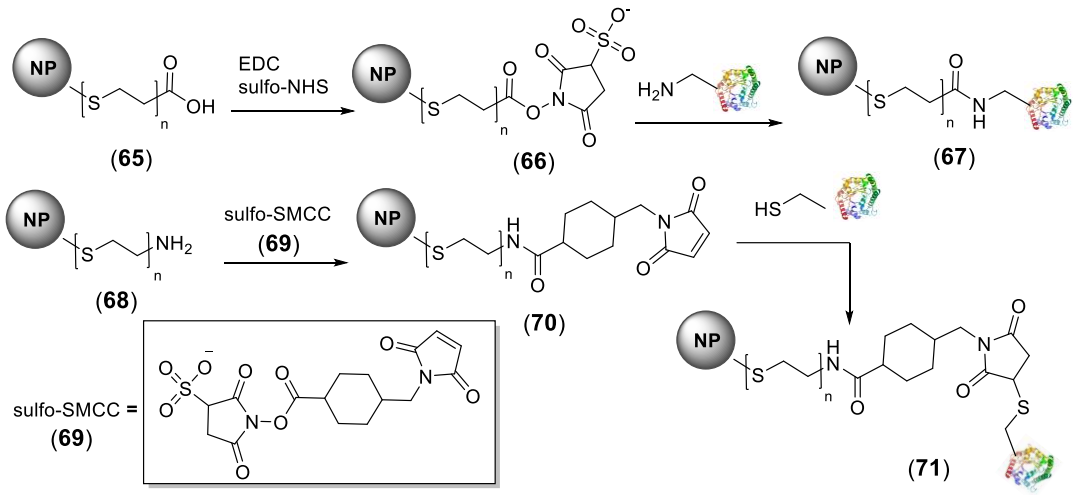

Scheme 4-2: *Common conjugation reactions of proteins with activated NPs.*

One of the key challenges in using nanoparticles for applications in sensing and therapy is to achieve specific and selective bioconjugation.[131,133,149,150] This is an

important aspect as many proteins have multiple amino and thiol groups. Recently, click chemistry has been widely used to attach NPs at a specific site of biomolecules such as DNA[82] and proteins[131,133] (see Section 1.3.3.1). This reaction proceeds under mild conditions using azide- or alkyne-modified biomolecules. For example, Brust's group developed a facile approach to immobilise lipase molecules onto azide-functionalised AuNPs via CuAAC reaction without loss of their enzymatic activity.[131] This method proceeded in two steps involving covalent attachment of azide-functionalised PEG thiolate ligand (**72**, Scheme 4-3) to AuNPs followed by a click reaction with acetylene-functionalised lipase molecules (**73**).

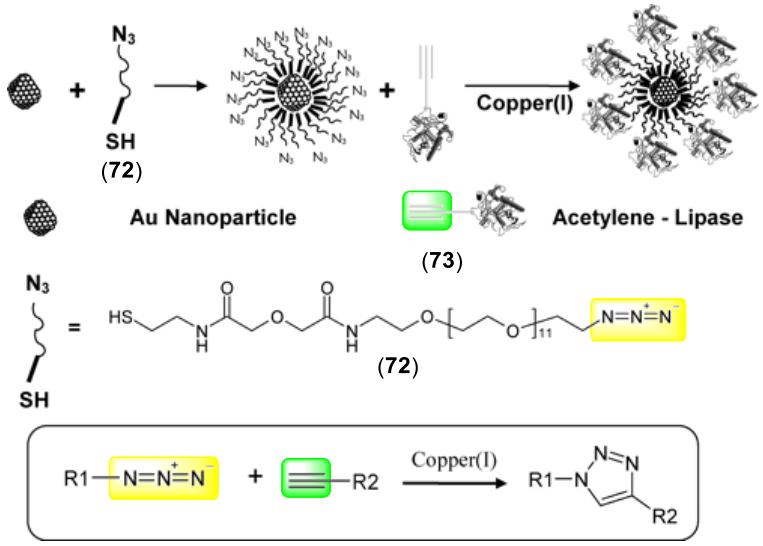

Scheme 4-3: *Schematic representation of the preparation of lipase-coated AuNPs. Figure adapted with permission from Reference 131. Copyright (2006) American Chemical Society.*

4.1.2 Copper-free click chemistry

Although CuAAC reactions have become efficient synthetic tools for functionalisation biomolecules, they have some distinct disadvantages.[151-153] One major limitation is the use of Cu(I) that can produce reactive oxygen species (ROS)

such as H_2O_2 and $^{\cdot}OH$ via Fenton chemistry (Equations 13-15). The production of ROS can lead to damage of biomolecules such as DNA.[154-156]

$$Cu(II) + O_2^{\bullet -} \longrightarrow Cu(I) + O_2 \qquad \text{Equation (13)}$$

$$2O_2^{\bullet -} + 2H^+ \longrightarrow H_2O_2 + O_2 \qquad \text{Equation (14)}$$

$$Cu(I) + H_2O_2 \longrightarrow Cu(II) + {}^{\bullet}OH + OH^- \qquad \text{Equation (15)}$$

One approach to overcome the potential toxicity of copper ions is to use strain-promoted alkyne azide cycloaddition (SPAAC).[151-153] Initially, Witting and Kerbs[157] reported the fast reaction between cyclooctynes and phenyl azide to form a single triazole product with the rate constant of 1.2×10^{-3} $M^{-1}s^{-1}$.[158] Bertozzi *et al.* developed a bioconjugation version of this reaction and demonstrated its effectiveness in labelling biomolecules (Scheme 4-4).[159]

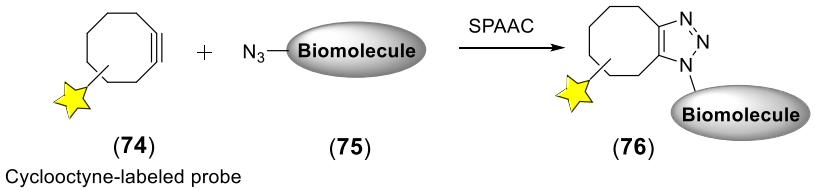

Scheme 4-4: *Schematic representation of labelling biomolecules via SPAAC.*

The reactivity of cyclooctynes to [3+2] cycloaddition reactions is attributed to the distortion of the triple bond in cyclooctynes (160°) compared to ideal angle bond in linear alkynes (180°) (Scheme 4-5a, b). Such destabilisation can enforce a high ring strain energy (18 kcal/mol), which in turn decreases the energy required to distort the reaction components toward the transition state of the reaction.[160] A typical reaction of cyclooctyne derivatives provide a regioisomeric mixture of triazoles (**83**) and (**84**) (Scheme 4-5c). Bertozzi *et al.* reported the use of a biotin cyclooctyne probe (**89**) to label azide-modified glycoprotein (**90**) selectively in living cells (Scheme 4-6b).[159]

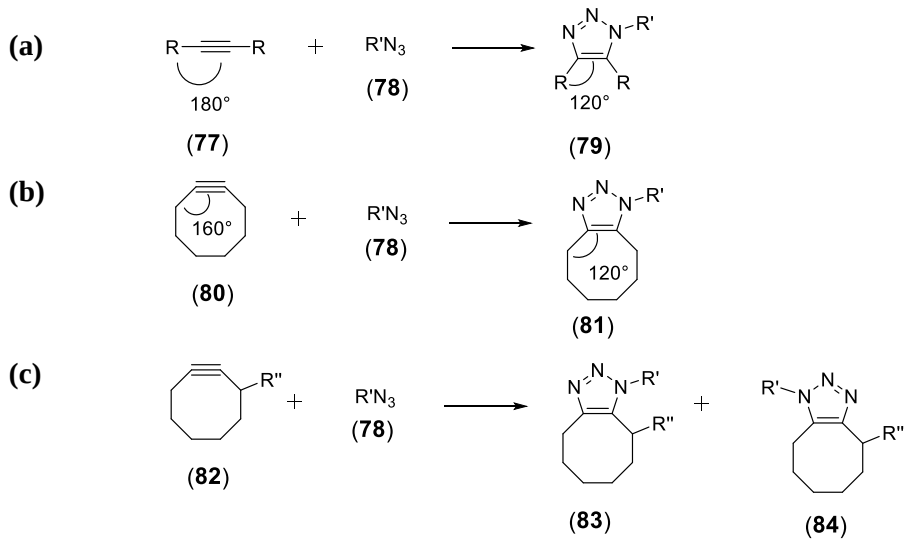

Scheme 4-5: *A comparison of bond angles between* ***(a)*** *linear alkynes and* ***(b)*** *cyclooctynes.* ***(c)*** *SPAAC reaction between cyclooctyne derivatives and azides.*

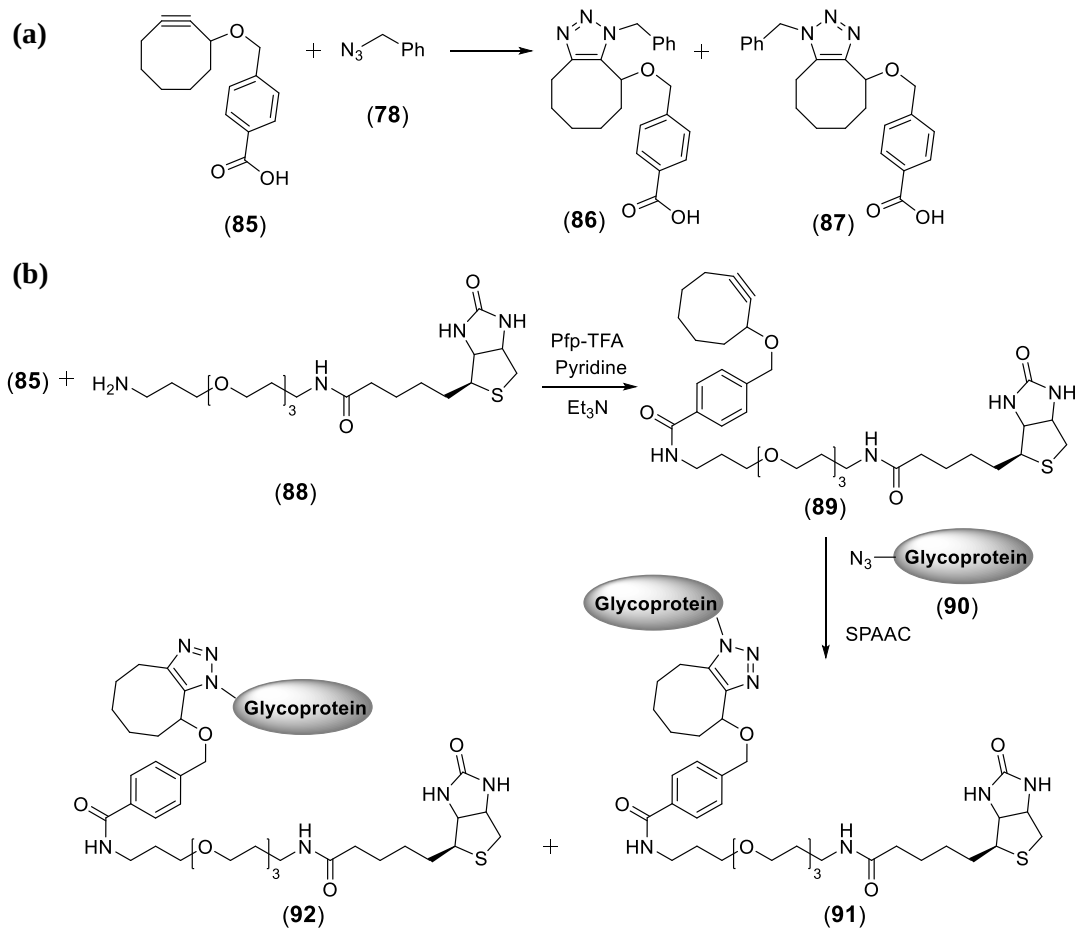

Scheme 4-6: ***(a)*** *General reaction between cyclooctyne* ***(85)*** *and benzyl azide* ***(78)****.* ***(b)*** *Labelling glycoproteins with biotin using copper-free click reaction.*

Following this initial exploration, a series of cyclooctyne derivatives have been investigated to improve the cycloaddition reactivity for biological applications (Figure 4-3).

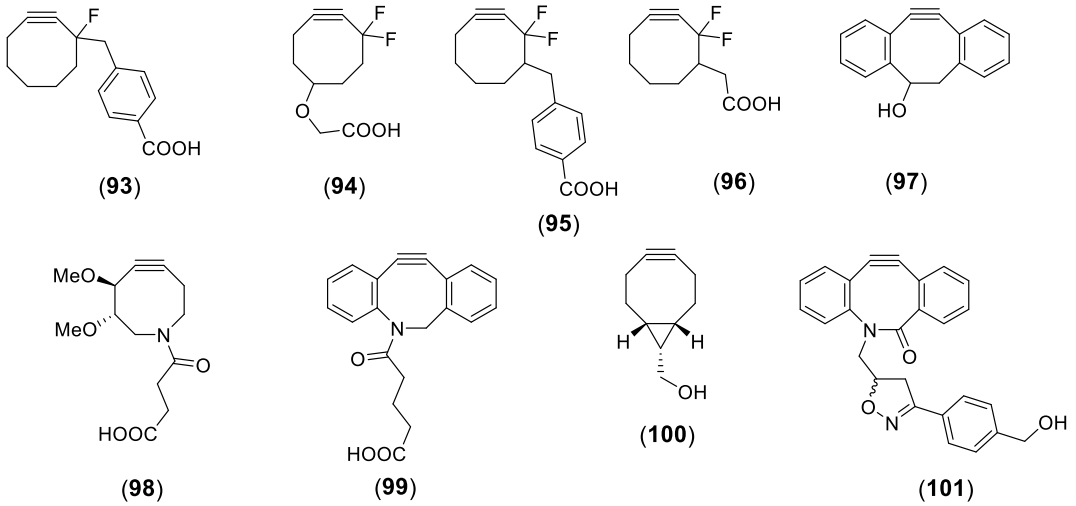

Figure 4-3: *Structures of common cyclooctyne reagents used in SPAAC.*

Bertozzi *et al.* reported that the addition of an electron-withdrawing group such as fluorine at the propargylic position in cyclooctyne (**93**) increases the rate of cycloaddition reactions by 4-fold compared to (**85**).[161] Interestingly, difluorinated cyclooctynes (DIFO) (**94-96**) afforded a 60-fold increase in the reaction rate.[162,163] Boons *et al.* reported an alternative approach to enhance the reactivity of cyclooctynes by introducing fused aromatic rings to increase the ring strain (**97**) affording a rate enhancement similar to (**94-96**).[164] This structure exhibited high stability due to the *ortho* hydrogens of the aromatic rings that can protect the alkyne from nucleophilic attack.

Other structures have been developed to improve the hydrophilic nature of these molecules. Bertozzi *et al.* synthesised a heterocyclooctyne called di-methoxy-aza-cyclooctyne (DIMAC) (**98**) as an example of polar cyclooctynes.[165] The

incorporation of a nitrogen atom into the ring provided a convenient attachment site for functionalisation. Delft *et al.* developed a novel cyclooctyne derivative, aza-dibenzocyclooctyne (DIBAC) (**99**), combining the reactivity feature of fused aromatic rings in DIBO (**97**) and the hydrophilic property in DIMAC (**98**).[166] Furthermore, they synthesised a symmetrical cyclooctyne, bicyclononyne (BCN) (**100**), that afforded a single regioisomer cycloadduct in reaction with azides.[167] Among these structures, biarylazacyclooctynone (BARAC) (**101**) developed by Bertozzi *et al.* has the highest sensitivity, solubility and reactivity toward cycloaddition.[168] The authors reported that this compound displayed a 800-fold rate enhancement relative to (**85**). This exceptional reactivity is attributed to the resonance structure of the amide within the ring in addition to the effect of fused dibenzo system.

The advent of SPAAC has led to the design of effective diagnostic tools for biological applications. One of the most recent technologies that can be used to recognise specific molecules such as carbohydrates, DNA, and fluorescent dyes is functionalisation of surfaces using metal-free click chemistry.[169,170] For example, Burley *et al.* developed a novel method to detect DNA sequences selectively using polyamide microarrays and SPAAC reactions.[169] The array was designed by immobilisation of polyamide-cyclooctyne (**102**) on azide-modified glass substrate (**103**) using microcontact printing (Figure 4-4). Thereby, a polydimethylsiloxane (PDMS) stamp was inked with polyamide-cyclooctyne which was then applied directly to the azide substrate in order to generate polyamide-patterned surfaces. This microarray pattern is an efficient tool to detect double-strand DNA sequences

selectively based on the affinity and specificity of binding polyamides via hydrogen bonding in the minor groove.[171]

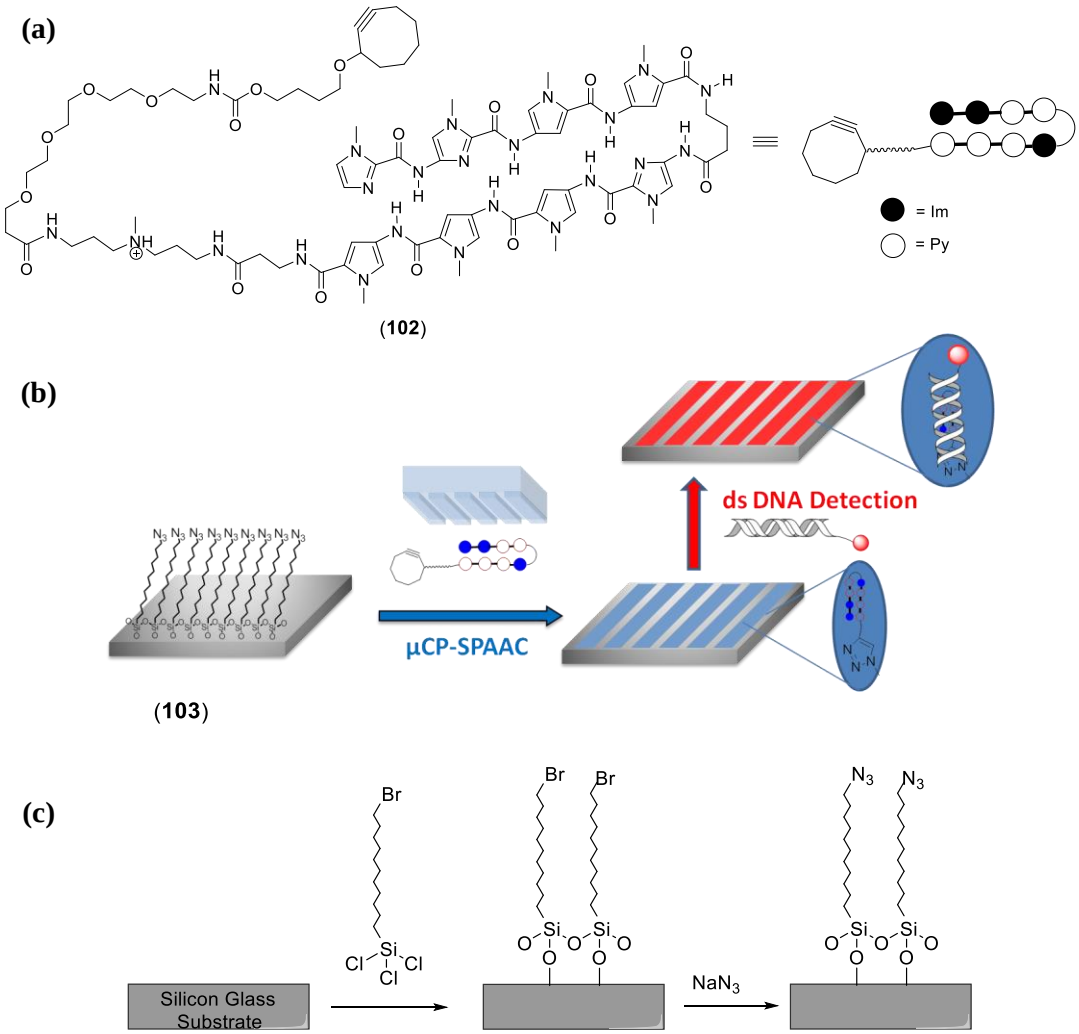

Figure 4-4: *Schematic representation of polyamide microarrays for DNA detection.* ***(a)*** *Structure of cyclooctyne-modified pyrrole (Py)-imidazole (Im) polyamide.* ***(b)*** *Immobilisation of polyamide-cyclooctyne on azide-modified glass substrate using microcontact printing (µCP) and SPAAC reaction. The polyamide detects target DNA-binding sites in duplex DNA tagged with fluorophore.* ***(c)*** *Preparation of azide-modified silicon and glass substrate.* ***(a)*** *and* ***(b)*** *Reproduced with permission from Reference 169. Copyright (2013) American Chemical Society.*

4.1.2.1 Applications of SPAAC for functionalisation of nanoparticles

The chemistry of cyclooctynes has been exploited to develop rapid and sensitive methods to functionalise NPs with biological molecules.[150] Texier *et al.*

demonstrated an example of SPAAC reaction to synthesise monosaccharide-functionalised QD (**108**) in two step using CdSe/ZnS QD coated with PEG amino groups (**104**) (Scheme 4-7a).[172] QD are known as semiconductor nanocrystals with highly fluorescent properties that allow their uses in imaging applications.[173] The authors reported the efficiency of SPAAC reaction between QD-cyclooctyne (**106**) and azido-modified monosaccharide (**107**) to provide more highly luminescent conjugates (**108**) compared to the standard Cu(I)-catalysed click reaction.[172] Copper ions can chelate with PEG groups that coated the NPs and significantly inhibit the fluorescent properties of QD due to photo-induced electron transfer between QD and Cu ions, resulting in irreversible fluorescence emission (Figure 4-5).[174,172] Texier *et al*. illustrated the ability of SPAAC as an excellent tool for imaging the biosynthesis of sialylated oligosaccharides,[172] a modification that occurs in pathologies such as carcinogenesis.[175] In this method, acetylated azido-mannosamine (**109**) was incorporated into glycoproteins to detect modified sialic acid (**110**) using cyclooctyne-functionalised QD (**106**) at low concentration (250 nM) (Scheme 4-7).[172]

Workentin *et al.* developed a biorthogonal method to synthesise water-soluble AuNPs functionalised with DBCO (**115**) (Scheme 4-8).[176] The synthesis was conducted by exchange reaction between methyl-terminated PEG3-coated AuNPs (**111**) and the thiol group in (**112**) to produce PEG-carboxy functionalised AuNPs (**113**) followed by amide coupling with DBCO-amine (**114**). The reactivity of (**115**) towards the interfacial SPAAC was reported by using azide-decorated polymersome vesicles **(116**) to afford a successful functionalisation of polymersomes with AuNPs (3nm) (Figure 4-6).

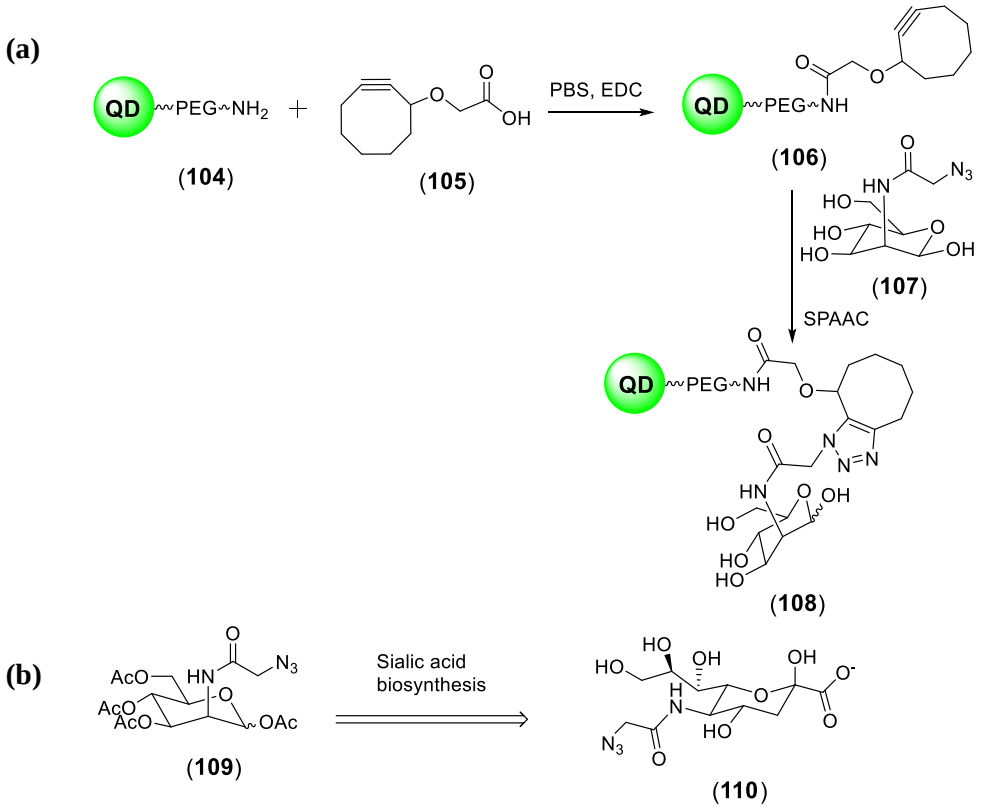

***Scheme 4-7**: **(a)** Schematic representation of monosaccharide-functionalised QD synthesis via SPAAC reaction. **(b)** Modification of mannosamine to biosynthesise modified sialic acid. Scheme reproduced with permission from Reference 172. Copyright (2010) American Chemical Society.*

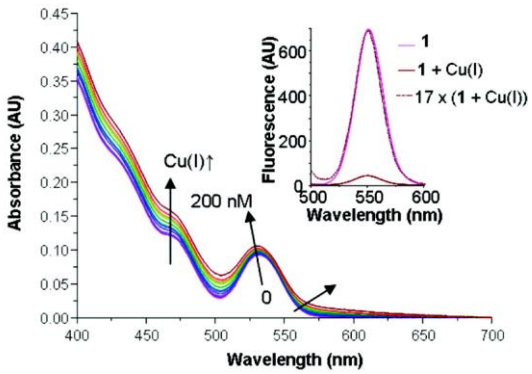

***Figure 4-5:** Absorption spectra of QD-amine (**104**) (17 nM) in the presence of increasing concentrations of Cu(I). Inset: luminescence spectra of QD-amine (**104**) (17 nM) in the absence and in the presence of 5 µM Cu(I). Figure reproduced with permission from Reference 172. Copyright (2010) American Chemical Society.*

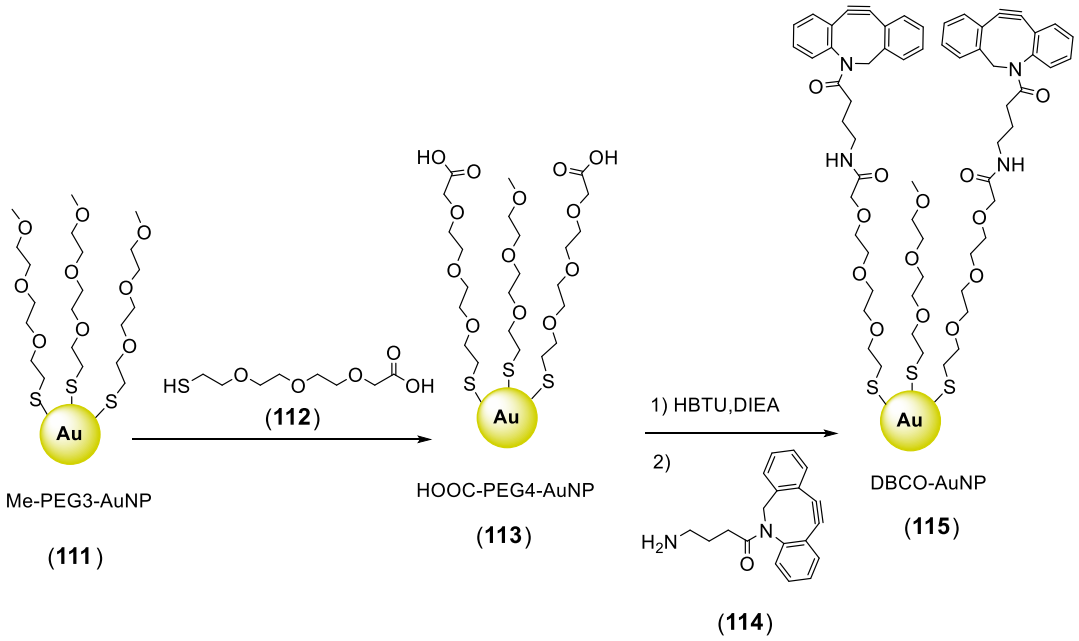

Scheme 4-8: *Schematic representation of DBCO-functionalised AuNP synthesis. Scheme adapted from Reference 176 with permission from the Royal Society of Chemistry.*

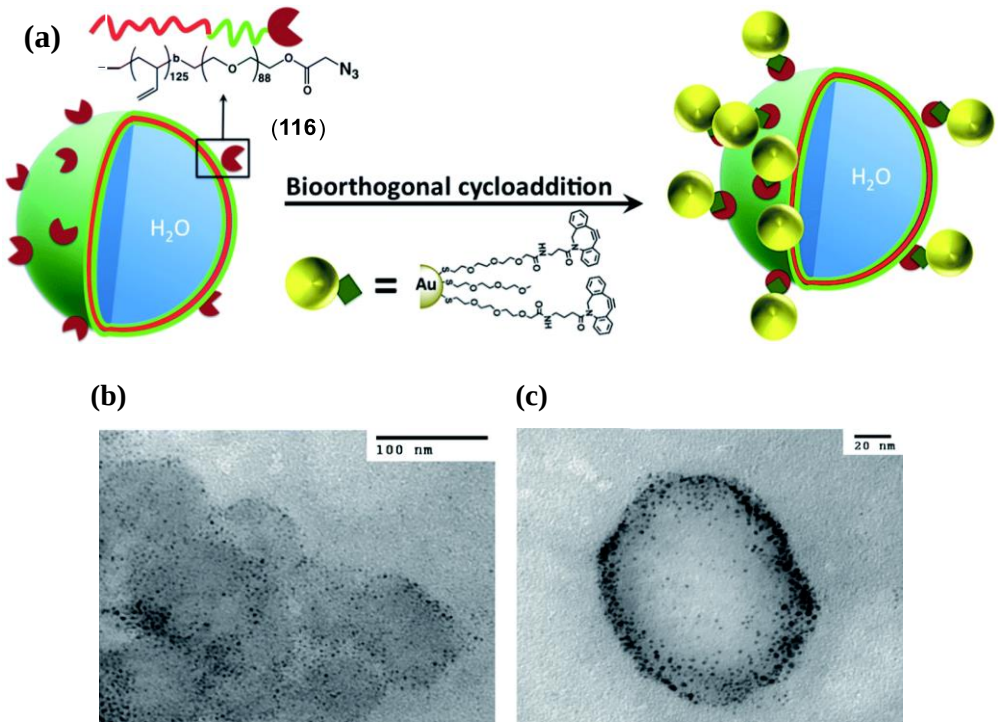

Figure 4-6: ***(a)*** *A cartoon representing the I-SPAAC reaction between DBCO–AuNPs* ***(115)*** *and azide-functionalised polymersomes* ***(116)****.* ***(b)*** *TEM image of the control experiment Me–EG3–AuNP with azide-functionalised polymersomes.* ***(c)*** *TEM image of vesicles covered with AuNPs through the I-SPAAC reaction. Figure adapted from Reference 176 with permission from the Royal Society of Chemistry.*

All of these investigations revealed the potential of using SPAAC as an effective tool for functionalisation of NPs with biological molecules. However, a key challenge in these applications is access to facile, reliable one-step preparative methods where the parameters of size, shape and surface coating can be easily controlled during the formation of the NP conjugate.[177,178] Based on a template-directed approach for the synthesis of size- and shape-controlled AgNP using Tollens' reagent and sugar triazoles (**18**, **23,** Chapter two), this chapter aims to develop the synthesis of PEGylated sugar triazoles (**24-26**, Figure 4-7) to enhance the modularity of this synthetic approach for the preparation of AgNP for biodiagnostic applications.

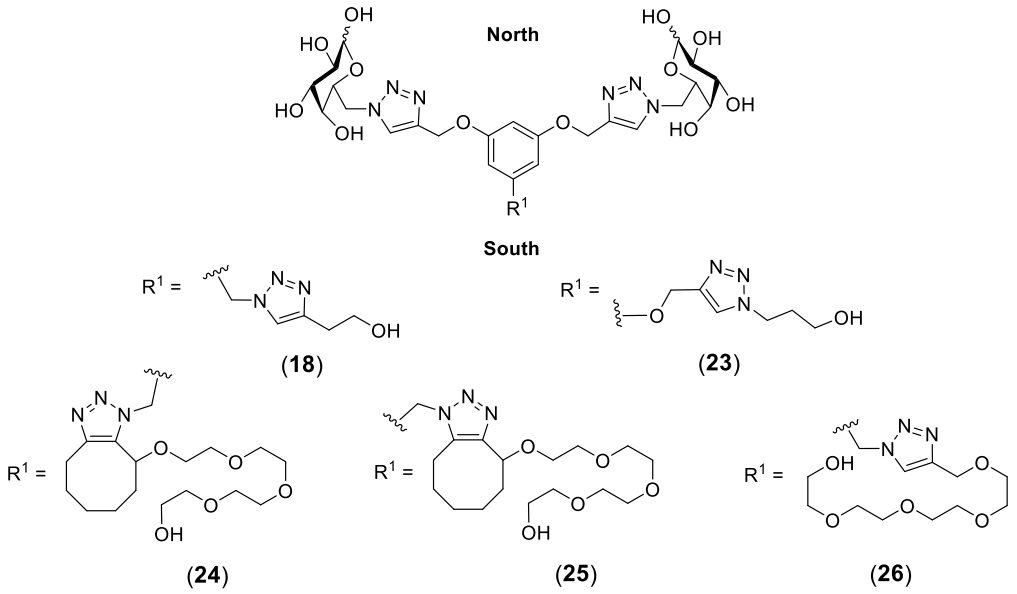

***Figure 4-7**: Structures of PEG-functionalised triazole ligands*

4.2 Hypothesis

In chapter two, the structural features of triazole ligands (**18**) and (**23**) were shown to influence size and shape of AgNPs. Importantly, the core structure of (**18**) and (**23**) influenced Ag(I)-binding affinity, with lower affinity ligands, producing monodisperse AgNP@(**23**) where the size and shape was tunable according to the

reaction conditions. Based on these results, the working hypothesis is that the southern part of the core of ligands (**24-26**, Figure 4-7) will influence AgNP formation. This effect was probed by introducing a triazole ring, using SPAAC to afford two triazole regioisomers (**24**) and (**25**). Increasing the rigidity of the southern portion ring using SPAAC reactions could affect the binding behaviour of ligands with Ag(I) and tune the size and shape of formed AgNPs. Finally, in order to explore the role of the cyclooctyne group attached to the southernmost triazole, the aliphatic alcohol chain in (**18**) was replaced with a PEG4 chain (**26**). Introducing PEG hydrophilic group to these ligands could play a defining role in the formation of AgNPs.

4.3 Aims

The aims of this chapter are:

1) To synthesise PEG-functionalised sugar triazole ligands (**24-26**, Figure 4-7).
2) To investigate the potential of ligands (**24-26**) to form AgNPs with controlled sizes and shapes using Tollens' reagent.
3) To study the binding characteristics of these ligands with Ag(I).
4) To determine the surface enhanced Raman scattering (SERS) properties of formed AgNPs.

4.4 Results and Discussion

4.4.1 Synthesis of cyclooctyne-functionalised PEG (120) for SPAAC

Compound (**120**) was prepared in three steps (Scheme 4-9). The first step was the bromination of commercially available cycloheptene (**117**) using bromoform and this afforded dibromobicycle (**118**) as a brown oil in 57% yield. The next step involved

ring opening of (**118**) with tetraethylene glycol in the presence of silver perchlorate afforded bromocyclooctene-PEG4 (**119**) in 54% yield. Finally, elimination of HBr using potassium *t*-butoxide and pyridine afforded (**120**) as a colourless oil in 70% yield after column chromatography.

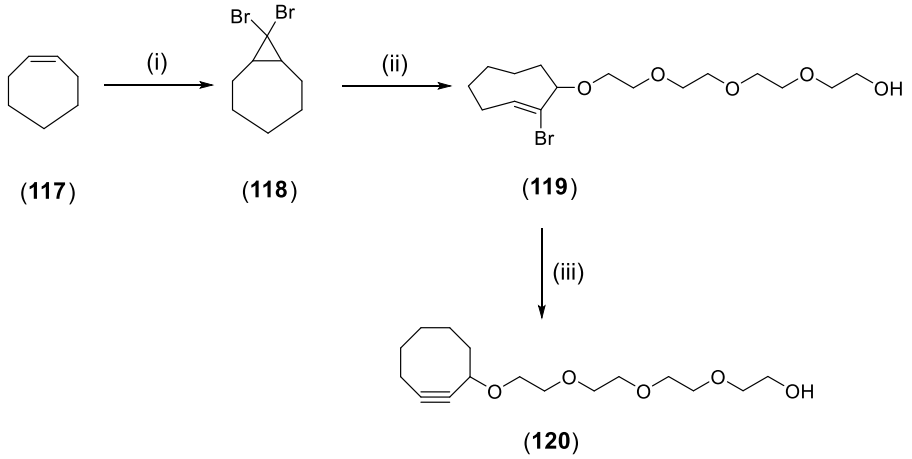

Scheme 4-9: *Reagents and conditions: (i) t-BuOK (1.2 equiv.), bromoform (1.2 equiv.), anhydrous pentane, RT, 57%; (ii) tetraethyleneglycol (30 equiv.), $AgClO_4$ (3.0 equiv.), pyridine (8.3 equiv.), toluene, Δ, 115°C, 4h in the dark, 54%; (iii) t-BuOK (3.0 equiv.), pyridine (17.2 equiv.), i-PrOH, RT, 3d, 70%.*

4.4.2 Synthesis of sugar triazole ligands (24-25)

Compounds (**24-25**) were prepared by SPAAC using (**120**) and (**35**) to afford the two triazole regioisomer ligands (**121**) and (**122**) after column chromatography. Acid deprotection of the isoprolylidene groups and purification by RP-HPLC yielded (**24-25**) (Scheme 4-10). The regiochemistry of each isomer was confirmed by 2D NOESY spectra. For (**121**), an nOes between H_{19} and H_{16} was observed, whereas no nOes was present in (**122**) (Figure 4-8).

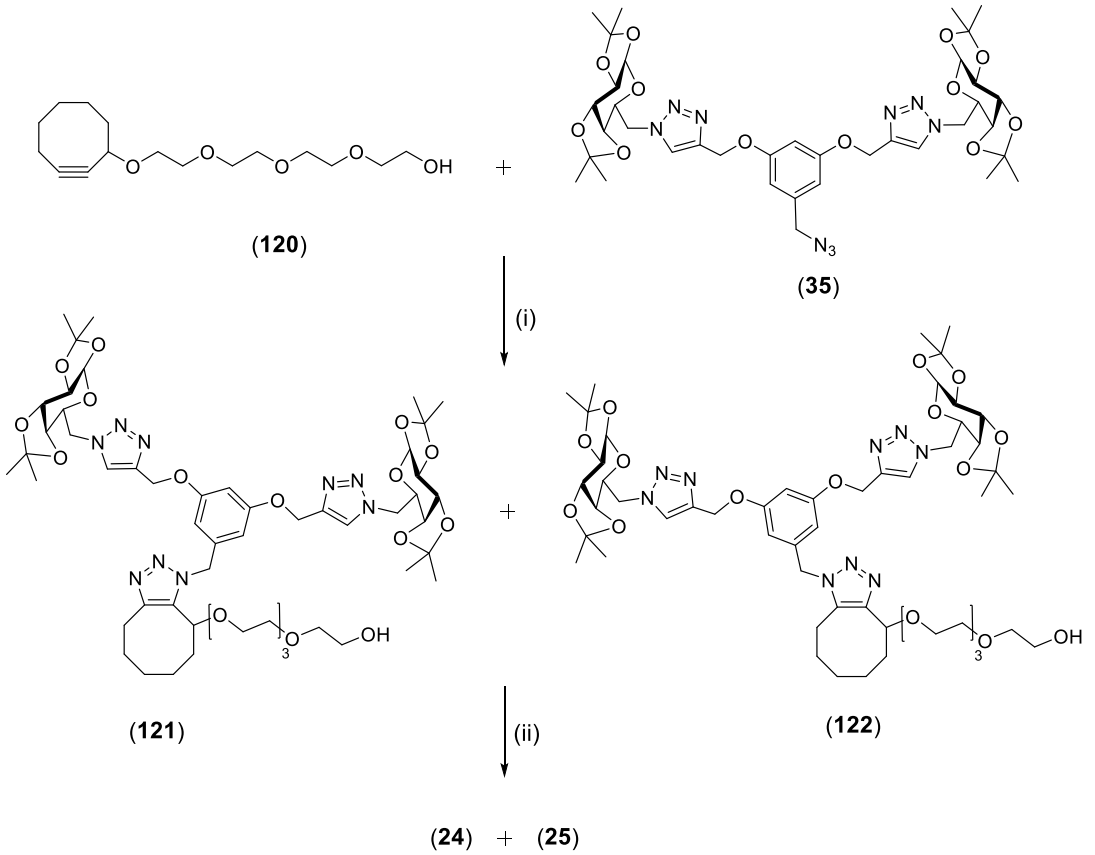

Scheme 4-10: *Reagents and conditions: (i) Compound (**120**) (1.8 equiv.), DMSO, RT, 24h, 37% : 26% (**24 : 25**); (ii) TFA:H_2O (1:1), Δ, 70°C, 3h, 77%.*

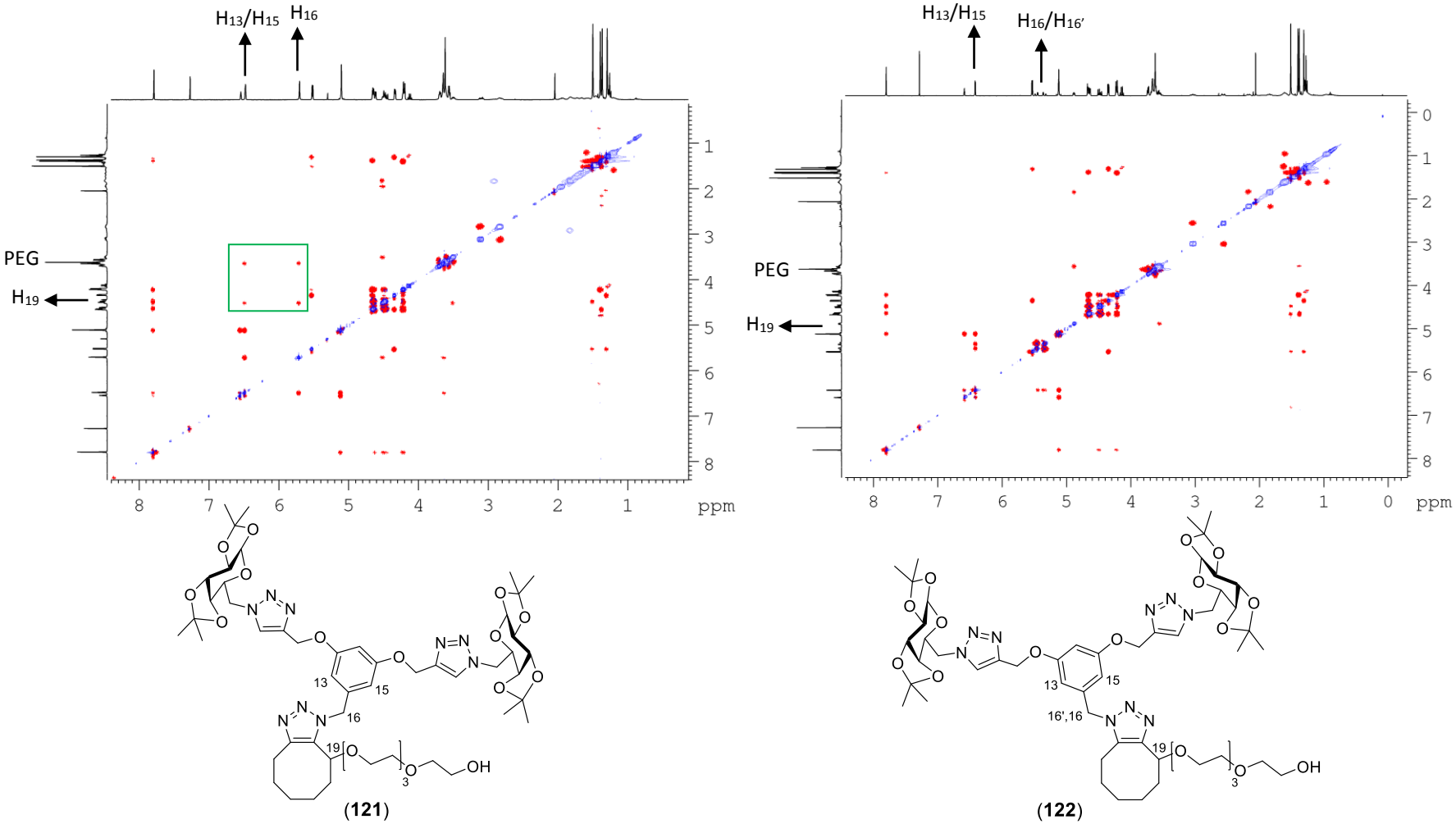

Figure 4-8: *NOESY NMR spectra of two triazole regioisomer ligands* ***(121)*** *and* ***(122)****.*

4.4.3 Synthesis of sugar triazole ligands (26)

Sugar triazole (**26**) was prepared from tetraethylene glycol (**124**) in three steps (Scheme 4-11). Alkylation of tetraethylene glycol (**124**) with propargyl bromide afforded (**125**) as a colourless oil in 80% yield after column chromatography. CuAAC between azide (**35**) and six equivalents of alkyne (**125**) under standard copper-catalysed Huisgen cycloaddition conditions afforded (**126**) as a white solid in 70% yield after column chromatography. Finally, acid deprotection of the isopropylidene groups of (**126**) and purification by RP-HPLC afforded (**26**) as a white powder in 40%.

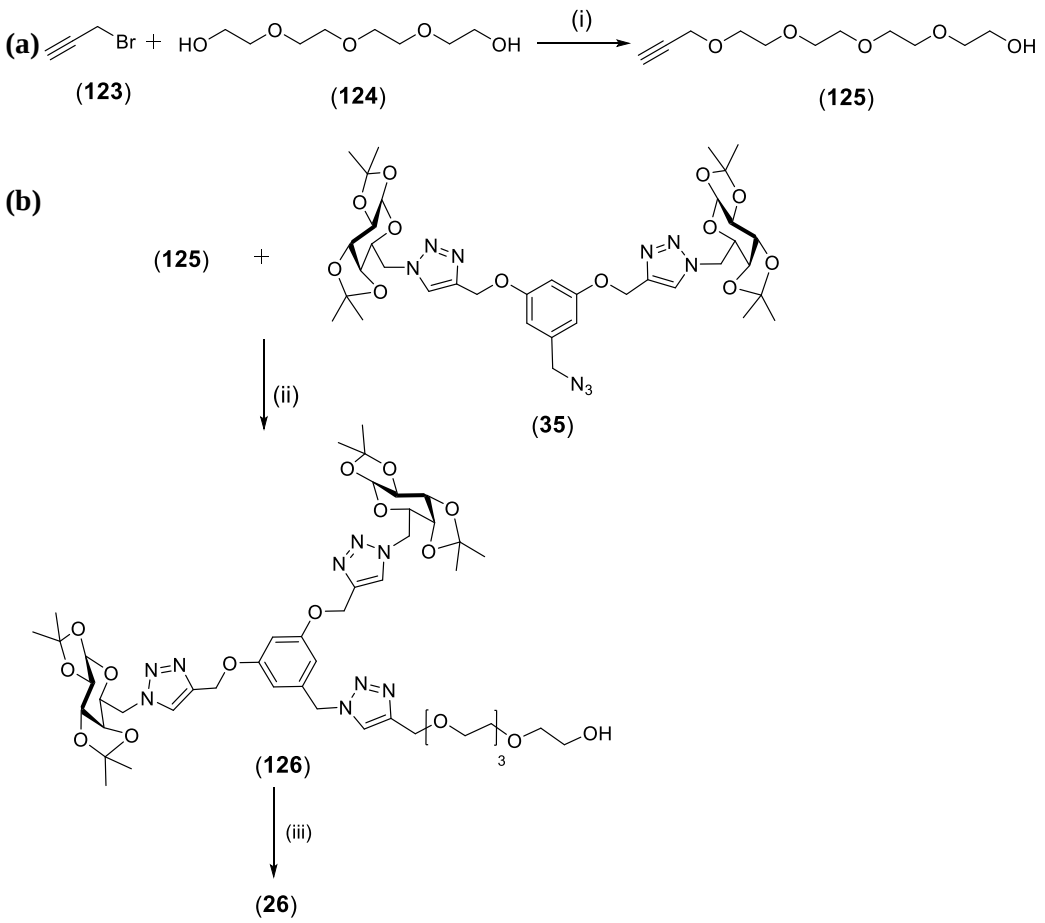

Scheme 4-11: *Reagents and conditions: Compound (**123**) (i) (4.0 equiv.), NaH (1.6 equiv.), dioxane, RT, 80%; (ii) (**125**) (6.0 equiv.), $CuSO_4$ (0.1 M, 1.2 equiv.), sodium ascorbate (2.0 equiv.), THF:H_2O (3:1), 70%; (iii) TFA:H_2O (1:1), Δ, 70°C, 4h, 40%.*

4.4.4 Synthesis of AgNPs using PEG-functionalised triazole ligands

4.4.4.1 AgNPs derived from sugar triazole (24)

A AgNP array was constructed over concentration ranges of 1 µM - 25 mM [(**24**)] and 10 µM - 50 mM [Tollens'] (Table 4-1). The formation of AgNP using (**24**) [i.e., AgNP@(**24**)] was confined to a region of high concentrations of (**24**) [10 mM - 25 mM] and Tollens' [10 mM - 50 mM]. Figure 4-9 shows the UV-vis spectra of AgNP@(**24**) formed in this region. The size distribution of the array of AgNP@(**24**) was slightly different from AgNP@(**18**) prepared by Burely *et al*.[87] No AgNPs were formed at low concentration of ligand (**24**) [i.e., 1mM]. Silver aggregation was observed at 10 mM [Tollens'] and 1mM (**24**). In contrast, yellow colloidal solutions were observed at 1 mM - 10 mM [Tollens'] and 1mM (**18**).

Table 4-1: *AgNP@(**24**) screening array prepared using sugar triazole (**24**) and Tollens' reagent. White boxes represent no AgNP formation, yellow boxes represent AgNP formation and grey box represents the formation of silver mirror.*

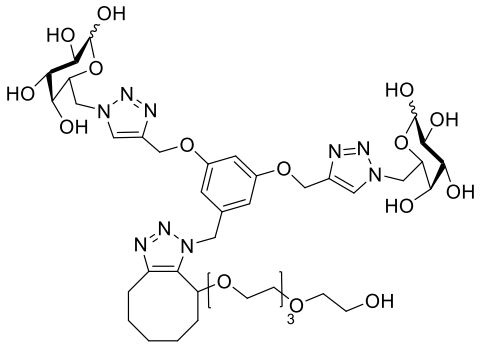

[(24)]

[Tollens']

	25 mM	10 mM	1 mM	100 µM	10 µM	1 µM
10 µM	#1	#2	#3	#4	#5	#6
100 µM	#7	#8	#9	#10	#11	#12
1 mM	#13	#14	#15	#16	#17	#18
10 mM	#19 19 ± 10 nm	#20 18 ± 7 nm	#21	#22	#23	#24
20 mM	#25	#26 15 ± 6 nm	#27	#28	#29	#30
50 mM	#31	#32	#33	#34	#35	#36

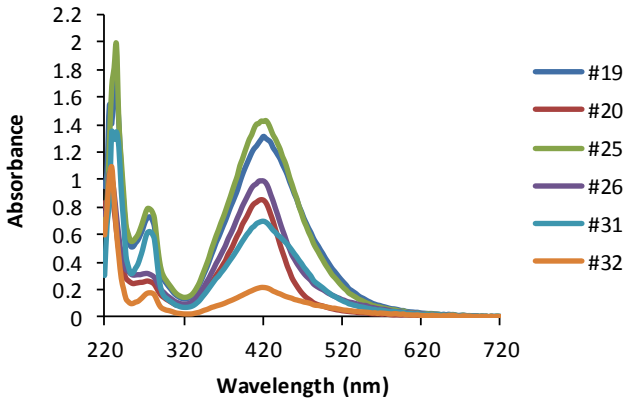

Figure 4-9: *UV-vis spectra of reactions #19-20, 25-26 and 31-32, which formed AgNP@(**24**) as observed by a SPR peak at 420 nm. Samples #19, 25, 31-32 were diluted 1:10 and #20, 26 were diluted 1:20 prior to each measurement.*

TEM analysis of several examples in this series produced angular AgNP@(**24**) with similar diameters ranging from 15 ± 6 nm (#26, Figure 4-10c) to 19 ± 10 nm (#19, Figure 4-10a).

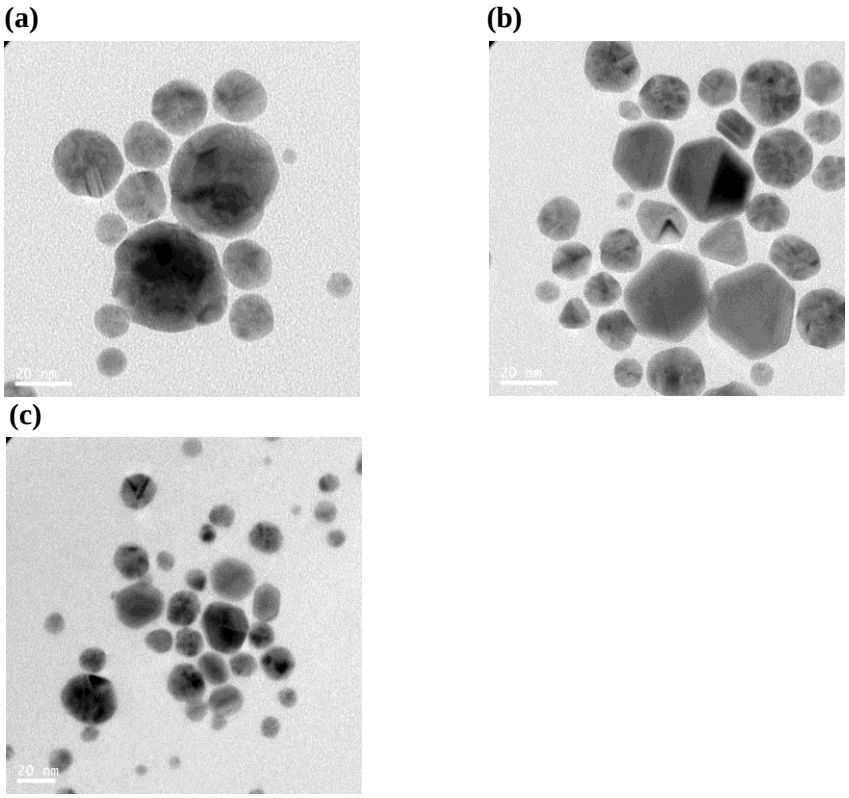

Figure 4-10: *TEM images of AgNP@(**24**) prepared using reaction conditions in Table 4.1.* ***(a)*** *#19, Ø = 19 ± 10 nm;* ***(b)*** *#20, Ø = 18 ± 7 nm;* ***(c)*** *#26, Ø = 15 ± 6 nm.*

4.4.4.2 AgNPs derived from sugar triazole (25)

Table 4-2 represents the AgNP@(**25**) array prepared over a concentration range of 1 µM - 25 mM [(**25**)] and 10 µM - 50 mM [Tollens'].

Table 4-2: *AgNP@(**25**) screening array prepared using sugar triazole (**25**) and Tollens' reagent. White boxes represent no AgNP formation, yellow boxes represent AgNP formation and grey boxes represent the formation of silver mirrors.*

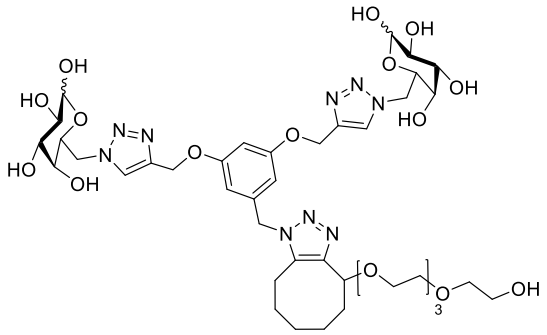

[(25)]

[Tollens']

	25 mM	10 mM	1 mM	100 µM	10 µM	1 µM
10 µM	#1	#2	#3	#4	#5	#6
100 µM	#7	#8	#9	#10	#11	#12
1 mM	#13	#14	#15	#16	#17	#18
10 mM	#19 38 ± 7 nm	#20 17 ± 5 nm	#21	#22	#23	#24
20 mM	#25	#26 25 ± 5 nm	#27	#28	#29	#30
50 mM	#31	#32	#33	#34	#35	#36

AgNP@(**25**) were formed over concentration ranges of 10 mM - 25 mM [(**25**)] and 10 mM - 50 mM [Tollens']. In contrast to AgNP@(**24**), silver aggregates were observed at the highest concentration of Tollens' at 50 mM and (**25**) at 10 mM - 25 mM. This observation revealed that the formation of AgNP@(**25**) was more dependent on the reaction conditions than AgNP@(**24**). All samples which formed AgNPs showed a SPR peak ~ 420 nm (Figure 4-11). TEM analysis of several examples in this series produced angular AgNP@(**25**) of tunable sizes that ranged from 17 ± 5 nm (#20, Figure 4-12b) to 38 ± 7 (#19, Figure 4-12a). The inherent size

tunability was not observed when ligand (**24**) was used. These results suggest that (**24**) and (**25**) behave differently in the formation of AgNPs.

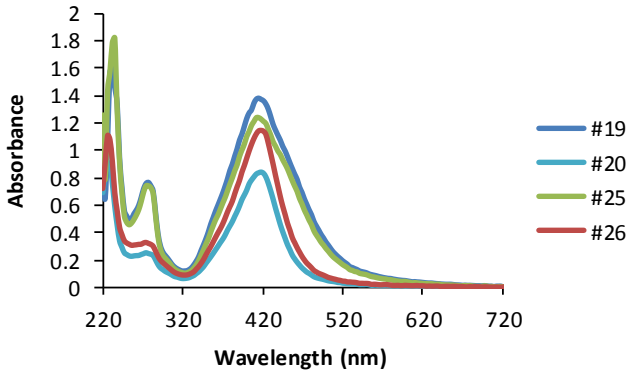

Figure 4-11: *UV-vis spectra of reactions #19-20 and 25-26, which formed AgNP@(**25**) as observed by a SPR peak. Samples #19, 25 were diluted 1:10 and #20, 26 were diluted 1:20 prior to each measurement.*

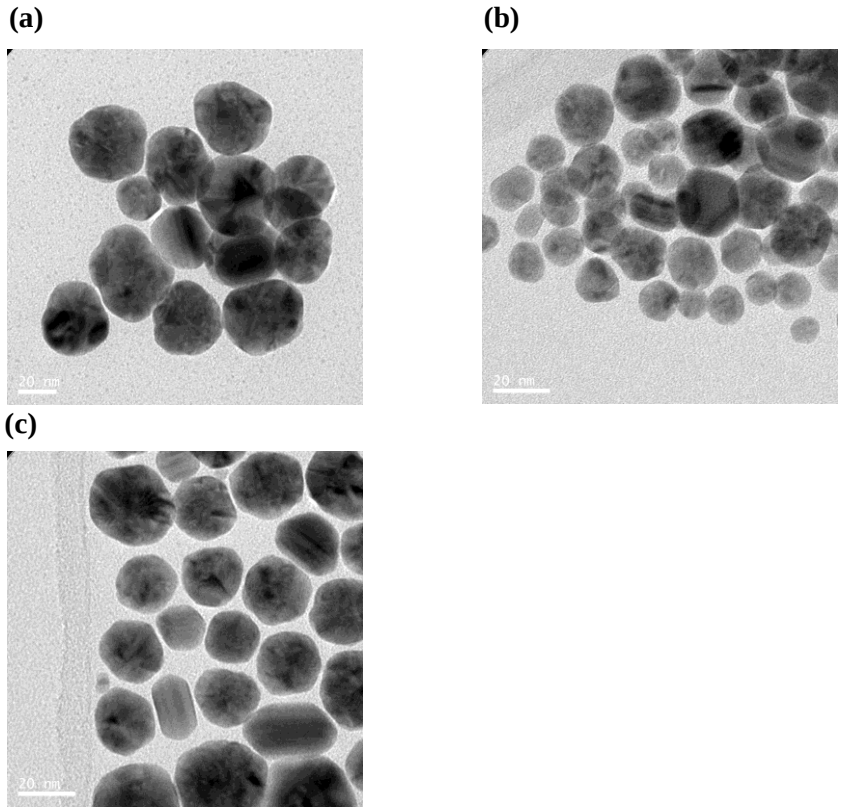

Figure 4-12: *TEM images of AgNP@(**25**) prepared using reaction conditions in Table 4.2.* ***(a)*** *#19, Ø = 38 ± 7 nm;* ***(b)*** *#20, Ø = 17 ± 5 nm;* ***(c)*** *#26, Ø = 25 ± 5 nm.*

4.4.4.3 AgNPs derived from sugar triazole (26)

The formation of AgNP@(**26**) was screened as a function of [(**26**)] and [Tollens'] with a similar concentration range used to prepare AgNP@(**24**) and AgNP@(**25**) (Table 4-3).

Table 4-3: *AgNP@(**26**) screening array prepared using sugar triazole (**26**) and Tollens' reagent. White boxes represent no AgNP formation, yellow boxes represent AgNP formation and grey boxes represent the formation of silver mirrors.*

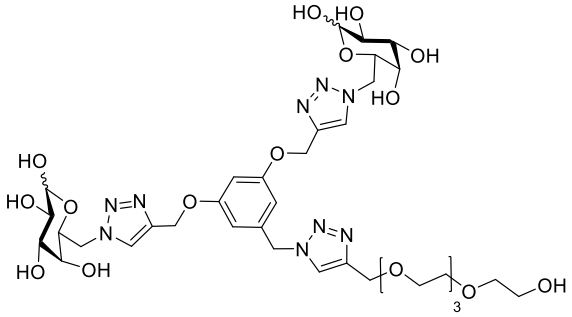

[(26)]

[Tollens']

	25 mM	10 mM	1 mM	100 µM	10 µM	1 µM
10 µM	#1	#2	#3	#4	#5	#6
100 µM	#7	#8	#9	#10	#11	#12
1 mM	#13	#14	#15	#16	#17	#18
10 mM	#19 15 ± 4 nm	#20 15 ± 4 nm	#21	#22	#23	#24
20 mM	#25	#26 16 ± 2 nm	#27	#28	#29	#30
50 mM	#31	#32	#33	#34	#35	#36

In contrast to AgNP@(**24**) and AgNP@(**25**), (**26**) facilitated the formation of AgNP@(**26**) over a wider range of [Tollens'] and [(**26**)]. The array showed that a low concentration of (**26**) [1 mM - 100 µM] formed AgNP@(**26**). This behavior was similar to AgNP@(**18**) prepared by Burley *et al.*[87] However, silver aggregates were observed at the highest concentration of Tollens' at 50 mM and (**26**) at 10 mM - 25 mM, while yellow colloidal solutions were observed at the same concentration of Tollens' and (**18**). Figure 4-13 shows the UV-vis spectra of AgNP@(**26**). TEM

analysis of several examples in this series produced angular AgNP@(**26**) with diameters of 15 ± 4 - 16 ± 2 nm (Figure 4-14).

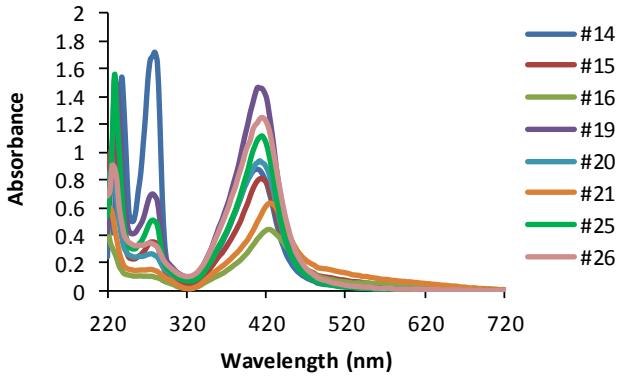

Figure 4-13: *UV-vis spectra of reactions #14-16, 19-21 and 25-26, which formed AgNP@(**26**) as observed by a SPR peak. Samples #19, 21, 25 were diluted 1:10 and #20, 26 were diluted 1:20 prior to each measurement.*

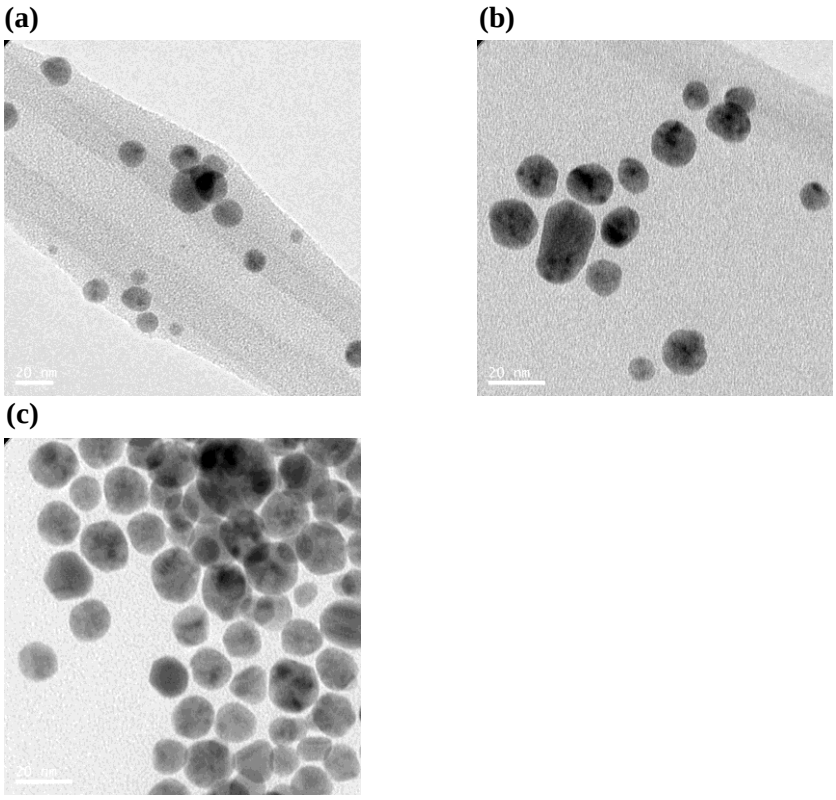

Figure 4-14: *TEM images of AgNP@(**26**) prepared using reaction conditions in Table 4.3.* ***(a)*** *#19, Ø = 15 ± 4 nm;* ***(b)*** *#20, Ø = 15 ± 4 nm;* ***(c)*** *#26, Ø = 16 ± 2 nm.*

4.4.5 Stability of AgNPs in high salt buffers

The stability of AgNP@(**24**), AgNP@(**25**) and AgNP@(**26**) to increasing concentrations of an aqueous solution of NaCl was tested after 24 hours at room temperature. AgNP@(**24**) and AgNP@(**25**) were stable in 0.5 M NaCl and aggregated at 1.0 M (Figure 4-15), whereas AgNP@(**26**) aggregated at a lower NaCl concentration (0.5 M) (Figure 4-15).

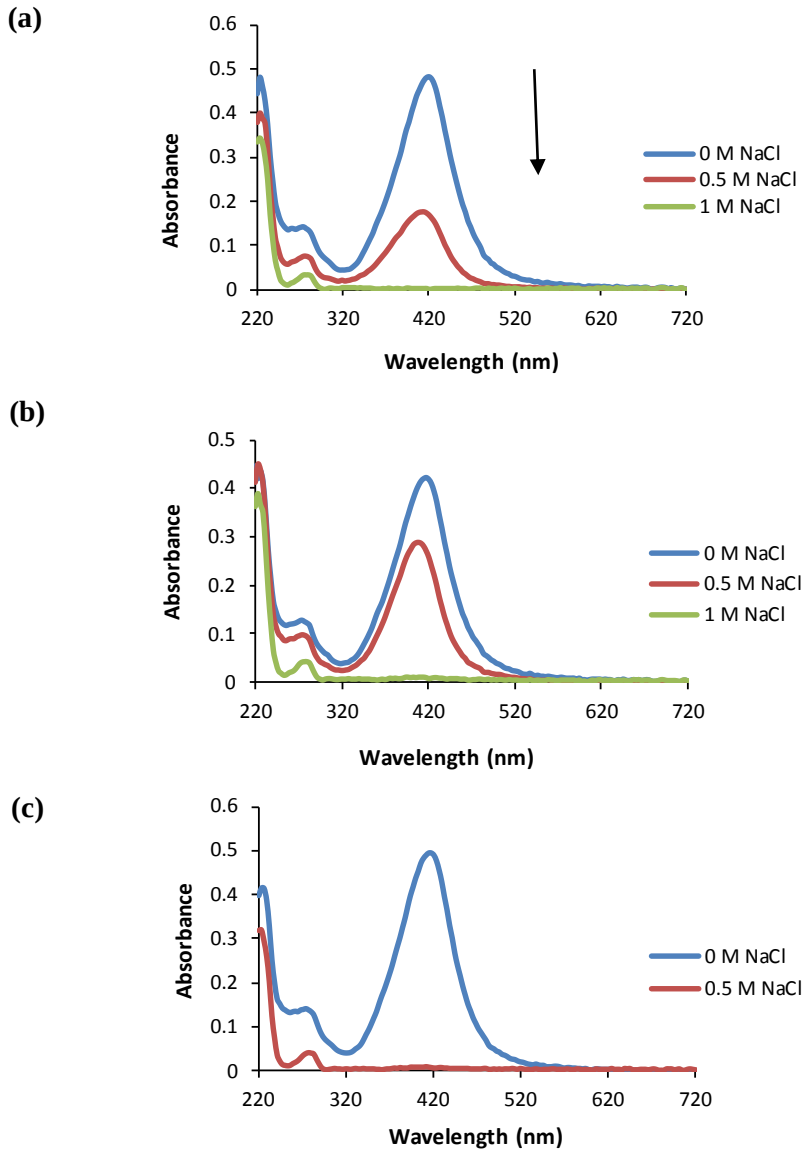

Figure 4-15: *Stability of* ***(a)*** *AgNP@(**24**),* ***(b)*** *AgNP@(**25**) and* ***(c)*** *AgNP@(**26**) to increasing concentrations of an aqueous solution of NaCl. Aggregation was observed by a loss of the SPR peak at ~ 420 nm.*

4.4.6 Summary of AgNPs synthesis

The key conclusion arising from this study was the formation of larger AgNPs in diameter and of different shape when (**24**), (**25**) and (**26**) were used as a ligand compared to (**18**) that produced spherical AgNP@(**18**) with a diameter of 8 ± 5 nm. These results provide further justification that the nature of southern half of the ligand structure plays a significant role in tuning the size and shape of AgNPs. Ligands (**24**), (**25**) and (**26**) retain the same features in the northern part of the structure as (**18**). Table 4-4 summarises the results of AgNPs in this study.

Table 4-4: *Summary of AgNPs formed using ligands (**24**, **25** and **26**)*

Tollens' : Ligand	AgNP@(**24**) size (nm)	AgNP@(**25**) size (nm)	AgNP@(**26**) size (nm)
10 mM : 25 mM (2:5)	19 ± 10	38 ± 7	15 ± 4
10 mM : 10 mM (1:1)	18 ± 7	17 ± 5	15 ± 4
20 mM : 10 mM (2:1)	15 ± 6	25 ± 5	16 ± 2

4.4.7 The kinetics of AgNP formation

In order to understand the effect of ligands (**24**), (**25**) and (**26**) on AgNP formation, kinetic experiments were conducted by monitoring the onset of the surface plasmon peak at 400 nm using 20 mM [(ligand)] and 20 mM [Tollens'] (Figure 4-16). The onset of formation of AgNP@(**24**) was observed at ~ 200 s with an end-point at ~ 1000 s. A significantly slower reaction rate (onset ~ 1100 s) with an end-point (~ 2900 s) was observed for the formation of AgNP@(**25**). This could be a contributing factor to the size tunability observed when ligand (**25**) was used. A slightly faster reaction rate (onset ~ 900 s) with an end-point (~ 2000 s) was observed for the formation of AgNP@(**26**) relative to AgNP@(**25**). This kinetics for all three

ligands were significantly slower than the kinetics of AgNP@(**18**) reported by Burley *et al*. [the rate of onset ~ 120 s and end point ~ 588 s].[87] This infers that the hydrophilic PEG group attached to the southernmost triazole in our ligand system decreases the rate of AgNP formation.

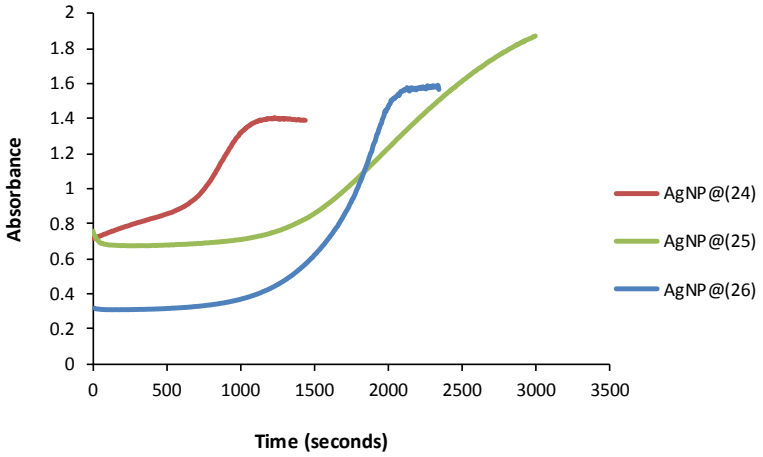

Figure 4-16: *Kinetics of formation of AgNP using (**24**, red), (**25**, green) and (**26**, blue) as monitored by the formation of the SPR peak at 400nm.*

4.4.8 ^{1}H NMR titration experiments

^{1}H NMR titration experiments were then conducted using ligands (**24**), (**25**) and (**26**) in the presence of $AgNO_3$ to explore the binding characteristics of these ligands to the silver ions (see Section 2.3.6). Triazole protons ($H^p/H^r/H^t$) and aromatic protons ($H^q/H^s/H^u$) were used as diagnostic markers of Ag(I) coordination (Figure 4-17, Figure 4-18 and Figure 4-19). Triazole protons of all three ligands showed a similar 0.1 ppm downfield shift upon the addition of two equivalents of Ag(I). A further downfield shift [0.2 ppm for H^p/H^r and 0.1 for H^t] was observed up to the addition of a further four equivalents Ag(I). In contrast, the behaviour of aromatic H^q in (**24**) and H^s in (**25**) was divergent from H^u in (**26**). An upfield shift [0.01 ppm for H^q and 0.03 ppm for H^s] was observed upon the addition of two equivalents of Ag(I) followed by

a gradual return to a similar chemical shift to its original position after the addition of a further four equivalents of Ag(I). This behaviour was similar to the aromatic proton of ligand (**18**) reported by Burley *et al.*[87] Whereas, a gradual 0.1 ppm upfield shift of the aromatic H^u was observed upon the addition of six equivalents of Ag(I).

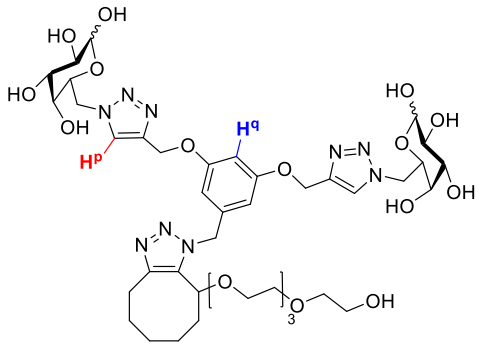

(**24**)

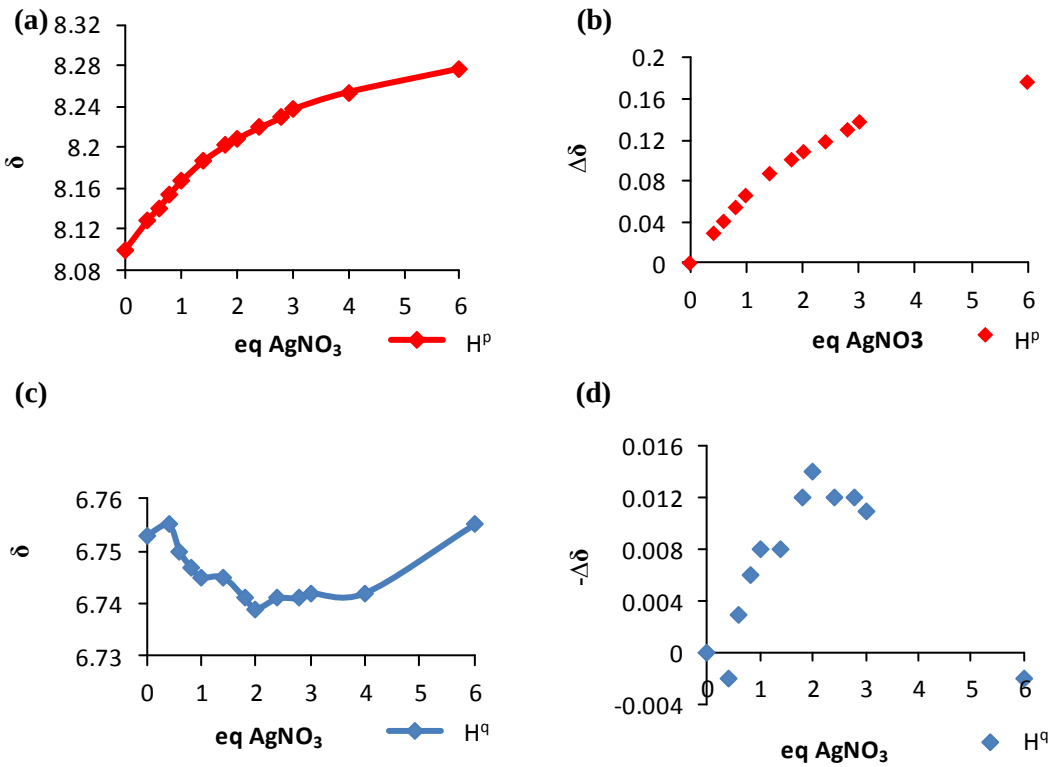

Figure 4-17: *Plots of the* ^{1}*H-NMR titration of sugar triazole ligand (**24**) with an increasing amount of* $AgNO_3$ *in* D_2O*. (**a** and **c**) Plots of the* ^{1}*H-NMR titration of* H^p *and* H^q *with* $AgNO_3$*. (**b** and **d**) Change in chemical shift of* H^p *and* H^q *as a function of* $AgNO_3$*.*

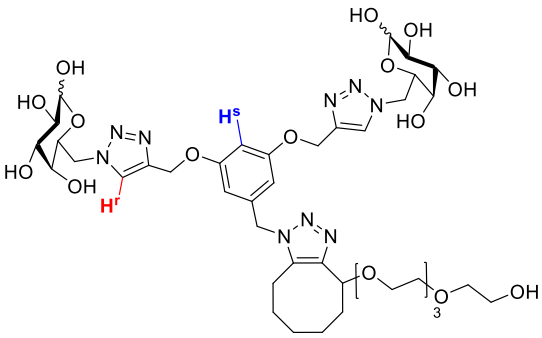

(**25**)

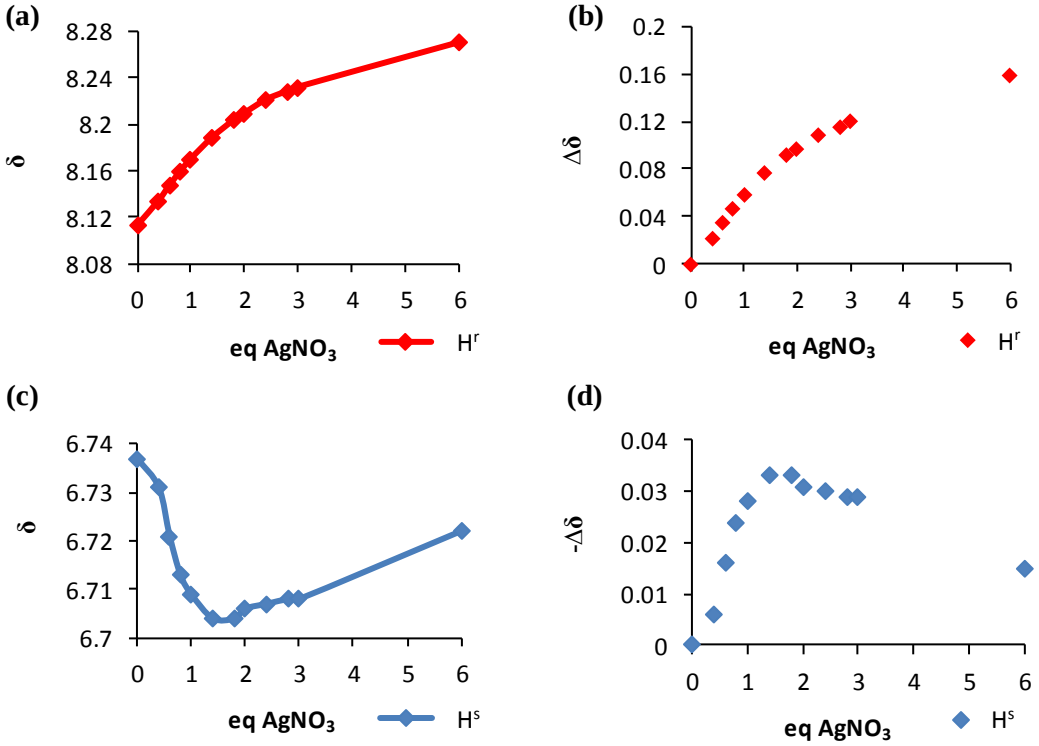

Figure 4-18: *Plots of the ^{1}H-NMR titration of sugar triazole ligand (**25**) with an increasing amount of $AgNO_3$ in D_2O.* ***(a** and **c)** Plots of the ^{1}H-NMR titration of H^r and H^s with $AgNO_3$.* ***(b** and **d)** Change in chemical shift of H^r and H^s as a function of $AgNO_3$.*

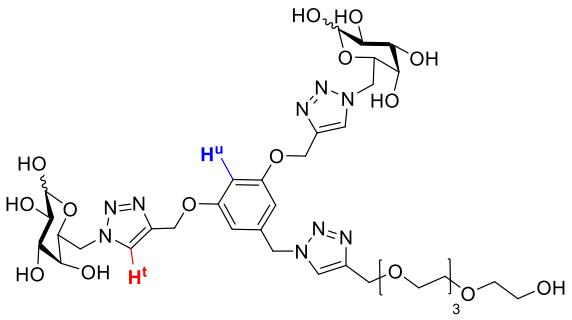

(**26**)

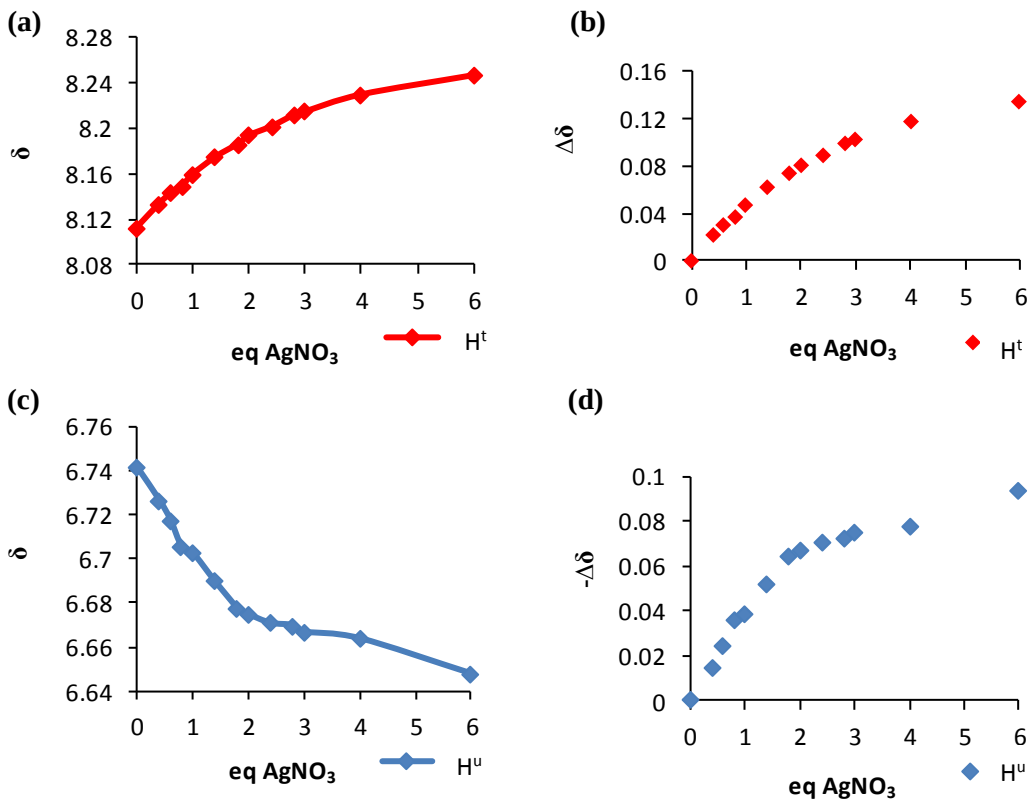

Figure 4-19: *Plots of the* ^{1}*H-NMR titration of sugar triazole ligand (**26**) with an increasing amount of* $AgNO_3$ *in* D_2O*. (**a** and **c**) Plots of the* ^{1}*H-NMR titration of* H^t *and* H^u *with* $AgNO_3$*. (**b** and **d**) Change in chemical shift of* H^t *and* H^u *as a function of* $AgNO_3$*.*

The binding constant of Ag(I) for ligands (**24**), (**25**), and (**26**) was then calculated by WinEQNMR2 software (Table 4-5).[108]

Table 4-5: *Ag(I) binding constant of (**24, 25** and **26**) calculated by non-linear curve fitting of ^{1}H NMR chemical shift data of the triazole protons using the software program WinEQNMR2.*[108]

Compound	**K** (M^{-1})	**Log K**
(**24**)	533 ±26	2.727 ± 0.021
(**25**)	752 ± 43	2.876 ± 0.025
(**26**)	478 ± 32	2.679 ± 0.029

A significant difference in Ag(I)-binding behaviour that was observed was the weaker Ag(I) binding affinity compared to (**18**) (72 393 ± 38011 M^{-1}).[109] An interesting observation was ligand (**26**) has a similar Ag(I) binding affinity compared to (**24**) and (**25**). Thus, the hydrophilic PEG group attached to the southernmost triazole ring reduced the binding affinity for Ag(I). Taken collectively with TEM results, this decrease in binding affinity resulted in producing larger AgNPs compared to (**18**). This effect was consistent with the results in chapter two where the southern ligand core was changed from (**18**) to (**23**) resulted in a significant reduction in Ag(I) binding and produced larger nanoparticles.

4.4.9 Surface enhanced Raman scattering (SERS) properties

In collaboration with David Thompson (Graham Group, University of Strathclyde), the SERS properties of produced AgNPs [i.e., AgNP@(**24**), AgNP@(**25**) and AgNP@(**26**) were studied using malachite green isothiocyanate (MGITC) (**127**) as a Raman reporter.

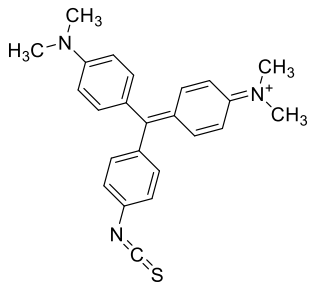

(**127**)

Compound (**127)** is a positively charged dye used as a common SERS substrate that adsorbs onto the negatively charged AgNPs surfaces.[179] A solution of MGITC in water (1.33 x 10^{-7} M) was mixed with a colloidal suspension of AgNPs and exposed to laser light. The SERS activity of AgNPs was measured by monitoring the intensity of the main Raman peaks of (**127**) (1618, 1370 with shoulder at 1390 and 1180 cm^{-1}). Figure 4-20 shows SERS spectra of malachite green isothiocyanate absorbed on AgNP. The highest SERS enhancement was achieved using AgNP@(**24**) in Table 4-1 (cell #20) (Figure 4-20b). In contrast, AgNP@(**24**) (Table 4-1, #19) provided a much lower SERS signal intensity (Figure 4-20a). These results suggested that the reaction conditions and choice of ligand used to prepare AgNP@(**24**) play a defining role in influencing the SERS enhancement because both samples prepared using ligand (**24**) produced similar sizes of AgNPs [i.e., #19, Ø = 19 ± 10 nm; #20, Ø = 18 ± 7 nm].

SERS enhancement was also obtained using AgNP@(**25**), cell #19 and cell #20 in Table 4-2. SERS spectra showed that smaller AgNP@(**25**) [#20 Ø = 17 ± 5 nm] provided higher SERS signal intensity (Figure 4-20d) compared to larger AgNP@(**25**) [#19, Ø = 38 ± 7 nm] (Figure 4-20c). SERS experiments were then conducted using AgNP@(**26**). A similar enhancement effect was obtained using AgNP@**(26)**, cell #19 and #20, Ø = 15 ± 4 nm in Table 4-3 (Figure 4-20e-f). A key

conclusion from this work was all three silver nanoparticles types, AgNP@(**24),** AgNP@(**25**) and AgNP@(**26**), are Raman active and could be potentially used as a potential diagnostic platform.

4.5 Conclusion

The synthesis of PEG-functionalised sugar triazole ligands (**24**, **25** and **26**) prepared size- and shape-controlled AgNPs using Tollens' reagent. The nature of the southernmost triazole of these ligands influenced the formation of AgNPs. The cyclooctyne in (**24**) and (**25**) resulted in a significant reduction in Ag(I) binding affinity relative to ligand (**18**). A similar effect was observed using ligand (**26**). This study revealed that introduction of PEG chain into the southernmost triazole ring produced weaker Ag(I)-binding ligands for the preparation of larger AgNPs.

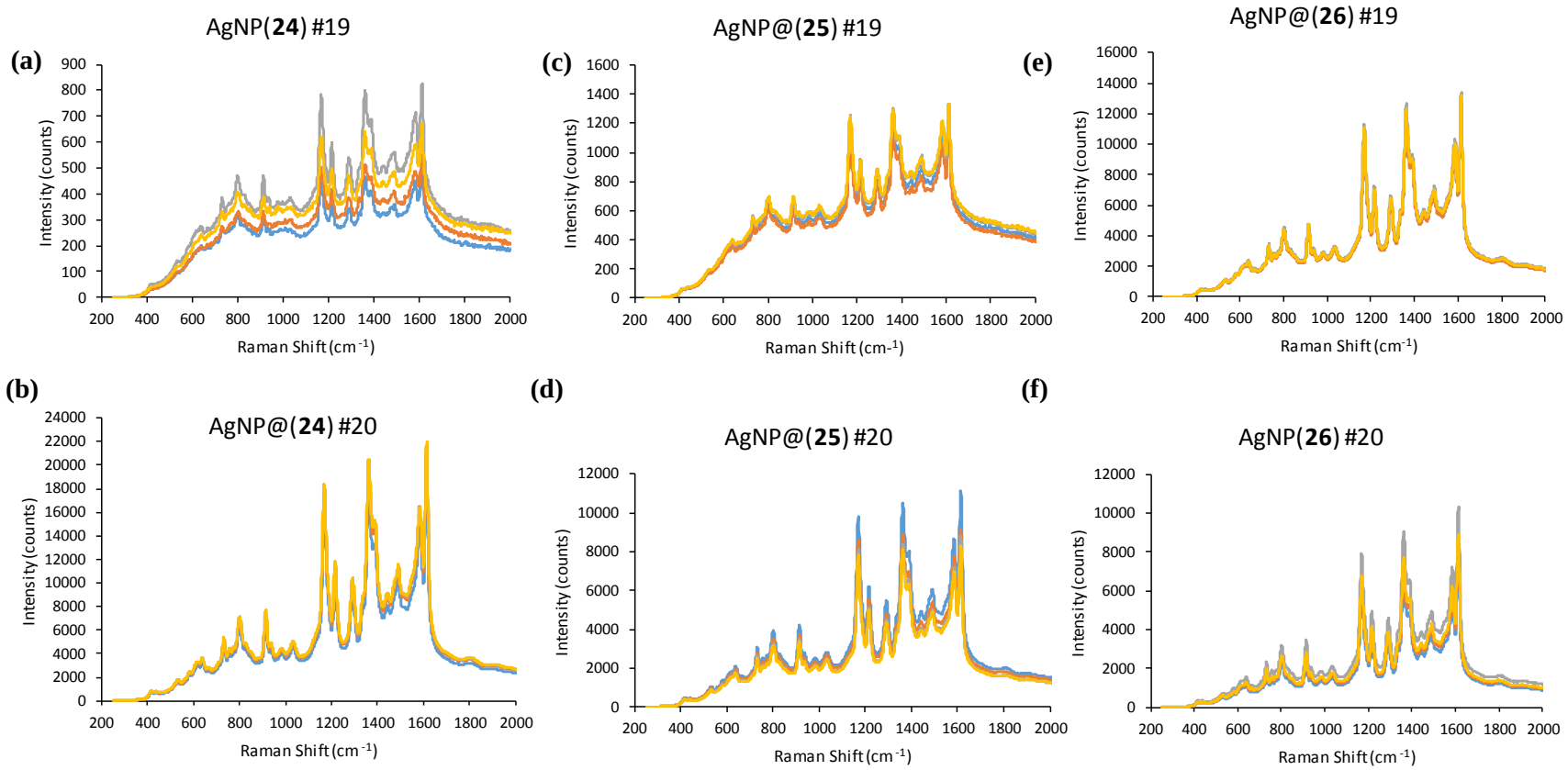

Figure 4-20: *SERS spectra (run 4 times) of malachite green isothiocyanate (**127**) adsorbed on **(a)** AgNP@(**24**), sample #19; **(b)** AgNP@(**24**), sample #20; **(c)** AgNP@(**25**), sample #19; **(d)** AgNP@(**25**), sample #20; **(e)** AgNP@(**26**), sample #19; **(f)** AgNP@(**26**), sample #20, using 532 nm laser line.*

4.6 Future work

In this preliminary work, the methodology described in this chapter for the preparation of AgNPs has been extended to investigate a new strategy for fabrication AgNPs array on glass surfaces. An interesting feature of this approach is the ability to form AgNPs on surfaces. In collaboration with Dr. Alasdair Clark at the University of Glasgow, an initial experiment was conducted to test the potential of functionalisation surfaces with sugar triazole groups on glass surfaces for formation of AgNPs using Tollens' reagent (Scheme 4-12). In this work, a square array of circular nano-features (diameter 500 nm) was patterned into a PMMA bi-layer using electron-beam lithography. The formation of Ag-nanostructures on the substrate was achieved in four steps. The glass surface exposed by the electron-beam patterning was modified with amino groups using 4% (3-aminopropyl)triethoxysilane in ethanol followed by a coupling reaction with NHS-PEG-cyclooctyne (**128**) (Scheme 4-13) in the presence of DIEA. The PMMA mask was then stripped using warm acetone before a SPAAC was performed using sugar azide (**8**) (Scheme 4-14), providing sugar-modified surfaces patterned at the noanoscale. The final step was metallisation the surface using 10 mM of Tollens' reagent. Figure 4-21 showed the selective metallisation on the surface using dark field microscopy. However, further work in this field is necessary to achieve the metallisation using a nanoscale range that is suitable for plasmonic applications.

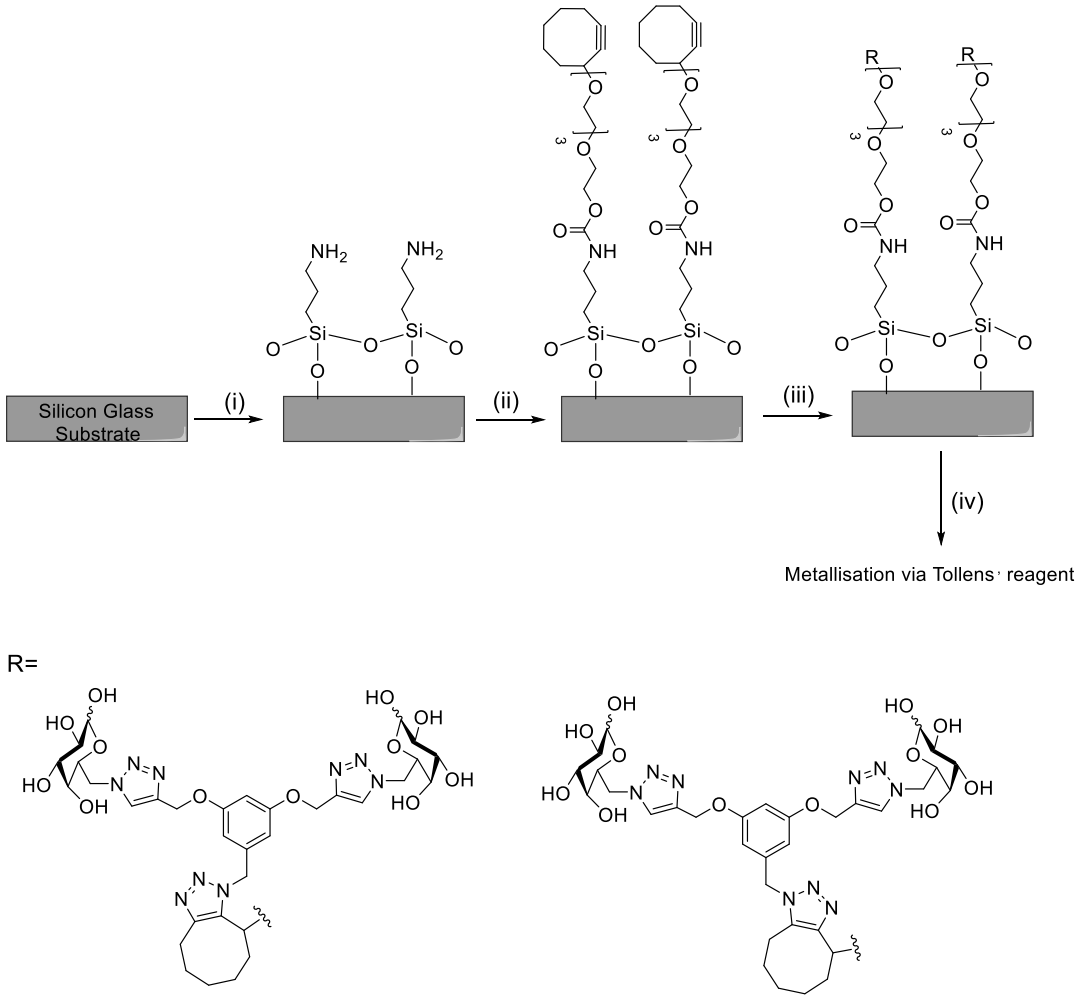

Scheme 4-12: *Schematic diagram for preparation of AgNPs on amino-modified surfaces. Reagents and conditions: (i) 4% (3-aminopropyl)triethoxysilane in ethanol; (ii) NHS-PEG-cyclooctyne (**128**), DIPEA, DMSO, 24h; (iii) Sugar azide (**8**), DMSO, 24h; (iv) 10 mM of Tollens' reagent, 15 min.*

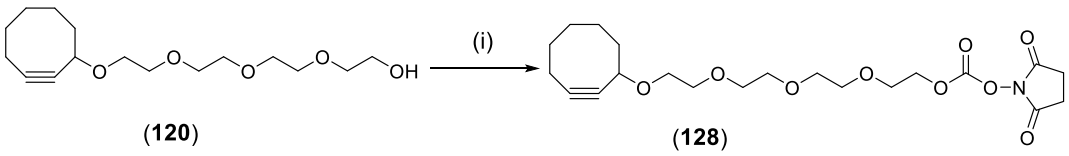

Scheme 4-13: *Reagents and conditions: (i) N,N'-Disuccinimidyl carbonate (3.0 equiv.), Et_3N (3.0 equiv.), MeCN, Rt, 24 h, 94%.*

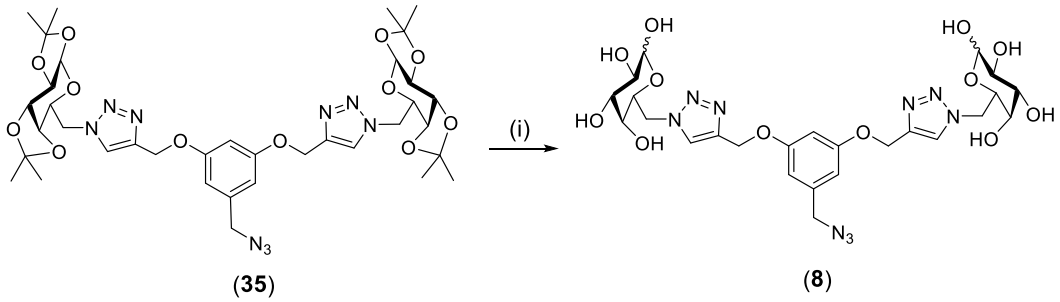

Scheme 4-14: *Reagents and conditions:(i) TFA:H_2O (1:1), Δ, 70°C, 4h, 58%.*

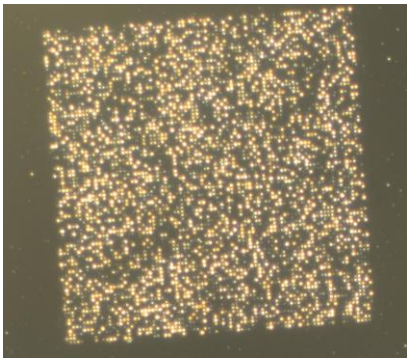

Figure 4-21: *Dark-field optical images of AgNPs array.*

4.7 Experimental

4.7.1 Synthesis of cyclooctyne-functionalised PEG

Synthesis of 8,8-dibromobicyclo[5.1.0]octane (118)[180,181]

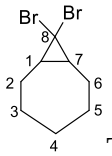

To a stirred suspension of cycloheptene (**117**) (3.77 g, 39 mmol) and *t*-BuOK (5.05 g, 45 mmol) in anhydrous pentane (100 mL) was added a solution of bromoform (11.40 g, 45 mmol, 4 mL) in anhydrous pentane (100 mL) dropwise in 2 h at 0°C under a nitrogen atmosphere. The reaction mixture was stirred overnight at room temperature. The mixture was diluted with H_2O (400 mL) and neutralised

with conc. HCl. The aqueous layer was then extracted with hexane (3 × 100 mL) and the organic layer washed with H_2O (3 × 100 mL) and dried over Na_2SO_4, filtered and concentrated *in vacuo* afforded 8,8-dibromobicyclo[5.1.0]octane **(118)** (6.00 g, 57%) as a brown oil.

^{1}H NMR ($CDCl_3$, 400 MHz): δ 1.18-1.26 (m, 3H, $H_2/H_4/H_6$), 1.32-1.43 (m, 2H, H_3/H_5), 1.70-1.74 (m, 2H, H_1/H_7), 1.80-1.94 (m, 3 H, $H_3/H_4/H_5$), 2.23-2.30 (m, 2 H, H_2/H_6).

^{13}C NMR ($CDCl_3$, 100 MHz): δ 28.2 (C_3, C_5), 29.1 (C_2, C_6), 32.4 (C_4), 34.9 (C_1, C_7), 40.9 (C_8).

Synthesis of (119)[182]

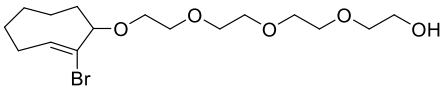

To a solution of 8,8-dibromobicyclo[5.1.0]octane **(118)** (4.00 g, 15 mmol) in a mixture of toluene (8 mL) and pyridine (10 mL) was added a solution of tetraethyleneglycol (87.00 g, 448 mmol, 77 mL) and $AgClO_4$ (9.35 g, 45 mmol) in toluene (18 mL). The reaction mixture was stirred and heated to reflux for 4 h in the dark. The mixture was then cooled to room temperature and concentrated *in vacuo* followed by the addition of brine (200 mL) and filtration. The aqueous layer was extracted with Et_2O (7 × 200 mL) and the organic layer washed with brine (300 mL), followed by H_2O (300 mL). The organic layer was then dried over Na_2SO_4, filtered and concentrated *in vacuo* afforded (**119**) (3.07 g, 54%) as a colourless oil.

^{1}H NMR ($CDCl_3$, 400 MHz): δ 0.76-2.32 (m, 9H), 2.41 (bs, 1H), 2.69-2.79 (m, 1H), 3.61-3.74 (m, 16H), 3.93 (dd, 1 H, J = 5 Hz, J = 10.4 Hz), 6.19 (dd, 1 H, J = 4.2 Hz, J = 11.7 Hz).

^{13}C NMR ($CDCl_3$, 100 MHz): δ 26.6, 28.3, 33.5, 36.7, 39.8, 62.0, 68.2, 70.6, 70.65, 70.7, 70.8, 70.85, 72.7, 85.5, 131.2, 133.3.

Synthesis of (120)[182]

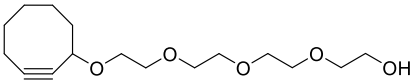

To a solution of (**119**) (1.55 g, 4 mmol) in *i*-PrOH (35 mL) was added pyridine (5.6 mL) followed by *t*-BuOK (1.37 g, 12 mmol). The reaction mixture was stirred for 3 days at room temperature. The mixture was neutralised with 5% HCl. and portioned between DCM (200 mL) and H_2O (100 mL) and extracted with DCM (7 × 100 mL). The organic layer was then dried over Na_2SO_4, filtered and concentrated *in vacuo* followed by purification by column chromatography (SiO_2) eluting with 5% MeOH in EtOAc afforded (**120**) (0.86 g, 70%) as a colourless oil.

^{1}H NMR ($CDCl_3$, 400 MHz): δ 1.19-2.29 (m, 10H, CH_2), 2.80 (bs, 1H, OH), 3.48-3.74 (m, 16H, CH_2), 4.20-4.24 (m, 1 H, CH).

^{13}C NMR ($CDCl_3$, 100 MHz): δ 20.9 (CH_2, 1C), 26.6 (CH_2, 1C), 29.9 (CH_2, 1C), 34.5 (CH_2, 1C), 42.4 (CH_2, 1C), 61.9 (1C), 68.7 (1C), 70.5 (1C), 70.6 (1C), 70.7 (1C), 70.8 (1C), 70.81 (1C), 72.8 (1C), 73.0 (1C), 93.2 (C≡**C**, 1C), 100.2 (**C**≡C, 1C).

4.7.2 Synthesis of sugar triazoles (24-25)

Synthesis of (121-122)

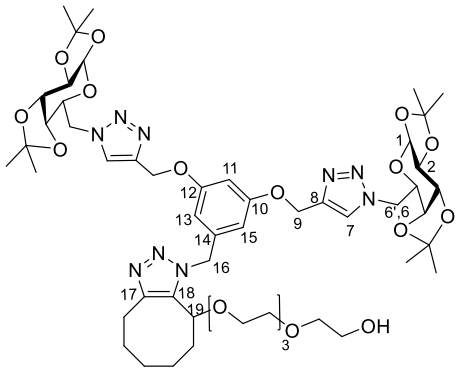

(**121**)

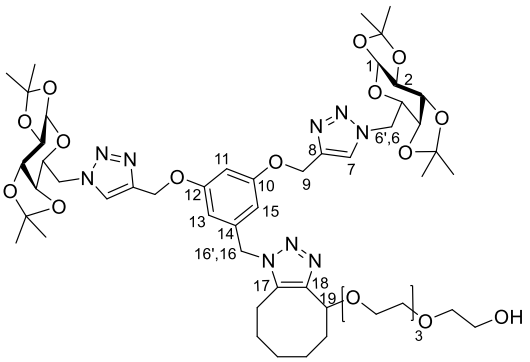

(**122**)

To a solution of **(35**) (0.30 g, 0.37 mmol) in DMSO (2 mL) was added (**120**) (0.20 g, 0.67 mmol) under a nitrogen atmosphere. The reaction mixture was stirred overnight at room temperature. The reaction mixture was diluted with EtOAc (50 mL) and the organic layer washed with H_2O (3 × 25 mL). The organic layer was then dried over $MgSO_4$, filtered and concentrated *in vacuo* followed by purification by column chromatography (SiO_2) eluting with 5% MeOH in EtOAc afforded (**121**) (0.15 g, 37%) and (**122**) (0.107, 26%) as white crystals. Identification of both regioisomers was achieved using 2D NMR NOESY (Figure 4-8), HSQC, HMBC and ROESY (see Appendix B68-B70, B76-B78).

Characterisation of compound (121)

HRMS (ESI-TOF) *m/z*: $[M + H]^+$ Calcd for $C_{53}H_{78}N_9O_{17}$ 1112.5516; Found 1112.5554.

MP. 75-77°C.

^{1}H NMR ($CDCl_3$, 400 MHz): δ 1.14-1.23 (m, 1H, OCT), 1.29 (s, 6H, CH_3), 1.37 (s, 6H, CH_3), 1.39 (s, 6H, CH_3), 1.34-1.48 (m, 2H, CH_2, OCT), 1.50 (s, 6H, CH_3), 1.55-

1.62 (m, 1H, OCT), 1.64-1.75 (m, 2H, CH_2, OCT), 1.79-1.88 (m, 1H, OCT), 1.90-1.98 (m, 1H, OCT), 2.78-2.86 (m, 1H, OCT), 3.07-3.13 (m, 1H, OCT), 3.46-3.70 (m, 16H, CH_2-PEG), 4.19-4.21(m, 4H, CH-sugar), 4.33 (dd, 2H, J = 2.5, 4.9 Hz, H_2), 4.44-4.51 (m, 3H, H_{19} + $H_{6'}$), 4.61-4.66 (m, 4H, CH-sugar + H_6), 5.10 (s, 4H, CH_2O [9]), 5.52 (d, 2H, J = 4.9 Hz, H_1), 5.70 (s, 2H, CH_2 [16]), 6.48 (s, 2H, *o*-Ar-H_{13}/H_{15}), 6.54 (s, 1H, *p*-Ar-H_{11}), 7.79 (s, 2H, NCH=C [7]).

^{13}C NMR ($CDCl_3$, 100 MHz): δ 23.1 (CH_2-OCT, 1C), 24.5 (CH_2-OCT, 1C) , 24.6 (CH_3, 2C), 24.9 (CH_2-OCT, 1C), 25.1 (CH_3, 2C), 26.1 (CH_3, 2C), 26.2 (CH_3, 2C), 28.2 (CH_2-OCT, 1C), 30.3 (CH_2-OCT, 1C), 50.8 (CH_6/$H_{6'}$, 2C), 52.4 (CH_2, 1C [16]), 61.8 (CH_2-PEG) , 62.2 (OCH_2, 2C [9]), 67.4 (CH-sugar, 2C), 68.2 (CH_2-PEG), 70.5 (CH-sugar, 2C), 70.7 (CH_2-PEG), 70.8 (CH_2-PEG), 70.84 (CH_2-PEG), 71.0 (CH-sugar, 2C), 71.3 (CH-sugar, 2C), 72.2 (CH_{19}, 1C), 72.8 (CH_2-PEG), 96.4 (CH_1, 2C), 101.7 (*p*-Ar-CH_{11}, 1C), 106.8 (*o*-Ar-CH_{13}/CH_{15}, 2C), 109.3 (Cq, 2C), 110.1 (Cq, 2C), 124.38 (N**C**H=C, 1C), 124.4 (N**C**H=C, 1C), 133.3 (C_{17}, 1C), 138.8 (*p*-Ar-C_{14}, 1C), 143.5 (C_8, 2C), 145.2 (C_{18}, 1C), 159.9 (*m*-Ar-C_{10}/C_{12}, 2C).

Characterisation of compound (122)

HRMS (ESI-TOF) *m/z*: $[M + H]^+$ Calcd for $C_{53}H_{78}N_9O_{17}$ 1112.5516; Found 1112.5559.

MP. 65-67°C.

^{1}H NMR ($CDCl_3$, 400 MHz): δ 0.92-0.99 (m, 1H, OCT), 1.29 (s, 6H, CH_3), 1.37 (s, 6H, CH_3), 1.39 (s, 6H, CH_3), 1.50 (s, 6H, CH_3), 1.34-1.66 (m, 5H, OCT), 1.79-1.86 (m, 1H, OCT), 2.13-2.20 (m, 1H, OCT), 2.52-2.58 (m, 1H, OCT), 2.99-3.06 (m, 1H, OCT), 3.49-3.73 (m, 16H, CH_2-PEG), 4.18-4.21 (m, 4H, CH-sugar), 4.33 (dd, 2H, J = 2.6, 4.9 Hz, H_2), 4.46 (dd, 2H, J = 8.4, 14.3 Hz, $H_{6'}$), 4.61-4.66 (m, 4H, CH-sugar

+ H_6), 4.87 (dd, 1H, *J* = 3.8, 5.7 Hz, H_{19}), 5.10 (s, 4H, CH_2O [9]), 5.33 (dd, 1H, *J* = 2.6, 15.7 Hz, $H_{16'}$), 5.45 (dd, 1H, *J* = 2.5, 15.7 Hz, H_{16}), 5.52 (d, 2H, *J* = 4.9 Hz, H_1), 6.40 (d, 2H, *J* = 2.2 Hz, *o*-Ar-H_{13}/H_{15}), 6.57 (t, 1H, *J* = 2.2 Hz, *p*-Ar-H_{11}), 7.79 (s, 2H, NCH=C [7]).

^{13}C NMR ($CDCl_3$, 100 MHz): δ 20.4 (CH_2-OCT, 1C), 21.1 (CH_2-OCT, 1C), 24.6 (CH_3, 2C), 25.1 (CH_3, 2C), 25.7 (CH_2-OCT, 1C), 26.1 (CH_3, 2C), 26.2 (CH_3, 2C), 26.6 (CH_2-OCT, 1C), 35.5 (CH_2-OCT, 1C), 50.8 (CH_6/$H_{6'}$, 2C), 51.8 (CH_{16}/$H_{16'}$, 2C), 61.9 (CH_2-PEG), 62.2 (OCH_2, 2C [9]), 67.4 (CH-sugar, 2C), 68.1 (CH_2-PEG), 70.5 (CH_2-PEG), 70.52 (CH-sugar, 2C), 70.6 (CH_2-PEG), 70.7 (CH_2-PEG), 70.8 (CH_2-PEG), 71.0 (CH, 1H-sugar, 2C), 71.4 (CH-sugar, 2C), 72.8 (CH_2-PEG), 74.8 (CH_{19}, 1C), 96.4 (CH_1 , 2C), 101.8 (*p*-Ar-CH_{11}, 1C), 106.6 (*o*-Ar-CH_{13}/CH_{15}, 2C), 109.3 (Cq, 2C), 110.1 (Cq, 2C) , 124.4 (N**C**H=C, 2C [7]), 134.5 (C_{18}, 1C), 138.0 (*p*-Ar-C_{14}, 1C), 143.4 (C_8, 2C), 145.8 (C_{17}, 1C), 160.1 (*m*-Ar-C_{10}/C_{12}, 2C).

Synthesis of (24)

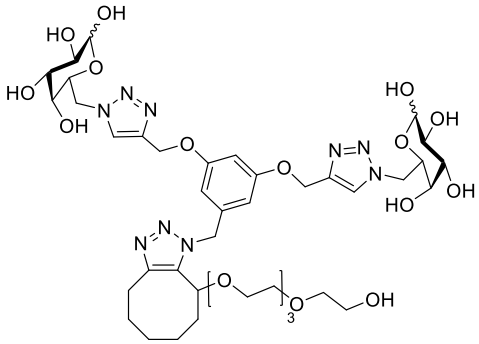

To a mixture of TFA:H_2O (1:1, 8 mL) was added (**121**) (0.13 g, 0.12 mmol) under a nitrogen atmosphere. The reaction mixture was heated to reflux for 3 h. The mixture was then cooled to room temperature followed by concentration *in vacuo*. The crude residue was diluted with H_2O (20 mL) and concentrated *in vacuo* again to remove excess TFA. The product was diluted with MeOH and precipitated using Et_2O. The crude residue was diluted in

H_2O and purified by semi-preparative HPLC using H_2O and MeCN. The gradient was started at 5% MeCN (solvent B), held at 5 min, then increased to 90% solvent B over 20 min. The product was freeze-dried to afford **(24)** (0.088 g, 77%) as a white powder. This compound was isolated as a mixture of diastereomers (see Appendix B81).

HRMS (ESI-TOF) *m/z*: $[M + H]^+$ Calcd for $C_{41}H_{62}N_9O_{17}$ 952.4264; Found 952.4309.

MP. 93-95°C.

^{1}H NMR (D_2O, 600 MHz): δ 1.01-1.86 (m), 2.80-2.83 (m), 3.00-3.05 (m), 3.39-3.65 (m), 3.66-3.68 (m), 3.83-3.88 (m), 3.92-3.93 (m), 3.99-4.00 (m), 4.05-4.07 (m), 4.42-4.44 (m), 4.50 (dd, *J* = 0.5, 7.9 Hz), 4.58-4.71 (m), 5.16 (s), 5.21 (d, *J* = 3.6 Hz), 5.60 (s), 6.43 (d, *J* = 1.7 Hz), 6.66 (s), 8.05 (s), 8.07 (s).

^{13}C NMR (D_2O, 150 MHz): δ 22.0, 23.4, 23.9, 27.9, 30.6, 50.9, 51.0, 52.1, 60.4, 61.4, 67.4, 67.44, 68.2, 68.8, 68.9, 69.1, 69.5, 69.6, 69.65, 69.7, 71.7, 71.73, 72.6, 73.2, 92.4, 96.5, 102.6, 107.3, 125.7, 125.8, 134.3, 138.5, 143.1, 146.3, 159.1).

Synthesis of (25)

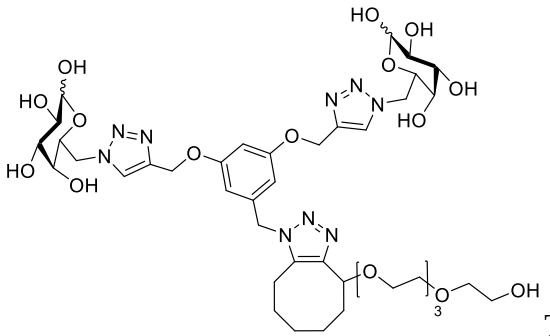

To a mixture of TFA:H_2O (1:1, 8 mL) was added (**122**) (0.09 g, 0.08 mmol) under a nitrogen atmosphere. The reaction mixture was heated to reflux for 3 h. The mixture was then cooled to room temperature followed by concentrationd *in vacuo*. The crude residue was diluted with H_2O (20 mL) and concentrated *in vacuo* again to remove excess TFA. The product was

diluted with MeOH and precipitated using Et_2O. The crude residue was diluted in H_2O and purified by semi-preparative HPLC using H_2O and MeCN. The gradient was started at 5% MeCN (solvent B), held at 5 min, then increased to 90% solvent B over 20 min. The product was freeze-dried to afford **(25)** (0.059 g, 77%) as a white powder. This compound was isolated as a mixture of diastereomers (see Appendix B86).

HRMS (ESI-TOF) *m/z*: $[M + H]^+$ Calcd for $C_{41}H_{62}N_9O_{17}$ 952.4264; Found 952.4293.

MP. 96-98°C.

^{1}H NMR (D_2O, 600 MHz): δ 0.81-1.48 (m), 1.87-2.00 (m), 2.62-2.67 (m), 2.88-2.93 (m), 3.52-3.68 (m), 3.70-3.72 (m), 3.82-3.88 (m), 3.92 (d, *J* = 3.5 Hz), 3.99 (d, *J* = 2.6 Hz), 4.04-4.06 (m), 4.42 (dd, *J* = 4.1, 9.0 Hz), 4.49 (d, *J* = 7.9 Hz), 4.57-4.70 (m), 5.14 (s), 5.21 (d, *J* = 3.5 Hz), 5.47 (d, *J* = 4.3 Hz), 6.45 (s), 6.63 (s), 8.06 (s), 8.07 (s).

^{13}C NMR (D_2O, 150 MHz): δ 20.0, 21.0, 24.7, 25.9, 34.3, 50.9, 51.0, 51.2, 60.4, 61.4, 67.5, 68.2, 68.8, 68.9, 69.1, 69.5, 69.6, 69.7, 69.8, 71.7, 71.8, 72.6, 73.2, 74.4, 92.4, 96.5, 102.7, 107.4, 125.7, 125.9, 136.0, 138.2, 143.0, 145.3, 159.1.

4.7.3 Synthesis of sugar triazole (26)

Synthesis of 3,6,9,12-tetraoxapentadec-14-yn-1-ol (125)[183]

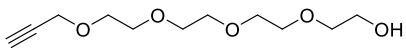

To a stirred suspension solution of NaH (50% oil dispersion, 4.00 g, 80 mmol) in dioxane (40 mL) was added tetraethyleneglycol (**124**) (40.00 g, 200 mmol slowly at 0°C followed by the addition of a solution of propargyl bromide (**123**) (80% in toluene, 5.95 g, 77.82 g, 50 mmol, 7.5 mL) in dioxane (60 mL) dropwise over a period of 1 h. The reaction mixture was then stirred for 2 h at room temperature followed by the addition of H_2O (20 mL). After 15 min, the solvent was evaporated *in vacuo*. The resulting residue was diluted with DCM

(400 mL) and the organic layer washed with brine (3 × 100 mL), dried over $MgSO_4$, filtered and concentrated *in vacuo.* Purification by column chromatography (SiO_2) eluting with 10% acetone in DCM afforded 3,6,9,12-tetraoxapentadec-14-yn-1-ol (**125**) (9.29 g, 80%) as a colourless oil.

^{1}H NMR ($CDCl_3$, 500 MHz): δ 2.41 (t, 1H, *J* = 2.4 Hz, CH≡C), 3-54-3.68 (m, 16H, CH_2-PEG), 4.15 (d, 2H, *J* = 2.4 Hz, CH≡CC**H$_2$**).

^{13}C NMR ($CDCl_3$, 125 MHz): δ 58.4 (CH≡C**C**H_2, 1C), 61.7 (CH_2OH, 1C), 69.2 (CH_2-PEG, 1C), 70.4 (CH_2-PEG, 1C), 70.44 (CH_2-PEG, 1C), 70.6 (CH_2-PEG, 1C), 70.62 (CH_2-PEG, 1C), 70.7 (CH_2-PEG, 1C), 72.6 (CH_2-PEG, 1C), 74.7 (**C**H≡C, 1C), 79.7 (CH≡**C**, 1C).

Synthesis of (126)

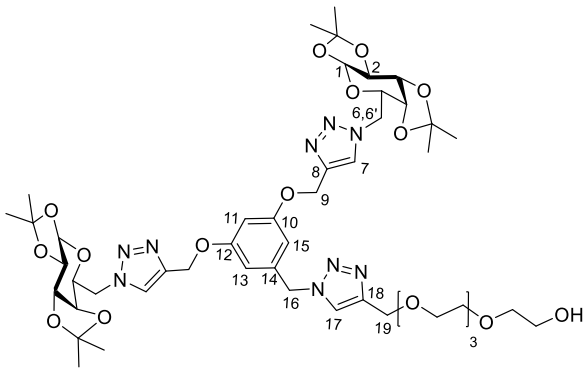

To a solution of (**35**) (0.10 g, 0.12 mmol) and (**125**) (0.17 g, 0.73 mmol) in THF:H_2O:DMSO (3:1:2, 1.4 mL) was added a solution of 0.5 M $CuSO_4$ in H_2O (0.28 mL) followed by solid sodium ascorbate (0.05 g, 0.25 mmol). The reaction mixture was stirred overnight at room temperature. The suspension was diluted with H_2O (2 mL), cooled to 0°C and treated with conc. NH_4OH (0.17 mL) for 10 min. The reaction mixture was diluted with DCM (100 mL) and the organic layer washed with brine (2 × 20 mL), followed by H_2O (2 × 20 mL). The organic layer was then dried over $MgSO_4$, filtered and concentrated

in vacuo. Purification by column chromatography (SiO_2) eluting with 10% of acetone in DCM afforded (**126**) (0.09, 70%).

HRMS (ESI-TOF) *m/z*: $[M + H]^+$ Calcd for $C_{48}H_{70}N_9O_{17}$ 1044.4890; Found 1044.4935.

MP. 65-66°C.

^{1}H NMR ($CDCl_3$, 500 MHz): δ 1.29 (s, 6H, CH_3), 1.36 (s, 6H, CH_3), 1.38 (s, 6H, CH_3), 1.50 (s, 6H, CH_3), 3.58-3.71 (m, 16H, CH_2-PEG), 4.19-4.21 (m, 4H, CH-sugar), 4.33 (dd, 2H, *J* = 2.5, 4.9 Hz, H_2), 4.47 (dd, 2H, *J* = 8.5, 14.3 Hz, $H_{6'}$), 4.62-4.65 (m, 4H, CH-sugar, H_6), 4.68 (s, 2H, CH_2 ^{19}), 5.14 (s, 4H, CH_2O ^{9}), 5.44 (s, 2H, CH_2 ^{16}), 5.51 (d, 2H, *J* = 4.9 Hz, H_1), 6.52 (d, 2H, *J* = 2.1 Hz, *o*-Ar-H_{13}/H_{15}), 6.62 (t, 1H, *J* = 2.1 Hz, *p*-Ar-H_{11}), 7.57 (s, 1H, NCH=C ^{17}), 7.80 (s, 2H, NCH=C ^{7}).

^{13}C NMR ($CDCl_3$, 125 MHz): δ 24.6 (CH_3, 2C), 25.1 (CH_3, 2C), 26.1 (CH_3, 2C), 26.2 (CH_3, 2C), 41.2 (CH_2, 1C ^{19}), 50.8 (CH_6/$H_{6'}$, 2C), 54.2 (CH_2, 1C ^{16}), 61.8 (CH_2-PEG), 62.3 (OCH_2, 2C ^{9}), 64.9 (CH_2-PEG), 67.4 (CH-sugar, 2C), 69.9 (CH_2-PEG), 70.4 (CH_2-PEG), 70.5 (CH-sugar, 2C), 70.65 (CH_2-PEG), 70.7 (CH_2-PEG), 70.74 (CH_2-PEG), 71.0 (CH-sugar, 2C), 71.4 (CH-sugar, 2C), 72.8 (CH_2-PEG), 96.4 (CH_1, 2C), 102.1 (*p*-Ar-CH_{11}, 1C), 107.7 (*o*-Ar-CH_{13}/CH_{15}, 2C), 109.3 (Cq, 2C), 110.1 (Cq, 2C), 123.0 (N**C**H=C, 1C ^{17}), 124.4 (N**C**H=C, 2C ^{7}), 137.1 (*p*-Ar-C_{14}, 1C), 143.4 (C_8, 2C), 145.7 (C_{18}, 1C), 160.1 (*m*-Ar-C_{10}/C_{12}, 2C).

Synthesis of (26)

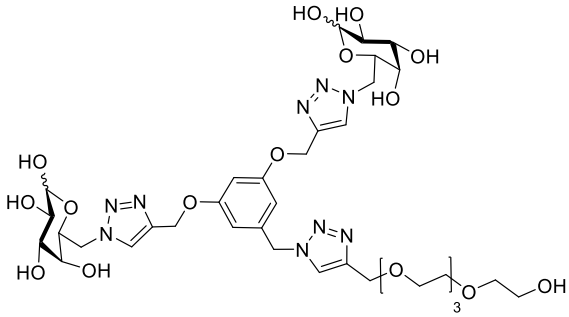

To a mixture of TFA:H_2O (1:1, 8 mL) was added (**126**) (0.08 g, 0.08 mmol) under a nitrogen atmosphere. The reaction mixture was heated to reflux for 4 h. The mixture was then cooled to room temperature followed by concentration *in vacuo*. The crude residue was diluted with H_2O (20 mL) and concentrated *in vacuo* again to remove excess TFA. The product was diluted with MeOH and precipitated using Et_2O. The crude residue was diluted in H_2O and purified by semi-preparative HPLC using H_2O and MeCN. The gradient was started at 5% MeCN (solvent B), held at 5 min, then increased to 90% solvent B over 20 min. The product was freeze-dried to afford (**26**) (0.028g, 40%) as a white powder. This compound was isolated as a mixture of diastereomers (see Appedix B95).

HRMS (ESI-TOF) *m/z*: $[M + H]^+$ Calcd for $C_{36}H_{54}N_9O_{17}$ 884.3638; Found 884.3612.

MP. 93-95°C.

^{1}H NMR (D_2O, 600 MHz): δ 3.55-3.68 (m), 3.70-3.72 (m), 3.86-3.91 (m), 3.95 (d, *J* = 3.3 Hz), 4.02 (d, *J* = 2.5 Hz), 4.06-4.08 (m), 4.46 (dd, *J* = 4.1, 8.9 Hz), 4.52 (d, *J* = 7.9 Hz), 4.60-4.73 (m), 5.15 (s), 5.24 (d, *J* = 3.5 Hz), 5.54 (s), 6.61 (d, *J* = 1.9 Hz), 6.64 (t, J = 1.9 Hz), 8.07 (s), 8.09 (s).

^{13}C NMR (D_2O, 150 MHz): δ 50.8, 51.0, 53.5, 60.3, 61.3, 63.1, 68.2, 68.8, 68.9, 68.91, 69.0, 69.4, 69.43, 69.46, 69.5, 69.52, 69.6, 71.66, 71.7, 72.6, 73.2, 92.4, 96.5, 102.5, 108.0, 125.2, 125.7, 125.9, 137.7, 142.9, 144.3, 159.1.

4.7.4 Silver nanoparticle (AgNP) formation

Preparation of sugar stock solutions: The corresponding sugar triazoles (**24-26**) were dissolved in ultrapure H_2O and diluted to a standard concentration of 50 mM. These stock solutions were then used to screen the optimal conditions for AgNP formation.

Preparation of Tollens' reagent stock solutions: Stock solutions of Tollens' reagent were prepared in three different concentrations (100, 20 and 3 mM) and diluted as required with ultrapure H_2O for the preparation of the nanoparticle arrays.

100 mM Tollens: To 1.8 mL H_2O was added $AgNO_3$ (0.5 M, 500 µL), followed by NaOH (3 M, 100 µL) and finally NH_4OH (28%, 110 µL).

20 mM Tollens: To 4.1 mL H_2O was added $AgNO_3$ (0.5 M, 279 µL), followed by NaOH (3 M, 56 µL) and finally NH_4OH (28%, 61 µL).

3 mM Tollens: To 9.9 mL H_2O was added $AgNO_3$ (0.5 M, 60 µL), followed by NaOH (3 M, 12 µL) and finally NH_4OH (28%, 13 µL).

AgNPs were formed by the addition of 25 µL of Tollens' reagent to 25 µL of a solution of an appropriate sugar ligand in a plastic eppendorf. The solution was vortexed and left in the dark overnight. The mixture was centrifuged for 30 seconds to afford a suspension of colloidal of AgNPs.

4.7.5 Reaction kinetics of AgNP formation

Time course: 200 µL of sugar solutions (**24**, **25** or **26**) at 200 µM and 200 µL of Tollens' solution (20 mM) were mixed in a low-volume quartz cuvette; UV-Vis measurements were taken at 400 nm every 5 seconds using a UV-Vis spectrophotometer.

4.7.6 General procedure for ^{1}H NMR titration studies

Stock solutions of triazole ligands (**24, 25** or **26**) at 2 mM and $AgNO_3$ (12 mM) were prepared in D_2O. 300 µL of aliquots of the ligands were mixed with increasing amounts of $AgNO_3$ and diluted with D_2O up to 600 µL. The recorded spectra are shown in Appendix C9-C11 and ordered at different concentrations of $AgNO_3$ from 0 to 6 mM. The acquired ^{1}H NMR data of the triazole sugar ligands and the concentration of the Ag(I) was used to calculate the Ag(I) binding constants using WinEQNMR2 software.[108]

4.7.7 Surface Enhanced Raman scattering

SERS analysis was performed using an Avalon Instruments Plate reader (532 nm) using a 96 well plate. The solution of prepared nanoparticle was diluted 1:200 with double distilled deionised H_2O. 15 µL of malachite green isothiocyanate (**127**) was added to a well, followed by 25 µL of double distilled deionised H_2O and 100 µL of the diluted nanoparticles. This solution was thoroughly aspirated and 10 µL of 0.1 M spermine hydrochloride was added and the nanoparticles allowed to aggregate for 1 min before immediate SERS analysis.

4.7.8 Synthesis of compounds (128) and (8) for preparation AgNPs on amino modified glass surfaces

Synthesis of (128) [182]

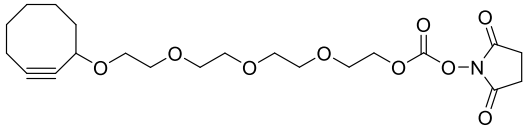

To a solution of (**120**) (0.76 g, 3 mmol) and Et_3N (0.77 g, 8 mmol, 1 mL) in MeCN (10 mL) was added N,N′ Disuccinimidyl carbonate (1.94 g, 8 mmol). The reaction mixture was stirred overnight at room temperature. The mixture was then cooled to room temperature, concentrated *in vacuo* and portioned between DCM (200 mL) and H_2O (100 mL). The aqueous layer was extracted with DCM (2 × 100 mL) and the organic layer washed with 5% $NaHCO_3$ (2 × 100 mL). The organic layer was then dried over $MgSO_4$, filtered and concentrated *in vacuo* followed by purification by column chromatography (SiO_2) eluting with 30% EtOAc in hexane afforded (**128**) (1.04 g, 94%) as a colourless syrup.

LRMS (ESI) m/z: $[M + Na]^+$ 464.

^{1}H NMR ($CDCl_3$, 500 MHz): δ 1.39-2.30 (m, 10H), 2.84 (s, 4H,$COCH_2CH_2CO$), 3.49-3.80 (m, 16H, CH_2-PEG), 4.21-4.24 (m, 1H, CH).

^{13}C NMR ($CDCl_3$, 125 MHz): δ 20.9 (CH_2, 1C), 25.7 (CO**C**H_2**C**H_2CO, 2C), 26.6 (CH_2, 1C), 29.9 (CH_2, 1C), 34.5 (CH_2, 1C), 42.5 (CH_2, 1C), 68.5 (1C), 68.7 (1C), 70.5 (1C), 70.6 (1C), 70.7 (1C), 70.8 (1C), 70.9 (1C), 71.1 (1C), 72.9 (1C), 93.1 (C≡**C**, 1C),, 100.1 (**C**≡C, 1C), 151.8 (O**C**OO, 1C), 168.7 (**C**OCH_2CH_2**C**O, 2C).

Synthesis of (8) [82]

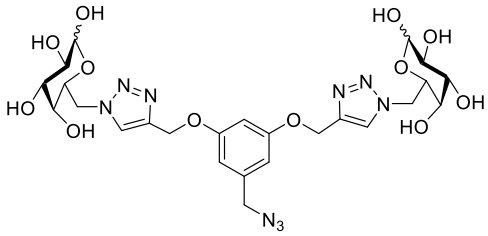

To a mixture of TFA:H_2O (1:1, 20 mL) was added (**35**) (0.64 g, 0.79 mmol) under a nitrogen atmosphere. The reaction mixture was heated to reflux for 4 h. The mixture was then cooled to room temperature followed by concentration *in vacuo*. The crude residue was diluted with H_2O (20 mL) and concentrated *in vacuo* again to remove excess TFA. The product was diluted with MeOH and precipitated using Et_2O. The crude residue was diluted in H_2O and purified by semi-preparative HPLC using H_2O and MeCN. The gradient was started at 5% MeCN (solvent B), held at 5 min, then increased to 90% solvent B over 20 min. The product was freeze-dried to afford **(8)** (0.30 g, 58%) as a white powder. This compound was isolated as a mixture of diastereomers.

LRMS (ESI) m/z: $[M + Na]^+$ 674.

MP. 185-186°C.

^{1}H NMR (DMSO-d_6, 400 MHz): δ 3.53-3.63 (m), 3.70-3.74 (m), 3.89-3.92 (m), 4.19-4.35 (m), 4.37 (s), 4.48-4.53 (m), 4.73-4.78 (m), 4.90-4.98 (m), 5.13 (d, J = 4.1 Hz), 6.60-6.57 (m), 8.20 (s).

^{1}H NMR (DMSO-d_6, 100 MHz): δ 51.0, 53.5, 61.2, 68.3, 68.9, 69.5, 71.6, 72.8, 72.9 92.6, 97.3, 101.1, 101.8, 107.4, 125.3, 137.9, 142.1, 159.4.

CHAPTER 5: SILVER NANOPARTICLE SYNTHESIS USING SUGAR-MODIFIED PEPTIDES

5.1 Introduction

This chapter focuses on the investigation of modified peptides and their role to template the size and shape of AgNPs. Chains of 2-50 amino acids are known as peptides (Figure 5-1a).[68] The majority of proteins and peptides are composed of twenty common L-amino acids, which have the general structure shown in Figure 5-1b. The simplest one is glycine, which has two hydrogen atoms attached to the alpha carbon atom. The rest of the amino acids are classified according to their side-chains (R). The first class includes aliphatic amino acids such as alanine, valine, leucine, isoleucine, proline and methionine. Secondly, phenylalanine, tyrosine and tryptophan are examples of compounds that have aromatic side-chains. The next type refers to uncharged amino acids which contain hydroxyl groups in serine and threonine, thiol group in cysteine and carboxamides in asparagine and glutamine. Finally, some amino acids such as aspartate and glutamate are acidic and have negatively charged side-chains. Whereas, lysine arginine and histidine are basic compounds and carry positive charges at neutral pH. Figure 5-2 summarises the twenty naturally occurring amino acids.

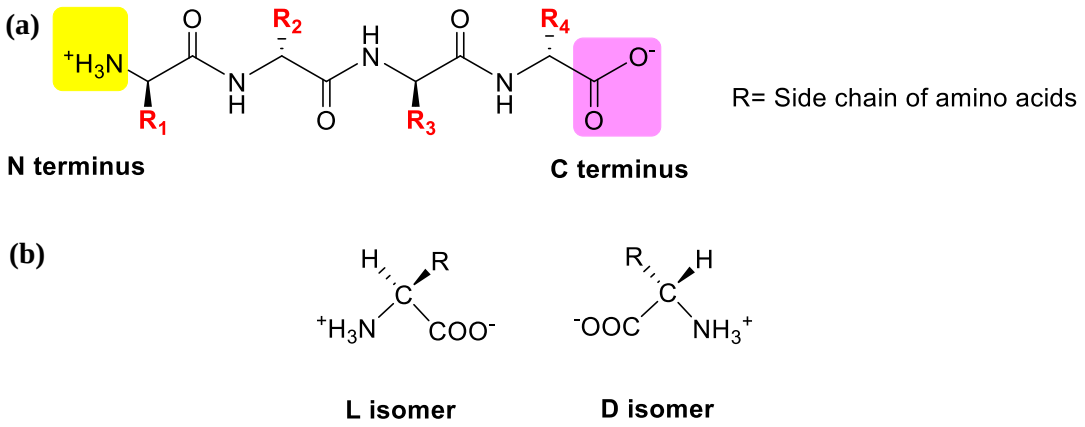

Figure 5-1: (a) *Primary peptide sequence.* ***(b)*** *The L and D isomers of amino acids.*

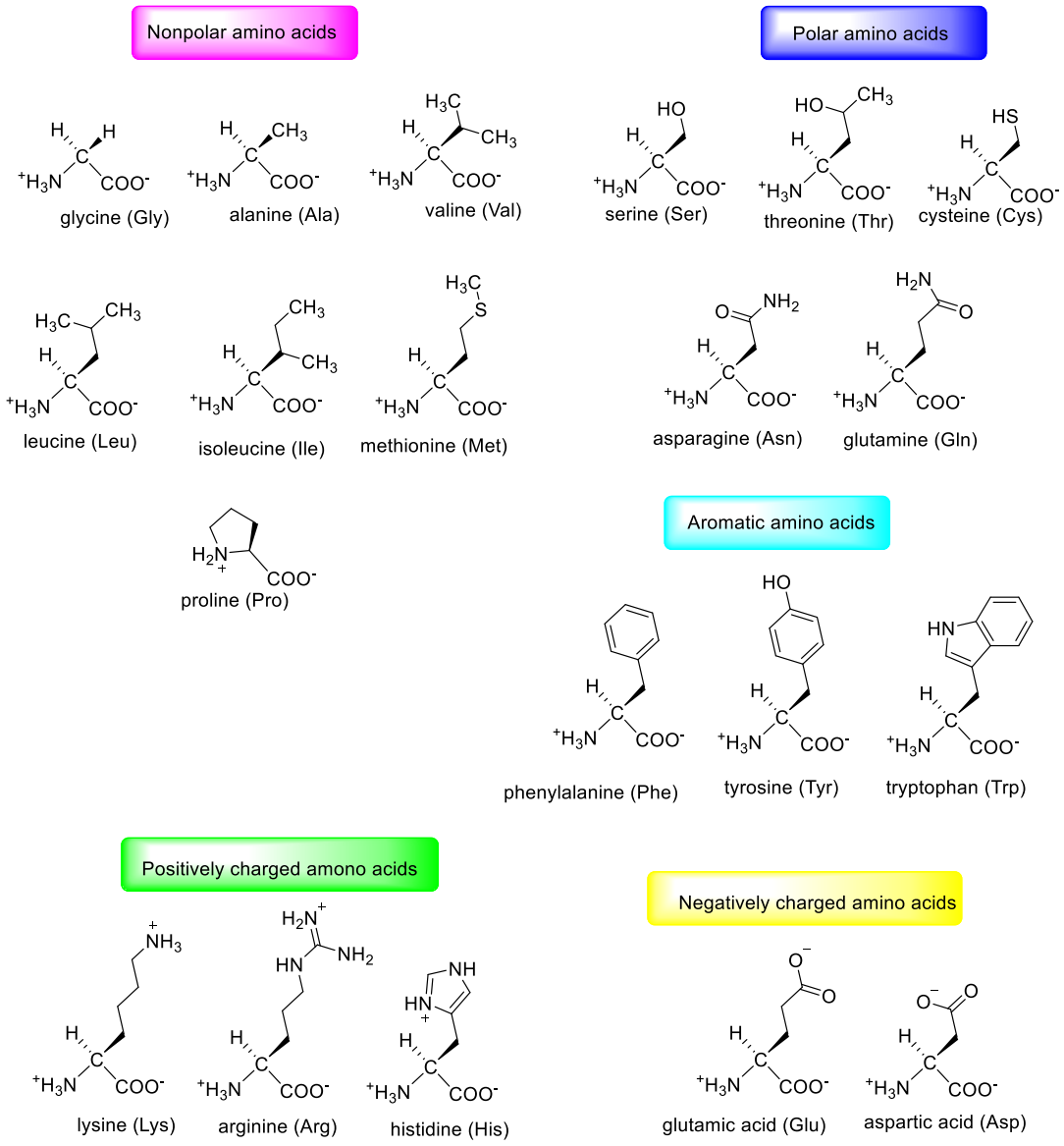

***Figure 5-2**: The twenty naturally-occurring amino acids.*

Polypeptide chains can fold to form secondary structures such as α helix and β sheet (Figure 5-3). A β-sheet is a linear structure formed either by intra- or inter-molecular hydrogen-bonding between the backbone C=O and NH groups.[68]

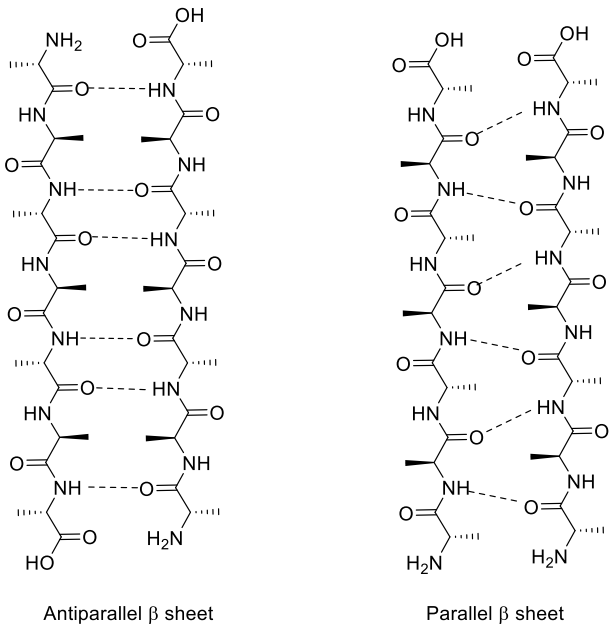

Figure 5-3: *β-sheet peptide secondary structures.*

5.1.1 Solid phase peptide synthesis

Peptides are generally synthesised from C-terminus to N-terminus using solid phase methods originally developed by Merrifield.[184] The basic principle of this approach involves covalent attachment of amino acid residues onto an insoluble polymeric support or resin (Scheme 5-1). In this technique, the most important aspect to control during synthesis is the reactivity of both amino and carboxylic groups. For this purpose, α-amino groups are masked with temporary protecting groups that are removed prior to the desired coupling. Orthogonal protecting groups are used to protect the functional groups of the amino acid side-chain that can be removed at the end of the synthesis.

In general, there are two methods for solid phase peptide synthesis. The first approach was developed by Merrifield based on the use of *tert*-butoxycarbonyl (Boc) groups for the protection of α-amino groups and benzyl derivatives (Bn) for side-

chain carboxy protection.[185] The first step in the synthesis is to link the first amino acid through its carboxyl group to the resin. The Boc group of this amino acid is then deprotected using trifluoroacetic acid (TFA) to allow coupling with an incoming activated ester of a corresponding N-α-protected amino acid to form the first peptide bond. The cycle of deprotection and coupling is repeated until the desired peptide sequence is assembled. Unreacted reagents are easily removed by filtration and washing after each step of the synthesis. At the end of the synthesis, the peptide is cleaved from the resin under strong acidic conditions such as hydrogen fluoride (HF).[186] The cleavage reagent also removes side-chain protecting groups. One of the main drawbacks of Boc solid phase peptide synthesis is that both N-α-protecting groups and side-chain groups are acid labile. This can lead to deprotection some of the side-chains during TFA treatment, forming undesired products at the end of the synthesis.

An alternative orthogonal strategy is Fmoc solid phase peptide synthesis. A base labile 9-fluorenylmethoxycarbonyl (Fmoc) group is used to protect the α-amino groups.[187] Acid labile side-chain protecting groups such as *tert*-butyl (*t*-Bu) are also used. In this method, deprotection of the Fmoc groups can be achieved under mild basic conditions using 20% piperidine in DMF. The side-chain protecting groups and the peptide are cleaved at the end of the synthesis using TFA. Another advantage of this strategy is that Fmoc derivatives have strong UV absorbance that enables the monitoring of each coupling at the deprotection stage. This feature leads to the development of automated peptide synthesisers with a UV-absorbance detector to monitor the efficiency of the synthesis.

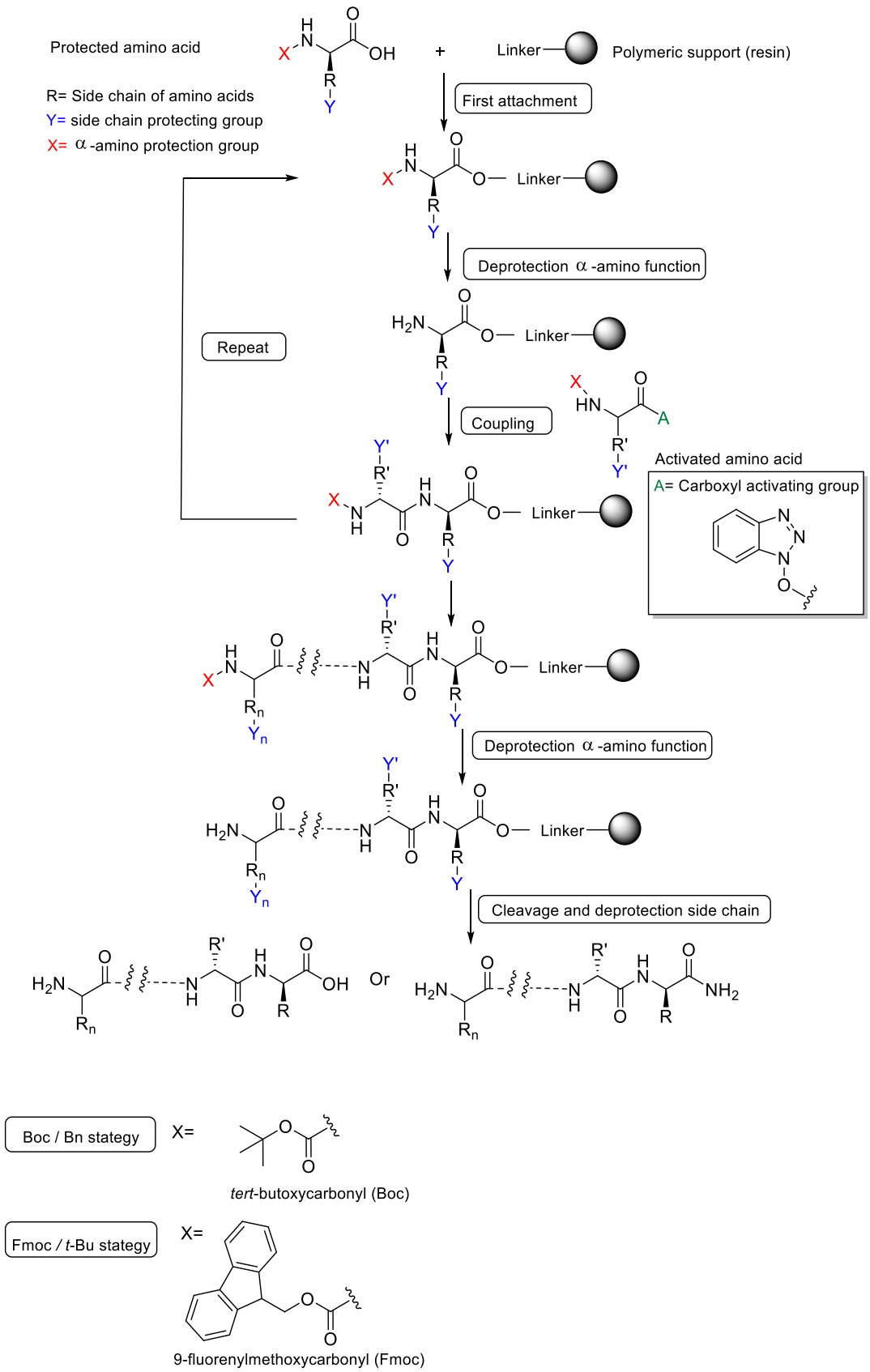

Scheme 5-1: *Overview of solid phase peptide synthesis.*

5.1.2 Protein- and peptide-directed synthesis of AgNPs

Natural proteins and peptides are attractive candidates for the development of green chemistry approaches for the synthesis of biocompatible AgNPs.[58,59,188-198] An example of the protein-mediated synthesis of AgNPs was reported by Lee *et al.*[192] Ag nanoplates with diameter of 44 nm were prepared using proteins extracted from green algae *Chlorella vulgaris* as reducing and shape-directed agents.[192] This study showed the following aspects: (i) hydroxyl groups in tyrosine residues were responsible for the reduction of silver ions. This effect was probed by chemical modification of tyrosine residues using N-acetylimidazole (**129**). The authors showed that acetylated protein derivatives did not form AgNPs, while deacetylation produced Ag nanoplates with a diameter of 46 nm; (ii) acidic side-chains in aspartic and glutamic residues were the most active functional groups to control the shape of the resulting nanoparticles and (iii) modified proteins through amination of aspartic and glutamic residues produced spherical AgNPs. On the basis of these results, tripeptide (Asp-Asp-Tyr) was designed to generate Ag nanoplates with a narrow size distribution (28 nm). This study showed how the nature of the proteins and peptides influenced the formation and morphologies of AgNPs (Scheme 5-2).

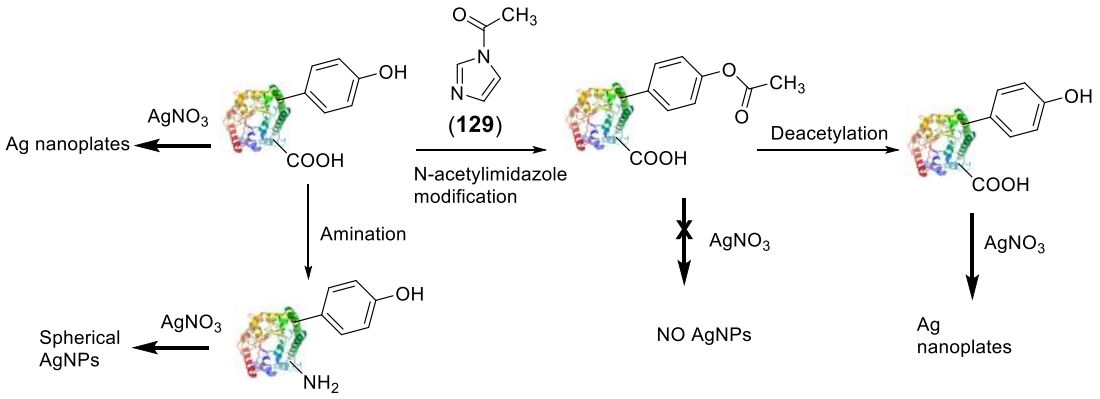

Scheme 5-2: *Schematic representation of manipulating algal proteins for the synthesis of different shapes of AgNPs.*

Another example of peptide-based methods for the synthesis of size-controlled spherical AgNPs was developed by Wennemers *et al*. using aldehyde-functionalised oligoprolines (**130**) and Tollens' reagent (Scheme 5-3).[59] The aldehyde groups were attached on every third residue on the backbone of oligoprolines which adopt a symmetric α-helical secondary structure found in polyproline II proteins.[199] This approach demonstrated that the length and rigidity of oligoproline peptides were important parameters to control the size of the AgNPs ranging from 2 nm into 9 nm. The authors also reported that increasing the number of aldehyde moieties in rigid oligoproline scaffolds produced larger spherical AgNPs. The influence of the rigidity of this system was confirmed by preparing flexible peptides (**131**) that displayed no correlation between the length of the peptides with the size of AgNPs.

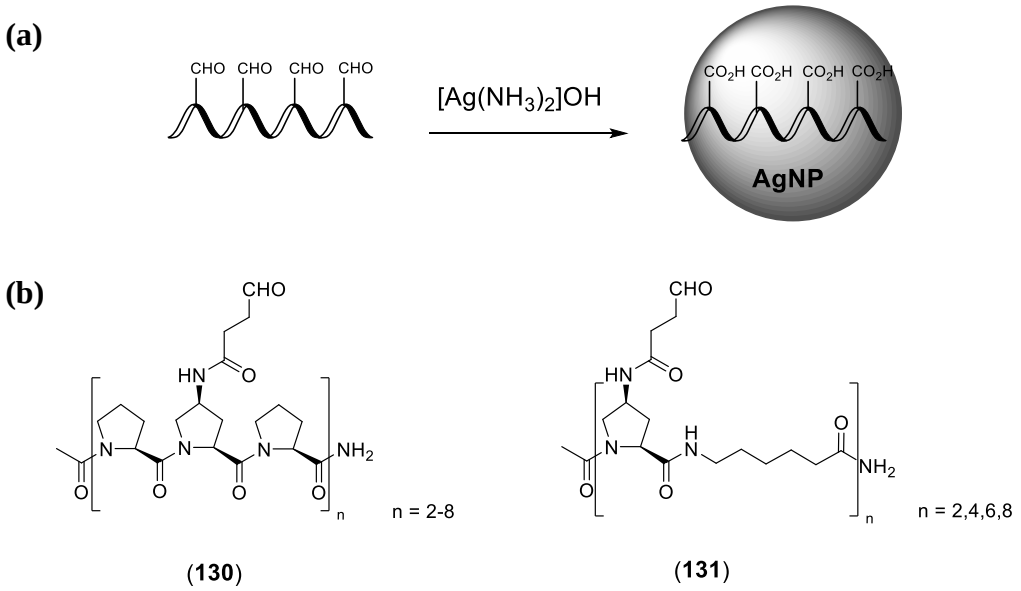

Scheme 5-3: (a) *General scheme for the formation of AgNPs templated by aldehyde-functionalised oligoprolines.* ***(b)*** *Structures of rigid and flexible aldehyde-functionalised oligoprolines. Figure adapted with permission from Reference 59. Copyright (2012) John Wiley and Sons.*

5.2 Hypothesis

In chapter one (Section 1.3.3.1), Carell *et al.*[82] showed how the incorporation of sugar triazoles into DNA by click reaction of alkyne-modified DNA with sugar azides can direct the deposition of silver nanoparticles using Tollens' reagent. Based on this work, sugar-functionalised peptides (**27-28**, Figure 5-4) were prepared to explore the size- and shape-controlled synthesis of AgNPs. We hypothesised that the density and position of sugars in the peptide will influence the morphology of AgNPs and form rod-shaped AgNPs that are different from those prepared using sugar triazole ligands in chapter two and four.

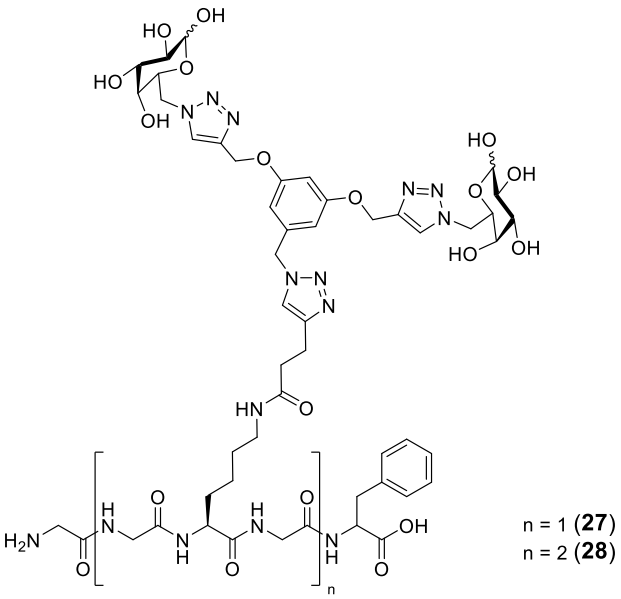

Figure 5-4: *Structures of sugar-functionalised peptides.*

5.3 Aims of the study

The aims of this chapter are:

1) To synthesise the Fmoc-alkyne lysine amino acid building block (**132**).

2) To synthesise alkyne-modified peptides (**133-134**) (Figure 5-5) by Fmoc solid phase peptide synthesis.

3) To synthesise sugar-functionalised peptides (**27-28,** Figure 5-4) for the synthesis of AgNPs using Tollens' reagent.

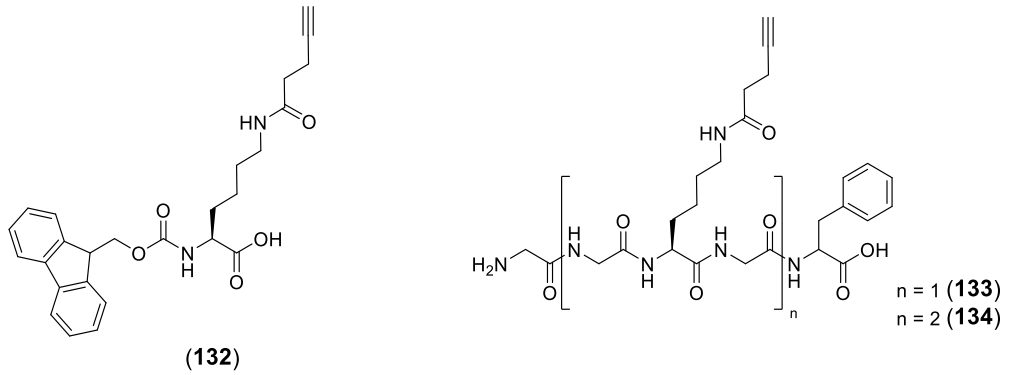

Figure 5-5: *Structures of Fmoc-alkyne lysine amino acid building block (**132**) and alkyne-modified peptides (**133-134**).*

5.4 Results and Discussion

5.4.1 Synthesis of Fmoc-alkyne lysine-OH monomer (132)

Two synthetic methods were used to prepare (**132**). The first approach started from the commercially available N^{α}-Boc-N^{ε}-(carbobenzyloxy)-L-lysine (**135**) (Scheme 5-4). The first step was the esterification of (**135**) using *t*-butanol to afford (**136**) as a yellow oil in 63% after purification by column chromatography. Deprotection of the Cbz group by Pd-catalysed hydrogenation afforded (**137**) as a yellow oil in 92%. The next step involved coupling of the free ε-amine group of (**137**) with 4-pentynoic acid (**138**) to afford (**139**) as a yellow oil in 64%. Acid deprotection of the *t*-Bu and Boc protecting groups was achieved in a single step using TFA:phenol:water (TPW) to afford (**140**) as a yellow oil in 86%. Finally, Fmoc protection of (**140**) afforded (**132**) as a pale yellow solid in 46% after purification by RP-HPLC. While this approach

achieved average yields, it has some disadvantages including the long preparative route to access (**132**) and the difficulty in purification by RP-HPLC due to its hydrophobic nature.

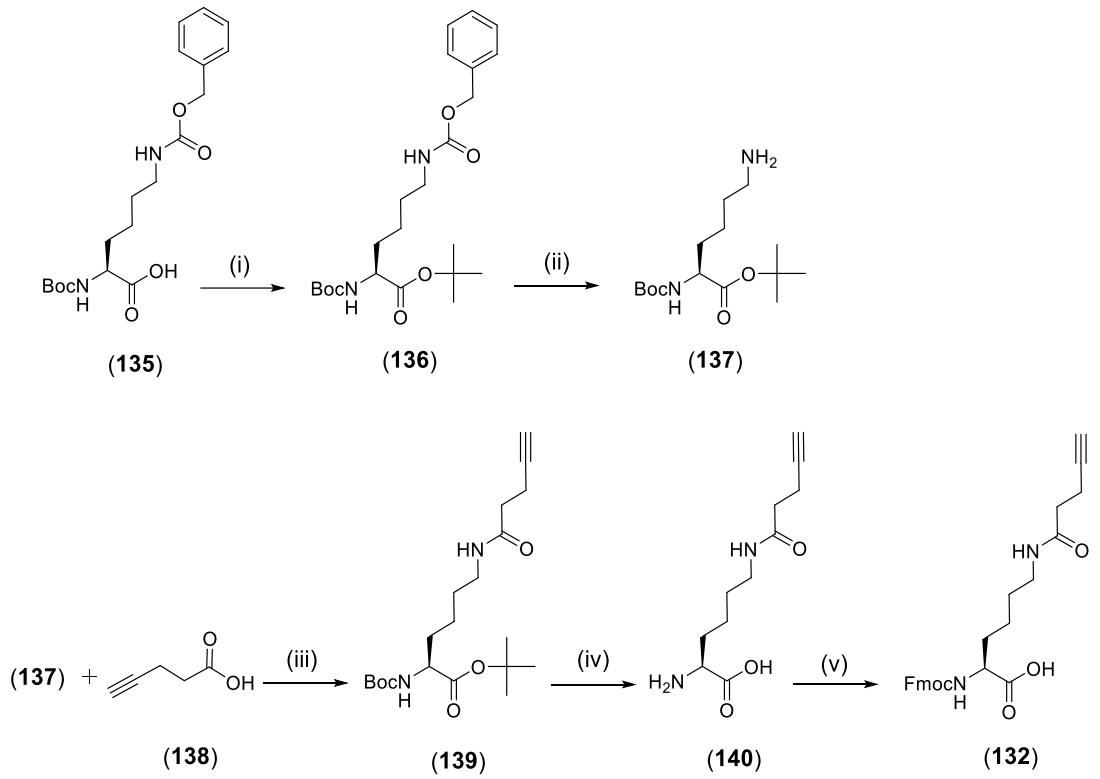

Scheme 5-4: *Reagents and conditions: (i) EDC (2.1 equiv.), DMAP (0.6 equiv.), dry t-BuOH (12 equiv.), dry DCM, RT, 24h, 63%; (ii) H_2, Pd/C (1.0 equiv.), MeOH, RT, 24h, 92%; (iii) compound (**138**) (1.2 equiv.), HOAt (1.2 equiv.), EDC (1.2 equiv.), DIEA (4.0 equiv.), anhydrous DMF, 0°C to RT, 24h, 64%; (iv) TFA:phenol:H_2O (92.5:5:2.5), RT, 1h, 86%; (v) Fmoc-OSu (0.95 equiv.), $NaHCO_3$, 1,4-dioxane:H_2O (1:1), 0°C to RT, 4h, 46%.*

An alternative method for the preparation of (**132**) was performed in two steps outlined in Scheme 5-5. The synthesis commenced with the activation of the carboxyl group of (**138**) using NHS and DCC to afford the corresponding NHS ester (**141**) as a white solid in 78%. Activated ester (**141**) was then reacted with the commercially available Fmoc-lysine-OH (**142**) to afford (**132**) as a pale yellow solid

in 71%. Compound (**132**) was then used directly for solid phase peptide synthesis without further purification.

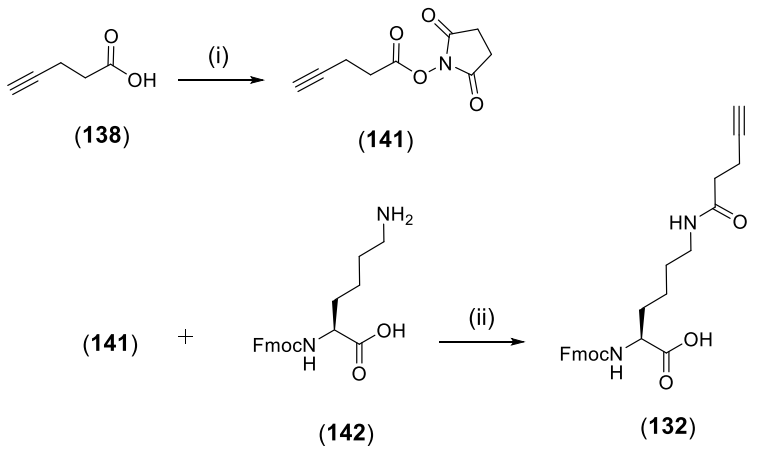

Scheme 5-5: *Reagents and conditions: (i) NHS (1.0 equiv.), DCC (1.0 equiv.), dry EtOAc:Dioxane (1:1), 0°C to RT, 5h, 78%; (ii) compound (**142**) (1.0 equiv.), DIEA (1.1 equiv.), DMF, RT, 2h, 71%.*

5.4.2 Synthesis of alkyne-modified peptides (133-134)

Alkyne-modified peptides (**133-134**) were prepared by Fmoc-based solid phase synthesis starting with Fmoc-Phe-Wang resin (**143**). The Fmoc was removed using 20% piperidine in DMF to afford (**144**). In order to minimise the loading of the resin, **(144**) was treated with 0.5 equivalent of acetic anhydride and 1 equivalent of DIEA in DMF for 30 min. Fmoc-Gly-OH (**145**) (4 equivalents) was pre-activated for 10 min with 3.9 equivalents of HATU in the presence of DIEA prior to addition to (**144**). The coupling of (**145**) with **(144**) proceeded for 2 h. Unreacted amino groups on the resin were capped with a solution of acetic anhydride:pyridine:DMF (5:5:95). The cycle of Fmoc-deprotection, coupling and capping was repeated until the desired peptide sequences (**149-150**) were formed. After deprotection of the final Fmoc group, the peptide was cleaved from the resin using TFA in the presence of 5% triethylsilane (TES) as scavenger. The cleaved peptides (**133-134**) were lyophilised

and used directly in click reactions without purification. The general protocol for the synthesis of alkyne-modified peptides (**133-134**) is summarised in Schemes 5-6 and 5-7.

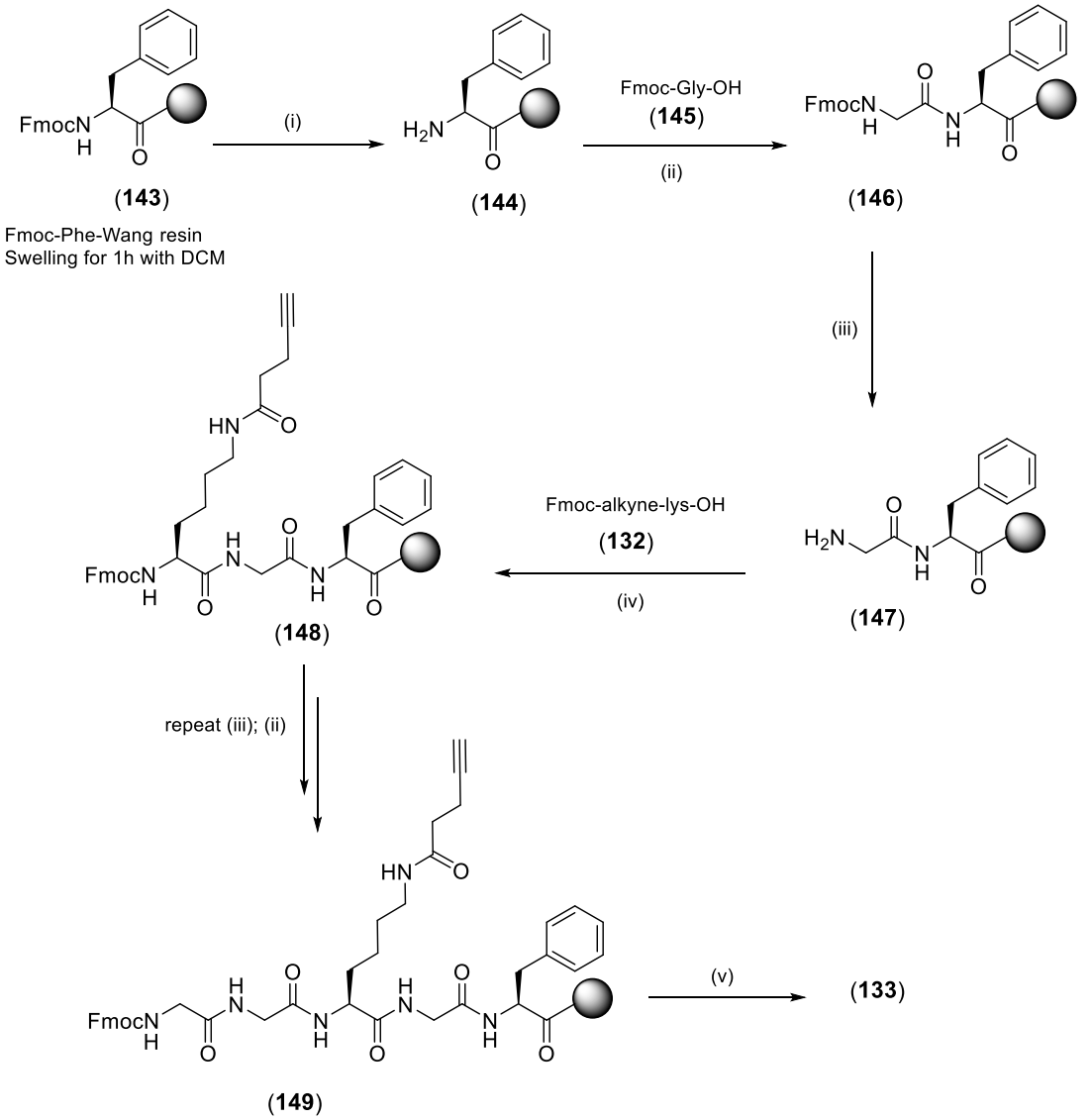

Scheme 5-6: *Reagents and conditions: (i) washing 3x DMF, 20% Piperidine in DMF (2x15 min), washing 6x DMF; (ii) compound (**145**) (4.0 equiv.), HATU (3.9 equiv.), DIEA (21 equiv.), 2h, washing 4x DMF, 3x DCM; (iii) Ac_2O:Pyridine:DMF (5:5:95)(2x10 min), washing 5x DMF, 3x DCM, 20% Piperidine in DMF (2x15 min), washing 6x DMF; (iv) (**132**) (2.5 equiv.), HATU (2.4 equiv.), DIEA (21 equiv.), 2h, washing 4x DMF, 3x DCM;(v) 20% Piperidine in DMF (2x15 min), washing 4x DMF, 4x DCM, TFA:TES (90:10).*

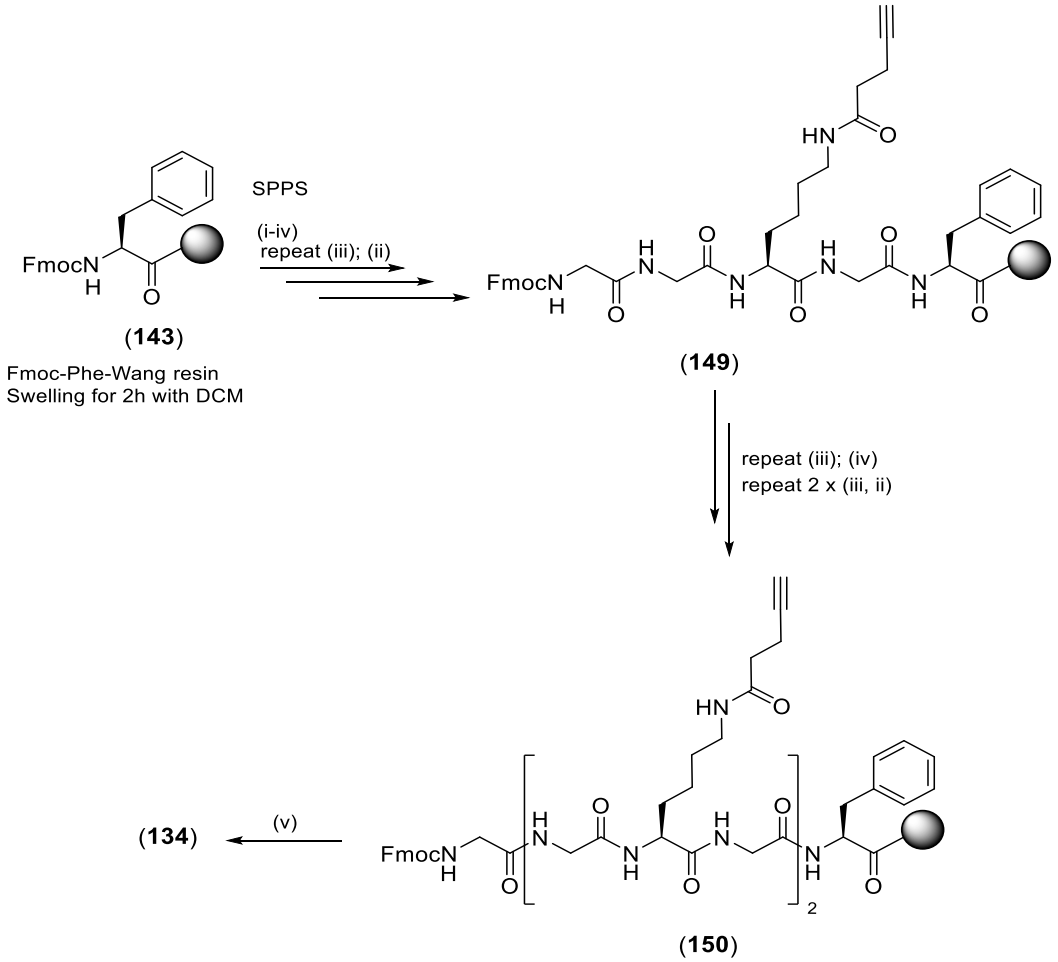

Scheme 5-7: *General protocol for the solid phase peptide synthesis (SPPS) for the preparation of octamer peptide (**134**). See Scheme 5-6 for reagents and conditions.*

5.4.3 Synthesis of sugar-functionalised peptides

A click reaction between alkyne-modified peptides (**133-134**) and azide (**35**) using copper sulfate in the presence of sodium ascorbate afforded (**151**) in 23% yield and (**152**) in 8% as a white powder after purification by RP-HPLC. Acid deprotection of the isopropylidene groups of (**151-152**) and purification by RP-HPLC afforded (**27**) in 48% yield and (**28**) in 37% as a white powder (Scheme 5-8).

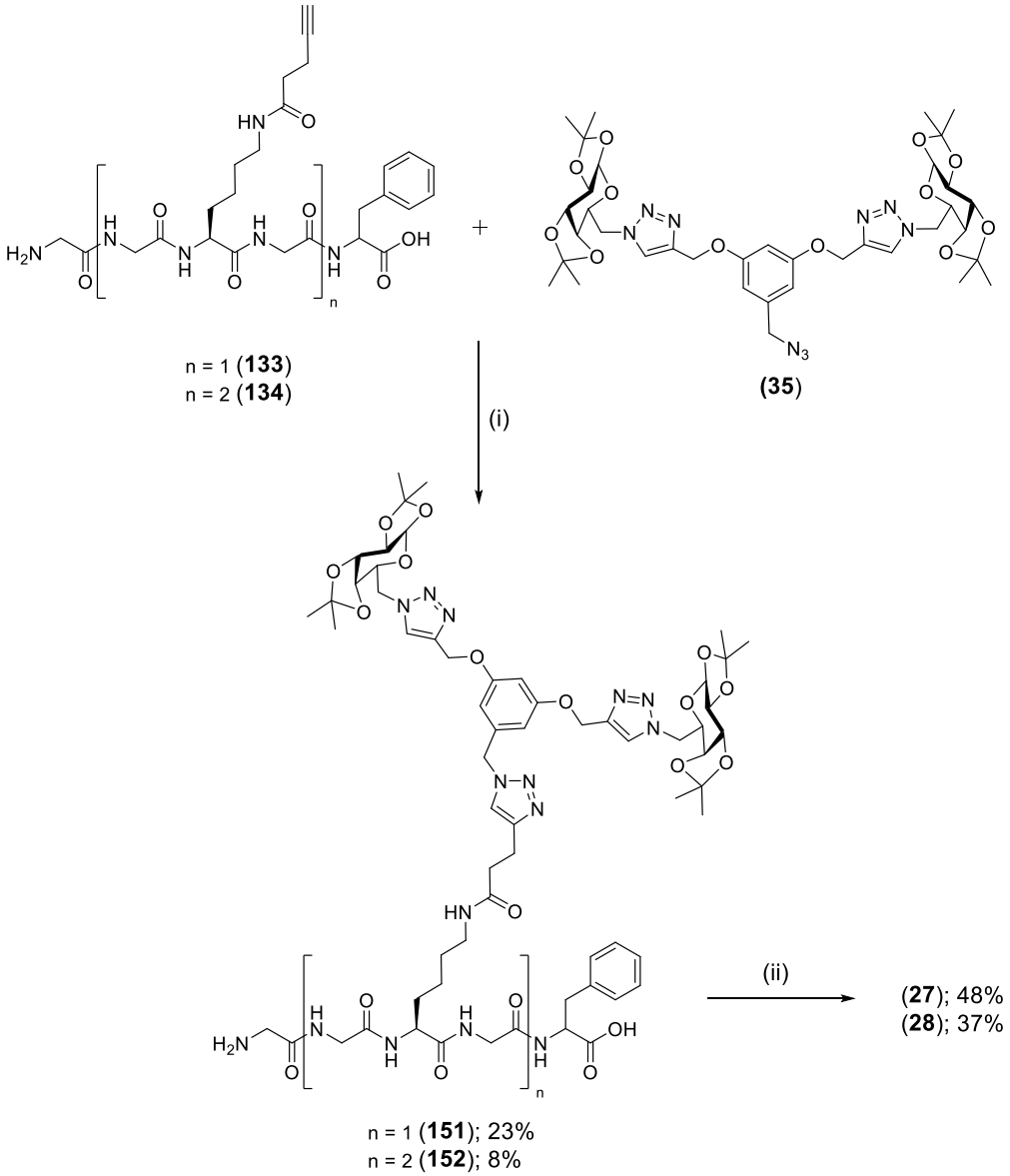

Scheme 5-8: *Reagents and conditions: (i) (**35**) (2.0 equiv. per alkyne), $CuSO_4$, sodium ascorbate (2.0 equiv.), THF:H_2O: DMSO (iii.) TFA:H_2O (1:1), 70°C, 4h.*

5.4.4 Synthesis of AgNPs using sugar-functionalised peptides

5.4.4.1 AgNPs derived from peptide (27)

A AgNP array using compound (**27**) was constructed over concentration ranges of 1 mM - 25 mM [(**27**)] and 1 mM - 50 mM [Tollens'] (Table-5-1)

Table 5-1: *AgNP@(**27**) screening array prepared using sugar triazole (**27**) and Tollens' reagent. White boxes represent no AgNP formation, yellow boxes represent AgNP formation and grey box represents the formation of silver mirror.*

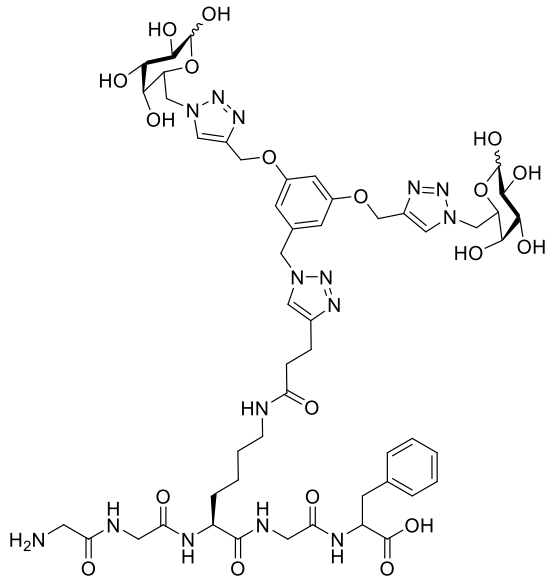

[(27)]

[Tollens']

	25 mM	10 mM	5 mM	1 mM
1 mM	#1	#2	#3	#4
10 mM	#5	#6	#7 20 ± 3 nm	#8 32 ± 4 nm
20 mM	#9	#10 16 ± 2 nm	#11	#12 32 ± 6 nm
50 mM	#13	#14	#15 23 ± 2 nm	#16

The reaction screen of [(**27**)] and [Tollens'] produced AgNP@(**27**) in two regions (yellow boxes in Table 5-1): (i) a region at 10 mM - 20 mM [Tollens'] and 1 mM - 10 mM (**27**) and (ii) a region at 50 mM [Tollens'] and 5 mM - 25 mM (**27**). Figure 5-6 shows the UV-vis spectra of AgNP@(**27**) formed in these regions. Silver aggregation was observed at 50 mM [Tollens'] and 1 mM (**27**).

SEM analysis of several examples in this series produced AgNP@(**27**) of tunable sizes that ranged from 16 ± 2 when a higher concentration of (**27**) was used (#10, Figure 5-7c) to 32 ± 6 nm when a lower concentration of (**27**) was used (#12, Figure 5-7d). TEM analysis revealed the formation of angular AgNP@(**27**) (Figure 5-8).

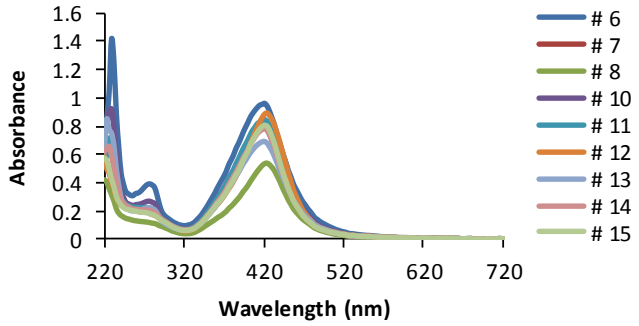

Figure 5-6: *UV-vis spectra of reactions #6-8 and 10-15, which formed AgNP@(**27**) as observed by a SPR peak. Sample #6 was diluted 1:10, #7-8, 10-12 were diluted 1:16 and #13-15 were diluted 1:50 prior to each measurement.*

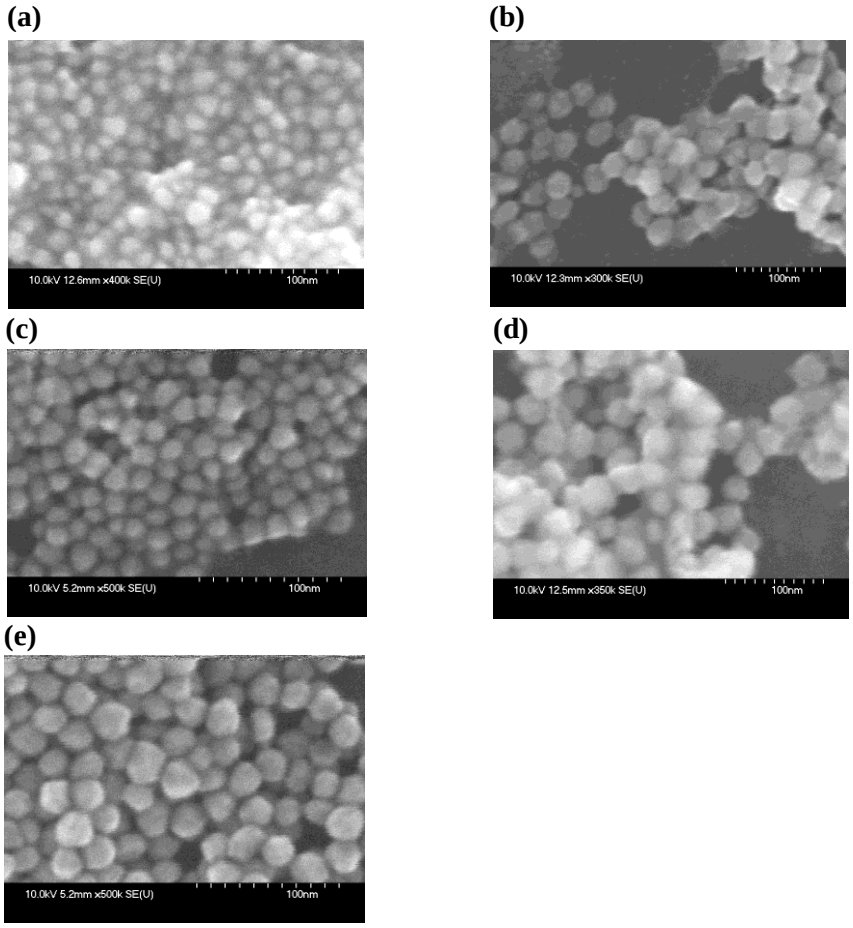

Figure 5-7: *SEM images of AgNP@(**27**) prepared using reaction conditions in Table 5-1.* ***(a)*** *#7, Ø = 20 ± 3 nm;* ***(b)*** *#8, Ø = 32 ± 4 nm;* ***(c)*** *#10, Ø = 16 ± 2 nm;* ***(d)*** *#12, Ø = 32 ± 6 nm;* ***(e)*** *#15, Ø = 23 ± 2 nm.*

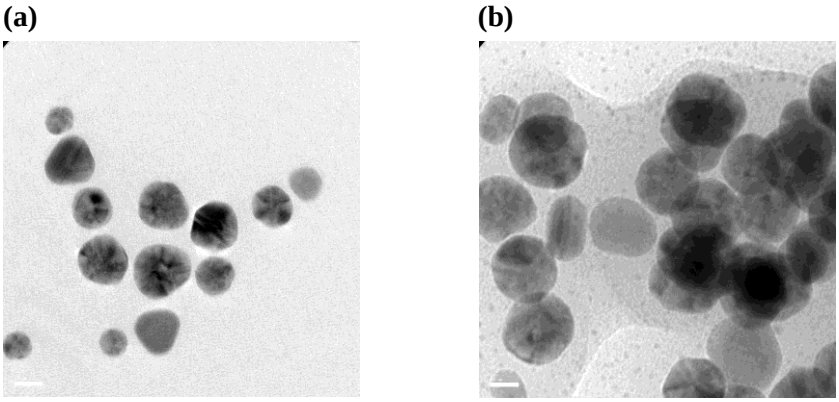

Figure 5-8: *TEM images of AgNP@(**27**) prepared using reaction conditions in Table 5-1.* ***(a)****#10;* ***(b)*** *#15.*

5.4.4.2 AgNPs derived from peptide (28)

Table 5-2 represents the AgNP@(**28**) array prepared over a concentration range of 10 µM - 10 mM [(**28**)] and 10 mM - 50 mM [Tollens']. The concentration of peptide (**28**) in this array was lower than that used for the preparation of AgNP@(**27**) array due to its high molecular weight.

In contrast to AgNP@(**27**), no silver mirrors or formation of Ag aggregates were observed when ligand (**28**) was used. Another difference is that the addition of 10 mM - 20 mM [Tollens'] to 5 mM - 10 mM [(**28**)] formed AgNP@(**28**) only with sample #7. However, yellow colloidal solutions were observed at 10 mM - 20 mM [Tollens'] and 5 mM - 10 mM [(**27**)] (#6, #7, #10 and #11, Table 5-1). Figure 5-9 shows the UV-vis spectra of AgNP@(**28**).

Table 5-2: *AgNP@(**28**) screening array prepared using sugar triazole (**28**) and Tollens' reagent. White boxes represent no AgNP formation and yellow boxes represent AgNP formation.*

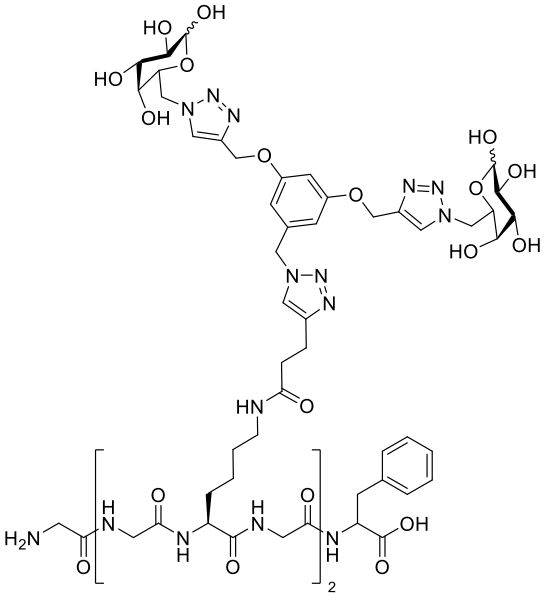

[(28)]

[Tollens']

	10 mM	5 mM	1 mM	100 µM	10 µM
10 mM	#1	#2	#3	#4 18 ± 3 nm	#5 23 ± 2 nm
20 mM	#6	#7	#8 12 ± 1 nm	#9 21 ± 2 nm	#10
50 mM	#11	#12 10 ± 1 nm	#13 21 ± 4 nm	#14	#15

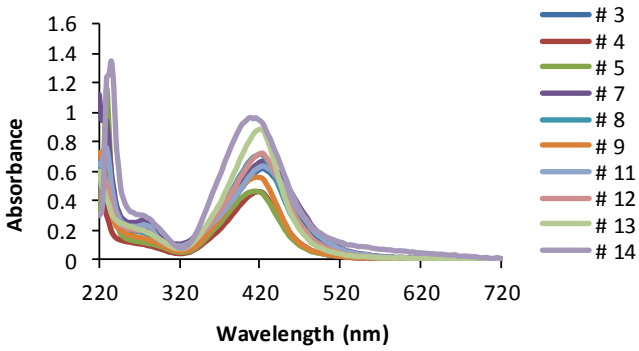

Figure 5-9: *UV-vis spectra of reactions #3-5, 7-9 and 11-14, which formed AgNP@(**28**) as observed by a SPR. Samples #3-4, 9 were diluted 1:10, #7-8 were diluted 1:16 and 11-13 were diluted 1:50 prior to each measurement.*

SEM analysis of several examples in this series produced AgNP@(**28**) with diameters ranging from 10 ± 1 nm (#12, Figure 5-10e) to 23 ± 2 nm (#5, Figure

5-10b). TEM analysis revealed the formation of angular AgNP@(**28**) (Figure 5-11). These AgNP@(**28**) were smaller in diameter compared to AgNP@(**27**). For example, #8 and #12 in Figure 5-10 afforded AgNP@(**28**) with diameters of 12 ± 1 nm and 10 ± 1 nm respectively. Using the same conditions [i.e., #12 and #15 in Table 5-1], AgNP@(**27**) were formed with diameters of 32 ± 6 nm and 23 ± 2 nm respectively. This behaviour was consistent with Kvitek's *et al*. results in chapter one (Section 1.3.2.2), showing that an increase in the number of reducing sugar units using disaccharides produced smaller AgNPs with a narrower size distribution relative to monosaccharides.[65] In contrast, Burley *et al*. reported that increasing sugar units from two (**18**) to four (**19**) resulted in the formation of AgNPs with similar diameters [AgNP @(**18**) produced 8 ± 5 nm and AgNP@(**19**) produced 10 ± 2 nm].[87]

5.5 Conclusion

A novel mild and one-step method was reported for the preparation of size- and shape-controlled AgNPs using sugar-functionalised peptides (**27-28**) and Tollens' reagent. The results of SEM and TEM analysis in this chapter indicated that angular monodispersed AgNPs were obtained with inherently tunable sizes. Increasing the density of reducing sugar units using octamer peptide (**28**) resulted in the formation of smaller AgNP@(**28**) compared to AgNP@(**27**) using pentamer peptide (**27**).

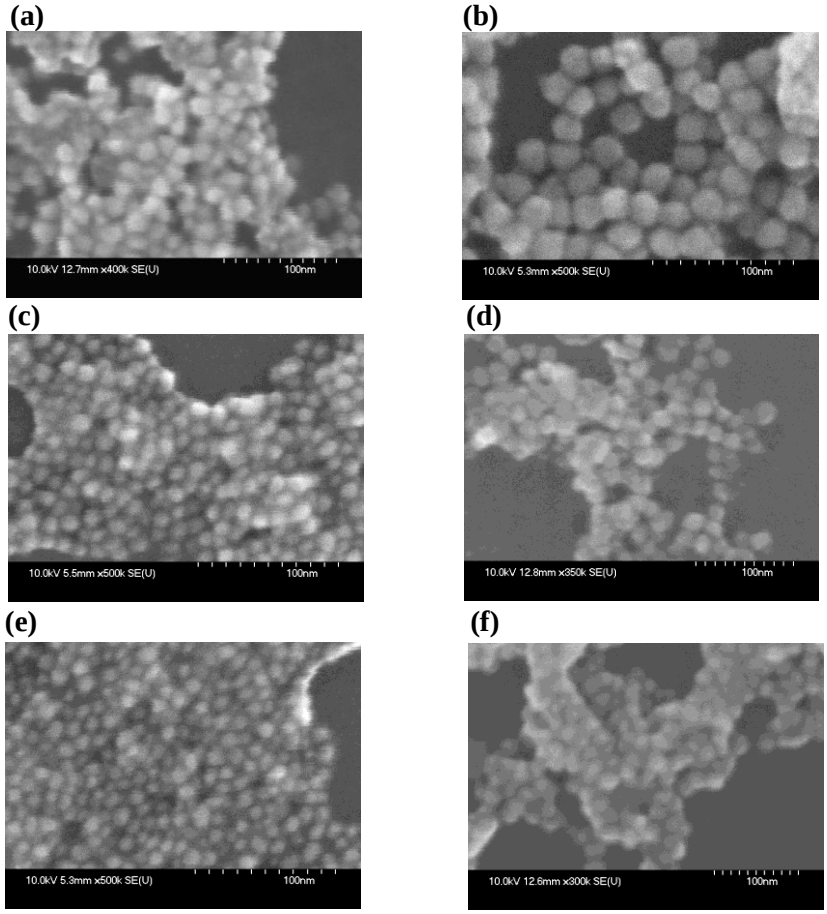

Figure 5-10: *SEM images of AgNP@(**28**) prepared using reaction conditions in Table 5-2.* ***(a)*** *#4, Ø = 18 ± 3 nm;* ***(b)*** *#5, Ø = 23 ± 2;* ***(c)*** *#8, Ø = 12 ± 1 nm;* ***(d)*** *#9, Ø = 21 ± 2 nm;* ***(e)*** *#12, Ø = 10 ± 1 nm;* ***(f)*** *#13, Ø = 21 ± 4 nm.*

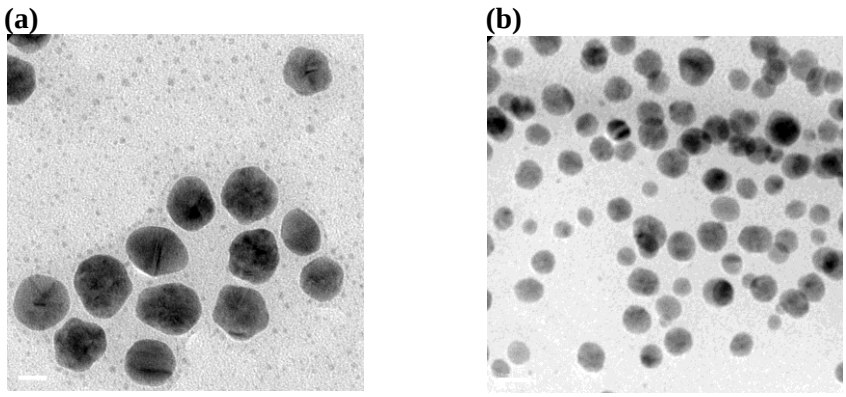

Figure 5-11: *TEM images of* ***(a)*** *AgNP@(**28**), sample #4;* ***(b)*** *AgNP@(**28**), sample #12 prepared using reaction conditions in Table 5-2.*

5.6 Future Work

Further investigation is necessary to study the correlation between the length of the peptide scaffolds with the size and shape of AgNPs. For this purpose, a series of sugar-functionalised peptides of different lengths will be prepared. Replacement of flexible amino acids with unnatural rigid amino acids (**153-154**, Figure 5-12) could have the potential to form rod-shaped AgNPs.

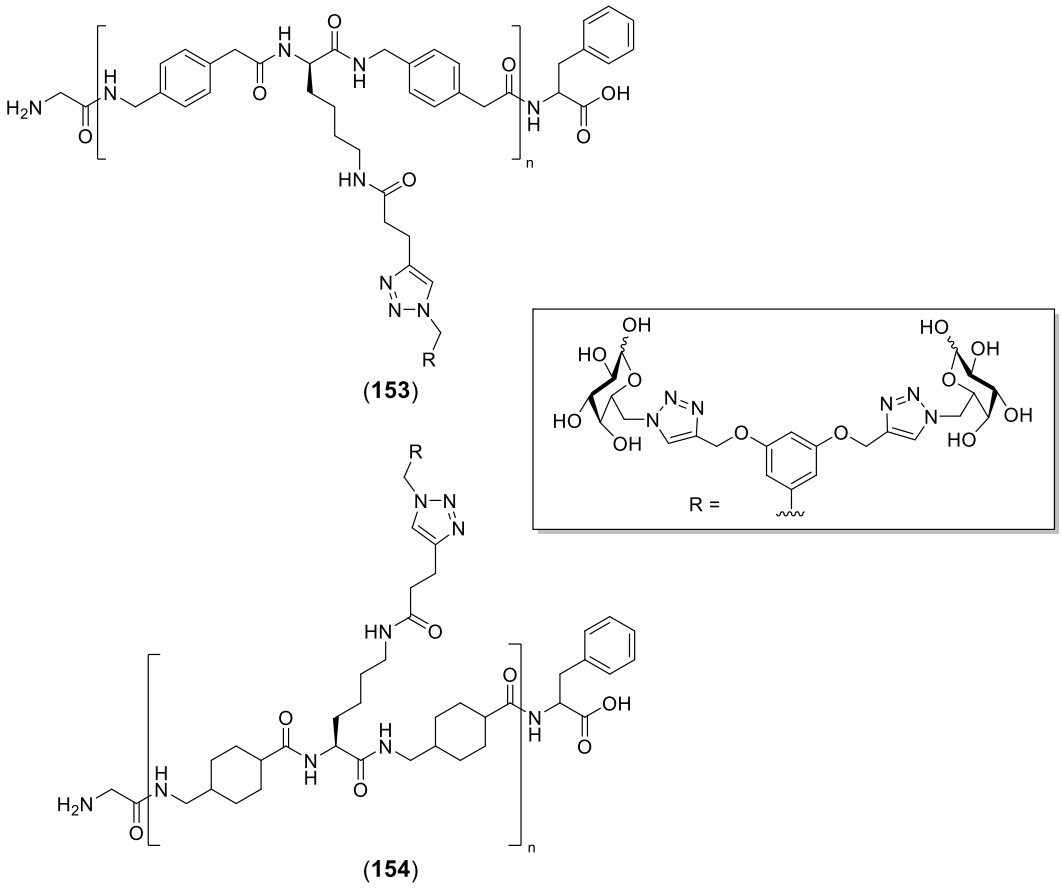

Figure 5-12: *Example of sugar-functionalised peptides (**153-154**) using rigid Fmoc-amino acids: Fmoc-4-aminomethyl-phenylacetic acid in (**153**) and Fmoc-4-aminomethyl-cyclohexane carboxylic acid in (**154**).*

5.7 Experimental

5.7.1 Synthesis of Fmoc-alkyne lysine-OH monomer starting from N^{α}-Boc-N^{ε}-Cbz-L-lysine (135)

Synthesis of N^{α}-*t*Boc-N^{ε}-(carbobenzyloxy)-L-lysine-*tert*-butyl ester (136)[200]

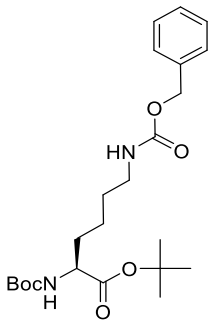

To a solution of N^{α}-Boc-N^{ε}-(carbobenzyloxy)-L-lysine (**135**) (10.00 g, 26 mmol) in dry DCM (25 mL) was added DMAP (1.96 g, 16 mmol) and EDC (10.50 g, 55 mmol). The reaction mixture was then stirred for 30 min. Dry *t*-butanol (312 mmol, 30 mL) was added to the reaction mixture and left stirring overnight at room temperature under an argon atmosphere. The reaction mixture was diluted with DCM (150 mL) and washed with H_2O (2 × 100 mL), followed by brine (2 × 100 mL). The organic layer was then dried over Na_2SO_4, filtered and concentrated *in vacuo*. Purification by column chromatography (SiO_2) eluting with 1:1 hexane:acetone afforded N^{α}-*t*Boc-N^{ε}-(carbobenzyloxy)-L-lysine-*tert*-butyl ester (**136**) (7.2 g, 64%) as a yellow oil. The pure product was directly used in the next step.

LRMS (ESI) m/z: $[M + Na]^+$ 459.

Synthesis of N$^{\alpha}$-(1,1-dimethylethoxycarbonyl)-L-lysine-tert-butyl ester (137) [200]

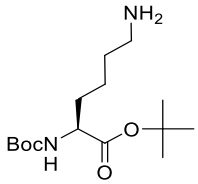

To a solution of N$^{\alpha}$-*t*Boc-N$^{\varepsilon}$-(carbobenzyloxy)-L-lysine-*tert*-butyl ester (**136**) (7.2 g, 16 mmol) in MeOH (80 mL) was added 10% palladium-activated carbon (1.70 g, 16 mmol) and stirred for 2 h under a hydrogen atmosphere. The catalyst was filtered and the solution concentrated *in vacuo* afforded N$^{\alpha}$-(1,1-dimethylethoxycarbonyl)-L-lysine-*tert*-butyl ester (**137**) (4.43 g, 92%) as a yellow oil.

LRMS (ESI) m/z: $[M + H]^+$ 303.

^{1}H NMR ($CDCl_3$, 400 MHz): δ 1.44 (s, 9H), 1.45 (s, 9H), 1.23-2.19 (m, 8H), 2.69 (t, 2H, J = 7.0 Hz), 3.88-4.30 (m, 1H), 5.02-5.08 (m, 1H).

^{13}C NMR ($CDCl_3$, 100 MHz): δ 22.7, 28.2, 28.5, 29.2, 32.9, 33.3, 42.0, 54.1, 79.8, 81.9, 155.6, 172.2.

Synthesis of N$^{\alpha}$-*t*Boc-N$^{\varepsilon}$-(pent-4-ynoyl)-L-lysine-tert-butyl ester (139)

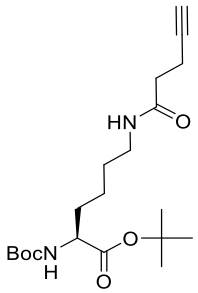

To a solution of (**138**) (1.48 g, 15 mmol) in anhydrous DMF (20 ml) was added HOAt (2.05 g, 15 mmol) followed by EDC (2.89 g, 15 mmol) at 0°C under an argon atmosphere. After stirring for 10 min, a solution of (**137**) (3.80 g, 13 mmol) in anhydrous DMF (20 mL) was added to the reaction mixture followed by DIEA (8.74 mL, 50 mmol) under a nitrogen atmosphere and left stirring overnight at

room temperature. The reaction mixture was diluted with EtOAc (500 mL) and washed with H_2O (1 × 100 mL). The organic layer was then washed with 3% brine (3 × 100 mL), followed by 1M HCl (1 × 100 mL), saturated $NaHCO_3$ (1 × 100 mL) and finally brine (3 × 100 mL). The organic layer was then dried over $MgSO_4$, filtrated and concentrated *in vacuo*. Purification by column chromatography (SiO_2) eluting with 1:1 hexane:acetone afforded N^{α}-*t*Boc-N^{ε}-(pent-4-ynoyl)-L-lysine-*tert*-butyl ester (**139**) (3.41 g, 64%) as a yellow oil.

$[\alpha]_D^{20}$ = -2.167.

HRMS (ESI-TOF) *m/z*: $[M + H]^+$ Calcd for $C_{20}H_{35}N_2O_5$ 383.2546; Found 383.2552.

^{1}H NMR ($CDCl_3$, 500 MHz): δ 1.46 (s), 1.47 (s), 1.63-1.78 (m), 1.99 (t, *J* = 2.6 Hz), 2.04 (t, *J* = 2.6 Hz) , 2.39 (t, *J* = 7.1 Hz), 2.50-2.59 (m), 3.24-3.32 (m), 3.68-3.71 (m), 4.16 (t, *J* = 6.5 Hz), 5.10 (bs), 5.83 (bs). The peaks cannot be assigned due to the presence of rotamers (see Appendix B99).

^{13}C NMR ($CDCl_3$, 125 MHz): δ 14.4, 15.0, 22.5, 25.1, 28.0, 28.4, 28.9, 29.1, 32.8, 33.4, 35.4, 39.3, 53.7, 62.3, 64.5, 69.0, 69.4, 76.8, 77.0, 77.3, 79.7, 81.92, 82.49, 83.1, 155.6, 171.0, 171.8, 171.9.

Synthesis of N^{ε}-(pent-4-ynoyl)-L-lysine (140)

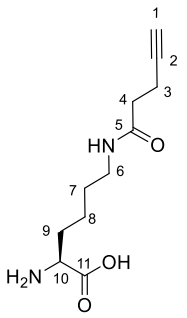

TPW (TFA:phenol:water, 92.5:5:2.5, 5 mL) was added to N^{α}-*t*Boc-N^{ε}-(pent-4-ynoyl)-L-lysine-*tert*-butyl ester (**139**) (0.50 mg, 2 mmol) and stirred for 1 h at room temperature. The reaction mixture was diluted with H_2O (20 mL) and

washed with DCM (4 × 20 mL). The aqueous layer was freeze-dried to afford N^{ε}-(pent-4-ynoyl)-L-lysine (**140**) (0.61 g, 86%) as a yellow oil.

$[\alpha]_D^{20}$ = -1.

HRMS (ESI-TOF) *m/z*: $[M + H]^+$ Calcd for $C_{11}H_{19}N_2O_3$ 227.1396; Found 227.1397.

^{1}H NMR (D_2O, 500 MHz): δ 1.41-1.55 (m, 2H, CH_2 ^{8}), 1.57-1.63 (m, 2H, CH_2 ^{7}), 1.90-2.04 (m, 2H, CH_2 ^{9}), 2.39 (t, 1H, *J* = 2.6 Hz, C≡C**H** ^{1}), 2.43-2.46 (m, 2H, CH_2 ^{4}), 2.49-2.53 (m, 2H, CH_2 ^{3}), 3.25 (t, 2H, J = 6.8 Hz, CH_2 ^{6}), 4.05 (t, 1H, J = 6.3 Hz, CH ^{10}).

^{13}C NMR (D_2O, 125 MHz): δ 14.6 (CH_2, 1C ^{3}), 21.5 (CH_2, 1C ^{8}), 27.9 (CH_2, 1C ^{7}), 29.4 (CH_2, 1C ^{9}), 34.5 (CH_2, 1C ^{4}), 38.8 (CH_2, 1C ^{6}), 53.0 (CH, 1C ^{10}), 70.2 (C≡**C**H, 1C ^{1}), 83.3 (**C**≡CH, 1C ^{2}), 172.4 (CO, 1C ^{5}), 174.6 (CO, 1C ^{11}).

Synthesis of N^{α}-Fmoc-N^{ε}-(pent-4-ynoyl)-L-lysine (132)

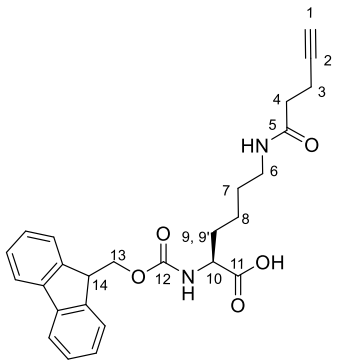

To a solution of N^{ε}-(pent-4-ynoyl)-L-lysine (**140**) (0.300 g, 1 mmol) in dioxane:H_2O (1:1, 10 mL) was added a solution of $NaHCO_3$ in H_2O until pH~8 at 0°C. After stirring for 10 min, Fmoc-OSu (0.42 g, 1 mmol) was added to the reaction mixture and left stirring at 0°C for 1 h followed by warming to room temperature for 3 h. The mixture was then concentrated *in vacuo*. The residue was diluted with H_2O (50 mL) and extracted with 1:1 EtOAc:Et_2O (1 × 100 mL). The aqueous layer was acidified to pH~2 and extracted with EtOAc (3 × 100 mL) and

n-butanol (4 × 50 mL). The organic layer was then dried over $MgSO_4$, filtrated and concentrated *in vacuo*. Purification by semi-preparative HPLC afforded N^{α}-Fmoc-N^{ε}-(pent-4-ynoyl)-L-lysine (**132**) (0.270 mg, 46%) as a pale yellow solid.

$[\alpha]_D^{20}$ = -1.33.

HRMS (ESI-TOF) *m/z*: $[M + H]^+$ Calcd for $C_{26}H_{29}N_2O_5$ 449.2076; Found 449.2074.

^{1}H NMR (DMSO, 500 MHz): δ 1.30-1.42 (m, 4H, CH_2 $^{7-8}$), 1.56-1.63 (m, 1H ^{9}), 1.66-1.74 (m, 1H $^{9'}$), 2.24 (t, 2H, CH_2 ^{4}), 2.33-2.36 (m, 2H, CH_2 ^{3}), 2.73 (t, 1H, *J* = 2.6 Hz, C≡CH ^{1}), 3.01-3.05 (m, 2H, CH_2 ^{6}), 3.88-3.93 (m, 1H, CH ^{10}), 4.21-4.29 (m, 3H $^{13-14}$), 7.33 (t, 2H, *J* = 7.5 Hz, Ar), 7.42 (t, 2H, *J* = 7.5 Hz, Ar), 7.61 (d, 1H, *J* = 8.1 Hz, NH), 7.73 (d, 2H, *J* = 7.5 Hz, Ar-H), 7.86 (t, 1H, J = 5.5 Hz, NH), 7.89 (d, 2H, *J* = 7.5 Hz, Ar), 12.54 (bs, 1H, OH).

^{13}C NMR (DMSO, 125 MHz): δ 14.3 (CH_2, 1C ^{3}), 23.0 (CH_2, 1C ^{8}), 28.6 (CH_2, 1C ^{7}), 30.4 (CH_2, 1C ^{9}), 34.2 (CH_2, 1C ^{4}), 38.2 (CH_2, 1C ^{6}), 46.6 (CH, 1C ^{14}), 53.7 (CH, 1C ^{10}), 65.6 (CH_2, 1C ^{13}), 71.2 (C≡**C**H, 1C ^{1}), 83.8 (**C**≡CH, 1C ^{2}), 120.1 (Ar-CH, 2C), 125.3 (Ar-CH, 2C), 127.0 (Ar-CH, 2C), 127.6 (Ar-CH, 2C), 140.7 (Ar-C, 2C), 143.8 (Ar-C, 2C), 156.1 (CO, 1C ^{12}), 170.0 (CO, 1C ^{5}), 174 (CO, 1C ^{11}).

5.7.2 Synthesis of Fmoc-alkyne lysine-OH monomer using NHS coupling reaction

Synthesis of 4-pentynoic acid succinimidyl ester (141) [201]

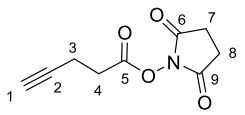

To a solution of 4-pentynoic acid (**138**) (2.00 g, 20 mmol) and NHS (2.36 g, 20 mmol) in dry EtOAc:dioxane (1:1, 120 mL) was added DCC (4.20 g, 20 mmo) at 0°C. The reaction mixture was stirred for 5 h at room temperature. The N,N'-dicyclohexylurea (DCU) was filtered off and the solution concentrated

in vacuo to a small volume. The residue was dissolved in EtOAc (400 mL) and washed with 5% $NaHCO_3$ (2 × 100 mL), followed by H_2O (1 × 100 mL) and brine (1 × 100 mL). The organic layer was then dried over $MgSO_4$, filtrated and concentrated *in vacuo*. The residue was dissolved in EtOAc:hexane (1:1, 100 mL), sonicated and filtrated to remove the residual DCU. The filtrate was then concentrated *in vacuo* afforded (**141**) (3.10 g, 78%) as a white solid.

^{1}H NMR ($CDCl_3$, 400 MHz): δ 2.06 (t, 1H, *J* = 2.7 Hz, C≡CH ^{1}), 2.60-2.64 (m, 2H, CH_2 ^{3}), 2.84 (s, 4H, CH_2 $^{7\text{-}8}$), 2.87-2.90 (m, 2H, CH_2 ^{4}).

^{13}C NMR ($CDCl_3$, 100 MHz): δ 14.3 (CH_2, 1C ^{3}), 25.7 (CH_2, 2C $^{7\text{-}8}$), 30.5 (CH_2, 1C ^{4}), 70.2 (C≡CH, 1C ^{1}), 81.0 (**C**≡CH, 1C ^{2}), 167.2 (CO, 1C ^{5}), 169.1 (CO, 2C ^{6,9}).

Synthesis of N$^{\alpha}$-Fmoc-N$^{\varepsilon}$-(pent-4-ynoyl)-L-lysine (132) [201]

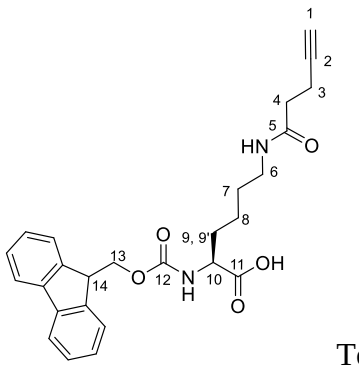

To a stirred solution (**142**) (4.29 g, 12 mmol) and DIPEA (1.65 g, 13 mmol, 2.23 mL) in anhydrous DMF (60 mL) was added a solution of (**141**) (2.27 g, 12 mmol) in anhydrous DMF (25 mL) dropwise over 15 min at room temperature. The pH of the mixture was adjusted to ~2 by addition of DIPEA. The reaction mixture was stirred for 2 h at room temperature. The mixture was concentrated *in vacuo* to a small volume. The residue was diluted with EtOAc (60 mL) and washed with a concentrated citric acid (2 × 30 mL), followed by H_2O (1 × 30 mL) and brine (1 × 30 mL). The organic layer was then dried over $MgSO_4$,

filtered and concentrated *in vacuo*. The product was dissolved in dry dioxane and freeze-dried to afford (**132**) (3.70 g, 71%) as a pale yellow solid. Compound (**132**) was used directly for solid phase peptide synthesis without further purification.

See 5.7.1.5 for HRMS, ^{1}H NMR and ^{13}C NMR.

5.7.3 Fmoc-solid phase peptide synthesis

Peptides (**133-134**) were synthesised manually using Fmoc-Phe-Wang resin (**143**) at 0.27 mmol/g scale using a glass vial flitted with a sintered frit. Before starting the synthesis, a small amount of resin (11.8 mg) was added to a solution of 20% piperidine in DMF (10 mL) in order to quantify the first residue onto the resin using the Fmoc UV titration method. The UV absorbance of the cleavage solution was measured at 302 nm and the loading was calculated (0.54 mmol/g) according to the following equation:

$$L = \frac{V * Abs_{302nm} * 10}{\varepsilon * M} \qquad \text{Equation (16)}$$

Where

L = Resin loading (mmol/g)

V = Volume of the cleavage solution (mL)

Abs_{302nm} = Absorbance of the cleavage solution at 302 nm

ε = Extinction coefficient = 7.8

M = Weight of the resin sample

The synthesis was performed using the following protocols:

(i) Cleavage of the Fmoc group in N-terminal: Fmoc-Phe-Wang resin (**143**) (1.00 g) was swollen in DCM for 1 h followed by washing with DMF (3× 7 mL, 2 min). Fmoc-Phe was deprotected twice using freshly prepared 20% piperidine in DMF for 15 min each. The resin was then washed with DMF (5× 7 mL, 2 min).

(ii) Reduction of resin loading: The resin was treated with acetic anhydride (0.27 mmol, 25 µL, 0.5 equiv. relative to the resin loading calculated from equating) and DIEA (0.54 mmol, 100 µL) in DMF (7 mL) for 30 min. The resin was then washed with DMF (5× 7 mL, 2 min) and once with anhydrous DMF.

(iii) Coupling of Fmoc-Gly-OH: The coupling solution was prepared in a small vial by adding DIEA (1 mL) and HATU (0.40 g, 1.05 mmol, 3.9 equiv. relative to the minimised resin loading) to a solution of Fmoc-Gly-OH (0.32 g, 1.08 mmol, 4.0 equiv.) in DMF (7ml). The mixture was shaken for 10 min and added quickly to the resin. After shaking for 2 h, the resin was washed with DMF (4× 7 mL, 2 min), followed by DCM (3× 7 mL, 2 min).

(iv) Capping unreacted amino group on the resin: The resin was treated with a freshly prepared mixture of Ac_2O:Pyridine:DMF (5:5:95) (7 mL) twice for 10 min each in order to cap unreacted amino group on the resin. The resin was then washed with DMF (5× 7 mL, 2 min) and DCM (3× 7 mL, 2 min).

(v) Repeat the cycle: The Fmoc-deprotection, coupling and capping steps were repeated to afford the desired peptide. The coupling of Fmoc-alkyne modified lysine-OH (**132**) was performed using 2.5 equivalents of (**132**) and 2.4 equivalents of HATU in the presence of DIEA (1mL). The Fmoc was then removed from the final

peptide product followed by washing with DMF (4× 7 mL, 2 min) and DCM (4× 7 mL, 2 min).

(vi) Cleavage of the resin: To the dried resin was added a solution of TFA:TES (90:10, 10 mL) and the mixture was shaken for 3 h at room temperature. The acid solution was transferred into a 50 ml centrifuge tube, cooled to 0°C and precipitated using Et_2O. The mixture was centrifuged for 10 min at 4000 rpm, and the supernatant discarded. The precipitate was washed twice with Et_2O and dried at room temperature. The crude product was used directly for the next step.

Peptides (**133-134**) were characterised by LRMS (ESI) (see Appedix B120-121).

(**133**): LRMS (ESI) m/z: $[M + H]^+$ 545.

(**134**): LRMS (ESI) m/z: $[M + Na]^+$ 889.

5.7.4 Synthesis of sugar-functionalised peptides (27-28)

Synthesis of (151)

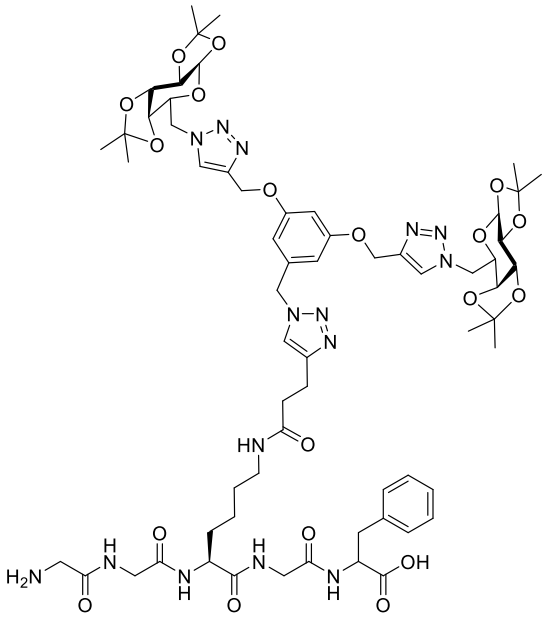

To a solution of (**133**) (0.075 g, 0.14 mmol) and (**35**) (0.224 g, 0.28 mmol) in THF:H_2O:DMSO (3:1:2, 2.7 mL) was added an aqueous solution of $CuSO_4$ (0.5 M, 0.54 mL) followed by solid sodium ascorbate

(0.055 g, 0.28 mmol). The reaction mixture was stirred overnight at room temperature. The crude residue was diluted in DMSO/H_2O mixture and purified by semi-preparative HPLC using H_2O and MeCN. The product was freeze-dried to afford (**151**) (0.043 g, 23%) as a white powder.

LRMS (ESI) m/z: $[M + H]^+$ 1356.

Synthesis of (27)

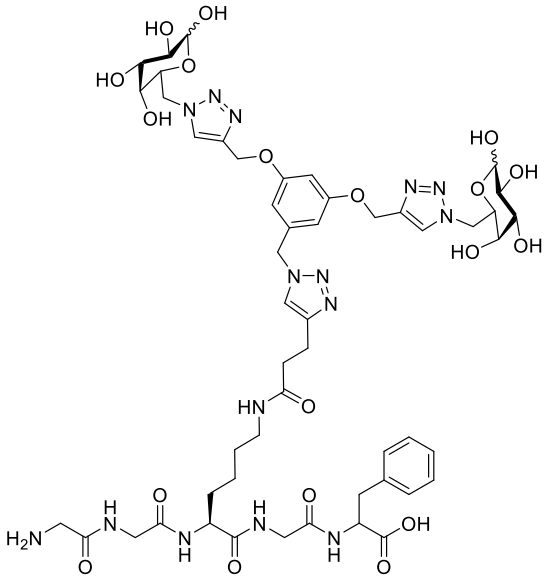

To a mixture of TFA:H_2O (1:1, 10 mL) was added (**151**) (0.040 g, 0.03 mmol) under a nitrogen atmosphere. The reaction mixture was heated to reflux for 4 h. The mixture was then cooled to room temperature followed by concentration *in vacuo*. The crude residue was diluted in H_2O and purified by semi-preparative HPLC using H_2O and MeCN. The product was freeze-dried to afford (**27**) (0.017 g, 48%) as a white powder.

LRMS (ESI) m/z: $[M + Na]^+$ 1218.

Synthesis of (152)

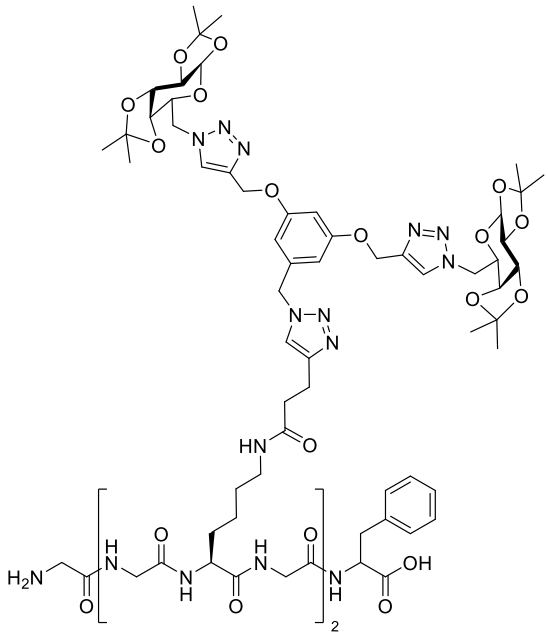

To a solution of (**134**) (0.096 g, 0.11 mmol) and (**35**) (0.36 g, 0.44 mmol) in THF:H_2O:DMSO (3:1:2, 2.4 mL) was added an aqueous solution of $CuSO_4$ (0.5 M, 0.24 mL) followed by solid sodium ascorbate (0.044 g, 0.22 mmol). The reaction mixture was stirred overnight at room temperature. The crude residue was diluted in DMSO-H_2O mixture and purified by semi-preparative HPLC using H_2O and MeCN. The product was freeze-dried to afford (**152**) (0.022 g, 8%) as a white powder.

MALDI-TOF *m/z*: $[M + Na]^+$ 2513.

Synthesis of (28)

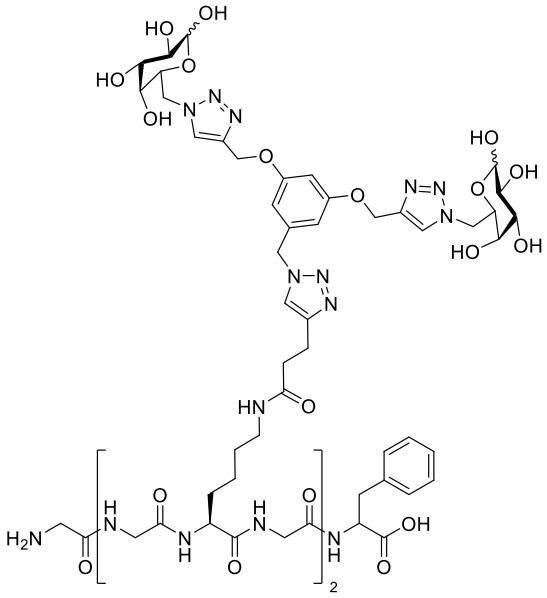

To a mixture of TFA:H_2O (1:1, 10 mL) was added (**152**) (0.022 g, 0.010 mmol) under a nitrogen atmosphere. The reaction mixture was heated to reflux for 4 h. The mixture was then cooled to room temperature followed by concentrateion *in vacuo*. The crude residue was diluted in H_2O and purified by semi-preparative HPLC using H_2O and MeCN. The product was freeze-dried to afford (**28**) (0.008 g, 37%) as a white powder.

6 CONCLUSION AND FUTURE WORK

The ability to prepare silver nanoparticles in a size- and shape-controlled fashion is a vital component for their use in optoelectronic diagnostic and nanomedical devices and assemblies. At present, the development of preparative methods for the synthesis of silver nanoparticles has mainly focused on a select few reactions that require elevated temperatures or strong reducing agents.

This thesis identifies key structural parameters that control the synthesis of AgNPs by a template-directed approach where the size, shape and colloidal stability are inherently tunable. This tunability arises from the use of novel sugar triazol ligands that template the reduction of silver nuclei using Tollens' reagent. Underpinning this work, we present kinetic and spectroscopic evidence which correlates the Ag(I) binding affinity of the triazole ligands with the size and shape of AgNPs.

The synthetic methodology outlined in this thesis could facilitate the growth of their wider utilisation of silver nanoparticles in diagnostics and medical nanotechnology by providing facile and simple methodology for the synthesis.

Future directions of this research are:

1) To investigate the potential of these AgNPs to be interfaced with biomolecules such as DNA for biosensing applications.
2) To investigate the synthesis of AgNPs using triazole ligands functionalised with different sugars such as lactose, fructose and maltose.

3) To synthesise other ligands with a triazine core using the click of 2,4,6-tris(prop-2-ynyloxy)-1,3,5-triazine with sugar azides (Scheme 6-1).

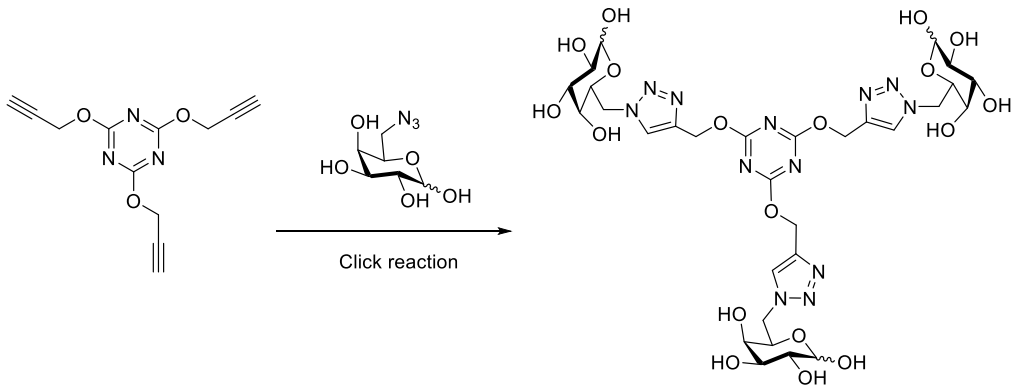

Scheme 6-1: *Proposed synthesis of sugar triazole ligand with triazine core.*

4) To use triazole ligands for the synthesis of other metal nanoparticles such as gold and copper NPs.

APPENDIX

The Appendix contains:

- ES-MS analysis of ligands (**22**, **23** and **39**) with $AgNO_3$ (Appendix A).
- HPLC, Mass and NMR characterisation data (Appendix B).
- ^{1}H NMR titration data (Appendix C)

REFERENCES

1. The Royal Society and The Royal Academy of Engineering. *Nanoscience and Nanotechnologies: Opportunities and Uncertainties;* The Royal Society: London, 2004.

2. Rosi, N. L.; Mirkin, C. A., Nanostructures in Biodiagnostics. *Chemical Reviews* **2005,** *105* (4), 1547-1562.

3. Tiwari, P.; Vig, K.; Dennis, V.; Singh, S., Functionalized Gold Nanoparticles and Their Biomedical Applications. *Nanomaterials* **2011,** *1* (1), 31-63.

4. Howes, P. D.; Chandrawati, R.; Stevens, M. M., Colloidal nanoparticles as advanced biological sensors. *Science* **2014,** *346* (6205).

5. Seeman, N. C., Nucleic acid junctions and lattices. *Journal of Theoretical Biology* **1982,** *99* (2), 237-247.

6. Fu, T. J.; Seeman, N. C., DNA double-crossover molecules. *Biochemistry* **1993,** *32* (13), 3211-3220.

7. LaBean, T. H.; Yan, H.; Kopatsch, J.; Liu, F.; Winfree, E.; Reif, J. H.; Seeman, N. C., Construction, Analysis, Ligation, and Self-Assembly of DNA Triple Crossover Complexes. *Journal of the American Chemical Society* **2000,** *122* (9), 1848-1860.

8. Lin, C.; Liu, Y.; Rinker, S.; Yan, H., DNA Tile Based Self-Assembly: Building Complex Nanoarchitectures. *ChemPhysChem* **2006,** *7* (8), 1641-1647.

9. Chen, J.; Seeman, N. C., Synthesis from DNA of a molecule with the connectivity of a cube. *Nature* **1991,** *350* (6319), 631-633.

10. Shih, W. M.; Quispe, J. D.; Joyce, G. F., A 1.7-kilobase single-stranded DNA that folds into a nanoscale octahedron. *Nature* **2004,** *427* (6975), 618-621.

11. Goodman, R. P.; Schaap, I. A. T.; Tardin, C. F.; Erben, C. M.; Berry, R. M.; Schmidt, C. F.; Turberfield, A. J., Rapid Chiral Assembly of Rigid DNA Building Blocks for Molecular Nanofabrication. *Science* **2005,** *310* (5754), 1661-1665.

12. Rothemund, P. W. K., Folding DNA to create nanoscale shapes and patterns. *Nature* **2006,** *440* (7082), 297-302.

13. He, Y.; Ye, T.; Su, M.; Zhang, C.; Ribbe, A. E.; Jiang, W.; Mao, C., Hierarchical self-assembly of DNA into symmetric supramolecular polyhedra. *Nature* **2008,** *452* (7184), 198-201.

14. Douglas, S. M.; Dietz, H.; Liedl, T.; Hogberg, B.; Graf, F.; Shih, W. M., Self-assembly of DNA into nanoscale three-dimensional shapes. *Nature* **2009,** *459* (7245), 414-418.

15. Lin, C.; Liu, Y.; Yan, H., Designer DNA Nanoarchitectures. *Biochemistry* **2009,** *48* (8), 1663-1674.

16. Seeman, N. C., DNA in a material world. *Nature* **2003,** *421* (6921), 427-431.

17. Niemeyer, C. M.; Simon, U., DNA-Based Assembly of Metal Nanoparticles. *European Journal of Inorganic Chemistry* **2005,** *2005* (18), 3641-3655.

18. Sharma, J.; Chhabra, R.; Cheng, A.; Brownell, J.; Liu, Y.; Yan, H., Control of Self-Assembly of DNA Tubules Through Integration of Gold Nanoparticles. *Science* **2009,** *323* (5910), 112-116.

19. Eustis, S.; El-Sayed, M. A., Why gold nanoparticles are more precious than pretty gold: Noble metal surface plasmon resonance and its enhancement of the radiative and nonradiative properties of nanocrystals of different shapes. *Chemical Society Reviews* **2006,** *35* (3), 209-217.

20. Faraday, M., The Bakerian Lecture: Experimental Relations of Gold (and Other Metals) to Light. *Philosophical Transactions of the Royal Society of London* **1857,** *147*, 145-181.

21. nanoComposix. Silver Nanoparticles: Optical Properties. http://nanocomposix.com/pages/silver-nanoparticles-optical-properties (accessed Jun 5, 2015)

22. Lal, S.; Link, S.; Halas, N. J., Nano-optics from sensing to waveguiding. *Nature Photonics* **2007,** *1* (11), 641-648.

23. Xia, Y.; Campbell, D. J., Plasmons: Why Should We Care? *Journal of Chemical Education* **2007,** *84* (1), 91.

24. Rycenga, M.; Cobley, C. M.; Zeng, J.; Li, W.; Moran, C. H.; Zhang, Q.; Qin, D.; Xia, Y., Controlling the Synthesis and Assembly of Silver Nanostructures for Plasmonic Applications. *Chemical Reviews* **2011,** *111* (6), 3669-3712.

25. Haes, A.; Van Duyne, R., A unified view of propagating and localized surface plasmon resonance biosensors. *Analytical and Bioanalytical Chemistry* **2004,** *379* (7-8), 920-930.

26. Takahara, J.; Yamagishi, S.; Taki, H.; Morimoto, A.; Kobayashi, T., Guiding of a one-dimensional optical beam with nanometer diameter. *Optics Letters* **1997,** *22* (7), 475-477.

27. Xia, Y.; Halas, N. J., Shape-Controlled Synthesis and Surface Plasmonic Properties of Metallic Nanostructures. *MRS Bulletin* **2005,** *30* (05), 338-348.

28. Wiley, B. J.; Im, S. H.; Li, Z.-Y.; McLellan, J.; Siekkinen, A.; Xia, Y., Maneuvering the Surface Plasmon Resonance of Silver Nanostructures through

Shape-Controlled Synthesis. *The Journal of Physical Chemistry B* **2006,** *110* (32), 15666-15675.

29. Wiley, B. J.; Chen, Y.; McLellan, J. M.; Xiong, Y.; Li, Z.-Y.; Ginger, D.; Xia, Y., Synthesis and Optical Properties of Silver Nanobars and Nanorice. *Nano Letters* **2007,** *7* (4), 1032-1036.

30. Lu, X.; Rycenga, M.; Skrabalak, S. E.; Wiley, B.; Xia, Y., Chemical Synthesis of Novel Plasmonic Nanoparticles. *Annual Review of Physical Chemistry* **2009,** *60* (1), 167-192.

31. Ru, E. L.; Etchegoin, P. *Principles of Surface Enhanced Raman Spectroscopy;* Elsevier: Oxford, U.K., 2009.

32. West, P. R.; Ishii, S.; Naik, G. V.; Emani, N. K.; Shalaev, V. M.; Boltasseva, A., Searching for better plasmonic materials. *Laser & Photonics Reviews* **2010,** *4* (6), 795-808.

33. Edelstein, A. S.; Cammarata, R. C. *Nanomaterials: Synthesis, Properties and Applications;* Institute of Physics Publishing: Bristol, 1998.

34. Abid, J. P.; Wark, A. W.; Brevet, P. F.; Girault, H. H., Preparation of silver nanoparticles in solution from a silver salt by laser irradiation. *Chemical Communications* **2002,** (7), 792-793.

35. Kim, S.-E.; Han, Y.-H.; Lee, B. c.; Lee, J.-C., One-pot fabrication of various silver nanostructures on substrates using electron beam irradiation. *Nanotechnology* **2010,** *21* (7), 075302.

36. Burshtain, D.; Zeiri, L.; Efrima, S., Control of Colloid Growth and Size Distribution by AdsorptionSilver Nanoparticles and Adsorbed Anisate. *Langmuir* **1999,** *15* (9), 3050-3055.

37. Henglein, A.; Giersig, M., Formation of Colloidal Silver Nanoparticles: Capping Action of Citrate. *The Journal of Physical Chemistry B* **1999,** *103* (44), 9533-9539.

38. Shirtcliffe, N.; Nickel, U.; Schneider, S., Reproducible Preparation of Silver Sols with Small Particle Size Using Borohydride Reduction: For Use as Nuclei for Preparation of Larger Particles. *Journal of Colloid and Interface Science* **1999,** *211* (1), 122-129.

39. Ito, T.; Okazaki, S., Pushing the limits of lithography. *Nature* **2000,** *406* (6799), 1027-1031.

40. Stewart, M. E.; Anderton, C. R.; Thompson, L. B.; Maria, J.; Gray, S. K.; Rogers, J. A.; Nuzzo, R. G., Nanostructured Plasmonic Sensors. *Chemical Reviews* **2008,** *108* (2), 494-521.

41. Arvizo, R. R.; Bhattacharyya, S.; Kudgus, R.; Giri, K.; Bhattacharya, R.; Mukherjee, P., Intrinsic Therapeutic Applications of Noble Metal Nanoparticles: Past, Present and Future. *Chemical Society Reviews* **2012,** *41* (7), 2943-2970.

42. Polte, J. r.; Tuaev, X.; Wuithschick, M.; Fischer, A.; Thuenemann, A. F.; Rademann, K.; Kraehnert, R.; Emmerling, F., Formation Mechanism of Colloidal Silver Nanoparticles: Analogies and Differences to the Growth of Gold Nanoparticles. *ACS Nano* **2012,** *6* (7), 5791-5802.

43. Schneider, S.; Halbig, P.; Grau, H.; Nickel, U., REPRODUCIBLE PREPARATION OF SILVER SOLS WITH UNIFORM PARTICLE SIZE FOR APPLICATION IN SURFACE-ENHANCED RAMAN SPECTROSCOPY. *Photochemistry and Photobiology* **1994,** *60* (6), 605-610.

44. Agnihotri, S.; Mukherji, S.; Mukherji, S., Size-controlled silver nanoparticles synthesized over the range 5-100 nm using the same protocol and their antibacterial efficacy. *RSC Advances* **2014,** *4* (8), 3974-3983.

45. Pillai, Z. S.; Kamat, P. V., What Factors Control the Size and Shape of Silver Nanoparticles in the Citrate Ion Reduction Method? *The Journal of Physical Chemistry B* **2004,** *108* (3), 945-951.

46. Caswell, K. K.; Bender, C. M.; Murphy, C. J., Seedless, Surfactantless Wet Chemical Synthesis of Silver Nanowires. *Nano Letters* **2003,** *3* (5), 667-669.

47. Dong, X.; Ji, X.; Wu, H.; Zhao, L.; Li, J.; Yang, W., Shape Control of Silver Nanoparticles by Stepwise Citrate Reduction. *The Journal of Physical Chemistry C* **2009,** *113* (16), 6573-6576.

48. Wiley, B.; Sun, Y.; Xia, Y., Synthesis of Silver Nanostructures with Controlled Shapes and Properties. *Accounts of Chemical Research* **2007,** *40* (10), 1067-1076.

49. Xia, Y.; Xiong, Y.; Lim, B.; Skrabalak, S. E., Shape-Controlled Synthesis of Metal Nanocrystals: Simple Chemistry Meets Complex Physics? *Angewandte Chemie International Edition* **2009,** *48* (1), 60-103.

50. Skrabalak, S. E.; Wiley, B. J.; Kim, M.; Formo, E. V.; Xia, Y., On the Polyol Synthesis of Silver Nanostructures: Glycolaldehyde as a Reducing Agent. *Nano Letters* **2008,** *8* (7), 2077-2081.

51. Wiley, B.; Herricks, T.; Sun, Y.; Xia, Y., Polyol Synthesis of Silver Nanoparticles: Use of Chloride and Oxygen to Promote the Formation of Single-Crystal, Truncated Cubes and Tetrahedrons. *Nano Letters* **2004,** *4* (9), 1733-1739.

52. Siekkinen, A. R.; McLellan, J. M.; Chen, J.; Xia, Y., Rapid synthesis of small silver nanocubes by mediating polyol reduction with a trace amount of sodium sulfide or sodium hydrosulfide. *Chemical Physics Letters* **2006,** *432* (4-6), 491-496.

53. Sun, Y.; Mayers, B.; Herricks, T.; Xia, Y., Polyol Synthesis of Uniform Silver Nanowires: A Plausible Growth Mechanism and the Supporting Evidence. *Nano Letters* **2003,** *3* (7), 955-960.

54. Wiley, B. J.; Xiong, Y.; Li, Z.-Y.; Yin, Y.; Xia, Y., Right Bipyramids of Silver: A New Shape Derived from Single Twinned Seeds. *Nano Letters* **2006,** *6* (4), 765-768.

55. Cobley, C. M.; Rycenga, M.; Zhou, F.; Li, Z.-Y.; Xia, Y., Etching and Growth: An Intertwined Pathway to Silver Nanocrystals with Exotic Shapes. *Angewandte Chemie International Edition* **2009,** *48* (26), 4824-4827.

56. Wiley, B.; Sun, Y.; Xia, Y., Polyol Synthesis of Silver Nanostructures: Control of Product Morphology with Fe(II) or Fe(III) Species. *Langmuir* **2005,** *21* (18), 8077-8080.

57. Xiong, Y.; Siekkinen, A. R.; Wang, J.; Yin, Y.; Kim, M. J.; Xia, Y., Synthesis of silver nanoplates at high yields by slowing down the polyol reduction of silver nitrate with polyacrylamide. *Journal of Materials Chemistry* **2007,** *17* (25), 2600-2602.

58. Wennemers, H., Peptides as asymmetric catalysts and templates for the controlled formation of Ag nanoparticles. *Journal of Peptide Science* **2012,** *18* (7), 437-441.

59. Upert, G.; Bouillère, F.; Wennemers, H., Oligoprolines as Scaffolds for the Formation of Silver Nanoparticles in Defined Sizes: Correlating Molecular and

Nanoscopic Dimensions. *Angewandte Chemie International Edition* **2012,** *51* (17), 4231-4234.

60. Liebig, J., Ueber Versilberung und Vergoldung von Glas. *Justus Liebigs Annalen der Chemie* **1856,** *98* (1), 132-139.

61. Le, A.-T.; Huy, P. T.; Tam, P. D.; Huy, T. Q.; Cam, P. D.; Kudrinskiy, A. A.; Krutyakov, Y. A., Green synthesis of finely-dispersed highly bactericidal silver nanoparticles via modified Tollens technique. *Current Applied Physics* **2010,** *10* (3), 910-916.

62. Kvitek, L.; Vanickova, M.; Panacek, A.; Soukupova, J.; Dittrich, M.; Valentova, E.; Prucek, R.; Bancirova, M.; Milde, D.; Zboril, R., Initial Study on the Toxicity of Silver Nanoparticles (NPs) against Paramecium caudatum. *The Journal of Physical Chemistry C* **2009,** *113* (11), 4296-4300.

63. Soukupova, J.; Kvitek, L.; Panacek, A.; Nevecna, T. J.; Zboril, R., Comprehensive study on surfactant role on silver nanoparticles (NPs) prepared via modified Tollens process. *Materials Chemistry and Physics* **2008,** *111* (1), 77-81.

64. Kvitek, L.; Panacek, A.; Soukupova, J.; Kolar, M.; Vecerova, R.; Prucek, R.; Holecova, M.; Zboril, R., Effect of Surfactants and Polymers on Stability and Antibacterial Activity of Silver Nanoparticles (NPs). *The Journal of Physical Chemistry C* **2008,** *112* (15), 5825-5834.

65. Panacek, A.; Kvitek, L.; Prucek, R.; Kolar, M.; Vecerova, R.; Pizurova, N.; Sharma, V. K.; Nevecna, T. J.; Zboril, R., Silver Colloid Nanoparticles: Synthesis, Characterization, and Their Antibacterial Activity. *The Journal of Physical Chemistry B* **2006,** *110* (33), 16248-16253.

66. Kvitek, L.; Prucek, R.; Panacek, A.; Novotny, R.; Hrbac, J.; Zboril, R., The influence of complexing agent concentration on particle size in the process of SERS active silver colloid synthesis. *Journal of Materials Chemistry* **2005,** *15* (10), 1099-1105.

67. Yin, Y.; Li, Z.-Y.; Zhong, Z.; Gates, B.; Xia, Y.; Venkateswaran, S., Synthesis and characterization of stable aqueous dispersions of silver nanoparticles through the Tollens process. *Journal of Materials Chemistry* **2002,** *12* (3), 522-527.

68. Berg, J. M.; Tymoczko, J. L.; Stryer, L. *Biochemistry*, 6th ed.; W. H. Freeman and company: New York, 2006.

69. Kammerlander, N. *Metallized DNA: Synthesis, Analysis and Properties*; Diplomica Verlag: Hamburg, 2009.

70. Blackburn, R. S.; Harvey, A., Green Chemistry Methods in Sulfur Dyeing: Application of Various Reducing d-Sugars and Analysis of the Importance of Optimum Redox Potential. *Environmental Science & Technology* **2004,** *38* (14), 4034-4039.

71. Becerril, H. A.; Woolley, A. T., DNA-templated nanofabrication. *Chemical Society Reviews* **2009,** *38* (2), 329-337.

72. Blackburn, G. M.; Gait, M. G.; Loakes, D.; Williams, D. M. *Nucleic Acids in Chemistry and Biology*, 3rd ed.; The Royal Society of Chemistry: Cambridge, 2006.

73. Tian, Y.; He, Y.; Ribbe, A. E.; Mao, C., Preparation of branched structures with long DNA duplex arms. *Organic & Biomolecular Chemistry* **2006,** *4* (18), 3404-3405.

74. Zhang, J.; Liu, Y.; Ke, Y.; Yan, H., Periodic Square-Like Gold Nanoparticle Arrays Templated by Self-Assembled 2D DNA Nanogrids on a Surface. *Nano Letters* **2006,** *6* (2), 248-251.

75. Berti, L.; Burley, G. A., Nucleic acid and nucleotide-mediated synthesis of inorganic nanoparticles. *Nature Nanotechnology* **2008,** *3* (2), 81-87.

76. Hinds, S.; Taft, B. J.; Levina, L.; Sukhovatkin, V.; Dooley, C. J.; Roy, M. D.; MacNeil, D. D.; Sargent, E. H.; Kelley, S. O., Nucleotide-Directed Growth of Semiconductor Nanocrystals. *Journal of the American Chemical Society* **2006,** *128* (1), 64-65.

77. Braun, E.; Eichen, Y.; Sivan, U.; Ben-Yoseph, G., DNA-templated assembly and electrode attachment of a conducting silver wire. *Nature* **1998,** *391* (6669), 775-778.

78. Mertig, M.; Colombi Ciacchi, L.; Seidel, R.; Pompe, W.; De Vita, A., DNA as a Selective Metallization Template. *Nano Letters* **2002,** *2* (8), 841-844.

79. Richter, J.; Seidel, R.; Kirsch, R.; Mertig, M.; Pompe, W.; Plaschke, J.; Schackert, H. K., Nanoscale Palladium Metallization of DNA. *Advanced Materials* **2000,** *12* (7), 507-510.

80. Monson, C. F.; Woolley, A. T., DNA-Templated Construction of Copper Nanowires. *Nano Letters* **2003,** *3* (3), 359-363.

81. Seidel, R.; Colombi Ciacchi, L.; Weigel, M.; Pompe, W.; Mertig, M., Synthesis of Platinum Cluster Chains on DNA Templates: Conditions for a Template-Controlled Cluster Growth. *The Journal of Physical Chemistry B* **2004,** *108* (30), 10801-10811.

82. Burley, G. A.; Gierlich, J.; Mofid, M. R.; Nir, H.; Tal, S.; Eichen, Y.; Carell, T., Directed DNA Metallization. *Journal of the American Chemical Society* **2006,** *128* (5), 1398-1399.

83. Fischler, M.; Simon, U.; Nir, H.; Eichen, Y.; Burley, G. A.; Gierlich, J.; Gramlich, P. M. E.; Carell, T., Formation of Bimetallic Ag–Au Nanowires by Metallization of Artificial DNA Duplexes. *Small* **2007,** *3* (6), 1049-1055.

84. Gierlich, J.; Burley, G. A.; Gramlich, P. M. E.; Hammond, D. M.; Carell, T., Click Chemistry as a Reliable Method for the High-Density Postsynthetic Functionalization of Alkyne-Modified DNA. *Organic Letters* **2006,** *8* (17), 3639-3642.

85. Rostovtsev, V. V.; Green, L. G.; Fokin, V. V.; Sharpless, K. B., A Stepwise Huisgen Cycloaddition Process: Copper(I)-Catalyzed Regioselective "Ligation" of Azides and Terminal Alkynes. *Angewandte Chemie International Edition* **2002,** *41* (14), 2596-2599.

86. Chan, T. R.; Hilgraf, R.; Sharpless, K. B.; Fokin, V. V., Polytriazoles as Copper(I)-Stabilizing Ligands in Catalysis. *Organic Letters* **2004,** *6* (17), 2853-2855.

87. Dondi, R.; Su, W.; Griffith, G. A.; Clark, G.; Burley, G. A., Highly Size- and Shape-Controlled Synthesis of Silver Nanoparticles via a Templated Tollens Reaction. *Small* **2012,** *8* (5), 770-776.

88. Wu, P.; Feldman, A. K.; Nugent, A. K.; Hawker, C. J.; Scheel, A.; Voit, B.; Pyun, J.; Fréchet, J. M. J.; Sharpless, K. B.; Fokin, V. V., Efficiency and Fidelity in a Click-Chemistry Route to Triazole Dendrimers by the Copper(I)-Catalyzed Ligation of Azides and Alkynes. *Angewandte Chemie International Edition* **2004,** *43* (30), 3928-3932.

89. Benet, W. E.; Lewis, G. S.; Yang, L. Z.; Hughes, P. D. E., The mechanism of the reaction of the Tollens reagent. *Journal of Chemical Research* **2011,** *35* (12), 675-677.

90. Sharma, V. K.; Yngard, R. A.; Lin, Y., Silver nanoparticles: Green synthesis and their antimicrobial activities. *Advances in Colloid and Interface Science* **2009,** *145* (1-2), 83-96.

91. Mirkin, C. A.; Letsinger, R. L.; Mucic, R. C.; Storhoff, J. J., A DNA-based method for rationally assembling nanoparticles into macroscopic materials. *Nature* **1996,** *382* (6592), 607-609.

92. Elghanian, R.; Storhoff, J. J.; Mucic, R. C.; Letsinger, R. L.; Mirkin, C. A., Selective Colorimetric Detection of Polynucleotides Based on the Distance-Dependent Optical Properties of Gold Nanoparticles. *Science* **1997,** *277* (5329), 1078-1081.

93. Chi, X.; Huang, D.; Zhao, Z.; Zhou, Z.; Yin, Z.; Gao, J., Nanoprobes for inÂ vitro diagnostics of cancer and infectious diseases. *Biomaterials* **2012,** *33* (1), 189-206.

94. Nie, S.; Emory, S. R., Probing Single Molecules and Single Nanoparticles by Surface-Enhanced Raman Scattering. *Science* **1997,** *275* (5303), 1102-1106.

95. Qian, X. M.; Nie, S. M., Single-molecule and single-nanoparticle SERS: from fundamental mechanisms to biomedical applications. *Chemical Society Reviews* **2008,** *37* (5), 912-920.

96. Faulds, K.; Littleford, R. E.; Graham, D.; Dent, G.; Smith, W. E., Comparison of Surface-Enhanced Resonance Raman Scattering from Unaggregated and Aggregated Nanoparticles. *Analytical Chemistry* **2004,** *76* (3), 592-598.

97. Graham, D.; Thompson, D. G.; Smith, W. E.; Faulds, K., Control of enhanced Raman scattering using a DNA-based assembly process of dye-coded nanoparticles. *Nature Nanotechnology* **2008,** *3* (9), 548-551.

98. Cao, Y. C.; Jin, R.; Mirkin, C. A., Nanoparticles with Raman Spectroscopic Fingerprints for DNA and RNA Detection. *Science* **2002,** *297* (5586), 1536-1540.

99. photonics 4 life. European Network of Excellence for Biophotonics. Surface enhanced Ramam Spectroscopr. http://www.photonics4life.eu/Consortium/P4L-DB/All-items/Surface-enhanced-Raman-Spectroscopy (accessed Jun 5, 2015).

100. Cassar, R. N.; Graham, D.; Larmour, I.; Wark, A. W.; Faulds, K., Synthesis of size tunable monodispersed silver nanoparticles and the effect of size on SERS enhancement. *Vibrational Spectroscopy* **2014,** *71*, 41-46.

101. Lu, Z.; Rong, K.; Li, J.; Yang, H.; Chen, R., Size-dependent antibacterial activities of silver nanoparticles against oral anaerobic pathogenic bacteria. *Journal of Materials Science: Materials in Medicine* **2013,** *24* (6), 1465-1471.

102. Pal, S.; Tak, Y. K.; Song, J. M., Does the Antibacterial Activity of Silver Nanoparticles Depend on the Shape of the Nanoparticle? A Study of the Gram-Negative Bacterium Escherichia coli. *Applied and Environmental Microbiology* **2007,** *73* (6), 1712-1720.

103. Mallard-Favier, I.; Blach, P.; Cazier, F.; Delattre, F., Efficient synthesis of a fluorescent tripod detection system for pesticides by microwave-assisted click chemistry. *Carbohydrate Research* **2009,** *344* (2), 161-166.

104. Bosco, M. l.; Gall, S. L.; Rihouey, C.; Couve-Bonnaire, S.; Bardor, M.; Lerouge, P.; Pannecoucke, X., 6-Azido D-galactose transfer to N-acetyl-D-

glucosamine derivative using commercially available β-1,4-galactosyltransferase. *Tetrahedron Letters* **2008,** *49* (14), 2294-2297.

105. Crowley, J. D.; Bandeen, P. H., A multicomponent CuAAC "click" approach to a library of hybrid polydentate 2-pyridyl-1,2,3-triazole ligands: new building blocks for the generation of metallosupramolecular architectures. *Dalton Transactions* **2010,** *39* (2), 612-623.

106. Crowley, J. D.; Bandeen, P. H.; Hanton, L. R., A one pot multi-component CuAAC "click" approach to bidentate and tridentate pyridyl-1,2,3-triazole ligands: Synthesis, X-ray structures and copper(II) and silver(I) complexes. *Polyhedron* **2010,** *29* (1), 70-83.

107. Gower, M. L.; Crowley, J. D., Self-assembly of silver(i) metallomacrocycles using unsupported 1,4-substituted-1,2,3-triazole "click" ligands. *Dalton Transactions* **2010,** *39* (9), 2371-2378.

108. Hynes, M. J., EQNMR: a computer program for the calculation of stability constants from nuclear magnetic resonance chemical shift data. *Journal of the Chemical Society, Dalton Transactions* **1993,** (2), 311-312.

109. Dondi, R., Directed Metallisation Using Molecular Recognition Tools. Ph.D. Thesis, University of Leicester, 2012.

110. Appukkuttan, P.; Dehaen, W.; Fokin, V. V.; Van der Eycken, E., A Microwave-Assisted Click Chemistry Synthesis of 1,4-Disubstituted 1,2,3-Triazoles via a Copper(I)-Catalyzed Three-Component Reaction. *Organic Letters* **2004,** *6* (23), 4223-4225.

111. Li, P.; Wang, L.; Zhang, Y., SiO_2-NHC-Cu(I): an efficient and reusable catalyst for [3+2] cycloaddition of organic azides and terminal alkynes under

solvent-free reaction conditions at room temperature. *Tetrahedron* **2008,** *64* (48), 10825-10830.

112. Hong, V.; Presolski, S. I.; Ma, C.; Finn, M. G., Analysis and Optimization of Copper-Catalyzed Azide–Alkyne Cycloaddition for Bioconjugation. *Angewandte Chemie International Edition* **2009,** *48* (52), 9879-9883.

113. Thordarson, P., Determining association constants from titration experiments in supramolecular chemistry. *Chemical Society Reviews* **2011,** *40* (3), 1305-1323.

114. Bowmaker, G. A.; Effendy; Marfuah, S.; Skelton, B. W.; White, A. H., Syntheses, structures and vibrational spectroscopy of some 1:1 and 1:2 adducts of silver(I) oxyanion salts with 2,2'-bis(pyridine) chelates. *Inorganica Chimica Acta* **2005,** *358* (14), 4371-4388.

115. Seward, C.; Chan, J.; Song, D.; Wang, S., Anion Dependent Structures of Luminescent Silver(I) Complexes. *Inorganic Chemistry* **2003,** *42* (4), 1112-1120.

116. Effendy; Marchetti, F.; Pettinari, C.; Pettinari, R.; Skelton, B. W.; White, A. H., Synthesis and Spectroscopic Characterization of Silver(I) Complexes with the Bis(1,2,4-triazol-1-yl)alkane Ligand $tz_2(CH_2)$. X-ray Structures of Two- and Three-Dimensional Coordination Polymers. *Inorganic Chemistry* **2003,** *42* (1), 112-117.

117. Zhang, Q.; Li, W.; Wen, L.-P.; Chen, J.; Xia, Y., Facile Synthesis of Ag Nanocubes of 30 to 70 nm in Edge Length with CF_3COOAg as a Precursor. *Chemistry – A European Journal* **2010,** *16* (33), 10234-10239.

118. Wang, Y.; Zheng, Y.; Huang, C. Z.; Xia, Y., Synthesis of Ag Nanocubes 18-32 nm in Edge Length: The Effects of Polyol on Reduction Kinetics, Size Control, and Reproducibility. *Journal of the American Chemical Society* **2013,** *135* (5), 1941-1951.

119. Sun, T.; Teja, A. S., Density, Viscosity, and Thermal Conductivity of Aqueous Ethylene, Diethylene, and Triethylene Glycol Mixtures between 290 K and 450 K. *Journal of Chemical & Engineering Data* **2003,** *48* (1), 198-202.

120. Lee, Y.; Oh, S.-G., Counter-ion effects of silver salt on the production yield of silver nanoparticles in alcohol reduction process. *Colloids and Surfaces A: Physicochemical and Engineering Aspects* **2014,** *459*, 172-176.

121. Link, S.; Ei-Sayed, M. A., Optical properties and ultrafast dynamics of metallic nanocrystals. *Annual Review of Physical Chemistry* **2003,** *54*, 331-366.

122. Bhui, D. K.; Bar, H.; Sarkar, P.; Sahoo, G. P.; De, S. P.; Misra, A., Synthesis and UV-vis spectroscopic study of silver nanoparticles in aqueous SDS solution. *Journal of Molecular Liquids* **2009,** *145* (1), 33-37.

123. Simakov, P.; Gautier, J.; Prochazka, M.; Herve-Aubert, K.; Chourpa, I., Polyethylene-glycol-Stabilized Ag Nanoparticles for Surface-Enhanced Raman Scattering Spectroscopy: Ag Surface Accessibility Studied Using Metalation of Free-Base Porphyrins. *The Journal of Physical Chemistry C* **2014,** *118* (14), 7690-7697.

124. Karakoti, A. S.; Das, S.; Thevuthasan, S.; Seal, S., PEGylated Inorganic Nanoparticles. *Angewandte Chemie International Edition* **2011,** *50* (9), 1980-1994.

125. Sperling, R. A.; Parak, W. J., *Surface modification, functionalization and bioconjugation of colloidal inorganic nanoparticles*. 2010; Vol. 368, p 1333-1383.

126. Roberts, M. J.; Bentley, M. D.; Harris, J. M., Chemistry for peptide and protein PEGylation. *Advanced Drug Delivery Reviews* **2002,** *54* (4), 459-476.

127. Eck, W.; Craig, G.; Sigdel, A.; Ritter, G.; Old, L. J.; Tang, L.; Brennan, M. F.; Allen, P. J.; Mason, M. D., PEGylated Gold Nanoparticles Conjugated to

Monoclonal F19 Antibodies as Targeted Labeling Agents for Human Pancreatic Carcinoma Tissue. *ACS Nano* **2008,** *2* (11), 2263-2272.

128. Abuchowski, A.; van Es, T.; Palczuk, N. C.; Davis, F. F., Alteration of immunological properties of bovine serum albumin by covalent attachment of polyethylene glycol. *Journal of Biological Chemistry* **1977,** *252* (11), 3578-81.

129. Abuchowski, A.; McCoy, J. R.; Palczuk, N. C.; van Es, T.; Davis, F. F., Effect of covalent attachment of polyethylene glycol on immunogenicity and circulating life of bovine liver catalase. *Journal of Biological Chemistry* **1977,** *252* (11), 3582-6.

130. Deiters, A.; Cropp, T. A.; Summerer, D.; Mukherji, M.; Schultz, P. G., Site-specific PEGylation of proteins containing unnatural amino acids. *Bioorganic & Medicinal Chemistry Letters* **2004,** *14* (23), 5743-5745.

131. Brennan, J. L.; Hatzakis, N. S.; Tshikhudo, T. R.; Razumas, V.; Patkar, S.; Vind, J.; Svendsen, A.; Nolte, R. J. M.; Rowan, A. E.; Brust, M., Bionanoconjugation via Click Chemistry: The Creation of Functional Hybrids of Lipases and Gold Nanoparticles. *Bioconjugate Chemistry* **2006,** *17* (6), 1373-1375.

132. Shenoy, D.; Fu, W.; Li, J.; Crasto, C.; Jones, G.; DiMarzio, C.; Sridhar, S.; Amiji, M., Surface functionalization of gold nanoparticles using hetero-bifunctional poly(ethylene glycol) spacer for intracellular tracking and delivery. *International Journal of Nanomedicine* **2006,** *1* (1), 51-57.

133. Gole, A.; Murphy, C. J., Azide-Derivatized Gold Nanorods: Functional Materials for "Click" Chemistry. *Langmuir* **2008,** *24* (1), 266-272.

134. Rana, S.; Yeh, Y.-C.; Rotello, V. M., Engineering the nanoparticle-protein interface: applications and possibilities. *Current Opinion in Chemical Biology* **2010,** *14* (6), 828-834.

135. Chen, J.; Spear, S. K.; Huddleston, J. G.; Rogers, R. D., Polyethylene glycol and solutions of polyethylene glycol as green reaction media. *Green Chemistry* **2005,** *7* (2), 64-82.

136. Bo, L.; Yang, W.; Chen, M.; Gao, J.; Xue, Q., A Simple and 'Green' Synthesis of Polymer-Based Silver Colloids and Their Antibacterial Properties. *Chemistry & Biodiversity* **2009,** *6* (1), 111-116.

137. Shameli, K.; Ahmad, M.; Jazayeri, S.; Shabanzadeh, P.; Sangpour, P.; Jahangirian, H.; Gharayebi, Y., Investigation of antibacterial properties silver nanoparticles prepared via green method. *Chemistry Central Journal* **2012,** *6* (1), 73.

138. Shameli, K.; Bin Ahmad, M.; Jazayeri, S. D.; Sedaghat, S.; Shabanzadeh, P.; Jahangirian, H.; Mahdavi, M.; Abdollahi, Y., Synthesis and Characterization of Polyethylene Glycol Mediated Silver Nanoparticles by the Green Method. *International Journal of Molecular Sciences* **2012,** *13* (6), 6639-6650.

139. Jokerst, J. V.; Lobovkina, T.; Zare, R. N.; Gambhir, S. S., Nanoparticle PEGylation for imaging and therapy. *Nanomedicine (London, England)* **2011,** *6* (4), 715-728.

140. Zhao, W.; Brook, M. A.; Li, Y., Design of Gold Nanoparticle-Based Colorimetric Biosensing Assays. *ChemBioChem* **2008,** *9* (15), 2363-2371.

141. Howard, M. D.; Jay, M.; Dziubla, T. D.; Lu, X., PEGylation of Nanocarrier Drug Delivery Systems: State of the Art. *Journal of Biomedical Nanotechnology* **2008,** *4* (2), 133-148.

142. Wuelfing, W. P.; Gross, S. M.; Miles, D. T.; Murray, R. W., Nanometer Gold Clusters Protected by Surface-Bound Monolayers of Thiolated Poly(ethylene glycol) Polymer Electrolyte. *Journal of the American Chemical Society* **1998,** *120* (48), 12696-12697.

143. Foos, E. E.; Snow, A. W.; Twigg, M. E.; Ancona, M. G., Thiol-Terminated Di-, Tri-, and Tetraethylene Oxide Functionalized Gold Nanoparticles: A Water-Soluble, Charge-Neutral Cluster. *Chemistry of Materials* **2002,** *14* (5), 2401-2408.

144. Kanaras, A. G.; Kamounah, F. S.; Schaumburg, K.; Kiely, C. J.; Brust, M., Thioalkylated tetraethylene glycol: a new ligand for water soluble monolayer protected gold clusters. *Chemical Communications* **2002,** (20), 2294-2295.

145. Tshikhudo, T. R.; Wang, Z.; Brust, M., Biocompatible gold nanoparticles. *Materials Science and Technology* **2004,** *20* (8), 980-984.

146. Krpetic, Z.; Saleemi, S.; Prior, I. A.; See, V.; Qureshi, R.; Brust, M., Negotiation of Intracellular Membrane Barriers by TAT-Modified Gold Nanoparticles. *ACS Nano* **2011,** *5* (6), 5195-5201.

147. Otsuka, H.; Akiyama, Y.; Nagasaki, Y.; Kataoka, K., Quantitative and Reversible Lectin-Induced Association of Gold Nanoparticles Modified with α-Lactosyl-ω-mercapto-poly(ethylene glycol). *Journal of the American Chemical Society* **2001,** *123* (34), 8226-8230.

148. Brust, M.; Walker, M.; Bethell, D.; Schiffrin, D. J.; Whyman, R., Synthesis of thiol-derivatised gold nanoparticles in a two-phase Liquid-Liquid system. *Journal of the Chemical Society, Chemical Communications* **1994,** (7), 801-802.

149. Erathodiyil, N.; Ying, J. Y., Functionalization of Inorganic Nanoparticles for Bioimaging Applications. *Accounts of Chemical Research* **2011,** *44* (10), 925-935.

150. Sapsford, K. E.; Algar, W. R.; Berti, L.; Gemmill, K. B.; Casey, B. J.; Oh, E.; Stewart, M. H.; Medintz, I. L., Functionalizing Nanoparticles with Biological Molecules: Developing Chemistries that Facilitate Nanotechnology. *Chemical Reviews* **2013,** *113* (3), 1904-2074.

151. Sletten, E. M.; Bertozzi, C. R., Bioorthogonal Chemistry: Fishing for Selectivity in a Sea of Functionality. *Angewandte Chemie International Edition* **2009,** *48* (38), 6974-6998.

152. Debets, M. F.; van der Doelen, C. W. J.; Rutjes, F. P. J. T.; van Delft, F. L., Azide: A Unique Dipole for Metal-Free Bioorthogonal Ligations. *ChemBioChem* **2010,** *11* (9), 1168-1184.

153. Jewett, J. C.; Bertozzi, C. R., Cu-free click cycloaddition reactions in chemical biology. *Chemical Society Reviews* **2010,** *39* (4), 1272-1279.

154. Stohs, S. J.; Bagchi, D., Oxidative mechanisms in the toxicity of metal ions. *Free Radical Biology and Medicine* **1995,** *18* (2), 321-336.

155. Burrows, C. J.; Muller, J. G., Oxidative Nucleobase Modifications Leading to Strand Scission. *Chemical Reviews* **1998,** *98* (3), 1109-1152.

156. Kennedy, D. C.; McKay, C. S.; Legault, M. C. B.; Danielson, D. C.; Blake, J. A.; Pegoraro, A. F.; Stolow, A.; Mester, Z.; Pezacki, J. P., Cellular Consequences of Copper Complexes Used To Catalyze Bioorthogonal Click Reactions. *Journal of the American Chemical Society* **2011,** *133* (44), 17993-18001.

157. Wittig, G.; Krebs, A., Zur Existenz niedergliedriger Cycloalkine, I. *Chemische Berichte* **1961,** *94* (12), 3260-3275.

158. Chenoweth, K.; Chenoweth, D.; Goddard Iii, W. A., Cyclooctyne-based reagents for uncatalyzed click chemistry: A computational survey. *Organic & Biomolecular Chemistry* **2009,** *7* (24), 5255-5258.

159. Agard, N. J.; Prescher, J. A.; Bertozzi, C. R., A Strain-Promoted [3 + 2] Azide-Alkyne Cycloaddition for Covalent Modification of Biomolecules in Living Systems. *Journal of the American Chemical Society* **2004,** *126* (46), 15046-15047.

160. Ess, D. H.; Jones, G. O.; Houk, K. N., Transition States of Strain-Promoted Metal-Free Click Chemistry: 1,3-Dipolar Cycloadditions of Phenyl Azide and Cyclooctynes. *Organic Letters* **2008,** *10* (8), 1633-1636.

161. Agard, N. J.; Baskin, J. M.; Prescher, J. A.; Lo, A.; Bertozzi, C. R., A Comparative Study of Bioorthogonal Reactions with Azides. *ACS Chemical Biology* **2006,** *1* (10), 644-648.

162. Baskin, J. M.; Prescher, J. A.; Laughlin, S. T.; Agard, N. J.; Chang, P. V.; Miller, I. A.; Lo, A.; Codelli, J. A.; Bertozzi, C. R., Copper-free click chemistry for dynamic in vivo imaging. *Proceedings of the National Academy of Sciences of the United States of America* **2007,** *104* (43), 16793-16797.

163. Codelli, J. A.; Baskin, J. M.; Agard, N. J.; Bertozzi, C. R., Second-Generation Difluorinated Cyclooctynes for Copper-Free Click Chemistry. *Journal of the American Chemical Society* **2008,** *130* (34), 11486-11493.

164. Ning, X.; Guo, J.; Wolfert, M. A.; Boons, G.-J., Visualizing Metabolically-Labeled Glycoconjugates of Living Cells by Copper-Free and Fast Huisgen Cycloadditions. *Angewandte Chemie International Edition* **2008,** *47* (12), 2253-2255.

165. Sletten, E. M.; Bertozzi, C. R., A Hydrophilic Azacyclooctyne for Cu-Free Click Chemistry. *Organic Letters* **2008,** *10* (14), 3097-3099.

166. Debets, M. F.; van Berkel, S. S.; Schoffelen, S.; Rutjes, F. P. J. T.; van Hest, J. C. M.; van Delft, F. L., Aza-dibenzocyclooctynes for fast and efficient enzyme PEGylation via copper-free (3+2) cycloaddition. *Chemical Communications* **2010,** *46* (1), 97-99.

167. Dommerholt, J.; Schmidt, S.; Temming, R.; Hendriks, L. J. A.; Rutjes, F. P. J. T.; van Hest, J. C. M.; Lefeber, D. J.; Friedl, P.; van Delft, F. L., Readily Accessible Bicyclononynes for Bioorthogonal Labeling and Three-Dimensional Imaging of Living Cells. *Angewandte Chemie International Edition* **2010,** *49* (49), 9422-9425.

168. Jewett, J. C.; Sletten, E. M.; Bertozzi, C. R., Rapid Cu-Free Click Chemistry with Readily Synthesized Biarylazacyclooctynones. *Journal of the American Chemical Society* **2010,** *132* (11), 3688-3690.

169. Singh, I.; Wendeln, C.; Clark, A. W.; Cooper, J. M.; Ravoo, B. J.; Burley, G. A., Sequence-Selective Detection of Double-Stranded DNA Sequences Using Pyrrole-Imidazole Polyamide Microarrays. *Journal of the American Chemical Society* **2013,** *135* (9), 3449-3457.

170. Manova, R. K.; Pujari, S. P.; Weijers, C. A. G. M.; Zuilhof, H.; van Beek, T. A., Copper-Free Click Biofunctionalization of Silicon Nitride Surfaces via Strain-Promoted Alkyne-Azide Cycloaddition Reactions. *Langmuir* **2012,** *28* (23), 8651-8663.

171. Dervan, P. B.; Edelson, B. S., Recognition of the DNA minor groove by pyrrole-imidazole polyamides. *Current Opinion in Structural Biology* **2003,** *13* (3), 284-299.

172. Bernardin, A.; Cazet, A.; Guyon, L.; Delannoy, P.; Vinet, F.; Bonnaffe, D.; Texier, I., Copper-Free Click Chemistry for Highly Luminescent Quantum Dot Conjugates: Application to in Vivo Metabolic Imaging. *Bioconjugate Chemistry* **2010,** *21* (4), 583-588.

173. Michalet, X.; Pinaud, F. F.; Bentolila, L. A.; Tsay, J. M.; Doose, S.; Li, J. J.; Sundaresan, G.; Wu, A. M.; Gambhir, S. S.; Weiss, S., Quantum Dots for Live Cells, in Vivo Imaging, and Diagnostics. *Science* **2005,** *307* (5709), 538-544.

174. Isarov, A. V.; Chrysochoos, J., Optical and Photochemical Properties of Nonstoichiometric Cadmium Sulfide Nanoparticles: Surface Modification with Copper(II) Ions. *Langmuir* **1997,** *13* (12), 3142-3149.

175. Dennis, J. W.; Granovsky, M.; Warren, C. E., Glycoprotein glycosylation and cancer progression. *Biochimica et Biophysica Acta (BBA) - General Subjects* **1999,** *1473* (1), 21-34.

176. Gobbo, P.; Mossman, Z.; Nazemi, A.; Niaux, A.; Biesinger, M. C.; Gillies, E. R.; Workentin, M. S., Versatile strained alkyne modified water-soluble AuNPs for interfacial strain promoted azide-alkyne cycloaddition (I-SPAAC). *Journal of Materials Chemistry B* **2014,** *2* (13), 1764-1769.

177. Xia, Y.; Xia, X.; Wang, Y.; Xie, S., Shape-controlled synthesis of metal nanocrystals. *MRS Bulletin* **2013,** *38* (04), 335-344.

178. Guerrini, L.; Graham, D., Molecularly-mediated assemblies of plasmonic nanoparticles for Surface-Enhanced Raman Spectroscopy applications. *Chemical Society Reviews* **2012,** *41* (21), 7085-7107.

179. Liang, H.; Li, Z.; Wang, W.; Wu, Y.; Xu, H., Highly Surface-roughened "Flower-like" Silver Nanoparticles for Extremely Sensitive Substrates of Surface-enhanced Raman Scattering. *Advanced Materials* **2009,** *21* (45), 4614-4618.

180. Skattebol, L.; Solomon, M. J., 1,2-CYCLONONADIENE. *Organic Synthesis* **1973,** *Coll. Vol. 5*, 306-310.

181. Neef, A. B.; Schultz, C., Selective Fluorescence Labeling of Lipids in Living Cells. *Angewandte Chemie International Edition* **2009,** *48* (8), 1498-1500.

182. Lallana, E.; Fernandez-Megia, E.; Riguera, R., Surpassing the Use of Copper in the Click Functionalization of Polymeric Nanostructures: A Strain-Promoted Approach. *Journal of the American Chemical Society* **2009,** *131* (16), 5748-5750.

183. Pinter, G.; Bereczki, I.; Roth, E.; Sipos, A.; Varghese, R.; Udo, E. E.; Ostorhazi, E.; Rozgonyi, F.; Phillips, O. A.; Herczegh, P., The Effect of Systematic Structural Modifications on the Antibacterial Activity of Novel Oxazolidinones. *Medicinal Chemistry* **2011,** *7* (1), 45-55.

184. Merrifield, R. B., Solid Phase Peptide Synthesis. I. The Synthesis of a Tetrapeptide. *Journal of the American Chemical Society* **1963,** *85* (14), 2149-2154.

185. Merrifield, R. B., Solid Phase Peptide Synthesis. II. The Synthesis of Bradykinin. *Journal of the American Chemical Society* **1964,** *86* (2), 304-305.

186. Sakakibara, S.; Shimonishi, Y.; Kishida, Y.; Okada, M.; Sugihara, H., Use of Anhydrous Hydrogen Fluoride in Peptide Synthesis. I. Behavior of Various

Protective Groups in Anhydrous Hydrogen Fluoride. *Bulletin of the Chemical Society of Japan* **1967,** *40* (9), 2164-2167.

187. Carpino, L. A.; Han, G. Y., 9-Fluorenylmethoxycarbonyl function, a new base-sensitive amino-protecting group. *Journal of the American Chemical Society* **1970,** *92* (19), 5748-5749.

188. Tolaymat, T. M.; El Badawy, A. M.; Genaidy, A.; Scheckel, K. G.; Luxton, T. P.; Suidan, M., An evidence-based environmental perspective of manufactured silver nanoparticle in syntheses and applications: A systematic review and critical appraisal of peer-reviewed scientific papers. *Science of The Total Environment* **2010,** *408* (5), 999-1006.

189. Chen, C.-L.; Rosi, N. L., Peptide-Based Methods for the Preparation of Nanostructured Inorganic Materials. *Angewandte Chemie International Edition* **2010,** *49* (11), 1924-1942.

190. Belser, K.; Vig Slenters, T.; Pfumbidzai, C.; Upert, G.; Mirolo, L.; Fromm, K. M.; Wennemers, H., Silver Nanoparticle Formation in Different Sizes Induced by Peptides Identified within Split-and-Mix Libraries. *Angewandte Chemie International Edition* **2009,** *48* (20), 3661-3664.

191. Dickerson, M. B.; Sandhage, K. H.; Naik, R. R., Protein- and Peptide-Directed Syntheses of Inorganic Materials. *Chemical Reviews* **2008,** *108* (11), 4935-4978.

192. Xie, J.; Lee, J. Y.; Wang, D. I. C.; Ting, Y. P., Silver Nanoplates: From Biological to Biomimetic Synthesis. *ACS Nano* **2007,** *1* (5), 429-439.

193. Si, S.; Mandal, T. K., Tryptophan-Based Peptides to Synthesize Gold and Silver Nanoparticles: A Mechanistic and Kinetic Study. *Chemistry – A European Journal* **2007,** *13* (11), 3160-3168.

194. Li, S.; Shen, Y.; Xie, A.; Yu, X.; Qiu, L.; Zhang, L.; Zhang, Q., Green synthesis of silver nanoparticles using Capsicum annuum L. extract. *Green Chemistry* **2007,** *9* (8), 852-858.

195. Slocik, J. M.; Wright, D. W., Biomimetic Mineralization of Noble Metal Nanoclusters. *Biomacromolecules* **2003,** *4* (5), 1135-1141.

196. Reches, M.; Gazit, E., Casting Metal Nanowires Within Discrete Self-Assembled Peptide Nanotubes. *Science* **2003,** *300* (5619), 625-627.

197. Slocik, J. M.; Moore, J. T.; Wright, D. W., Monoclonal Antibody Recognition of Histidine-Rich Peptide Encapsulated Nanoclusters. *Nano Letters* **2002,** *2* (3), 169-173.

198. Naik, R. R.; Stringer, S. J.; Agarwal, G.; Jones, S. E.; Stone, M. O., Biomimetic synthesis and patterning of silver nanoparticles. *Nature Materials* **2002,** *1* (3), 169-172.

199. Rabanal, F.; Ludevid, M. D.; Pons, M.; Giralt, E., CD of proline-rich polypeptides: Application to the study of the repetitive domain of maize glutelin-2. *Biopolymers* **1993,** *33* (7), 1019-1028.

200. Gellett, A. M.; Huber, P. W.; Higgins, P. J., Synthesis of the unnatural amino acid N^{α}-N^{ε}-(ferrocene-1-acetyl)-l-lysine: A novel organometallic nuclease. *Journal of Organometallic Chemistry* **2008,** *693* (18), 2959-2962.

201. Galibert, M.; Dumy, P.; Boturyn, D., One-Pot Approach to Well-Defined Biomolecular Assemblies by Orthogonal Chemoselective Ligations. *Angewandte Chemie International Edition* **2009,** *48* (14), 2576-2579.